LYSOSOME DYNAMICS IN MODELS OF FRONTOTEMPORAL DEMENTIA AND ALZHEIMERS DISEASE

SAADIA HASAN
University College London
UCL QUEEN SQUARE INSTITUTE OF NEUROLOGY

Submitted to University College London (UCL) in partial fulfilment of the requirements for the award of the degree of Doctor of Philosophy.

Primary supervisor: **DR. SOYON HONG**

Primary supervisor: **DR. MICHAEL E WARD**

Secondary supervisor: **DR. ADRIAN ISAACS**

Examining committee: **DR. CHRIS SHAW, DR. CARA CROFT**

Thesis submission date: **May 2023**

Declaration

I, **Saadia Hasan**, confirm that the work presented in this thesis is my own. Where information has been derived from other sources, I confirm that this has been indicated in the thesis.

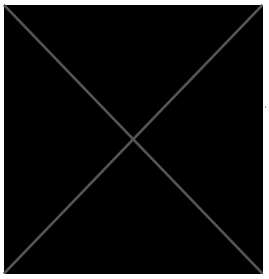

Saadia Hasan
London, United Kingdom
May 3rd 2023

Abstract

Lysosomal dysfunction is linked to several neurodegenerative diseases. Recent GWAS studies have implicated genes in endo-lysosomal pathways as risk factors for developing frontotemporal dementia (FTD) and Alzheimer's disease (AD). However current tools to study protein interactions of these pathways *in situ* are limited. In this thesis, I enhanced a proximity-based proteomics tool to capture an unbiased interactome of a protein of interest in mouse brains. The tool, called Biotinylation by Antibody Recognition (BAR), utilizes existing immunohistochemistry protocols on fixed tissue in addition to activating HRP-conjugated secondaries bound to primary of interest. Activation of HRP generates biotin radicals that bind to proteins in the vicinity that can be collected for proteomics. I investigated the robustness of this method targeting lysosomes in *GRN*$^{-/-}$ mice. *GRN* codes for progranulin, a lysosomal glycoprotein, and is implicated as an FTD and AD GWAS hit. I used human inducible pluripotent stem cell (iPSC) derived neurons and microglia for follow up studies. Additionally, I tested a cell type-specific marker for microglia using BAR to assess its applicability to generate whole cell interactomes *in situ* for FTD and AD using *GRN*$^{-/-}$ and *APP*^{NLF} mice respectively. Here, I showed that lysosomes have an increased abundance of proteolytic enzymes with progranulin loss. Subsequently, I showed that despite this increase, there is a decrease in the enzymatic activity. Additionally, there was an upregulation of microglial proteins in this dataset consistent with literature. Proximity labeled proteomics of *GRN*$^{-/-}$ microglia showed increased lysosomal enzymes and components of the complement pathway as seen before. Lastly, I demonstrated that endo-lysosomal pathways are affected early in microglia from *APP*^{NLF} brains, consistent with lysosomal dysfunction seen in AD. Collectively, these findings confirm the validity of using BAR-based proteomics in fixed brain slices. And lastly, this dataset implicates endo-lysosomal dysfunction as the converging pathway in neurodegenerative diseases.

Impact Statement

Commonly used methods to probe region and cell type-specific biology in disease involve spatial transcriptomics and proteomics. These methods, however, are extensive and elaborate. In this thesis, I propose a simpler method to potentially achieve similar results with complement coverage to the spatial -omics methods. The method described is Biotinylation by Antibody Recognition developed by Bar et al. (2018) that uses horseradish peroxidase conjugated secondary antibody targeted to primary antibody of target protein to tag proteins in proximity. Here I've showed its applicability to mouse tissue that consistently produces target-relevant hits. I have mentored and taught this protocol to members of other labs, who have proceeded to apply it to human tissue. The applicability of this protocol to human tissue is the final impact of this method.

I have submitted my work, along with the work of my collaborators, for publication in a peer-reviewed journal. The research presented in this paper has the potential to advance the field of frontotemporal dementia research, as the findings presented are significant. Additionally, I have also had the opportunity to present my work at several scientific conferences through posters and talks, providing an opportunity to engage with other members of the scientific community and further the impact of my research.

Dedication

In loving memory of my brother, Ebad Hasan.

You instilled in me the love for science since I can remember, and the drive for medicine when you left your legacy behind.

Acknowledgements

Firstly, I would like to thank my two mentors Dr. Michael Ward and Dr. Soyon Hong. Michael, without your faith in me and superior advocacy for me, I would not have made it to where I am now. Thank you for mentoring me not only scientifically, but also professionally. For the times when I could just walk into your office for counseling, from experiments to questions about career paths, you always took the time to mentor me. Soyon, thank you for taking the leap of faith in accepting me into your lab at its infancy. It was a mold-breaking experience to have the opportunity to be mentored by you from across the pond. Through the countless zoom meetings, you always kept me accountable, and nurtured my scientific curiosity. Even though my physical time in the lab was brief, there was never a time I felt like I wasn't your student. Your resilient perseverance through the pandemic and passion to mentor have inspired me. With the co-mentorship of both my primary supervisors, I have learned so much in the span of these past 4 years.

Secondly, I would like to thank Dr. Ling Hao for her indispensable contribution to my whole PhD experience. From hot pot excursions, standing on bench tops to reach the top shelf, sharing her love for meat, to single-handedly teaching me everything I know about proteomics, mass spectrometry sample preparation, handling, data analysis, and manuscript construction. Thank you for your persistence and perseverance through challenging times of setting up a new lab in the pandemic and juggling faculty responsibilities.

Thirdly, I would like to thank the NIH-UCL graduate partnership program, Ward Lab and Hong Lab members, both past and present, for enriching my PhD experience. To NIH-UCL graduate partnership program for taking the challenge of allowing me to embark on this endeavor as their first dual-degree graduate student. To Dr. Yan Li for performing some of my mass spectrometry experiments. To Maia Parsadanian for providing invaluable assistance with the BAR method, microtome, and cell culture work. To

Hebao for always being responsive to my asks from across the pond. To Michael Fernandopulle for always lending a helping hand when I needed it. To Seppe for providing mentorship from across the pond. To Jenn for always putting a smile on my face.

Fourthly, to all my friends who provided me the emotional support needed to get through the PhD. To Deeti for her constant encouragement, to Shaista for always lending a listening ear, to Hannah and Anum for their pride in me, to Christina for making my move to the UK fondly memorable, to Lia for being there for me, to Ger for his amazing humor, to Laís for being her sweet self, and all the other lab members in Cruciform wing 2.4.

And finally, and most importantly, to my husband Robert. Your contribution has been vital for my success. Thank you.

COVID Impact Statement

In September 2019, I joined the University College London (UCL) and National Institutes of Health (NIH) joint graduate program with the goal of spending the first year at the NIH in the United States (US) developing tools for studying the microglial interactome in the context of Alzheimer's disease. Specifically, I aimed to optimize the Biotinylation by Antibody Recognition (BAR) method and develop the split-BAR method. After that year, I planned to return to UCL in September 2020 to apply these tools to AD models and spend the next two years investigating hypotheses based on the data generated from the BAR and split-BAR methods. I intended to move back to the NIH in September 2022 to pursue follow-up questions in the inducible pluripotent stem cell (iPSC) system for biological mechanistic validations and complete my PhD by September 2023.

However, because of the COVID-19 pandemic in 2020, I made the choice to stay in the US and analyze existing data from the BAR method and a proximity labeling experiment conducted by another graduate student in the lab, instead of traveling to the Unites Kingdom (UK). Once the lab resumed with limited occupancy in March 2021, I conducted follow-up experiments, which led to a manuscript that delayed my arrival at UCL until September 2022. Upon arrival, I discovered that I had a limited time frame to complete my PhD before returning to medical school in the US in June 2023, due to technicalities regarding medical licensing exams and graduation requirements. Unfortunately, the COVID-19 extension offered could not be availed because of these technicalities.

Contents

LIST OF ACRONYMS **14**

LIST OF FIGURES **18**

LIST OF SUPPLEMENTAL FIGURES **20**

LIST OF TABLES **21**

LIST OF SUPPLEMENTAL TABLES **22**

CHAPTER: 1 INTRODUCTION **23**

1.1 NEURODEGENERATION 23

1.1.1 General Cellular Dysfunctions *23*

1.1.1.1 Protein Aggregation 24

1.1.1.2 Mitochondrial Dysfunction 24

1.1.1.3 Neuroinflammation 26

1.1.2 Complex Interplay of Key Players in Neurodegeneration *26*

1.2 GWAS STUDIES 27

1.2.1 Novel Loci Discoveries in Neurodegeneration *27*

1.2.2 GWAS in Frontotemporal Dementia *27*

1.2.3 GWAS in Alzheimer's Disease *29*

1.2.3.1 FTD and AD Overlap 29

1.2.3.2 Microglial Genes in AD GWAS 30

1.3 FRONTOTEMPORAL DEMENTIA 30

1.3.1 Incidence, Clinical Features, and Pathology *30*

1.3.1.1 Subtle Variations in Clinical Manifestations 31

1.3.1.2 Proteinopathies 33

1.3.2 Models/Tools Available to Study FTD *35*

1.3.2.1 *GRN* KO Mouse Models 35

1.3.2.2 Induced Pluripotent Stem Cells Derived Neurons 36

1.3.2.2.1 Complete Loss of Progranulin 37

1.3.2.2.2 FTLD-Patient Derived Cell Lines 37

1.4 ALZHEIMER'S DISEASE 38

1.4.1 Incidence, Clinical Features, and Pathology *38*

1.4.1.1 Amyloid Cascade Hypothesis 39

1.4.1.2 Tau Hypothesis 40

1.4.2 Models/Tools Available to Study Alzheimer's disease 41
1.4.2.1 Mouse Models 41
1.4.2.2 Advantages of APP^{NLF} Model 42
1.5 MICROGLIA IN DISEASE 42
1.5.1 Healthy Microglia and Heterogeneity 43
1.5.2 Reactive versus Sensing Microglia 44
1.5.3 Neuroinflammation in Neurodegeneration 46
1.5.4 Challenges in Studying Microglia 48
1.6 AIMS 49

CHAPTER: 2 GENERAL METHODS 51

2.1 I^{3}NEURONS 51
2.2 I^{3}MICROGLIA 52
2.3 LYSOSOMAL IMMUNOPRECIPITATION 53
2.4 SAMPLE PREPARATION FOR PROTEOMICS 54
2.5 LIQUID CHROMATOGRAPHY COUPLED TO TANDEM MASS SPECTROMETRY ANALYSIS . 55
2.6 DATA ANALYSIS 56
2.7 FLUORESCENCE IMAGING 57
2.8 STATISTICS 58

CHAPTER: 3 CORE METHOD DEVELOPMENT: BIOTINYLATION BY ANTIBODY RECOGNITION 60

3.1 INTRODUCTION 60
3.1.1 Aims 64
3.2 PROTOCOL A: OPTIMIZING LABELING WITH PRIMARY ANTIBODIES 64
3.2.1 Tissue Eligibility 65
3.2.2 Antibody Eligibility 68
3.2.3 Staining Buffers 72
3.3 PROTOCOL B: OPTIMIZING LABELING RADIUS 72
3.3.1 Serum vs. No Serum 73
3.3.2 Ratio of Serum to Staining Buffers 75
3.4 PROTOCOL C: OPTIMIZING LYSATE AND STREPTAVIDIN BEADS TITRATION 78
3.4.1 PFA De-Crosslinking and Protein Quantification 78
3.4.2 Generating Dot Blot Assay 79
3.4.3 Analyzing Dot Blot Assay 80
3.5 MASS SPECTROMETRY SAMPLE PREPARATION 83
3.6 ANALYSIS 86

3.6.1 Use of Proteome Discover Over MaxQuant 87
3.6.2 Generation of Volcano Plots Using GraphPad Prism 89
3.6.3 Use of GO Term Search Engines 93
3.6.4 Use of Network Search Engines 96
3.7 COMMENTARY 96
3.7.1 Background Information 96
3.7.2 Critical Parameters and Troubleshooting 97
3.7.3 Anticipated Results 98
3.7.4 Time Considerations 98

CHAPTER: 4 PROGRANULIN IS REQUIRED FOR NORMAL LYSOSOMAL FUNCTION 99

4.1 INTRODUCTION 99
4.1.1 Lysosomal Storage Associated Neurodegeneration 100
4.1.2 Progranulin in the Lysosome 100
4.1.3 Progranulin's Role in Neurons 101
4.1.4 Aims 103
4.2 METHODS 103
4.2.1 GRN KO i^{3}Neurons 103
4.2.2 GRN KO Mouse Model 104
4.2.3 Lysosomal Proximity Labeling 104
4.2.4 Lysosomal Immunoprecipitation 105
4.3 LYSOSOMAL ASSAYS 105
4.3.1 Magic Red Assay 105
4.3.2 Dynamic Stable Isotope Labelling in Cell Culture (dSILAC) 106
4.4 RESULTS 107
4.4.1 Lysosomal Immunoprecipitation Can Be Used on i^{3}Neurons 107
4.4.2 Loss of Progranulin Leads to Increased Lysosomal Enzymes in Neurons 111
4.4.3 Progranulin-lacking Lysosomes Have Decreased Degradative Capabilities 114
4.4.4 Genes Associated with Neurodegeneration Have Altered Protein Turnover Rates in the Absence of Progranulin 116
4.4.5 Mouse Brains Lacking Progranulin Upregulate Complement Markers 120
4.5 DISCUSSION 124
4.5.1 Loss of Progranulin Leads to an Increase in Lysosomal Enzymes 125
4.5.2 Progranulin Deficiency Leads to Lysosomal Degradation Dysregulation .. 126

4.5.3 Progranulin-Null Mouse Brains Have Increased Lysosome and Complement Associated Proteins 128

CHAPTER: 5 LOSS OF PROGRANULIN LEADS TO A REACTIVE MICROGLIAL RESPONSE 130

5.1 INTRODUCTION 130
5.1.1 Role of Progranulin in Microglia 130
5.1.2 Challenges of Studying Microglia in Isolation 131
5.1.3 Aims 133
5.2 METHODS 133
5.2.1 GRN KO iMicroglia 133
5.2.2 Lysosomal Immunoprecipitation Cell Lines 134
5.2.3 GRN KO Mouse Model 134
5.2.4 Microglial Proximity Labeling 134
5.3 RESULTS 135
5.3.1 iMicroglia Can Be Used to Isolate Intact Lysosomes 135
5.3.2 Further Optimizations are Needed to Characterize Lysosomes from iMicroglia Lacking Progranulin 140
5.3.3 Progranulin Lacking Mouse Microglia Have Increased Lysosomal, Immunity, and Synapse-pruning Proteins in Their Vicinity. 143
5.4 DISCUSSION 148
5.4.1 iMicroglia Can Be Used to Study Microglial Lysosomes 149
5.4.2 Microglial-BAR as a Tool to Study In Situ Microglial Changes 150

CHAPTER: 6 PATHWAYS AFFECTED IN PROXIMITY TO MICROGLIA IN EARLY AD MOUSE MODEL 155

6.1 INTRODUCTION 155
6.1.1 Synapse Loss Occurs Early in AD 155
6.1.2 Microglia's Role in AD 157
6.1.3 Aims 158
6.2 METHODS 158
6.2.1 APP^{NLF} Mouse Model 158
6.2.2 Microglial BAR in APP^{NLF} Mouse Brains 158
6.3 RESULTS 159
6.3.1 Comparison of P2y12 and Iba1 for Microglial-BAR on APP^{NLF} Cohort 159
6.3.2 Proteins increased in microglia in early AD are endocytosis-associated. . 163
6.4 DISCUSSION 171

CHAPTER: 7 DISCUSSION 175

7.1 INTRODUCTION 175
7.2 APPLICABILITY AND CHALLENGES OF THE BAR METHOD 176
7.3 PROGRANULIN'S ROLE IN LYSOSOMES 178
7.4 MICROGLIAL PROGRANULIN 181
7.5 PRE-PLAQUE AD-ASSOCIATED MICROGLIA 183
7.6 CONCLUSION 185

BIBLIOGRAPHY 186

APPENDIX 238

SUPPLEMENTAL FIGURES 238

SUPPLEMENTAL TABLES 248

LIST OF PUBLICATIONS 252

List of Acronyms

6-TF	Six transcription factor
AAV	Adeno-associated virus
ACN	Acetonitrile
ACUC	Animal Care and Use Committee
AD	Alzheimer's Disease
ADP	Adenosine 5′-Diphosphate
AGC	Automatic Gain Control
ALS	Amyotrophic Lateral Sclerosis
APEX2	ascorbate peroxidase 2
APP	Amyloid Precursor Protein
ATP	Adenosine 5′-Triphosphate
ATP/ADP	Adenosine Tri-Phosphate And Adenosine Di-Phosphate
Aβ	Amyloid-Beta
BAR	Biotinylation by Antibody Recognition
BASU	Bacillus subtilis
BBB	Blood-Brain Barrier
BSA	Bovine Serum Albumin
bvFTD	Behavioral variant frontotemporal dementia
C1q	Complement component 1q
C3	Complement component 3
C9ORF72	Chromosome 9 open reading frame 72
CBS	Corticobasal syndrome
CD68	Cluster of Differentiation 68
CEBPα	CCAAT Enhancer Binding Protein Alpha
CEBPβ	CCAAT Enhancer Binding Protein Beta
CNS	Central Nervous System
CRISPR-Cas9	Clustered regularly interspaced short palindromic repeats and CRISPR-associated protein 9
CTSC	Cathepsin C
CX3CR1	CX3C chemokine receptor 1
DCA	Detergent Compatible Protein Assay
DNA	Deoxyribonucleic acid
dox	Doxycycline

dSILAC	Dynamic Stable Isotope Labeling Using Amino Acids in Cell Culture
DTT	Dithiothreitol
EDTA	Ethylenediaminetetraacetic acid
ELISA	Enzyme-linked immunosorbent assay
EMP	Erythromyeloid precursor
ER	Endoplasmic reticulum
FA	Formic acid
FACS	Fluorescence-activated cell sorting
FBS	Fetal bovine serum
FDR	False discovery rate
FTD	Frontotemporal dementia
FUS	Fused in sarcoma
GABA	Gamma-aminobutyric acid
GDP	Guanosine diphosphate
GM-CSF	Granulocyte macrophage colony-stimulating factor
GO	Gene ontology
GPCR	G protein-coupled receptor
GRN	Gene for progranulin
GTP	Guanosine triphosphate
GWAS	Genome-wide association studies
H_2O_2	Hydrogen peroxide
HA	Human influenza hemagglutinin
HCD	Higher-energy collisional dissociation
HEK 293T	Human Embryonic Kidney cells 293T
HEPES	N-2-hydroxyethylpiperazine-N'-2-ethanesulfonic acid
hiPSC	Human inducible pluripotent stem cell
HLA	Human leukocyte antigen
hnRNP	Heterogeneous nuclear ribonucleoprotein
HRP	Horseradish peroxidases
i^3	Integrated, inducible, and isogenic
i^3Microglia	Inducible, integrate, isogenic microglia
i^3Neurons	Inducible, integrate, isogenic neurons
IAA	Iodoacetamide
IFN	Interferon
IL-1β	Interleukin-1 beta
IL-6	Interleukin-6
iMG	Inducible, integrate, isogenic microglia
iPSC	Induced pluripotent stem cells
IRF5	Interferon regulatory factor 5

IRF8	Interferon regulatory factor 8
KEGG	Kyoto Encyclopedia of Genes and Genomes
KO	Knock out
KPBS	Potassium phosphate buffered saline
LAMP1	Lysosome associated membrane protein
LC-MS/MS	Liquid chromatography coupled to tandem mass spectrometry
LRRK2	Leucine-rich repeat kinase 2
Lyso-IP	Lysosomal immunoprecipitation
MAFB	Maf bzip transcription factor b
MAPT	Microtubule-associated protein tau
MCM	Microglia conditioned media
MCSF	Macrophage colony-stimulating factor
MHC II	Major histocompatibility complex II
MMSE	Mini-mental status examination
MND	Motor neuron disease
mRNA	Messenger ribonucleic acid
NCL	Neuronal ceroid lipofuscinosis
NDRI	National disease research interchange
NFTs	Neurofibrillary tangles
nfvFTD	Progressive non-fluent variant frontotemporal dementia
NGN2	Neurogenin2
NIH	National Institutes of Health
NO	Nitric oxide
P2Y12	P2Y purinoceptor 12
PAMP	Pathogen-associated molecular patterns
PBS	Phosphate-buffered saline
PBST	Phosphate buffered saline solution/1% Tween-20
PCAs	Protein-fragment complementation assays
PCCA	Propionyl-coa carboxylase alpha chain
PFA	Paraformaldehyde
PLO	Poly-L-ornithine
PPA	Primary progressive aphasia
PPIs	Protein-protein interactions
PSD-95	Postsynaptic density protein 95
PSPS	Progressive supranuclear palsy syndrome
RCF	Relative centrifugal field
RNA	Ribonucleic acid
ROS	Reactive oxygen species
SA	Streptavidin

SDS	Sodium dodecyl sulfate
SILAC	Stable isotope labeling using amino acids in cell culture
SNPs	Single-nucleotide polymorphisms
SV-40	Simian virus 40
svFTD	Semantic variant frontotemporal dementia
TBST	Tris buffered saline containing 0.1% Tween-20
TCEP	Tris(2-carboxyethyl)phosphine
TDP-43	TAR DNA binding protein 43
TFA	Trifluoroacetic acid
TLRs	Toll-like receptors
TMEM192	Transmembrane protein 192
TMT	Tandem Mass Tag
TNF-α	Tumor necrosis factor alpha
TREM2	Triggering receptor expressed on myeloid cells 2
Tris-HCl	Tris (hydroxymethyl) aminomethane (THAM) hydrochloride
UCL	University College London
VCP	Valosin containing protein
WT	Wildtype
WTC11	Wildtype human induced pluripotent stem cell

List of Figures

Figure 1-1: Locations of frontotemporal dementia pathologies. 31

Figure 3-1: Biotinylation by antibody recognition representation. 63

Figure 3-2: Antibodies for LAMP1, PGRN and P2Y12 are highly specific. 70

Figure 3-3: No difference exists between 100% FBS and 0% FBS buffer. 74

Figure 3-4: FBS buffer does not decrease the labeling radius. 75

Figure 3-5: Varying percentages of serum yield inconclusive results. 77

Figure 3-6: Dot Blot assay for BAR-treated lysates. 80

Figure 3-7: Intensity plots for dot blots from LAMP1-BAR and PGRN-BAR using wildtype and *GRN*$^{-/-}$ mouse brain. 82

Figure 3-8: Enriched proteins in bait group versus control no-bait group. 90

Figure 3-9: Majority of the enriched proteins are cell-substrate junction proteins. 91

Figure 3-10: Lyso-BAR pulls down lysosome-relevant proteins. 93

Figure 3-11: Gene Ontology (GO) term analysis reveals Lyso-BAR enriched proteins associate with lysosomal terms and Microglia-BAR enriched proteins associate with membrane terms. 95

Figure 4-1: HA tagged to LAMP1 pulls down lysosomes and colocalizes with lysosomal marker LAMTOR4. 110

Figure 4-2: Isolated lysosomes are enriched for lysosomal proteins. 111

Figure 4-3: Loss of progranulin leads to an increase in lysosomal enzymes in human neurons. 113

Figure 4-4: Lysosomal proteins related to pH maintenance and bond breakage are upregulated in human neurons with progranulin loss. 114

Figure 4-5: Progranulin loss leads to decreased cathepsin B activity. 116

Figure 4-6: Frontotemporal dementia (FTD) patient-derived i^{3}Neurons with mutant *GRN* reveal altered protein turnover of lysosomal enzymes and FTD-associated proteins.... 119

Figure 4-7: Mouse brains lacking progranulin upregulate pathways associated with autophagy, starvation response and complement activation. 121

Figure 4-8: Progranulin lacking lysosomes have more synaptic and complement peptides. 123

Figure 5-1: HA tagged to TMEM192 pulls down cleaner lysosome lysates than HA tagged to LAMP1. 136

Figure 5-2: Lysosome associated proteins are isolated using HA tagged to TMEM192 from day 8 iMicroglia. 138

Figure 5-3: Lysosome lysates are enriched for lysosomal proteins. 139

Figure 5-4: Progranulin lacking lysosomes from iMicroglia have altered abundance of proteins associated with translation and cell-cell junctions. 142

Figure 5-5: Biotinylated proteins colocalize with microglial marker in fixed mouse tissue. 145

Figure 5-6: Microglia lacking progranulin have increased proteins associated with cell-cell junctions and lysosomes. 146

Figure 5-7: Literature confirmed hits from progranulin lacking microglia are associated with protein transport, lysosomal activity, and classical complement pathways..... 148

Figure 6-1: P2Y12 and IBA1 as microglial marker for BAR in fixed mouse brain. 160

Figure 6-2: Volcano plots for IBA1-BAR and P2Y12-BAR comparing *APP*^{NLF} to wildtype. 162

Figure 6-3: Comparison of raw abundances between groups. 162

Figure 6-4: IBA1-BAR data could not be used post-normalization..... 163

Figure 6-5: *APP*^{NLF} brains have altered protein abundances related to oxidative phosphorylation, phagocytosis, and protein translation. 165

Figure 6-6: *APP*^{NLF} brains have more proteins associated with endocytosis and phagosome increased at 6 months of age. 167

Figure 6-7: String network analysis of increased proteins in *APP*^{NLF} associated with endocytosis and phagosome. 168

Figure 6-8: KEGG Pathways associated with synaptic terms in *APP*^{NLF} microglial-BAR compared to wildtype. 170

List of Supplemental Figures

Supplemental Figure 3-1: Overlap of P2Y12-BAR enriched proteins from *GRN*^{WT} and *APP*-WT mouse brains. ……..238

Supplemental Figure 4-1: Lysosomal proteins from i^{3}Neurons Lyso-IP pull down. …..239

Supplemental Figure 4-2: Complete loss of progranulin in i^{3}Neurons. ……...240

Supplemental Figure 4-3: Complete STRING diagram for Arsa, Sts, Arsf and Arsi. …241

Supplemental Figure 4-4: Dynamic Stable Isotope Labelling using Amino acids in Cell culture (dSILAC) workflow. ……242

Supplemental Figure 4-5: KEGG Pathways GO enrichment all proteins with changed turnover rates in *GRN* KO neurons. ……243

Supplemental Figure 4-6: Cellular component GO enrichment for 68 proteins upregulated only in Lyso-BAR from *GRN*$^{-/-}$ brains. ……..244

Supplemental Figure 5-1: GO term analysis for 41 decreased proteins in *GRN*$^{-/-}$ microglial-BAR. ……245

Supplemental Figure 5-2: 29% of microglia-BAR hits from *GRN*$^{-/-}$ brains overlap with existing literature. ……246

Supplemental Figure 6-1: KEGG Pathway Gene Ontology analysis showing synaptic terms in *APP*^{NLF} microglial-BAR compared to wildtype. ……247

List of Tables

Table 1-1: Gene mutations associated with FTD proteinopathies. 33

Table 2-1: List of human iPSC lines used in this study. 52

Table 2-2: Antibodies used for immunostaining. 58

List of Supplemental Tables

Supplemental Table 5-1: Known human lysosome, lysosomal membrane, and lysosomal lumen proteins from Uniprot.org. ……..248

Supplemental Table 5-2: Increased Lyso- and Microglial-BAR proteins overlap with whole brain proteomics in GRN-/- brains. ……..249

Supplemental Table 6-1: Proteins with altered abundances from *APP*^{NLF} brains compared to wildtype with their respective top KEGG pathways..……..250

Supplemental Table 6-2: Proteins with altered abundances from *APP*^{NLF} brains compared to wildtype with their respective synaptic KEGG pathways.……..251

Chapter: 1 Introduction

1.1 Neurodegeneration

Neurodegenerative diseases, such as Alzheimer's disease (AD) and frontotemporal dementia (FTD), are a vast group of disorders characterized by progressive loss of neurons, resulting in various clinical manifestations depending on the specific brain regions affected. These diseases significantly contribute to the global burden of disability and mortality, with Alzheimer's disease alone affecting approximately 50 million people worldwide and the numbers expected to rise due to an aging population (Prince et al., 2015). It is important to note that dementia, often associated with neurodegenerative diseases, is not a disease itself but a clinical symptom resulting from the loss of neurons and their connections. The complex clinical features of neurodegenerative diseases are determined by the combination of locations affected and extent of neuronal loss, leading to diverse cognitive, motor, and behavioral impairments. In this thesis, I will focus on Alzheimer's disease and frontotemporal dementia as examples of neurodegenerative dementias.

1.1.1 General Cellular Dysfunctions

There are several general cellular dysfunctions that are common in many neurodegenerative dementias. These dysfunctions contribute to the progression of various neurodegenerative diseases, such as Alzheimer's disease and frontotemporal dementia. Some of these dysfunctions include

protein aggregation, mitochondrial dysfunction, and neuroinflammation. In the following sections, I will briefly discuss each of these dysfunctions.

1.1.1.1 Protein Aggregation

The most extensively investigated and notable cellular dysfunction in neurodegenerative disorders is the presence of protein aggregates in the brain (Ross and Poirier, 2004; Chopra et al., 2022; Tsoi et al., 2023). For instance, the widely recognized protein aggregate amyloid-beta (Aβ) was first observed by Alois Alzheimer in 1906 in a patient who suffered memory loss, disorientation, and cognitive decline (Alzheimer, 1907). Subsequent studies validated this finding to be what is now known as Alzheimer's disease (Glenner & Wong, 1984; Masters et al., 1985; Selkoe et al., 1986). Shortly thereafter, researchers confirmed that the neurofibrillary tangles observed in AD consisted of aggregates of aberrantly misfolded tau proteins that were subject to post-translation modifications of hyperphosphorylation (Grundke-Iqbal et al, 1986; Ihara et al., 1986; Kosik et al, 1986). Tau aggregates were also identified in frontotemporal dementia, as initially demonstrated by Spillantini et al. (Spillantini et al., 1997a, Murrell et al., 1997). In 2006, two independent research groups reported the presence of TAR DNA-binding protein 43 (TDP-43) aggregates in the brains of amyotrophic lateral sclerosis (ALS) and frontotemporal dementia patients (Neumann et al., 2006; Arai et al., 2006). Finally, a small subset of FTD patients present with ubiquitin positive, TDP-43 negative inclusions that are identified as FUS protein aggregates coded by *fused in sarcoma* (*FUS*) gene (Neumann et al., 2009).

1.1.1.2 Mitochondrial Dysfunction

Extensive evidence supports the presence of mitochondrial dysmorphology in FTD and AD models. In the FTD model of TDP-43

patient samples, cells exhibit dysmorphic and fragmented mitochondria. Increased TDP-43 expression in mouse models reduces mitochondrial length and density in neurites, whereas loss of TDP-43 leads to an increase in both length and density (Wang et al., 2013; Wang et al., 2019; Onesto et al., 2016). Similarly, in mouse models of *C9ORF72* hexanucleotide repeats, mitochondria lose their cristae formation in the prefrontal cortex, while cultured neurons with FUS mutations display fragmented and shortened mitochondria (Choi et a., 2019; Tradewell et al., 2012; Deng et al., 2015, 2018). Reactive oxygen species (ROS) can cause cellular damage if produced in excess. Mitochondria is the typical site for oxidative stress induced damage (Guo et al., 2013). In neurons from *Drosophila melanogaster*, expression of mutant TDP-43 leads to ROS over-production (Wang et al., 2019). Likewise, in C9-derived patient neurons and fibroblasts exhibit increased ROS production (Lopez-Gonzalez et al., 2016; Onesto et al., 2016).

In AD models, Aβ and tau aggregates are often associated with multiple mitochondrial dysfunctions. In an AD mouse model, synaptic mitochondria displayed impaired respiratory rates, ROS production, membrane potential, and cytochrome C activity. The degree of impairment was observed to correlate with the amount of amyloid-beta (Aβ) plaques (Dragicevic et al., 2010). In human AD brain tissue, mitochondrial fission genes have been shown to be increased whereas mitochondrial fusion genes were downregulated with increased severity of Aβ plaques and hyperphosphorylated tau (Manczak et al., 2011; Manczak and Reddy, 2012). Studies conducted on mouse hippocampal neurons in culture have demonstrated that exposure to Aβ leads to a reduction in mitochondrial length, movement, and axonal transport (Du et al., 2010). Mitochondrial dysfunction in AD is a vast and complex area, and the scope of this discussion has been limited. For further details, please refer to Kalani et al. (2023).

1.1.1.3 Neuroinflammation

Microglia have been implicated in the release of pro-inflammatory cytokines, which can contribute to neurodegeneration, particularly in the context of aging and disease (Norden and Godbout, 2013). This topic will be discussed in greater depth in section, “Neuroinflammation in Neurodegeneration.”

1.1.2 Complex Interplay of Key Players in Neurodegeneration

It is worth noting that the cellular dysfunctions discussed earlier are not standalone phenomena, but rather a complex interplay of interlinked processes that affect each other at various points in disease development. However, deciphering these links across different cell types has been a challenge due to limited tools available. Recent advancements in spatial transcriptomics and proteomics have enabled a more detailed understanding of these dysfunctions at a physiological level, but limitations still exist due to restricted availability of human tissue, and the limitations of mouse model-to-human translation. Therefore, it is imperative to develop easily accessible tools with broad applicability. This thesis will focus on such a tool, namely Biotinylation by Antibody Recognition (BAR), which will be elaborated on in subsequent chapters.

1.2 GWAS Studies

1.2.1 Novel Loci Discoveries in Neurodegeneration

Genome-wide association studies (GWAS) have emerged as crucial tools for determining the risk associated with developing any given disease. Specifically, GWAS aims at detecting associations between common single-nucleotide polymorphisms (SNPs) and a disease of choice (Uffelmann et al., 2021). Many useful applications of this tool have yielded valuable insights into the pathophysiology of numerous diseases, including obesity, Crohn's disease, type 2 diabetes, and autoimmune disorders. Specifically in neurodegeneration, GWAS has facilitated the identification of novel connections, thereby providing a platform to investigate previously unexplored pathways. In the following sections, I will discuss some of these risk genes in the context of FTD and AD.

1.2.2 GWAS in Frontotemporal Dementia

One of the challenges in conducting GWAS is ensuring an adequate sample size. Despite this limitation, current studies have provided valuable insights into FTD even with sample sizes of only a few thousand patients. FTD is associated with three main genetic mutations; chromosome 9 open reading frame 72 (*C9ORF72*), progranulin (*GRN*), and microtubule-associated protein tau (*MAPT*) (Hutton et al., 1998; Baker et al., 2006; Cruts et al., 2006; DeJesus-Hernandez et al., 2011). Therefore, GWAS studies conducted on FTD patients would generally focus on one of these three mutations, with the goal of identifying new gene loci related to these mutations.

To date, six GWAS studies focusing on FTD have identified novel loci some of which include transmembrane protein 106B (*TMEM106B*), member RAS oncogene family (*RAB38*), cathepsin C (*CTSC*), and genes located in the human leukocyte antigen (*HLA*) locus (Van Deerlin et al., 2010; Ferrari et al., 2014). To this end, significant research has linked *TMEM106B* and FTD mechanistically. Most recently, a case report described a patient with behavioral variant of FTD in their 50s who had an asymptomatic parent and sibling that carried the same genetic mutation in *GRN* (Perneel et al., 2023). However, the parent and sibling also carried two alleles of the protective variant of *TMEM106B* whereas the patient was heterozygous. FTD patients can present with protein aggregates of a DNA binding protein, TDP-43, in their neurons. Jiang et al. recently showed that amyloid fibrils in these patients contain aggregates of TMEM106B and not TDP-43 as previously thought (Jiang et al., 2022). *TMEM106B* codes for a protein that localizes to the late endosomal/lysosomal membrane and is upregulated when the lysosomes are deacidified (Lang et al., 2012). In mice, loss of *TMEM106B* leads to increase in lysosomal sizes in the ventral horn of the spinal cord (Feng et al., 2020). A complete loss of progranulin and *TMEM106B* leads to severe motor deficits, increased microgliosis, and astrogliosis, highlighting a clear association between *GRN* and *TMEM106B*.

It is worth emphasizing that genetic loci found in GWAS studies of other neurodegenerative disorders may be applicable to FTD. This is particularly relevant given the limited sample size of GWAS studies in FTD caused by the low incidence of the disease. Therefore, it is crucial to explore potential overlaps in the genetic basis of FTD and other neurodegenerative disorders to enhance the scientific community's understanding of the disease.

1.2.3 GWAS in Alzheimer's Disease

Given the challenges with incorporating large enough sample sizes, AD presents a different concern. It is more prevalent than FTD and therefore larger population sizes can be included, however, AD diagnosis is quite heterogenous clinically. Several GWAS studies have managed to include large samples sizes (in the hundreds of thousands), however, it comes with the caveat of including clinically diagnosed AD, which is not always accurate. This runs the risk of creating an inaccurate GWAS study resulting in hits overlapping between possibly unique pathologies.

One of the largest AD GWAS studies was conducted by Bellenguez et al. incorporating over 85,000 AD cases, however, the majority of these were cases with a clinical diagnosis of AD rather than pathological (Bellenguez et al., 2022). This dataset identified 42 novel gene loci associated with clinically diagnosed dementia in addition to 33 already known loci. Although this dataset may not be specific to AD, it provides potential mechanistic overlap between common neurodegenerative pathologies.

1.2.3.1 FTD and AD Overlap

In the recent study, novel AD risk loci detected included *GRN*, *TMEM106B*, and genes encoding for cathepsins (*CTSB* and *CTSH*) (Bellenguez et al., 2022). These are all lysosomal proteins, implicating lysosomal dysfunction. The *GRN* gene codes for progranulin, a protein that localizes to the lysosome. However, the precise biological function of progranulin remains a topic of growing research (Paushter et al., 2018). Although it is possible these hits are from FTD patients misdiagnosed as AD, recent studies have implicated lysosomal dysfunction in AD (Lee et al., 2022). In this study, the authors show that there is lysosomal blebbing

in neurons of AD mouse models before plaque deposition. Therefore, these hits may hold potential merit.

1.2.3.2 Microglial Genes in AD GWAS

In several GWAS studies, the authors perform single-cell expression enrichment analysis in their dataset which has consistently uncovered microglial expression of their hits as most significant (Jansen et al., 2019; Wightman et al., 2021, Bellenguez et al., 2022). This potentially suggests that microglia expressing these mutations are likely involved in disease manifestation. These genes include *CR1, TREM2, ABI3,* and *GRN*, which have all been shown to be highly expressed by microglia (Satoh et al., 2017; Yeh et al, 2017; Daskoulidou et al., 2023). These findings suggest that microglial dysfunction and inflammation may play a crucial role in the development of AD.

1.3 Frontotemporal Dementia

1.3.1 Incidence, Clinical Features, and Pathology

Frontotemporal dementia is a clinically elusive disease with symptoms that can be easily overlooked, leading to misdiagnoses. Incidence of FTD has been shown to be 0.0 to 0.3 cases per 1000 person-years, accounting for 10.2% of patients with dementia under the age of 65 (Hogan et al., 2016). It is the second most common cause of dementia for patients 65 years and younger (Hodges et al., 2003; Knopman and Roberts, 2011). Patients typically present with a wide array of symptoms ranging from behavioral changes such as disinhibition, apathy, compulsions and hyperorality to changes in language and motor functions

(Olney et al., 2017). These symptoms can be classified into three main forms of FTD: behavioral variant (bvFTD), primary progressive aphasia (PPA) and FTD with motor neuron disease (MND).

1.3.1.1 Subtle Variations in Clinical Manifestations

The clinical features of these three variants are determined by the location of pathology within the brain (**Figure 1-1**). In general, FTD arises from atrophy in the frontal and temporal lobes, which may occur symmetrically or asymmetrically. Patients with bvFTD exhibit symptoms due to atrophy of the paralimbic regions (Rosen et al., 2005; Seeley et al., 2008). Disinhibition results from right orbital frontal cortex involvement, apathy is linked to medial prefrontal lobes and anterior cingulate engagement, compulsive behavior is connected to asymmetrical temporal lobe atrophy, and hyperorality is associated with orbital frontal cortex, right insular cortex, and striatum pathology (Rosso et al., 2001; Tranel et al., 2002; Rankin et al., 2006; Whitwell et al., 2007; Woolley et al., 2007). Over 50% of FTD patients are diagnosed with bvFTD (Johnson et al., 2005).

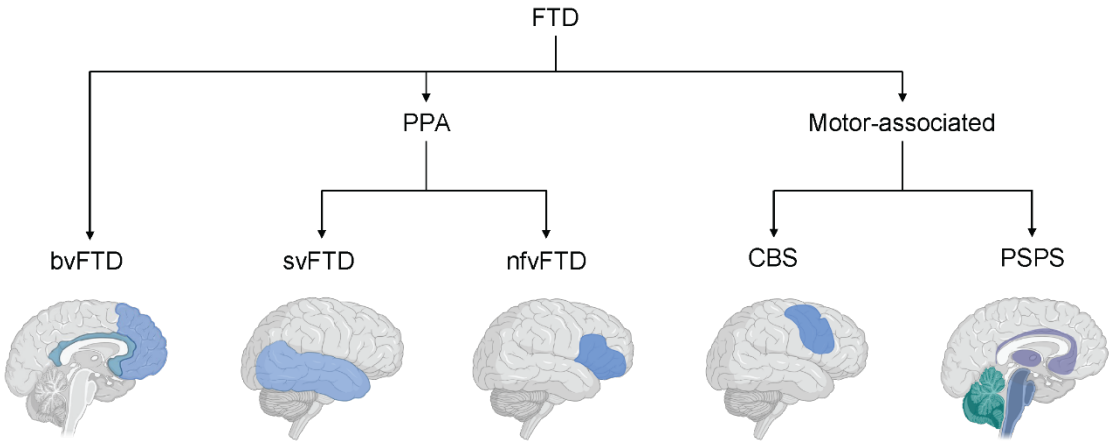

Figure 1-1: Locations of frontotemporal dementia pathologies.

Frontotemporal dementia (FTD) can be divided into 3 main groups: behavioral variant (bvFTD), primary progressive aphasia (PPA) and motor associated. The second arm of the schematic shows how PPA can further be divided into semantic variant (svFTD) and non-fluent variant (nfvFTD). As seen in the right arm of the diagram, there are two types of FTD associated with motor neuron disease (MND): corticobasal syndrome (CBS) and progressive supranuclear palsy syndrome (PSPS). Corresponding affected brain regions for each variant are highlighted in color. Image generated using Biorender.com.

PPA patients primarily experience language-associated disorders (Mesulam, 1982; Mesulam, 1987). These patients can be further divided into two categories: semantic variant (svFTD) and progressive non-fluent variant (nfvFTD). nfvFTD is the second most prevalent form of FTD, accounting for 25% of cases (Johnson et al., 2005), followed by svFTD. Patients with nfvFTD initially present with effortful speech, which declines to complete apraxia of speech or agrammatism. This is due to involvement of the left inferior frontal gyrus and anterior insula (Gorno-Tempini et al., 2004). Semantic variant, on the other hand, can manifest as either a language-based slow loss of semantic knowledge or behavioral changes, depending on which side of the temporal lobe degeneration begins. Left svFTD is language-associated, while right svFTD is behavior-associated (Seeley et al., 2005). While bvFTD presents with behavioral changes such as disinhibition, compulsion, hyperorality, and apathy, right svFTD presents with emotional distance, isolation, irritability, and disturbances in sleep, appetite, and libido (Miller et al., 1993; Edwards-Lee et al., 1997).

FTD that manifests with MND can be further classified into two types: progressive supranuclear palsy syndrome (PSPS) and corticobasal syndrome (CBS) (Olney et al., 2017; Sieben et al., 2012). PSPS is characterized by progressive dementia and extrapyramidal symptoms such as supranuclear ophthalmoplegia, and postural instability (Litvan et al., 1996). This results from involvement of the basal ganglia, and brainstem (Chambers et al., 1999). In contrast, CBS patients develop a

focal cortical deficit and progressive asymmetrical movement disorder (Kertesz et al., 2003). Cognitive dysfunctions manifest in the later stages of the disease in the form of frontotemporal behavioral syndrome although patients do not always present with early motor findings first (Lee et al., 2011). These various manifestations of FTD highlight the diverse range of symptoms and clinical presentations that can make diagnosis challenging. However, understanding the underlying neuroanatomical changes and their associations with specific clinical features can aid in the accurate identification and management of FTD patients.

1.3.1.2 Proteinopathies

The diagnosis of FTD is based on a constellation of symptoms presented by the patient. However, the underlying cause of these symptoms can be traced to molecular pathologies known as proteinopathies, which refer to abnormalities resulting from protein depositions in the brain. The three primary proteins identified in FTD are microtubule-associated protein tau, DNA-binding protein TDP-43, and tumor-associated protein FUS (Hutton et al., 1998; Neumann et al., 2006; Kwiatkowski Jr et al., 2009). Consequently, FTD molecular pathology can be categorized into three main groups based on the predominant protein deposited: FTLD-TDP, FTLD-tau, and FTLD-FUS (Mackenzie et al., 2010). Intriguingly, clinical symptoms are not determined by the specific proteinopathy but rather by the location of protein deposits. This is evident in the observation that nfvFTD typically presents with tau pathology and svFTD with TDP-43 deposits, although the inverse has also been observed (Sieben et al., 2012). In contrast, bvFTD can present with any of the three proteinopathies and lacks a defined neuropathological presentation (Josephs et al., 2011).

FTD-tau was the first discovered proteinopathy, accounting for up to 40% of FTD cases (Young et al., 2018). Among the remaining cases

initially labeled as FTD-U, 80%-95% comprised FTD-TDP, followed by a small percentage of FTD-FUS cases (Mackenzie et al., 2008; Roeber et al., 2008; Sieben et al., 2012). To date, a minor portion of FTD-U inclusions remains unidentified (Sieben et al., 2012). The genes responsible for these proteinopathies are listed in **Table 1-1** (Josephs et al., 2011). Approximately 70% of patients develop sporadic FTD, while 30% inherit the condition (Greaves and Rohrer, 2019). Among the inherited population, the majority of proteinopathies are attributed to TDP-43 inclusion bodies (Greaves and Rohrer, 2019).

Table 1-1: Gene mutations associated with FTD proteinopathies.

Major FTD- associated protein deposits include tau, TDP, FUS and other labeled as FTD-U. Each proteinopathy has a corresponding gene mutation as listed in the table below (Josephs et al., 2011*).*

Proteinopathy	**Associated gene**
FTD-tau	Microtubule associated protein tau (*MAPT*)
FTD-TDP	Progranulin (*GRN*)
	Chromosome 9 open reading frame 72 (*C9ORF72*)
	Valosin containing protein (*VCP*)
	Transactive response DNA binding protein (*TARDBP*)
FTD-FUS	Fused in sarcoma (*FUS*)
FTD-U	Charged multivesicular body protein 2B (*CHMP2B*)

The most common genetic cause of FTD is *C9ORF72*, followed by *GRN* and *MAPT* (Greaves and Rohrer, 2019). *MAPT* was the first identified causal gene mutation for FTD, closely followed by *GRN*, both located on chromosome 17 (Hutton et al., 1998; Spillantini et al., 1998; Baker et al., 2006; Cruts et al., 2006; Lashley et al., 2015).

1.3.2 Models/Tools Available to Study FTD

Currently, the available tools for studying FTD involve genetic mutation models targeting specific genes such as *MAPT, C9ORF72, GRN, VCP, FUS, CHMP2B,* and *TARDBP* (Roberson, 2012). The three most common genetic mutations in FTD are *MAPT, C9ORF72,* and *GRN*, each characterized by different types of mutations. In mouse models of *MAPT* mutations, human *MAPT* genes with the specific mutation are expressed instead of the mouse *MAPT* gene. *C9ORF72* mouse models involve the insertion of hexanucleotide GGGGCC repeat motifs, while *GRN* mouse models simulate the complete loss of function of the *GRN* protein. These mouse models offer the advantage of monitoring early pathological changes and uncovering molecular mechanisms that are difficult to assess in human patients. However, since the primary clinical outcomes of these mutations in patients are related to language and behavioral dysfunctions, it is challenging to assess these aspects in mice. Nonetheless, there are behavioral read-outs in mice that parallel human behavioral phenotypes, such as repetitive grooming for repetitive behaviors, hyperactivity in open field arena, reduced anxiety in various paradigms, and apathy and disinhibition in fear-conditioning paradigms (Ahmed et al., 2017). There are also challenges with these mouse models, such as the lack of phenotype in heterozygous loss of *GRN* models and the absence of TDP-43 aggregate formation in complete *GRN* knock-out models, which do not fully represent the pathophysiology observed in patients (Ahmed et al., 2010). In this thesis, I will discuss the two specific mouse models used.

1.3.2.1 *GRN* KO Mouse Models

GRN codes for the protein progranulin, and over 70 mutations have been identified in this gene that result in loss of function and cause disease through haploinsufficiency of progranulin (Baker et al., 2006;

Cruts et al., 2006; Gass et al., 2012). Majority of these mutations lead to nonsense-mediated decay of the *GRN* mRNA (Baker et al., 2006; Cruts et al., 2006). Others can cause a loss of the protein, entrapment of the protein in an intracellular compartment or inability to be cleaved (Gijselinck et al., 2008; Mukherjee et al., 2008; Shankaran et al., 2008; Wang et al., 2010). All these mutations lead to loss of function and therefore mouse models that are progranulin deficient have been made to study *GRN* associated FTD. Three such lines have been shown to have early social behavior abnormalities without issues with overall health or motor function. These mice exhibit enhanced microgliosis, astrogliosis, and accumulation of ubiquitin-positive autofluorescent lipofuscin. They also exhibit a specific type of neuronal loss in the hippocampus and thalamus (Ahmed et al., 2010). This loss is associated with an increased elimination of synapses by microglia, leading to the loss of neurons in these brain regions (Lui et al., 2016). These features make them valuable tools for studying *GRN*-associated FTD (Kayasuga et al., 2007; Yin et al., 2010a; Yin et al., 2010b; Ahmed et al., 2010; Ghoshal et al., 2012).

1.3.2.2 Induced Pluripotent Stem Cells Derived Neurons

In 2006, a groundbreaking technique was developed that has since proved to be an invaluable tool in biomedical research. Takahashi et al. reported the successful de-differentiation of human somatic cells into induced pluripotent stem cells (iPSC) (Takahashi et al., 2007). This breakthrough has opened up a new avenue of research possibilities for studying human-relevant hypotheses *in vitro*. The generation of human/patient iPSC-derived cortical neurons has been especially useful for investigating various hypotheses related to neurodegeneration. The two cell lines used in this thesis are described below.

1.3.2.2.1 Complete Loss of Progranulin

The Ward Lab at the NIH has created a full *GRN* knock-out model with an insertion at the 7 base-pair locus in one allele and a deletion at the 10 base-pair locus in the other, resulting in the complete absence of progranulin from a healthy male donor fibroblast-derived iPSC line. These lines also contain a stable, doxycycline-inducible neurogenin2 (*NGN2*) cassette integrated into their genome, which enables differentiation into cortical neurons.

1.3.2.2.2 FTLD-Patient Derived Cell Lines

We obtained a patient-derived cell line harboring a mutation in the coding DNA at position 26, resulting in a cytosine to adenine switch and a corresponding substitution of alanine with aspartic acid at position 9 of the protein (c.26 C > A, p.A9D), from Dr. Dimitri Krainc (Valdez et al., 2017), along with its isogenic control. The cell line was donated by a female patient who presented with progressive dysarthria and stuttering at the age of 63 (Wider et al., 2008). The lines were equipped with the *NGN2* cassette, which facilitated their differentiation into cortical neurons. We further modified the isogenic control by employing CRISPR-Cas-9 small guide RNA against *GRN* to generate a complete *GRN* knock-out line (Hasan et al., preprint 2023). Although studies on neurons with progranulin deficiency have not found a direct link to sex-specific dimorphism, there are observed sex-specific differences in progranulin-deficient microglia, leading to sex-specific immune responses where male pathology is more exacerbated than female (Houser et al., 2022; Zhang et al., 2023). Since no significant influence of sex-specific progranulin function in neurons was observed, the use of female patient-derived cell lines was not considered to have a major impact on the data.

1.4 Alzheimer's Disease

1.4.1 Incidence, Clinical Features, and Pathology

Alzheimer's disease, initially identified by Alois Alzheimer, is a progressive neurodegeneration disease and has emerged as the predominant form of dementia. It affects 1 in 3 people over the age of 65, with a prevalence ranging from 5% to 7% in most global regions and affecting over 50 million people in the world currently (Prince et al., 2013; Alzheimer's Association, 2020). The primary risk factor for AD development is aging, followed by a combination of genetic, environmental, and lifestyle factors (Scheltens et al., 2016). Typically, AD patients exhibit memory impairments and executive dysfunction that interfere with daily activities. In contrast, atypical presentations may involve cognitive impairments, such as language or visual difficulties, which manifest before memory deficits (Scheltens et al., 2016). The neuropathology of AD has historically been characterized by the presence of extracellular plaques and intracellular neurofibrillary tangles (NFTs) (Alzheimer, 1907). Over the past century, researchers have made significant progress in understanding the disease's pathophysiology and two primary hypotheses have been proposed. The first is the amyloid cascade hypothesis, which suggests that the accumulation of amyloid-beta (Aβ) peptides in the brain leads to the formation of extracellular amyloid plaques, followed by hyperphosphorylation of tau leading in neurofibrillary tangles, all of which ultimately results in neuronal dysfunction and cell death (Hardy and Allsop, 1991; Hardy and Higgins, 1992; Hardy and Selkoe, 2002). The second hypothesis is the tau hypothesis, which posits that the hyperphosphorylation of tau proteins

results in the formation of neurofibrillary tangles within neurons, leading to neuronal dysfunction and subsequent cell death (Mohandas, 2009).

1.4.1.1 Amyloid Cascade Hypothesis

The amyloid cascade hypothesis has been a central theory in Alzheimer's disease research since it was first introduced by Hardy and Higgins about 3 decades ago (Hardy and Higgins, 1992). This hypothesis proposes that the accumulation of Aβ peptides in the brain is the primary cause of the disease, ultimately leading to neurodegeneration, cognitive decline, and dementia (Hardy and Selkoe, 2002; Selkoe and Hardy, 2016). Aβ peptides are derived from the sequential proteolytic cleavage of amyloid precursor protein (APP) by β- and γ-secretases, producing fragments of varying lengths, with $A\beta_{42}$ being the most amyloidogenic (Zhang et al., 2011).

According to the amyloid cascade hypothesis, the accumulation of $A\beta_{42}$ peptides results in the formation of soluble oligomers and insoluble fibrils, which aggregate into senile plaques (Hardy and Selkoe, 2002). These plaques trigger a cascade of events, including microgliosis, astrogliosis, oxidative injury, and the hyperphosphorylation of tau protein, leading to the formation of neurofibrillary tangles (Hardy and Selkoe, 2002). Collectively, these pathological events disrupt neuronal communication, cause synaptic dysfunction, and ultimately lead to neuronal death and cognitive decline (Hardy and Selkoe, 2002).

Despite the wealth of evidence supporting the amyloid cascade hypothesis, some inconsistencies and challenges remain. There are cases where individuals have high Aβ burden but do not exhibit clinical symptoms of AD, while some clinically diagnosed AD patients have low amyloid burden upon autopsy (Davis et al., 1999; Price et al., 2009; Serrano-Pozo et al., 2014). Additionally, therapeutic approaches targeting

Aβ have not consistently demonstrated clinical efficacy, raising questions about the hypothesis's validity (Morris et al., 2014). However, counterarguments have been made where anti-amyloid therapies show promising results (Wang et al., 2022). Additionally, genetic links between *APP* mutations and development of AD are undeniable and so the amyloid hypothesis continues to hold merit (Selkoe and Hardy, 2016; Bellenguez et al., 2022).

1.4.1.2 Tau Hypothesis

The tau hypothesis is another key theory in AD research, focusing on the role of tau protein in the development and progression of the disease. Tau is a microtubule-associated protein that primarily functions in the stabilization of microtubules within neuronal axons, facilitating the transport of essential molecules and nutrients (Weingarten et al., 1975). In AD, abnormal hyperphosphorylation of tau protein leads to its detachment from microtubules, resulting in the formation of neurofibrillary tangles (NFTs) and the destabilization of the neuronal cytoskeleton (Weingarten et al., 1975; Grundke-Iqbal et al., 1986).

According to the tau hypothesis, the accumulation of hyperphosphorylated tau and NFTs correlates with the severity of cognitive decline in AD patients, as NFTs have been observed to spread through the brain in a pattern that closely mirrors the progression of cognitive symptoms (Braak et al., 1986; Braak and Braak, 1991). Additionally, several genetic mutations and risk factors have been identified in tau that have been linked to several other neurodegenerative disorders. For example, mutations in the MAPT gene, which encodes tau protein, have been linked to various tauopathies, including frontotemporal dementia, and some of these mutations have been shown to increase the propensity of tau to aggregate (Götz et al., 2019).

Although the tau hypothesis suggests that tau pathology is the primary driver of AD, there is still considerable debate in the field. While most studies show that Aβ presences exacerbates tau aggregation, Bright et al. showed that secreted tau leads to neuronal hyperactivity, which in turn leads to Aβ production in primary human cortical neurons (Bright et al., 2015; Vogel et al., 2020; Zhang et al., 2021). Additionally, others have shown that in mouse models with no or decreased levels of tau, Aβ-induced dysfunctions are ameliorated (Roberson et al., 2007). Hence, the relationship between tau and amyloid-beta is complex and not fully understood, implicating that a more interactive relationship between the two proteins exists in the pathogenesis of AD (Ittner and Götz, 2011). Despite these debates, the tau hypothesis continues to provide valuable insights into AD.

1.4.2 Models/Tools Available to Study Alzheimer's disease

1.4.2.1 Mouse Models

There are several mouse models available to study Alzheimer's disease, based on the two pathways discussed above: Aβ and tau. For the purposes of this thesis, only the Aβ models will be briefly covered. Most models are either overexpression or knock-in models of the human *APP* gene carrying mutations, as wildtype mice do not develop plaques or tangles at any point in their lives. Currently, there are numerous mouse models based on *APP* mutations, with 10 of them overexpressing the human *APP* gene with various mutations (Yokoyama et al., 2022). The only *APP* model that expresses the *APP* gene at endogenous levels in the mouse is the $APP^{NL\text{-}G\text{-}F}$. This mouse model carries the humanized Aβ sequence with three mutations - Swedish (KM670/671NL), Arctic (E693G), and Iberian (I716F) - introduced into the endogenous *APP*

mouse gene, which addresses overexpression artifacts (Saito et al., 2014).

1.4.2.2 Advantages of APP^{NLF} Model

In addition to the more aggressive *APP*$^{NL-G-F}$ model, the authors also created a less aggressive *APP*^{NLF} model with two mutations (Saito et al., 2014). The motivation for developing this model was to provide an alternative to overexpression transgenic models. These overexpression issues include the production of other Aβ fragments with biological functions that are overlooked, competition between artificial and endogenous promoters for transcription factors, destruction of the endogenous gene during insertion leading to downstream effects that are mistaken for those of the inserted gene, expression of the inserted gene in cells that do not normally express the endogenous gene, and artifacts arising from overexpressing Aβ and its unknown direct functions. In contrast, the *APP*^{NLF} model addresses these issues and is a more suitable tool to study the effects of Aβ on AD progression without interference from tau pathology. The model harbors mutations that result in elevated levels of $Aβ_{40}$ and $Aβ_{42}$ with an increased $Aβ_{42}/Aβ_{40}$ ratio. Plaque formation begins at around 6 months and increases with age. Given these factors, the *APP*^{NLF} model is a suitable tool for investigating questions related to Aβ biology (Saito et al., 2014).

1.5 Microglia in Disease

Microglia are the primary immune cells of the central nervous system (CNS) derived from primitive myeloid progenitors and play a crucial role in maintaining brain homeostasis (Ginhoux et al., 2010). Microglia have a distinct origin compared to other cells present in the CNS. In mouse

models, it has been demonstrated that microglia originate from prenatal hematopoietic progenitor cells located in the embryonic yolk sac and fetal liver (Alliot et al., 1999; Ginhoux et al., 2010; Ginhoux et al., 2013). They arise from erythromyeloid precursor (EMP) cells, which differentiate into macrophage ancestor populations before migrating into the brain prior to the closure of the blood-brain barrier (BBB) (Kierdorf et al., 2013; Salter and Stevens, 2017). After infiltrating the brain, microglia differentiate into their final state without any further contribution from the blood or bone marrow (Bruttger et al., 2015). Efforts to reproduce the development of microglia by utilizing monocytes derived from bone marrow have been unsuccessful in achieving a mature microglial transcriptome. This supports the notion that microglia's distinct ontogenic lineage from embryonic stages is critical to their function in the brain (De Schepper et al., 2020).

1.5.1 Healthy Microglia and Heterogeneity

In the healthy brain, microglia are distributed throughout the parenchyma, with a higher density in the gray matter than in the white matter. Specifically, they are more densely present in regions such as the hippocampus, olfactory telencephalon, basal ganglia, and substantia nigra, as opposed to fiber tracts, cerebellum, much of the brainstem, thalamus, and hypothalamus (Lawson et al., 1990). Microglia exhibit a highly branched morphology and were initially described to have three major morphological categories: compact cells, longitudinally branched cells, and radially branched cells depending on where they were present in the brain (Perry and Gordon, 1988; Lawson et al., 1990). We now know that microglial morphology results from them constantly surveying their local environment to detect potential threats or changes (Nimmerjahn et al., 2005). In the healthy brain state, microglia contribute to myelin growth

and maintenance, synaptic turnover, and neurogenesis (Wake et al., 2009; Sierra et al., 2010; McNamara et al., 2023). Recent single-cell RNA sequencing studies have revealed a substantial degree of heterogeneity among microglial populations, with distinct subpopulations identified across different brain regions and developmental stages (Hammond et al., 2019). This heterogeneity is likely to play a critical role in the context-specific functions of microglia during both physiological and pathological conditions.

1.5.2 Reactive versus Sensing Microglia

Microglia display a range of functional states depending on the specific signals they receive from their environment. These states fall on a spectrum of phenotypes, ranging from a sensing state where they monitor the cells around them via contact sites, to a reactive state where they release signaling factors and engage in phagocytosis (Town et al., 2005; Nimmerjahn et al., 2005; Davalos et al., 2005; Neumann et al., 2009).

Sensing microglia are characterized by their highly dynamic and ramified long, thin processes, and a very static soma (Nimmerjahn et al., 2005; Davalos et al., 2005). In this state, microglia make constant contacts with neuronal synapses for about 5 minutes per every hour to monitor synaptic activity (Wake et al., 2009). However, majority of neuronal contacts occur between the neuronal cell body and microglial processes, which can persist for 25 minutes to over an hour (Cserép et al., 2020). Any changes in ATP concentrations during this time lead to recruitment of microglial processes. The primary function of sensing microglia is to maintain homeostasis and provide support to neurons in their environment.

Reactive microglia respond to signals such as injury, inflammation, or cell debris (Hanisch and Kettenmann, 2007). They have been shown to express the whole gamut of toll-like receptors (TLRs) 1-9 that can recognize pathogen-associated molecular patterns (PAMP) (Bsibsi et al., 2002; Olson and Miller, 2004). In response to receptor activation, microglia release cytokines such as tumor necrosis factor (TNF-α), Interleukin (IL)-6, and IL-1β, as well as chemokines, reactive oxygen species (ROS), and nitric oxide (NO) (Dalpke et al., 2002; Olson and Miller, 2004; Smith et al., 2012). Downstream effects of these lead to antigen processing and presentation (Rock et al., 2005). Additionally, microglia act as the primary phagocytic cells in the brain, engulfing pathogens, cell debris, and synapses. This response can be modulated by classical complement cascade, cytokine, or chemokine release (Magnus et al., 2001; Butovsky et al., 2006; Schafer et al., 2012; Hong et al., 2016). While other cell types, such as astrocytes and oligodendrocytes, also play the role of phagocytosis by targeting synapses and myelin debris, microglia remain the major players (Galloway et al., 2019). Reactive microglia can be identified by their morphology, which change from highly ramified to compact and amoeboid.

A recent study provided evidence suggesting the existence of a distinct subset of aged microglia with decreased phagocytic abilities and increased production of reactive oxygen species and cytokines, referred to as lipid droplet accumulating microglia or LDAM (Marschallinger et al., 2020). In contrast to other microglia subsets associated with neurodegeneration or activation response, LDAM display a unique transcriptional profile indicating lysosomal dysfunction in aged microglia. These findings may have important implications for our understanding of microglia heterogeneity in aging and neurodegeneration.

In summary, microglia are highly responsive to their environment, and can mount an immune response to various stimuli. Recent studies have highlighted the connection between “sterile” inflammation in neurodegeneration, leading to interest in the role of microglial dysfunction. In the following paragraphs, I will provide a brief overview of how microglial dysfunction is implicated in neurodegeneration with a focus on FTD and AD.

1.5.3 Neuroinflammation in Neurodegeneration

Neuroinflammation can be defined as a type of inflammation in the central nervous system (CNS) that presents with increased production of pro-inflammatory cytokines and chemokines, such as tumor necrosis factor alpha (TNF-α), interleukin-1 beta (IL-1β), and interleukin-6 (IL-6) by reactive microglia and astrocytes responding to injury or infection (Becher et al., 2017). The release of these signaling molecules can lead to downstream effects that can disrupt the blood brain barrier (BBB), activate the complement system, and provide a positive feedback loop for continued inflammation. Typically, initial inflammation responses are protective, however, prolonged inflammation can lead to neuronal damage and cell death. Many neurodegenerative dementias present with neuroinflammation; however, it is unclear which comes first. Microglia have been shown to become primed to respond to insults with an increased pro-inflammatory response as they age (Niraula et al., 2017). In human prefrontal cortex samples, there is an increase in gene expression noted of several pro-inflammatory genes such as *NFKB1, TRAF6, TLR4, IL1R1, TSPO*, and *GFAP* (Primiani et al., 2014). Aged rodent microglia have increased expression of CD45, CD11, and complement components (Godbout et al, 2005; Ritzel et al., 2015). This

enhanced response may contribute to development of neurodegeneration in individuals with genetic predispositions.

In patients with FTD, Lant et al. observed increased levels of non-ramified microglia in the frontal and temporal cortical grey matter when compared to control groups in post-mortem studies (Lant et al., 2014). In their study, Lant et al. stained for CD68, a lysosomal microglial marker of activation, and observed increased CD68 immunoreactivity in FTD brains with microglia presenting as hypertrophied with thick processes. In animal models of progranulin deficiency, Lui et al. observed increased microglial lysosome size, as indicated by CD68 staining in Iba1-positive cells (Lui et al., 2016). They also noted an increase in the number of microglia isolated from progranulin deficient brains compared to wildtype via Fluorescence-activated cell sorting (FACS) sorting. Patients with FTD have protein aggregates of TDP-43 in their cells (Mackenzie et al., 2006; Arai et al., 2006), and microglia have been shown to exacerbate that pathology in progranulin deficiency (Zhang et al., 2020). When progranulin deficient primary neurons were incubated in microglia conditioned media (MCM) from progranulin sufficient and insufficient microglia, TDP-43 aggregation was noted. Specifically, MCM from progranulin deficient microglia resulted in the highest exacerbation of TDP-43 aggregation in progranulin deficient neurons via complement mediated pathways. Progranulin deficient mouse brains have been shown to express increased levels of complement components (Lui et al., 2016; Zhang et al., 2020), which further highlights the role microglia play in neurodegeneration. Overall, these studies suggest that microglial response and lysosomal dysfunction are key features in the pathogenesis of FTD, and that these processes are further exacerbated in the context of progranulin deficiency.

In AD patient brains post-mortem, microglia have been seen clustering around Aβ plaques (McGeer et al., 1987; Cras et al., 1990;

Sasaki et al., 1997). The same has been noted in transgenic mouse models overexpressing *APP* mutations (Stalder et al., 1999; Wegiel et al., 2001). Additionally, Maezawa et al. have shown that Aβ oligomers can induce microglial dysmorphology, and conditioned media from these microglia are sufficient to cause neuronal toxicity (Maezawa et al., 2011). Microglial TLR4 and TLR6 can bind Aβ fibrils via CD36, which results in an inflammatory response by release of reactive oxygen species (ROS) and nitric oxide (NO) (Stewart et al., 2010). Additionally, triggering receptor expressed on myeloid cells 2 (TREM2) is highly expressed in microglia and various TREM2 variants have been linked to risk of developing AD (Guerreiro et al., 2013; Hickman et al., 2013; Jonsson et al., 2013). Tau, the other AD-associated protein that leads to pathology, has been shown to spread via anatomically connected cell contacts (Liu et al., 2012; de Calignon et al., 2012). Microglia have been shown to be part of the perpetrators of this pathological spread of Tau (Maphis et al., 2015). These findings collectively suggest that microglia play a significant role in the pathogenesis of AD.

In summary, many studies have shown that microglia play a crucial role in the pathogenesis of neurodegeneration. Although this section provides only a brief overview, it is clear that microglia are highly reactive cells that can contribute to both the initiation and progression of disease. It is crucial to understand the underlying etiology of microglial contribution and their role in neurodegeneration.

1.5.4 Challenges in Studying Microglia

Despite the growing body of evidence implicating microglia in the pathogenesis of neurodegenerative diseases, several challenges remain in studying these cells. The isolation and culture of microglia from the brain can lead to significant alterations in gene expression profiles and

functional properties, which may not accurately reflect their *in vivo* state (Hammond et al., 2019; Cadiz et al., 2022). Moreover, any manipulation of the CNS tissue can cause damage, which microglia are predisposed to react to, thereby potentially impacting the research inquiry at hand (Stence et al., 2001).

Additionally, it is important to be aware of species-specific differences when studying microglia. Numerous transcriptomic studies conducted on isolated microglia have demonstrated that the gene expression between human and mouse microglia is largely conserved. However, there exist some species-specific differences that distinguish human microglia from their murine counterparts (Gosselin et al., 2017; Galatro et al., 2017). Therefore, studies on microglia from rodent models may not fully recapitulate the human microglial phenotype and function. Considering the above-mentioned challenges, it is crucial to develop methods that allow the study of microglia in their native environment in human brain tissue.

1.6 Aims

This chapter highlights the connections between FTD and AD, including mutations in lysosomal genes and the involvement of microglia in both diseases. As a result, the following aims were established for this thesis.

- Develop/modify a tool to capture *in situ* proteome of microglia in AD and FTD models.
- Given the link to *GRN* mutations associated with AD and FTD, determine progranulin's role in lysosomes of FTD models.

- Determine the dysfunctions associated with microglial proteome *in situ* of FTD and AD models.

Chapter: 2 General Methods

Note: Parts of this chapter are in preprint as: Hasan S*, Fernandopulle MS*, Humble SW*, Frankenfield AM, Li H, Prestil R, Johnson KR, Ryan BJ, Wade-Martins R, Ward ME, Hao L. Multi-modal Proteomic Characterization of Lysosomal Function and Proteostasis in Progranulin-Deficient Neurons. bioRxiv doi: 10.1101/2023.02.24.529955 *equal contribution.

2.1 i^{3}Neurons

The i^{3}Neuron culture is derived from the previously established human inducible pluripotent stem cell (hiPSC) line (Fernandopulle et al. 2018). It has a doxycycline inducible neurogenin2 (NGN2) cassette (Addgene #105840) stably integrated into its genome making it integrated, inducible, and isogenic (i^3). This allows differentiation of the iPSCs, in presence of doxycycline (dox), to glutamatergic cortical neurons (i^{3}Neurons) in 3 days. The hiPSCs were maintained on Matrigel (Corning Incorporated #354277) coated 10cm tissue culture dishes in Essential 8 media (Gibco #A1517001) as previously described (Fernandopulle et al. 2018). Once the cells were differentiated into neurons, they were maintained on poly-L-ornithine (PLO) coated plates in Brainphys medium (StemCellTechnologies #05790) with half media changes every two days. The identity of the cell lines and how they were attained is shown in **Table 2-1**.

Table 2-1: List of human iPSC lines used in this study.

Cell line	Description	Source
WT	WTC 11 line, Healthy 30-year-old Japanese male donor	Coriell Institute #GM25256
***GRN* KO**	WTC11 line with a 7 base pair insertion in one GRN allele and 10 base pair deletion in the other *GRN* allele resulting in complete loss of function	Generated in house
ptMut	FTD patient cell line harboring a heterozygous *GRN* mutation (c.26 C > A, p.A9D)	Dr. Dimitri Krainc[46]
ptWT	Isogenic control line by correcting the *GRN* mutation in ptMut line.	Dr. Dimitri Krainc[46]
ptKO	Complete knock out of *GRN* in ptWT line using CRISPR-Cas9 sgRNA gGTGGCCTTAACAGCAGGGC directed against *GRN*	Generated in house

Control male WTC11 human inducible pluripotent stem cells (hiPSCs) with a single-copy integration of a doxycycline-inducible NGN2 cassette at the AAVS1 locus (Fernandopulle et al., 2018) were used from Coriell to generate a *GRN* KO cell line with a 7 base pair insertion in one *GRN* allele and 10 base pair deletion in the other *GRN* allele resulting in complete loss of function by the lab.

2.2 i^{3}Microglia

The i^{3}Microglia (or iMicroglia) cell line was obtained from Dr. Martin Kampmann's group (Dräger et al., 2022) where iPSCs were integrated with 6 transcription factors to facilitate doxycycline-induced differentiation into iMicroglia: Hematopoietic Transcription Factor PU.1, MAF BZIP Transcription Factor B (MAFB), CCAAT Enhancer Binding Protein Alpha (CEBPα), CCAAT Enhancer Binding Protein Beta (CEBPβ), Interferon Regulatory Factor 5 (IRF5), Interferon Regulatory Factor 8 (IRF8). To induce differentiation, iPSCs were coated on to PLO and Matrigel coated 10cm tissue culture dishes into Essential 8 media (Gibco #A1517001)

containing Chroman1 (MedChem Express #HY-15392) and dox. On day 2 of differentiation, media was changed to Advanced DMEM-F12 (Thermo Scientific #12634028) containing dox, Glutamax (Life Technologies #35050061), IL-34 (PeproTech #200-34-250UG) and GM-CSF (PeproTech #300-03-250UG). On day 4 of differentiation, media was replaced with and maintained on Advanced DMEM-F12 containing dox, Glutamax, IL-34, GM-CSF, M-CSF (PeproTech #300-25-250UG), and TGF-β1 (PeproTech #100-21-250UG) with media changed every 2 days.

2.3 Lysosomal Immunoprecipitation

Lyso-IP protocol was carried out as described previously (Abu-Remaileh et al., 2017) with the following modifications. Prior to starting, 150µl of Pierce magnetic anti-HA beads (Thermo #88836/88837) per sample were rotated at 4°C with 1 ml of KPBS (136 mM KCl, 10 mM KH_2PO_4, pH 7.25 adjusted with KOH) containing 2-5% BSA for 30-45 minutes to reduce nonspecific binding. These beads were washed for a total of 3 times prior to the pull down. Cells were washed 2-3 times with room temperature PBS before released from the plate using forceful pipetting of 10 ml of PBS. After resuspension in 1 ml cold KPBS, cells were gently homogenized with 21 strokes through an isobiotec balch-style cell homogenizer with a 10um ball bearing. After pulldown, samples were resuspended in 100 µl lysis buffer (50 mM HEPES, 50 mM NaCl, 5 mM EDTA, 1% SDS, 1% TritonX, 1% NP-40, 1% Tween 20, 1% deoxycholate, 1% glycerol, 5 mM TCEP). The samples were heated at 60°C for 30 mins at 1000 RPM agitation. The supernatant was then transferred to a new tube for proteomics and the beads were washed with an additional 50µl of lysis buffer. This was added to the tube for proteomics resulting in 150µl of suspension per sample. Once cooled, the samples were incubated in

20 mM iodoacetamide (Sigma-Aldrich #A3221-10VL) for 30 minutes in the dark and then with 10 mM 1,4-Dithiothreitol (Sigma-Aldrich #10708984001) for 15 minutes at room temperature. The samples can be stored at -80°C indefinitely at this step. Routine bottom-up proteomics were conducted for these samples as described below.

2.4 Sample Preparation for Proteomics

Lysates were measured for protein amount using DC Protein Assay (Bio-Rad). Streptavidin magnetic beads (GE Healthcare # 28985799) were used to enrich biotinylated proteins from the lysates after proximity labeling. Beads titration assay was used to determine the optimal amount of streptavidin beads per mg of total input proteins for Lamp1-BAR, Iba1-BAR and P2y12-BAR. Detailed steps for beads titration assay and enrichment of biotinylated proteins are described previously (Frankenfield et al., 2020) and will be covered in Chapter 3. After sample incubated with streptavidin magnetic beads (with optimal beads/protein ratio) overnight at 4°C, four sequential buffers were used to wash the beads to remove non-specific binding proteins (see Chapter 3 for recipes). Each buffer was used twice for the wash with 8 minute rotation. Magnetic beads were then resuspended in 100 µL of 2M urea/50 mM Trish-HCl solution followed by protein reduction and alkylation on beads with 5 mM TCEP, 20 mM IAA, and 5 mM TCEP treatment, subsequently. The supernatant was removed, and magnetic beads were resuspended in 50 mM Tris-HCl buffer for a 16-hr on-beads digestion with Trypsin/Lys-C Mix enzyme (Promega #V5073) at 37°C in a ThermoMixer shaking at 1200 RPM. The amount of enzyme was optimized as previously described with 1 µg of enzyme per 250 µL of streptavidin magnetic beads (Frankenfield et al., 2020). Half the amount of enzyme was added for an additional 3 hours of digestion. Supernatants

were then collected from the magnetic beads. The magnetic beads were washed with 50 µL of 50 mM Tris buffer. Supernatants were combined and quenched with 10% TFA until pH <3. Waters Oasis HLB 96-well extraction plate was used for peptide desalting, followed by SpeedVac drying down and storage at -80°C.

2.5 Liquid Chromatography Coupled to Tandem Mass Spectrometry Analysis

This portion was executed by Dr. Ling Hao at George Washington University and Dr. Yan Li at the NIH. Liquid chromatography coupled to tandem mass spectrometry (LC-MS/MS) analyses were conducted on a Dionex UltiMate3000 nanoLC system coupled with a Thermo Scientific Q-Exactive HFX or a Fusion Lumos mass spectrometer. Dried peptide samples were reconstituted in 10 µL of 2% acetonitrile (ACN), 0.1% formic acid (FA) in LC-MS grade water before injection. Easy-spray PepMap C18 columns (2 µM, 100 Å, 75 µM ×75 cm) were used for peptide separation with an injection volume of 2 µL, flow rate of 0.2 µl/min and column temperature of 60°C. The mobile phase buffer A was 0.1% FA in water, and buffer B was 0.1% FA in ACN. A two-hour gradient was used for proximity labeling proteomics, and a three-hour gradient was used for stable isotope labeling using amino acids in cell culture (SILAC) proteomics. LC-MS/MS analyses were conducted with a top 40 data dependent acquisition with MS range of m/z 400-1500, MS resolution of 120K, isolation window of m/z 1.4, dynamic exclusion of 22.5 s, and collision energy of 30% for higher-energy collisional dissociation (HCD) fragmentation. Automatic gain control (AGC) targets were 1×106 for MS and 2×105 for MS/MS. Maximum injection times were 30 ms for MS and 35 ms for MS/MS.

2.6 Data Analysis

Mass spectrometer data processing was a courtesy of Dr. Ling Hao and Dr. Yan Li. Proteomics raw data was analyzed by Thermo Fisher Proteome Discoverer 2.4 software. For dynamic SILAC proteomic data, MaxQuant (1.6.17.0) software was used for data analysis. Swiss-Prot *Homo sapiens* database was used for i^{3}Neuron data and *Mus musculus* proteome database was used for protein identification with a 1% false discovery rate (FDR) cutoff. MS tolerance was 5 ppm and MS/MS tolerance was 0.01 Da. Fixed modification was cysteine carbamidomethylation, and variable modifications were methionine oxidation of methionine, acetylation of protein N-terminus, and biotin-phenol modification of tyrosine. The sequence of endogenous biotinylated protein (PCCA) was imported onto the Proteome Discoverer software for data normalization to reduce experimental variation based on our previously develop method (Frankenfield et al., 2020). Missing values were replaced with the minimum observed value per sample. Protein intensity was used for quantification after log_2-transformation followed by t-test for statistical analysis. P-values from t-test were corrected for multiple hypothesis testing. For SILAC proteomics in human i^{3}Neurons, raw LC-MS/MS data was analyzed by the MaxQuant software. Swiss-Prot Homo sapiens proteome database was used for protein identification with 1% FDR. Fixed modification was cysteine carbamidomethylation, and variable modifications were methionine oxidation of methionine and acetylation of protein N-terminus. Match between runs were conducted with a 0.7 min match time window. For single time point experiments, peptide level MaxQuant output files were processed with Python to calculate the peptide half-lives using the equation: $t_{1/2} = t_s \times [\ln 2 / \ln (1+\Psi)]$, where t_s represents the sampling time after media switch, and y represents the heavy-to-light abundant ratio of the peptide. Protein level

half-lives were calculated by averaging the half-lives of unique peptides belong to the specific protein. Statistical analysis was conducted with t-test, and multiple half-life datasets were merged by protein accession in Python.

2.7 Fluorescence Imaging

i^{3}Neurons were cultured on PLO-coated iBiDi slides (iBiDi #81506). The cells were fixed in 4% PFA for 10 minutes and then washed very gently with PBS. The cells were incubated in block (1% bovine serum albumin + 0.1% TritonX) for 1 hour at room temperature. Next, they were incubated with primary antibody in block buffer overnight at 4°C. The slides were gently washed with PBS and incubated in secondary antibody for 1 hour at room temperature. Following thorough washes, the slides were imaged. The mouse brain slices were handled as described above and treated to an extra step of incubation with secondary Alexafluors for visualization. All antibodies and their respective applications and dilutions are listed in **Table 2-2**. Confocal images were obtained using a Nikon Eclipse Ti spinning disk confocal microscope at 63X using an oil immersion objective with constant setting between experimental groups and analyzed using ImageJ software.

Table 2-2: Antibodies used for immunostaining.

Application	Antibody	Specifications	Dilutions
i^3Neurons	PGRN	R&D Systems #AF2420	1:1000
i^3Neurons	LAMP1	Developmental Studies Hybridoma Bank #H4A3	1:3000
i^3Neurons	LAMTOR4	Cell Signaling Technology #13140S	1:500
i^3Neurons	HA	Millipore Sigma # 11867423001	1:500
Mouse brain slice	PGRN	R&D Systems #AF2557-SP	1:1000
Mouse brain slice	P2Y12	AnaSpec #AS-55043A	1:3000
Mouse brain slice	IBA1	Wako Chemicals 019-19741	1:3000
Mouse brain slice	LAMP1	Developmental Studies Hybridoma Bank #1D4B	1:5000
Mouse brain slice	Streptavidin Alexa Fluor 488	Jackson Labs #016-540-084	1:1000
Mouse brain slice	Anti-sheep Alexa Flour 647	Thomas Scientific #C839N93	1:1000
Mouse brain slice	Anti-rat Alexa Fluor Rhodamine Red	JacksonLabs # 712-295-153	1:1000
Mouse brain slice	Anti-rabbit Alexa Fluor Rhodamine Red	JacksonLabs # 711-295-152	1:1000
Both	Hoechst	Thermo Scientific #62249	1:10,000
Western blot	LAMP2	Cell Signaling Technology #D5C2P	1:5000
Western blot	CTSD	Proteintech #21327-I-AP	1:5000
Western blot	P70S6K	Cell Signaling Technology #49D7	1:5000
Western blot	Catalase	Proteintech #2126-1-AP	1:5000
Western blot	Calreticulin	Cell Signaling Technology #D8P2K	1:5000
Western blot	Golga1	Cell Signaling Technology #D8P2K	1:5000
Western blot	VDAC	Cell Signaling Technology #D73D12	1:5000

2.8 Statistics

Statistical analyses were conducted using various software packages. GraphPad Prism 9 was utilized for statistical calculations, while Proteome Discoverer 2.4 software and MaxQuant (1.6.17.0) software were employed for specific data analysis tasks including statistics. A significance threshold of $p<0.05$ was applied to determine statistical significance. For the Lyso-IP data analysis, Proteome Discoverer 2.4 software was used with a total of 4 technical replicates (n=4). The Magic Red Assay data analysis involved GraphPad Prism 9, where an unpaired two-tailed t-test was performed on 8 fields of view per 3 replicates (n=3).

The BAR data analysis utilized a combination of Proteome Discoverer 2.4 software, MaxQuant (1.6.17.0) software, and Python. Statistical analysis was performed on 4 biological replicates per genotype (n=4) using t-tests, as indicated. The Dynamic SILAC data analysis involved a t-test performed via Python on 3 technical replicates (n=3). Additionally, p-values obtained from the t-tests were adjusted for multiple hypothesis testing to ensure statistical rigor.

Chapter: 3 Core Method Development: Biotinylation by Antibody Recognition

Note: Parts of this chapter are in preprint as: Hasan S*, Fernandopulle MS*, Humble SW*, Frankenfield AM, Li H, Prestil R, Johnson KR, Ryan BJ, Wade-Martins R, Ward ME, Hao L. Multi-modal Proteomic Characterization of Lysosomal Function and Proteostasis in Progranulin-Deficient Neurons. bioRxiv doi: 10.1101/2023.02.24.529955 *equal contribution.

3.1 Introduction

Traditional methods to study protein-protein interactions involve pulling down proteins of interest using immunoprecipitation, followed by probing for specific interactions using western blots or using unbiased approaches such as mass spectrometry-based proteomics. However, the drawback of this method is that any transient protein-protein interaction that does not involve the protein binding to the protein of interest is not captured, and valuable information is lost.

Three new related technological developments have enabled new methods to characterize protein interactions in living cells, including transient interactions, using peroxidases such as ascorbate peroxidase 2 (APEX2) (Lam et al., 2015), horseradish peroxidases (HRP) (Kotani et al., 2008), or biotin ligases. The fundamental principal underlying all these techniques is to genetically fuse the enzyme to a bait protein and express

it in cells. The enzyme labels proteins in the vicinity by conjugating biotin once activated. The biotinylated proteins can then be visualized or isolated through a pull-down assay against biotin. Examples of biotin ligases include engineered Escherichia coli-derived biotin ligase BirA or BioID (Choi-Rhee et al., 2004; Roux et al., 2012), BioID2 (Kim et al., 2016), biotin ligase derived from Bacillus subtilis (BASU) (Ramanathan et al., 2018), as well as TurboID and miniTurbo (Branon et al., 2018).

The main difference between peroxidases and biotin ligases is in the mechanism of how they create active biotin molecules. Peroxidases react with hydrogen peroxide and phenol biotin to generate biotin radicals that bind to any exposed electron-rich amino acid. On the other hand, biotin ligases use ATP and biotin to produce reactive biotin-5'-AMP that only reacts with free primary amines of exposed lysine residues of proteins in proximity (Mathew et al., 2022). These biotinylated proteins can then be isolated using magnetic streptavidin beads that will form a strong non-covalent bond with the biotin. Upon capture, following on-beads digestion, the biotinylated proteins can then be identified via mass spectrometry.

The various biotinylating enzymes have their own benefits over the other, proving useful for varying questions. APEX is the smallest tag at 27 kDa, whereas HRP is the largest at 44 kDa. BirA falls at 35 kDa, with two most recent variations being 35 kDa (TurboID) and 28 kDa (miniTurboID) (Mathew et al.,2022). Smaller tags have the advantage of being easier to clone into a target protein's end, and they are less likely to interfere with the function of the target protein due to their smaller size. Compared to BirA, APEX labels in a shorter time window (1 minute vs 18-24 hours), however, TurboID variants seem to have faster labelling kinetics than the traditional BirA (Rhee et al., 2013; Branon et al., 2018). This is important for addressing hypotheses that investigate quick or short-lived interactions between proteins. Another key difference between the enzymes is the

nature of biotinylation. Where APEX biotinylates at tyrosine and possibly tryptophan, cysteine, and histidine, BirA/TurboID biotinylates at lysines only. This feature can dictate the sensitivity of mass spectrometry methods depending on which Trypsin is used for digesting the proteins. Trypsin-LysC is a protease that cleaves at lysines only and using this in conjunction with BirA/TurboID would increase the sensitivity of LC-MS/MS detection. HRP, on the other hand, is not as active in the cytosol or other reducing agents but has been shown to work in pulling down biotinylated protein from fixed tissue. APEX and BirA have been useful *in vivo* protein-fragment complementation assays (PCAs) by fusing two proteins of interest to N- or C-terminal BirA* or APEX fragments and expressing them in cells.

However, these advantages come with their disadvantages too. Generating fusion proteins requires using cell lines, which may not be representative of an in-vivo model. Additionally, when working with genetically modified cell lines, adding tags, over-expression of protein of interest, and non-specific biotinylation introduced by the free enzyme due to unforeseen cleavage of the fusion protein, can all result in artifacts. Previous studies have used CHME-5 cells, obtained from embryonic fetal human microglia through transformation with simian virus 40 (SV-40) T antigen, primary pure rodent microglia cultures and Adeno-associated virus (AAV) to introduce tagged APEX in rodent brains, all of which are far from what happens *in vivo* and possibly over activated.

In this thesis, I pursued a recently developed modification of proximity labeling termed Biotinylation by Antibody Recognition (BAR) method, which enables proximity labeling of proteins surrounding bait proteins of interest in fixed tissue from animal models. BAR leverages horseradish peroxidase (HRP) conjugated antibodies that recognize primary antibodies targeting proteins of interest in fixed tissue as shown in **Figure**

3-1 (Bar et al., 2018). Use of BAR to study microglia may have substantial advantages over cellular models, since microglia are known to be reactive to any perturbations, such as physical via fluorescence-activated cell sorting (FACS) or chemical via cytokines (Butovsky et al., 2014; Bohlen et al., 2017; Gosselin et al., 2017). Other benefits of BAR include capturing sub-cellular compartments from cells in their native environment. This method, however, does carry its own caveats. Although it targets a protein of interest, HRP's labeling radius is 200-300nm (Kotani et al., 2008), substantially larger than the labeling radius of APEX (15nm). This is a wide field of coverage, given that the average diameter of a neuronal soma is 10 - 40 μm and microglia have even smaller soma (Nimmerjahn et al., 2005). Therefore, BAR could potentially capture irrelevant hits. In this chapter, I set out to test if this method can be applied to fixed mouse brain slices, optimize the sample preparation, and determine the specificity of this technique of capturing relevant hits to my protein of interest.

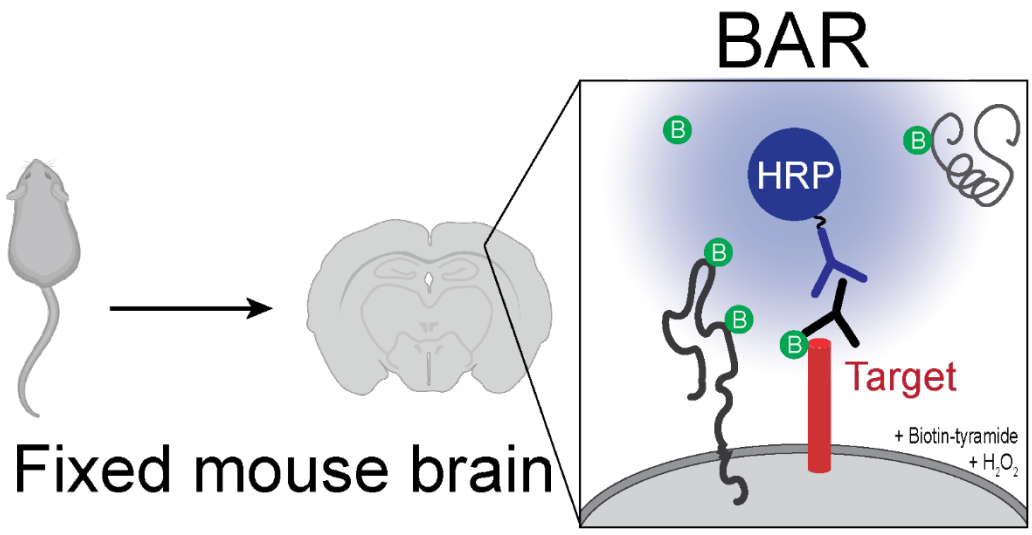

Figure 3-1: Biotinylation by antibody recognition representation.

This figure shows a theoretical transmembrane target protein as the protein of interest. A primary antibody to the target protein binds to it, followed by an HRP-conjugated antibody. This HRP can be activated with H_2O_2 to generate a cloud of biotin radicals that can bind to R chains of amino acids on neighboring peptides. This allows the capture of transiently interacting and proximal proteins. Schematic in not drawn to scale.

3.1.1 Aims

- Determine optimal BAR application to tissue, defining tissue eligibility and staining buffers.
- Assess starting sample size and preparation for mass spectrometry.
- Define a post-mass spectrometry analysis pipeline.

3.2 Protocol A: Optimizing Labeling with Primary Antibodies

In this section of the thesis, I aimed to assess the applicability of the immunostaining technique to fixed brain slices derived from mice. This process entailed several key optimization steps, including tissue preparation, antibody selection, and the determination of appropriate dilution factors and staining buffers. The successful optimization of these parameters is critical to ensuring the reliability and accuracy of the immunostaining procedure for subsequent experiments involving the BAR method on fixed mouse brain slices. By systematically investigating and fine-tuning these elements, I sought to establish a robust and reproducible protocol that can be employed throughout the course of this thesis. The following subsections provide a detailed account of the optimization process, covering the rationale behind the decisions made, the experimental methodologies employed, and the resulting outcomes.

Through this comprehensive analysis, I aimed to demonstrate the suitability of the optimized immunostaining technique for BAR on fixed mouse brain slices and to provide a foundation for future investigations in this area.

3.2.1 Tissue Eligibility

To establish the technique in lab, I first set out to determine tissue eligibility for the BAR method. To this effect, I closely examined the original study by Bar et al. and determined that the authors did not discuss methods of tissue acquisition other than stating National Disease Research Interchange (NDRI) biorepository as the source (Bar et al., 2017). The authors described using primary human skeletal and smooth muscle tissue, and adipose tissue from cadaveric samples without specifying fixation method. I speculated that these were fresh or fixed tissue. The authors also used mouse skeletal tissue and performed routine cardiac paraformaldehyde (PFA) fixation. Given that brain banks typically have fixed human tissue, I explored the fixed tissue avenue further using cardiac PFA perfused mouse brain. The study does not mention how thick the tissue sections need to be for adequate antibody penetration. I used a microtome to generate coronal sections and discovered that slices could be as thin as 35 μm thick before they became difficult to handle but were thin enough to have complete primary antibody penetration. I did note that 10 minutes of hydrogen peroxide (H_2O_2) stimulation was enough to generate biotin signal, but penetration was diminished in the middle of the slice. Bar et al. employed 1 to 7 minutes of stimulation, which did not prove to be adequate in our case. Despite the incomplete penetration, there was enough positive biotin signal colocalized to the primary antibody to ensure adequate sample acquisition. I therefore proceeded with these modifications as follows:

Reagents

1. Isoflurane (1.1%)
2. 16% paraformaldehyde (Invitrogen, # 28906)
3. PBS (Fisher Scientific, # BP39920)
4. Sucrose (Sigma-Aldrich, # S1888-500G)
5. Triton-X (Sigma-Aldrich, # 93443-500ML)
6. Donkey serum (GeneTex, Inc., # GTX73205)
7. 30% H_2O_2 in water (Thomas Scientific, # 7722-84-1)

Materials

8. Conical tubes
9. Paraffin film
10. Dissecting forceps
11. Hemostatic forceps
12. Tissue scissors
13. Fine scissors
14. Syringes (1cc, 50 cc)
15. Butterfly infusion needle
16. Spatula
17. 500 ml beakers
18. 6 well plates
19. Serological pipets
20. Paint brush
21. Pins

<u>Cardiac PFA perfusion and brain extraction</u>

1. Anesthetize mouse using 1.1% isoflurane
2. Pin anesthetized mouse to the operating workstation using dissection pins through the appendages

3. Cut open chest cavity using sharp scissors, starting at the naval and progressing towards the head
4. Expose the heart by cutting through the sternum
5. Gently rip open the pericardium to allow easy access to the heart
6. Inject butterfly needle into the left ventricle, careful not to go through the septum
7. Make an incision at the base of the right atrium
8. Perfuse 30 ml of PBS to clear out blood through the vessels
9. Perfuse 60 ml of 4% PFA until the liver and lungs clear
10. Separate head from body using large scissors
11. Cut across the nose bridge through the bone and cut off the skin to expose the skull
12. Starting from the back of the head, cut the skull through the midline to the cut nose bridge, ensuring the round end of the scissors are pointing towards the soft tissue while maintaining pressure upwards to avoid injuring the brain
13. Carefully evert the skull flaps laterally to expose the brain
14. Gently lift the brain off the base of the skull and drop into 4% PFA in a conical tube
15. Leave on rotator overnight at 4°C
16. Switch to 30% sucrose in PBS after 24 hours and leave on rotator overnight at 4°C
17. The brains can be stored at 4°C in 30% sucrose until ready to be sectioned
18. Use a microtome to generate 35 μm thick coronal slices of the whole brain and place in cryoprotectant in 6 well dishes
19. These can be stored at -30°C until ready for use

Immunohistochemistry

22. Take 21 coronal brain slices evenly through the brain per animal. Use 4 biological replicates per group
23. Wash the slices in PBS thrice to remove cryoprotectant
24. Quench endogenous peroxidases by incubating the slices in 0.3% H_2O_2 in PBS for 30 minutes
25. Wash thoroughly with PBS thrice
26. Permeabilize and block using 3% donkey serum and 0.25% Triton-X in PBS for 1 hour
27. Incubate with primary antibody in block buffer overnight on a rocker at 4°C

3.2.2 Antibody Eligibility

An essential aspect of immunostaining techniques is the utilization of high-quality antibodies that consistently yield reliable results. Antibodies must be highly specific, targeting only the intended antigen without cross-reacting with other proteins. This specificity is necessary for the success of the BAR method to ensure that the observed staining pattern for biotinylated proteins via streptavidin staining is an accurate representation of distribution of the target protein. A non-specific or "noisy" antibody may bind to multiple unrelated proteins, leading to false-positive signals. These artifacts can significantly impact data interpretation, making it challenging to draw accurate conclusions about the target protein's interactors or proximal microenvironment. Therefore, selecting a well-validated and highly specific antibody is crucial for obtaining clean and reliable BAR results.

To identify and employ an appropriate antibody, it is typical to test various antibodies against the target protein and optimize the staining

protocol by adjusting factors such as antibody dilution, incubation time, and blocking buffer composition. This optimization process minimizes background noise and maximizes signal-to-noise ratio, ensuring that the antibody staining reflects the true distribution of the target protein in the sample. This thesis focuses on investigating the lysosome and microglial interactomes, which will be further elaborated in the subsequent chapters. A typical marker for lysosomes is the lysosome associated membrane protein 1 (Lamp1) that is highly conserved (Chen et al., 1985). Progranulin, glycoprotein, has been shown to be trafficked to the lysosome, and its loss results in a lysosomal storage disorder called neuronal ceroid lipofuscinosis (NCL) (Hu et al., 2010; Smith et al., 2012). Microglial cell membranes are abundant in GTP-binding protein (G-protein)-coupled P2 receptors, and these cells specifically respond to adenosine tri-phosphate and adenosine di-phosphate (ATP/ADP) via these receptors (Honda et al., 2001; Inoue, 2002). One such receptor is the P2y12 receptor, sometimes referred to as P2ry12. Therefore, for this BAR method, I tested Lamp1, Pgrn, and P2y12 as target proteins. The results show that these three antibodies are highly specific for their targets, and the streptavidin stain displays remarkable colocalization with the primary stain (**Figure 3-2**). This is important for the success of the BAR method because we relied on biotinylated proteins being close to the target of interest. The following protocol was then established.

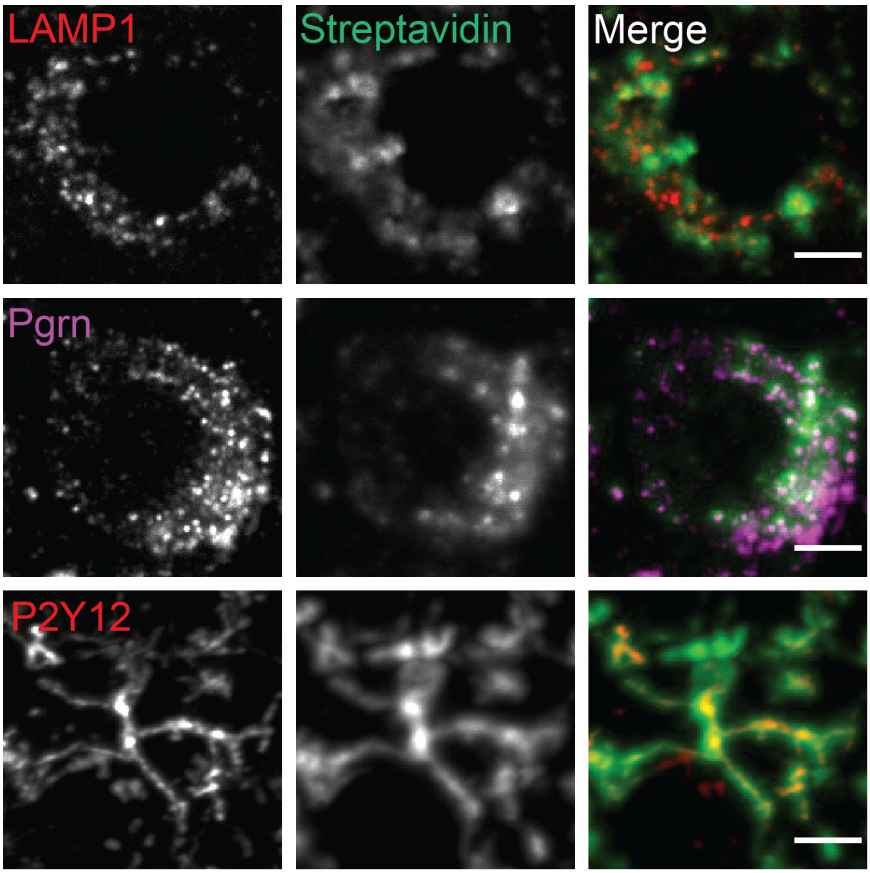

Figure 3-2: Antibodies for LAMP1, PGRN and P2Y12 are highly specific.

These are representative confocal images of successful primary stains on 6-month-old wildtype mouse brain. The top two rows represent neurons. The last row represents microglia. There is complete colocalization of biotinylated proteins represented in the streptavidin stain. Scale bar is 10 μm.

Reagents

- Tween 20 (Bio Rad, # 1706531)
- PBS (Fisher Scientific, # BP39920)
- Phenol-biotin (AdipoGen, # CDX-B0270-M500)
- 30% H_2O_2 in water (Thomas Scientific, # 7722-84-1)
- Sodium azide (Sigma-Aldrich, # S8032-100G)
- Sodium ascorbate (Millipore-Sigma, # A4034-500G)

- PrLong Gold Antifade Mountant (Thermo Fisher, # P10144)

Materials

- 6 well plates
- Conical tubes
- Paint brush
- Timer
- Glass slides
- Coverslips

BAR Application

28. After overnight incubation with the primary antibody, wash the slices thoroughly at room temperature with PBST (PBS + 0.1% Tween20) thrice
29. Incubate wit HRP-conjugated secondary for 1 hour at room temperature on the rocker
30. Wash with PBST thrice for 30 minutes each time at room temperature on the rocker
31. Incubate the slices in phenol-biotin for 1 hour on the rocker and room temperature
32. Activate the HRP using 0.003% H_2O_2 in PBS for 10 minutes at room temperature on the rocker
33. Stop the reaction using quench buffer (sodium azide and sodium ascorbate in water) for 5 minutes
34. Wash with PBST thrice
35. Take one slice per group and incubate in streptavidin AlexaFluor and AlexaFluor against the primary antibody for 1 hour at room temperature on the rocker
36. Wash off using PBS thrice
37. Mount the slice on a slide and let it dry

38. Rinse off the salts and apply mounting media and cover with coverslip
39. Let cure overnight before imaging

3.2.3 Staining Buffers

In this section, I received significant assistance from Maia Parsadanian, who utilized her extensive experience in immunostaining to devise the blocking buffers I ultimately used. The buffers comprised 3% donkey serum and 0.25% Triton-X in PBS. Additionally, Maia determined that 0.3% H_2O_2 effectively quenched endogenous peroxidases, while 0.003% H_2O_2 was sufficient for activating HRP-bound secondary antibodies.

3.3 Protocol B: Optimizing Labeling Radius

In my efforts to reduce the labeling radius, I experimented with incubating the samples in various concentrations of fetal bovine serum (FBS) in the stimulation buffer. The underlying rationale for this approach was based on the fact that the rate of biotin radical production follows a Gaussian distribution. Consequently, there would be a higher concentration of biotin radicals closer to the source point than further away. By introducing a high concentration of FBS in the reaction, the biotinylated proteins located further from the target site would preferentially be washed away, while proteins in close proximity to the target site would be more abundantly labeled due to the lower ratio of FBS to these true interaction partners. This method aimed to refine the labeling

process, allowing for a more accurate identification of proteins in close proximity to the target site.

3.3.1 Serum vs. No Serum

As an initial attempt, I compared a full serum buffer using 100% FBS to a buffer without FBS, using 100% phosphate-buffered saline (PBS). The protocol was followed as described until the stimulation step. For HRP activation, the buffers used were either 0.003% H_2O_2 in PBS or 0.003% H_2O_2 in FBS. The quench and following steps were performed as described above. Using confocal imaging, I observed no discernible difference between the two conditions in either the staining pattern or intensity (**Figure 3**). To further investigate any potential differences in the labeling radius that might not be immediately apparent, I generated line graphs from the representative images. Overall, the analysis revealed that the presence of FBS brought the pixel intensity of the streptavidin channel closer to the channel for P2y12, but it did not affect the labeling radius (**Figure 4**). This lack of effect on the labeling radius is likely due to a consistent ratio of cross-linked proteins to FBS being biotinylated, which results in a decrease in the overall signal of biotinylated proteins without altering the radius.

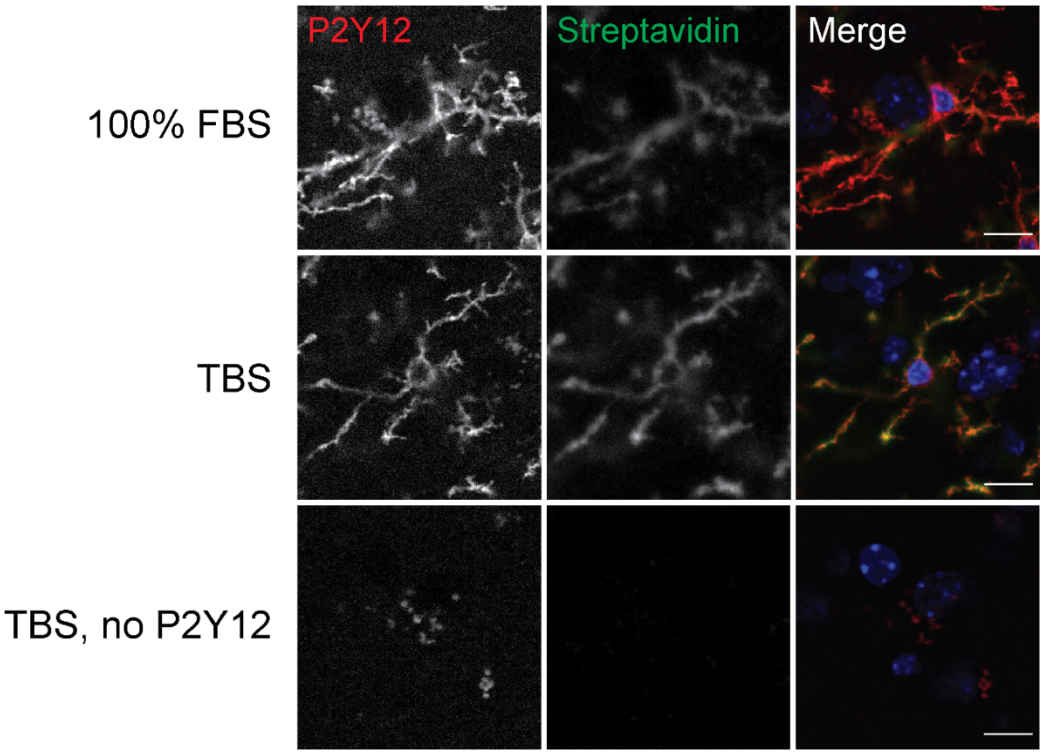

Figure 3-3: No difference exists between 100% FBS and 0% FBS buffer.

These are representative images of microglia from each staining condition. The last row is a negative control showing no streptavidin stain in the absence of the primary antibody. Scale bar is 10 μm.

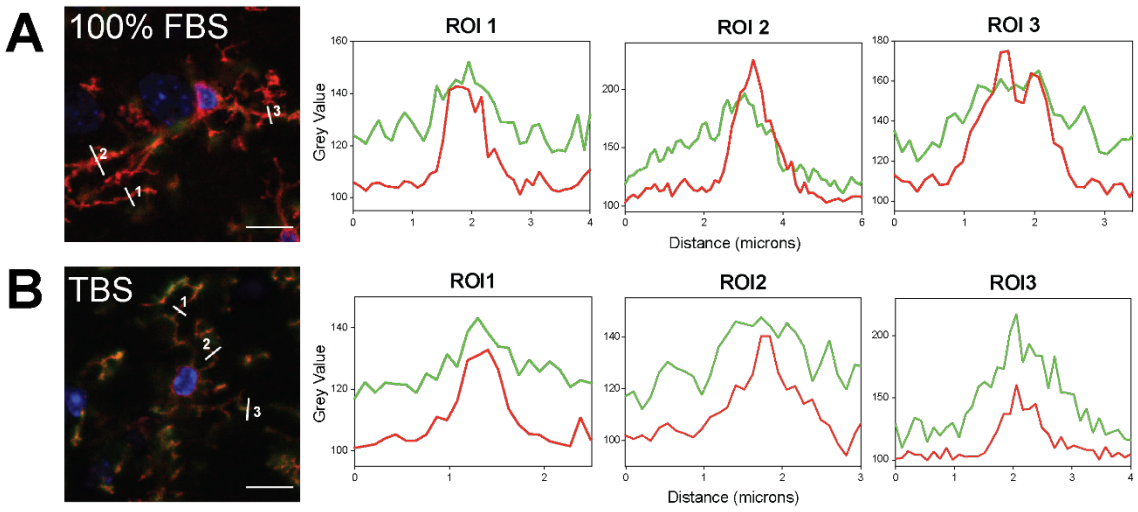

Figure 3-4: FBS buffer does not decrease the labeling radius.

Line graphs were generated using intensity plots over known distances. Each region of interest (ROI) was plotted separately, and corresponding lines are shown in the merge images. The red and green lines represent P2Y12 and streptavidin stain respectively. (A) This panel represents the 100% FBS condition. The streptavidin intensity closely follows the P2Y12 intensity. (B) This panel represents the 0% serum condition. Unlike the last panel, the streptavidin pixel intensities are higher than P2Y12 but are clearly colocalized. Scale bar 10 μm.

3.3.2 Ratio of Serum to Staining Buffers

Given the observation that a full serum buffer reduced the staining intensity of streptavidin, I focused on finding the ideal serum concentration next. My aim was to identify a concentration that could effectively reduce background noise while still allow the detection of relevant biotinylated proteins. To this end, I sought to investigate whether incorporating a certain amount of serum into the stimulation buffer could yield any benefits in terms of staining quality and specificity. To explore this, I tested four stimulation buffers containing increasing serum percentages: 1%, 5%, 10%, and 50% (all in 0.003% H_2O_2 and PBS). Interestingly, buffers with

serum exhibited higher streptavidin intensity compared to the no-serum condition (**Figure3-5**). The highest intensity was observed with 1% serum, followed by 50%, 5%, and 10%. This finding was unexpected. However, since adding serum did not alter the labeling radius in the 100% serum condition, I decided to include a small amount of serum (1%) in my subsequent experiments as a precautionary measure.

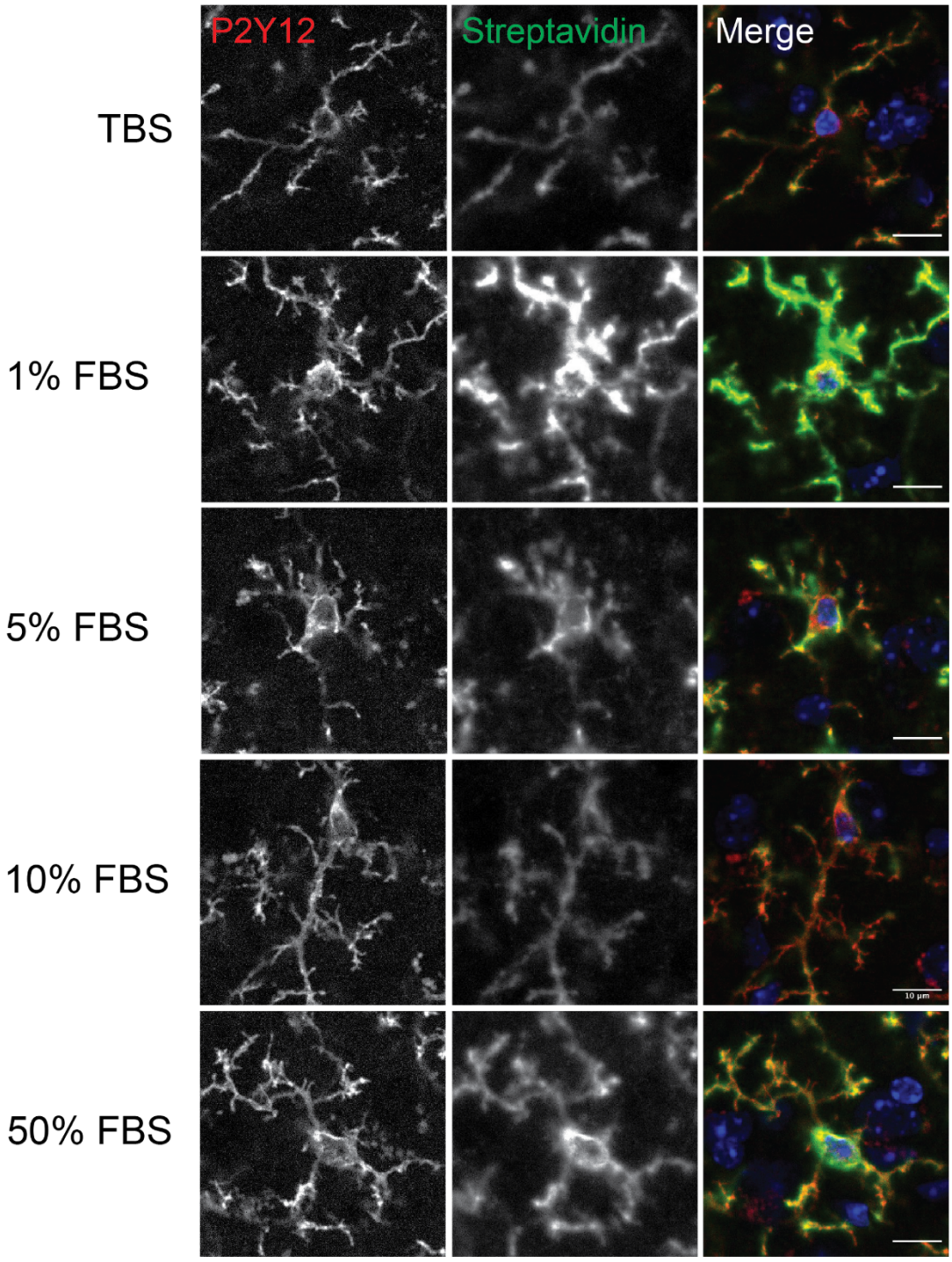

Figure 3-5: Varying percentages of serum yield inconclusive results.

Representative images of P2Y12-BAR on 6-month-old wildtype mouse brain. Highest streptavidin stain is seen with 1% FBS buffer, followed by 50%, 5% and 10% FBS buffer. P2Y12 stain is consistent between the different groups. Scale bar 10 μm.

3.4 Protocol C: Optimizing Lysate and Streptavidin Beads Titration

3.4.1 PFA De-Crosslinking and Protein Quantification

With the staining process optimized, the next challenge was to determine how to de-crosslink the bonds in fixed tissue. This step is necessary to release the biotinylated proteins into solution for mass spectrometry analysis. I modified the lysis buffer used by Bar et al. and changed the detergent concentrations to 3% sodium dodecyl sulfate (SDS) and 2% sodium deoxycholate in phosphate-buffered saline solution with a low-concentration detergent solution (PBST). Bar et al. had used 2% of SDS and 1.33% of sodium deoxycholate in PBST (Bar et al., 2017). With no clear instructions from the primary paper, I utilized 150 µl of lysis buffer for every 20 brain tissue slices. I heated the samples at 99°C for 1 hour while shaking to initiate the physical tissue breakdown. Subsequently, I applied high-power sonication at 4°C with 1 amp pulses (40 seconds on, 40 seconds off) for 15 minutes. The final step involved heating the samples once more for 30 minutes at 99°C. If the tissue had not fully dissociated, I repeated the sonication and heating steps.

After the tissue was dissolved into the solution, I centrifuged the samples at 18,000 RCF at 4°C and collected the supernatant on ice. I then used a Detergent Compatible Protein Assay (DCA) to determine the

protein content in each sample following boiling and sonication. The samples can then be frozen and stored at -80°C until the subsequent step.

3.4.2 Generating Dot Blot Assay

Upon de-crosslinking and quantifying the samples, the biotinylated proteins can be isolated using magnetic streptavidin beads. Since non-specific interactions with beads increases with an increase in the volume of beads used for the pull-down, it is crucial to perform a bead titration assay to identify the minimum volume of bead slurry required to effectively pull down all biotinylated proteins in the sample. Under the guidance and mentorship of Dr. Ling Hao, I developed a dot blot assay for the BAR method.

For the bead titration assay, magnetic streptavidin beads in varying volumes were incubated with 40 µg of protein lysates overnight at 4°C on a rotator. The different volumes tested included 0 µl, 0.5 µl, 1 µl, 2 µl, 5 µl, 10 µl, 15 µl, and 20 µl. Following a maximum of 16-hour incubation, 2 µl of supernatant from the bead and lysate mixture was blotted onto a nitrocellulose membrane after magnetizing and immobilizing the beads. After the membrane dried, it was blocked in Odyssey blocking buffer for 1 hour at room temperature on a rocker. The membrane was then washed thoroughly with tris buffered saline containing 0.1% Tween-20 (TBST) and incubated with streptavidin AlexaFluor for 1 hour. After another thorough wash, the membrane was imaged using the Li-Cor system.

The presented dot blot is an example from 6-month-old *GRN*$^{+/+}$ and *GRN*$^{-/-}$ mice using Lamp1 and Pgrn as targets. The increasing intensity of the blot indicates a decrease in bound biotinylated proteins to magnetic streptavidin beads (**Figure 3-6**). The no primary rows have fewer biotinylated proteins as expected.

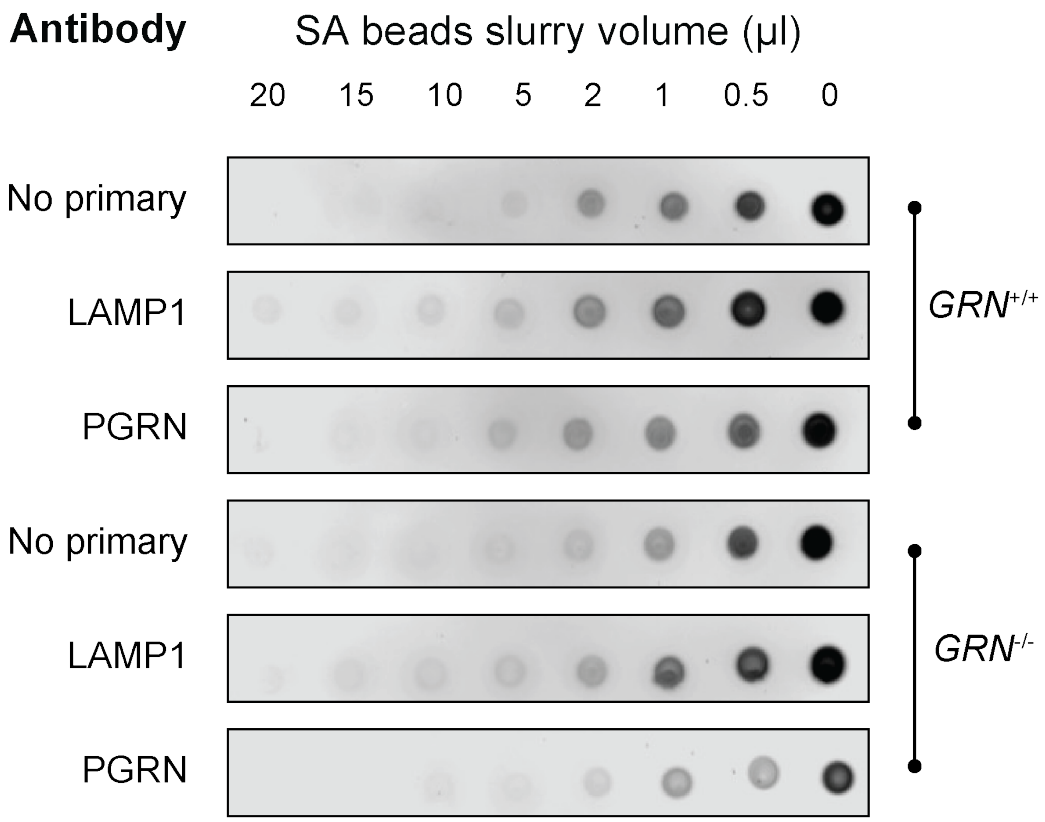

Figure 3-6: Dot Blot assay for BAR-treated lysates.

LAMP1-BAR and PGRN-BAR was performed on 6-month-old wildtype and *GRN*$^{-/-}$ mouse brain and lysates from these experiments were used for this dot blot assay. Samples of 40 µg of protein lysate were incubated with 0, 0.5, 1, 2, 5, 10, 15 and 20 µl of beads slurry overnight and 2 µl of the supernatant was blotted. Supernatant incubated with no beads had the highest intensity of streptavidin stain, whereas 20 µl of beads quenched the signal.

3.4.3 Analyzing Dot Blot Assay

After imaging the dot blot, it can be utilized to estimate the minimum volume of bead slurry needed for a complete protein pull-down. This is achieved by recording the intensities of each dot on the blot and plotting them on a graph using Excel, as demonstrated in **Figure 3-7**. By analyzing these graphs, we can determine the point at which adding more bead

slurry does not yield any further benefits. Most samples' biotinylated proteins can be fully captured by 10 μl of beads slurry for every 40 μg of protein loaded as can be seen in this example plot. Upon completion of the bead titration, the subsequent mass spectrometry sample preparation steps can be carried out to isolate the biotinylated proteins of interest.

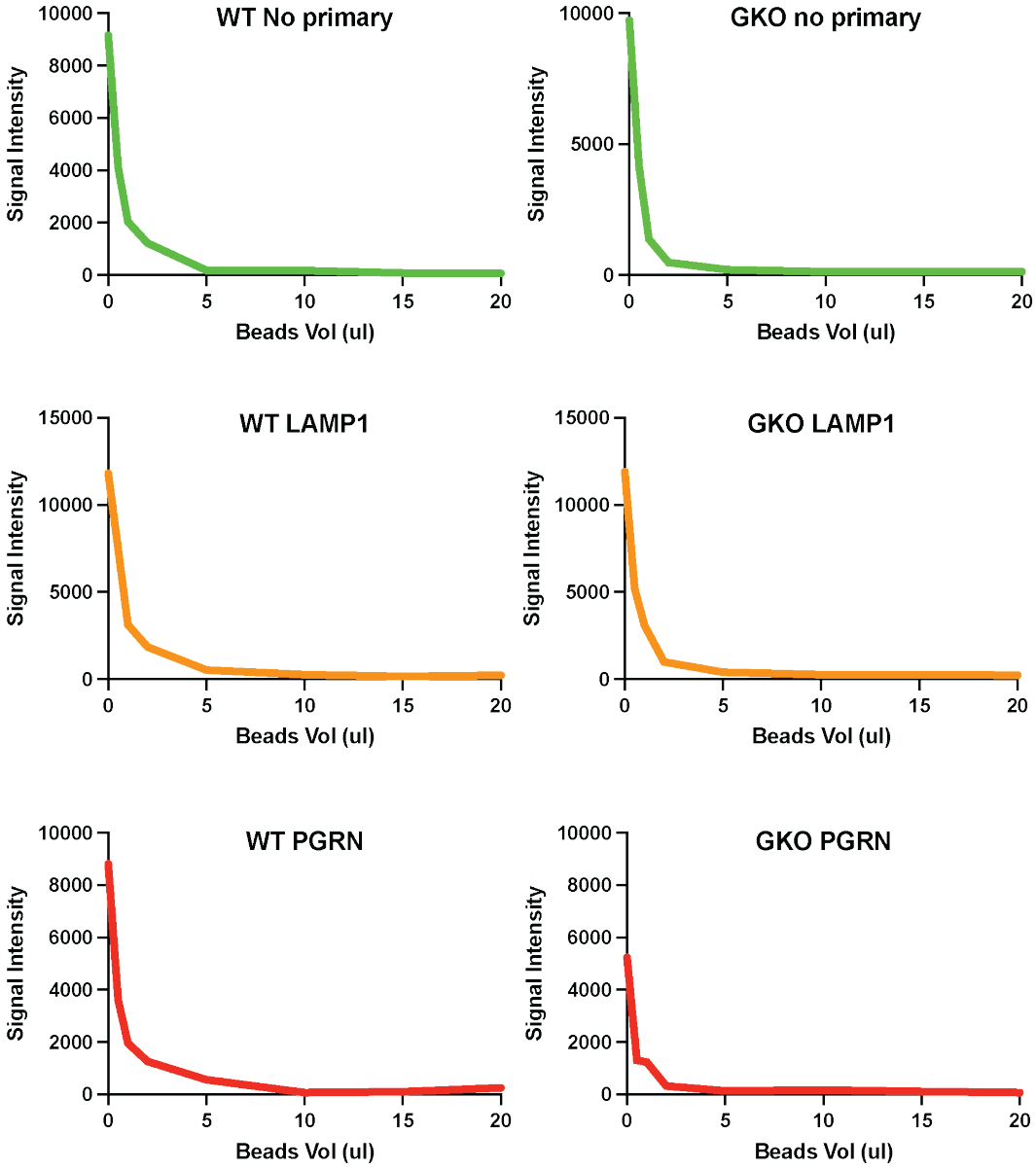

Figure 3-7: Intensity plots for dot blots from LAMP1-BAR and PGRN-BAR using wildtype and *GRN*$^{-/-}$ mouse brain.

Each biological replicate (4 per group) was pooled into one sample. Pixel intensity was recorded for each sample blot and graphed in excel to generate these graphs. Each graph represents pooled

samples for the respective group. All plots hit saturation of beads at 10 μl of beads slurry for 40 μg of protein loaded.

3.5 Mass Spectrometry Sample Preparation

The preparation of samples for mass spectrometry is a well-established procedure. To process the BAR samples, I utilized the following protocol.

Reagents

- PBS (Fisher Scientific, # BP39920)
- Streptavidin magnetic beads (Cytiva, # 28-9857-99)
- Lysis buffer (3% SDS + 2% sodium deoxycholate in PBST)
- Wash buffer 2 (50mM Tris-HCl, 500mM NaCl, 0.1% deoxycholic acid, 1% Triton-X, 1mM EDTA)
- Wash buffer 3 (10mM Tris-HCl, 250mM NaCl, 0.5% deoxycholic acid, 0.5% NP-40, 1mM EDTA)
- TCEP (Sigma-Aldrich, # 75259-1G)
- Iodoacetamide (IAA) (Sigma-Aldrich, # A3221-10VL)
- 10% SDS (Invitrogen, # 24730020)
- Sodium deoxycholate (Sigma-Aldrich, # 302-95-4)
- 1 M Tris-HCl (Fisher Scientific, # 15568025)
- 8M Urea (Fisher Scientific, # U15500)
- 5M NaCl (Fisher Scientific, # 24740011)
- 0.5M EDTA (Life Technologies, # 15575020)
- NP-40 (Fisher Scientific, # 28324)
- Deoxycholic acid (Sigma-Aldrich, # D2510-500G)

- Triton X-100 (Sigma-Aldrich, # 93443-500ML)
- Trypsin LysC (Promega Corporation, # V5073)
- 10% Trifluoroacetic acid (TFA) (Millipore Sigma, # 76-05-1)
- Methanol (MeOH) (Fisher Scientific, # A4524)

Materials

- Magnetic rack
- Lo-Bind tubes
- Heating block
- Rotators
- pH reading strip
- Oasis HLB 96-well Plate 30um (5mg) [Neta Scientific Inc, WAT-186000309]

Bitiotinylated Protein Pull-Down

1. Based on the bead titration assay, determine beads slurry volume to use. For most BAR experiments, 100-150 μl of beads slurry was used.
2. Wash beads thoroughly with lysis buffer to remove ethanol from beads storage solution.
3. Based on DCA, calculate amount volume of each sample needed for a pre-determined amount of protein. For most BAR-experiments, 300-400 μg of protein was loaded on to 100-150 μl of beads slurry.
4. Load samples to beads in Lo-Bind tubes and incubate overnight at 4°C on a rotator.
5. Do not let it incubate longer than 16 hours.

6. Wash bead-bound samples with wash buffer 1 (diluted lysis buffer) using a magnetic rack twice for 8 minutes each at room temperature on a rotator.
7. Wash twice with buffer 2 (50mM Tris-HCl, 500mM NaCl, 0.1% deoxycholic acid, 1% Triton-X, 1mM EDTA) using a magnetic rack for 8 mins in the cold room on a rotator.
8. Repeat wash steps in the same manner as previous step with wash buffer 3 (10mM Tris-HCl, 250mM NaCl, 0.5% deoxycholic acid, 0.5% NP-40, 1mM EDTA) twice.
9. For the final two washes, use buffer 4 (2M Urea, 250mM NaCl, 50mM Tris-HCl) on the rotator in the cold room.

On-Beads Digestion

1. Wash the beads in 2M urea/50mM Tris-HCl solution and resuspend in 100 μl of urea/Tris-HCl buffer.
2. Add TCEP to a final concentration of 5mM and incubate at 37°C for 30 minutes on a shaker.
3. Add IAA to a final concentration of 20mM and incubate in the dark at room temperature on a shaker
4. IAA needs to be made fresh before each use
5. Add TCEP to a final concentration of 5mM again to quench IAA and incubate at room temperature for 10 minutes on a shaker
6. Add 50mM Tris-HCl to dilute the urea concentration to less than 1M.
7. Add 3 μg of Trypsin LysC for every 1mg of protein loaded before pull-down and incubate overnight at 37°C on a shaker.
8. Do not incubate longer than 16 hours.
9. Add an additional 1 μg of Trypsin LysC to the samples and incubate for an additional 2 hours at 37°C while shaking.

10. Collect supernatant into clean Lo-Bind tubes and wash the beads with 50 μl of 50mM Tris-HCl and add it to the collected supernatant.
11. Quench Trypsin LysC by adding 10% TFA till pH falls below 2.

Reverse Phase SPE Column Clean-Up

1. Using Oasis HLB 96-well Plate, wet the column with 200 μl of 100% MeOH.
2. Equilibrate the columns with 200 μl of 1% TFA in water twice.
3. Load the digested samples on to the columns.
4. Wash the samples with 200 μl of 1% TFA, 5% MeOH, in water twice.
5. Finally, elute using 200 μl of 1% TFA, 80% MeOH, in water.
6. Transfer the eluate to Lo-Bind tubes for drying using a speed vacuum centrifuge.
7. Resuspend dried samples in 2% ACN/0.1% FA for LC-MS/MS.

3.6 Analysis

Mass spectrometry-based proteomics has emerged as a powerful tool for the large-scale identification and quantification of proteins in complex biological samples (Aebersold & Mann, 2003). The raw data generated by mass spectrometers are typically composed of thousands of spectra, each representing a unique peptide ion from the analyzed sample. To transform this complex data into biologically meaningful information, it is necessary

to apply sophisticated computational analysis methods (Eng, McCormack, & Yates III, 1994). In this regard, several software platforms have been developed, such as Proteome Discoverer and MaxQuant software, which enable the identification of peptides and proteins, as well as their quantification, by processing the raw mass spectrometry data (Cox & Mann, 2008). This section will provide an overview of these two widely used tools, discussing their respective strengths, limitations, and the databases they utilize for protein identification.

3.6.1 Use of Proteome Discover Over MaxQuant

Proteome Discoverer and MaxQuant are two widely used software platforms for mass spectrometry (MS)-based proteomics data analysis. Both platforms offer a range of features for processing and analyzing proteomics data, but they also have their respective advantages and limitations.

Proteome Discoverer is a comprehensive software suite developed by Thermo Fisher Scientific, which allows users to perform a variety of tasks, including protein identification, quantification, and post-translational modification analysis. One of the main strengths of Proteome Discoverer is its flexibility, as it supports a wide range of mass spectrometers from different manufacturers and can be easily customized using various algorithms and workflows. Additionally, Proteome Discoverer offers a user-friendly graphical interface, which can be particularly helpful for researchers who are new to proteomics data analysis (Thermo Fisher Scientific, Proteome Discoverer Software webpage).

MaxQuant is another popular software platform for proteomics data analysis, specifically designed for high-resolution MS data

(maxquant.org). Developed by the Max Planck Institute of Biochemistry, MaxQuant is particularly well-suited for isotope clusters and stable isotope labeling using amino acids in cell culture (SILAC) peptide pairs due to its advanced algorithms and computational efficiency (Cox & Mann, 2008). One notable feature of MaxQuant is its built-in support for label-free quantification (MaxLFQ) that is compatible with any peptide or protein separation prior to LC-MS analysis (Cox et al., 2014). Furthermore, MaxQuant offers an integrated statistical framework, Perseus, for downstream data analysis and visualization (maxquant.org).

When comparing Proteome Discoverer and MaxQuant, there are several key differences to consider. Zhao et al. determined that MaxQuant in MaxLFQ mode was more accurate and precise in whole proteome and low abundance proteome quantification when compared to 7 other commonly used label-free quantification methods. However, Proteome Discoverer using SEQUEST as a search engine outperformed for quantifying low abundance proteomes with exceptional coverage (Zhao et al., 2020).

Subsequently, Palomba et al. showed that in their comparative study, Proteome Discoverer was superior to MaxQuant for quantification yield, dynamic range, and reproducibility, yet MaxQuant yielded slightly higher specificity, accuracy, and precision values (Palomba et al., 2021). Although Proteome Discoverer was most accurate in estimating the abundance ratio between groups with high sensitivity for narrow abundance ratios. The choice between the two platforms may depend on the specific requirements of a given project and the experience of the researchers involved. For this thesis, both programs were used and yielded similar results.

3.6.2 Generation of Volcano Plots Using GraphPad Prism

Once data is analyzed using either of the programs, it generates a Microsoft Excel sheet with protein name, number of peptides, number of unique peptides, fold change and p-value detected. I filter the sheet by using proteins that have more than 2 unique peptides detected and calculate $\log_2$ fold change and $-\log_{10}$ p-value for each protein. Using these values, I generate volcano plots using GraphPad Prism. In this section, I tested a total of 5 groups: 6-month-old *GRN* wildtype mice with P2y12 and Iba1, 6-month-old *APP* wildtype mice with P2y12 and Iba1, and 20-month-old *GRN* wildtype mice with Lamp1. Each group had a corresponding non-specific control without primary antibody.

In the first set of experiments involving microglial-BAR using *GRN* wildtype mice, the data was analyzed using MaxQuant and MsStat. As shown in **Figure 3-8**, majority of proteins were enriched in the bait group for both Iba1 and P2y12 antibodies. There were only a few proteins enriched in the non-specific group, as indicated by the fewer proteins on the left side of the graph. The top enriched protein in both groups was P2y12. However, Iba1 was not detected since one unique peptide was identified, which fell below my filter criterion of two or more unique peptides.

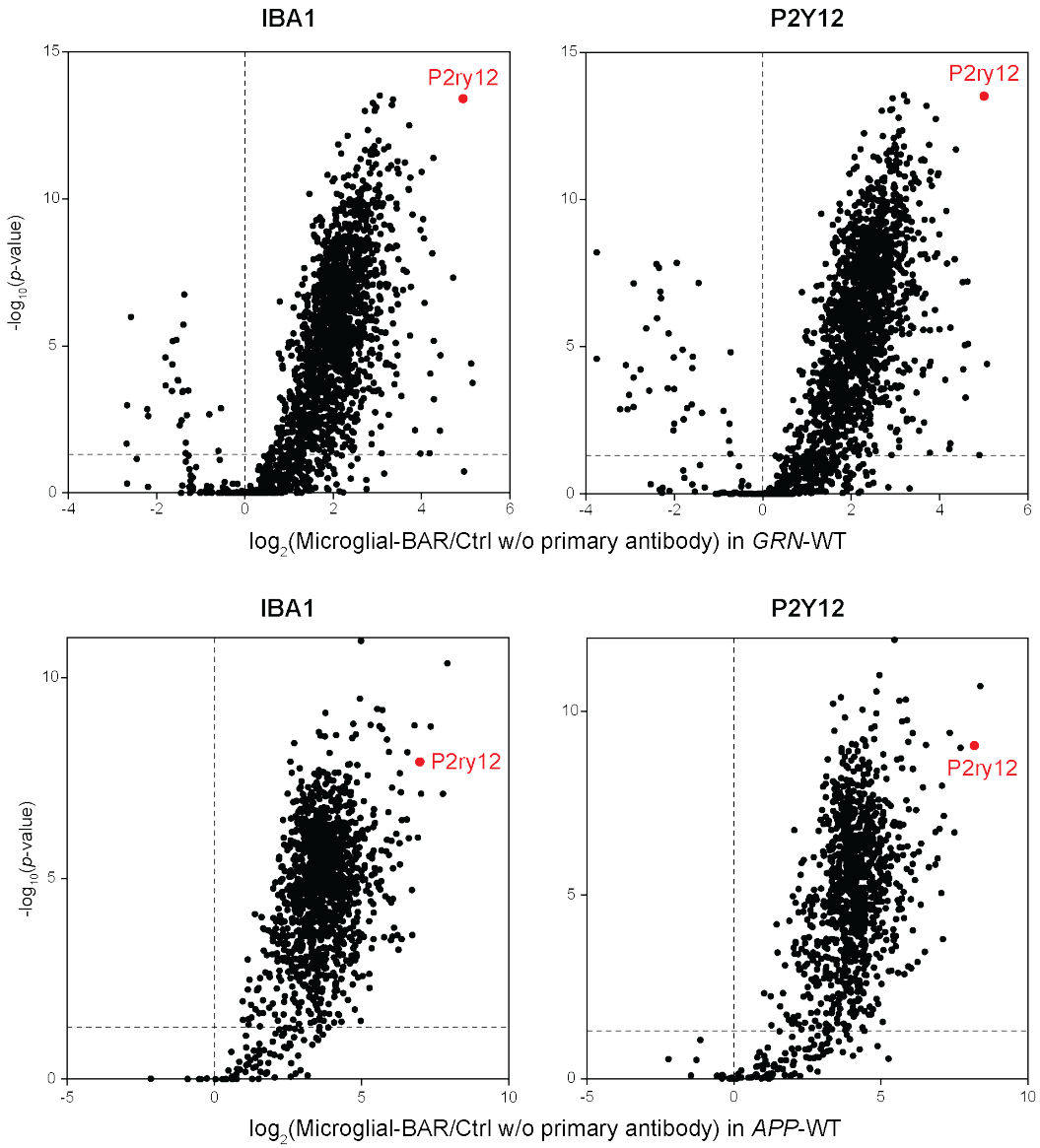

Figure 3-8: Enriched proteins in bait group versus control no-bait group.

Microglial-BAR was performed on 6-month-old wildtype mice from the *GRN*$^{-/-}$ and *APP*^{NLF} cohort using P2Y12 and IBA1 antibodies. Majority of the proteins detected were enriched in all groups with P2Y12 being one the highest enriched.

For the *APP*-wildtype group, the analysis was conducted using Proteome Discoverer, as the mass spectrometry experts recommended upgrading to this software by the time this experiment was performed. As

anticipated, it yielded similar results to the *GRN*-wildtype data analyzed by MaxQuant. Once again, P2y12 was enriched in both groups, while Iba1 remained undetected, with no unique peptide identified.

Since Iba1 was not detected in either group, I focused my analysis on the P2y12 group. I obtained a list of all known and reviewed mouse microglial proteins from Uniprot.org and compared it with my microglia-enriched dataset. The overlapping proteins are represented by blue dots in the plots (**Figure 3-9**). Surprisingly, only 10 of the 210 reviewed microglial proteins overlapped in the *GRN*-wildtype dataset, and 5 in the *APP*-wildtype dataset. The *GRN*-wildtype dataset detected Atp6v0a1, C1qa, Tmem35, Snca, App, Abhd6, P2ry12, Tspan2, Itgam, and Clu, while the *APP*-wildtype group identified Atp6v0a1, Snca, App, P2ry12, and Cmpk2.

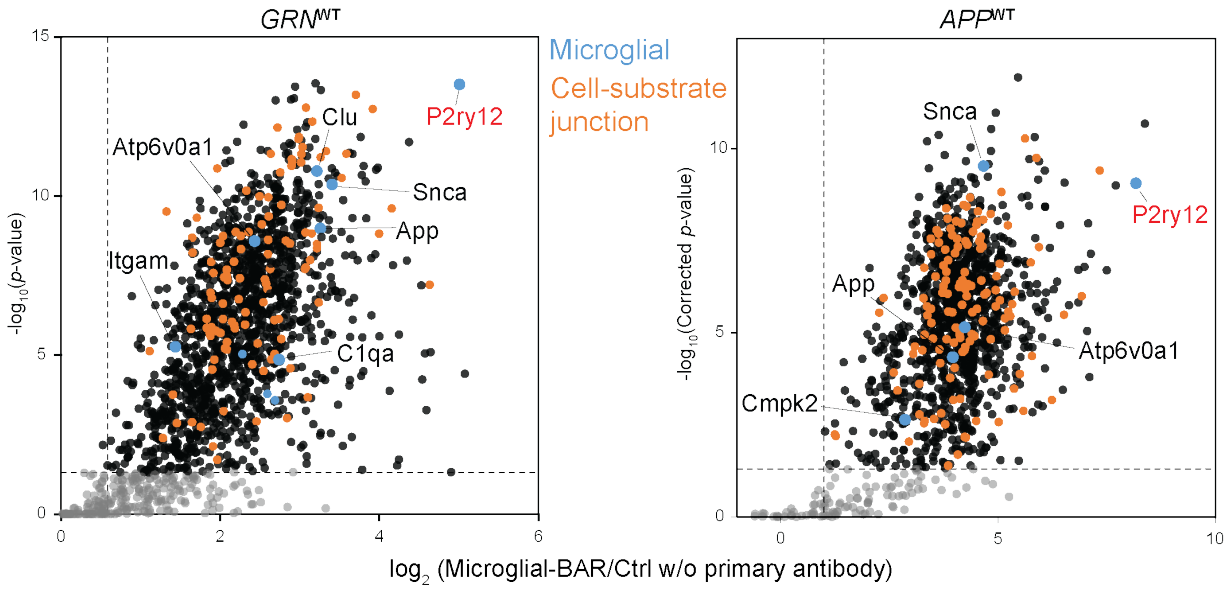

Figure 3-9: Majority of the enriched proteins are cell-substrate junction proteins.

Of the 1426 enriched proteins in the *GRN*^{WT} group, 125 were classified a cell-substrate junction proteins and 13 as microglial. Of the 1224 enriched proteins in the *APP*-WT group, 133 were classified as cell-substrate junction proteins and 5 as microglial.

However, a Gene Ontology (GO) term analysis, which will be discussed in more detail in the following section, revealed 110 proteins as cell-substrate junction proteins in the *GRN*-wildtype group, consistent with possibly microglial processes. These proteins are depicted as orange dots in **Figure 3-9**. The *APP*-wildtype group had 133 proteins classified as cell-substrate junction proteins. Of the 1426 enriched proteins in *GRN*^{WT} group, 846 overlapped with the 1224 enriched proteins in *APP*-WT group accounting for approximately 60% of the *GRN*^{WT} pull-downs and 70% of the *APP*-WT. Most significant cellular component GO term for these proteins was cell-substrate junction (**Supplemental Figure 3-1**). Other GO terms detected were synapse-related proteins suggestive of microglial contact sites.

Having demonstrated that P2y12 antibody can pull-down similar groups of proteins from two different experiments conducted at separate times, I sought to assess a different target protein to determine if this technique was specific to the target protein. To this end, I decided to test the lysosomal membrane protein Lamp1. For this experiment, I used 20-month-old wildtype mice, and the analysis was performed using Proteome Discoverer. The full plot shows majority of proteins enriched in the bait group, similar to previous results where 169 proteins were significantly enriched. A closer inspection of these proteins, using a list of reviewed lysosomal proteins from Uniprot.org, revealed that 70 of the identified proteins were lysosomal, as shown in **Figure 3-10**. The bait protein Lamp1 was also highly enriched. These results were promising, as 70 of the isolated proteins were lysosome related. Based on these findings, I am confident that the BAR method is indeed effective as Lamp1-BAR

dataset was enriched for lysosomal proteins, and P2y12-BAR was enriched for cell-substrate junction proteins.

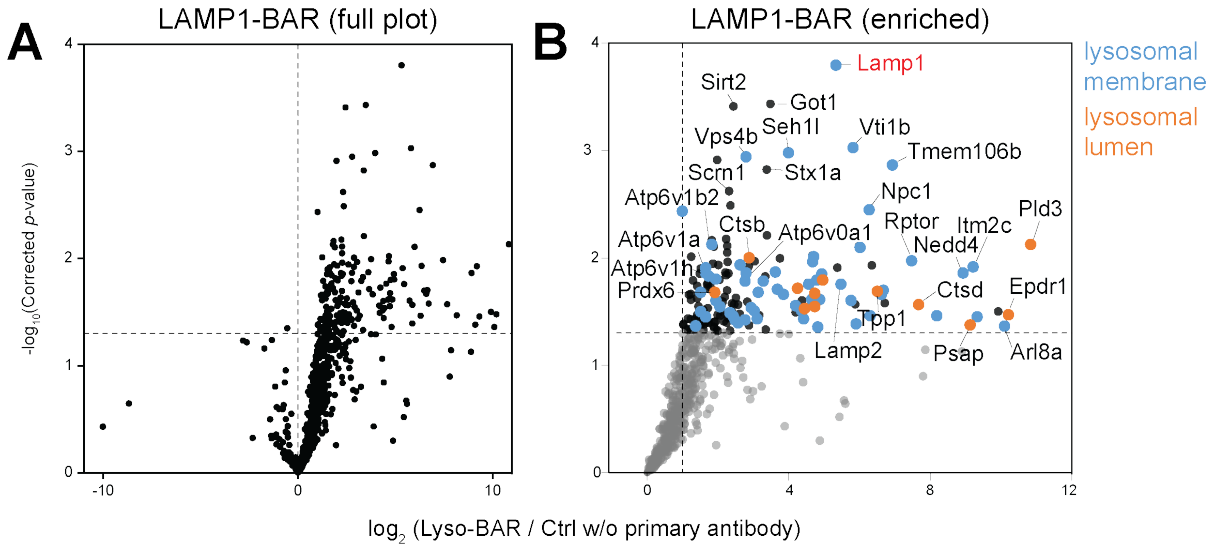

Figure 3-10: Lyso-BAR pulls down lysosome-relevant proteins.

(A) Full volcano plot for Lyso-BAR showing majority of the proteins as being enriched (169 proteins). **(B)** Enriched plot shows bait protein LAMP1 as highly enriched, and several other proteins related to lysosomal membrane (58 proteins) and lumen (12 proteins).

3.6.3 Use of GO Term Search Engines

Gene Ontology (GO) term analysis is a critical step in interpreting large-scale omics data, such as those generated from proteomics, transcriptomics, and genomics experiments. Various GO term analysis programs have been developed to identify overrepresented GO terms associated with a list of genes or proteins, providing insights into the underlying biological processes, molecular functions, and cellular components. Widely used tools for GO term analysis include ShinyGO (Ge et al., 2020), Enrichr (Kuleshov et al., 2016), g:Profiler (Reimand et al., 2007), DAVID (Huang et al., 2009), and WebGestalt (Liao et al., 2019),

among others. These user-friendly web-based tools offer unique features and visualization options, enabling researchers to explore their data in a broader biological context.

ShinyGO (Ge et al., 2020) is an interactive web-based tool that allows users to perform GO term enrichment analysis and visualize the results through various plots and networks. It also supports multiple species and provides the option to explore additional functional annotations. Enrichr (Kuleshov et al., 2016) is a comprehensive web-based tool that not only performs GO term enrichment analysis but also analyzes other functional annotations, such as pathways and transcription factors. Enrichr provides interactive visualization options, including bar graphs and scatter plots, to help interpret the results. g:Profiler (Reimand et al., 2007; Raudvere et al., 2019) is a web server that offers a set of tools for functional profiling of gene lists, including GO term enrichment analysis. It supports over 500 organisms and integrates various annotation databases.

In summary, these web-based tools are user-friendly programs that facilitate GO term enrichment analysis for proteomics data, providing valuable insights into the biological functions and pathways associated with protein sets. I preferred to use Enrichr and ShinyGO interchangeably for this thesis.

For the analysis included in this chapter, I utilized ShinyGO to examine the enriched proteins in both Lyso-BAR and Microglia-BAR from *GRN*-wildtype and *APP*-wildtype mice, respectively. For the Lyso-BAR graph, a Python algorithm generated the plot using data obtained from ShinyGO (**Figure 3-11A**). Conversely, for the Microglia-BAR, I used a combination of GraphPad Prism and Adobe Illustrator software with the downloaded data from ShinyGO, demonstrating that a Python algorithm is not necessary to create a similar plot (**Figure 3-11B**).

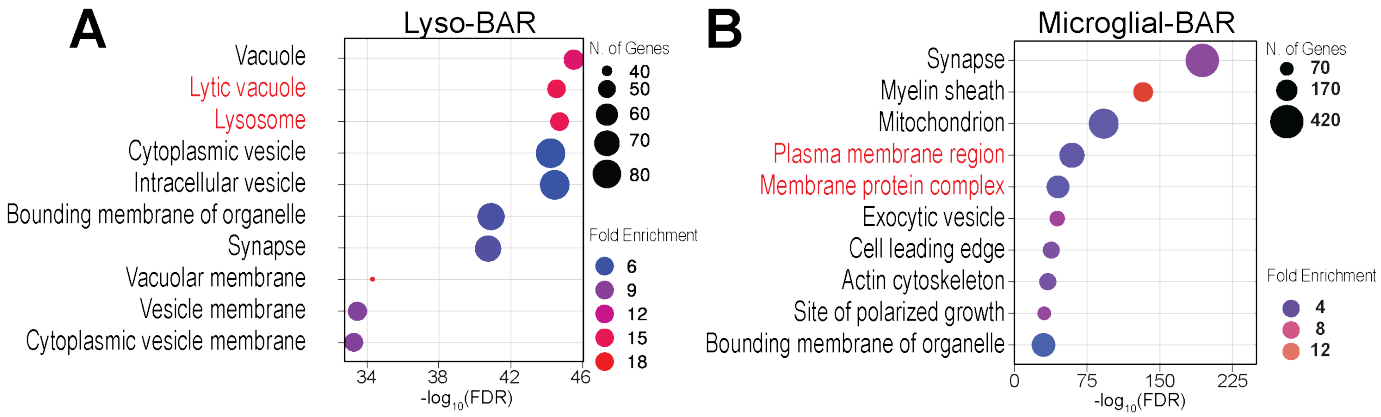

Figure 3-11: Gene Ontology (GO) term analysis reveals Lyso-BAR enriched proteins associate with lysosomal terms and Microglia-BAR enriched proteins associate with membrane terms.

GO term analysis was conducted using ShinyGO. **(A)** Lyso-BAR data shows several proteins under terms such as cytoplasmic vesicle and intracellular vesicle, but the highest fold enrichment was in terms such as vacuole, lytic vacuole and lysosome. **(B)** Microglia-BAR data shows several proteins under terms such as synapse and mitochondria, but the highest fold enrichment is represented by myelin sheath and exocytic vesicle. Relevant terms to Microglia-BAR were plasma membrane region and membrane protein complex.

The plots reveal that Lyso-BAR-enriched proteins are associated with relevant lysosomal GO terms, such as lytic vacuole and lysosome, while Microglia-BAR-enriched proteins fall under terms like plasma membrane region and membrane protein complex. Interestingly, both sets of GO analyses show additional terms, such as cytoplasmic vesicle, bounding membrane of organelle, and synapse for Lyso-BAR and synapse, myelin sheath, and mitochondria for Microglia-BAR. This is likely due to the large labeling radius of 200-300 nm associated with the BAR method, which captures proteins over a broader area than intended.

In this section, I have demonstrated how GO term analysis can be utilized as a quality control measure to validate the results obtained from the BAR method.

3.6.4 Use of Network Search Engines

Network search engines have become a valuable tool in the analysis of proteomics data, enabling researchers to explore protein-protein interactions (PPIs) and identify potential functional relationships between proteins. Several network search engines have been developed to facilitate the analysis of PPIs, such as STRING (Szklarczyk et al., 2019), Cytoscape (Shannon et al., 2003), and BioGRID (Oughtred et al., 2021). These tools offer comprehensive resources for visualizing and analyzing complex networks based on experimentally verified and predicted interactions from multiple databases. Examples of this search engine results will be shown in the following chapters.

3.7 Commentary

3.7.1 Background Information

Proteins typically do not operate solo and have been shown to form multimeric structures for their various functions in the eukaryotic system (Gavin et al., 2006; Krogan et al., 2006). The human proteome has been shown to have 52,569 verified PPIs involving 8275 proteins (Luck et al., 2020). Exploring the underlying mechanisms of aberrant protein interactions in disease can offer crucial insights into potential therapeutic targets. However, capturing protein-protein interactions *in vivo* requires genetic manipulation to introduce the labeling enzyme, a luxury not applicable to human tissue. Therefore, I set out to test a proximity labeling technique applicable to fixed tissues and chose to do so using mouse models given that it's an easier available resource than human tissue. To this end, in this chapter I have shown that fixed mouse brain slices can be

used to isolate proteins in proximity to two targets: lysosomes and microglial processes. One feature of the technique is that it covers a radius of 200-300nm around the target, regardless of any boundaries. In the BAR method, permeabilization is used to maximize efficient labeling with antibodies, which means that targets on only one side of a surface cannot be captured. This could potentially lead to false positives where a protein does not have interactors on the other side of the membrane *in vivo*, but sample preparation techniques may make it appear as if it does. This caveat should be kept in mind when interpreting results.

3.7.2 Critical Parameters and Troubleshooting

The BAR method is highly dependent on a successful stain. Therefore, it is important to ensure a proper labeling of targets using highly specific and efficient antibodies. All tissue slices from one animal should be considered as 1 biological replicate and each test group should have 4 biological replicates. Each test group should have its own negative control that lacks the primary antibody of choice. Do no proceed with mass spectrometry sample preparation without confirming a successful immunohistochemistry staining. It is crucial to ensure maximal tissue de-crosslinking after the BAR method by performing as many boiling and sonication steps needed without prolonging the protocol more than necessary. Once lysed, it is imperative to keep the samples cold at each mass spectrometry processing step to minimize protein loss. While using the magnetic beads described in this chapter, it is important to combine and mix the stock from different vials as there can be batch variability. For any step involving overnight incubation or digestion with magnetic beads, it is important to not let that time period pass 16 hours. Doing so will generate more non-specific results. For each experiment conducted, a negative control should always be included, and the Liquid

chromatography coupled to tandem mass spectrometry (LC-MS/MS) should be done in the same run as there is batch-to-batch variability between runs. Finally, this method has not been tested with paraffin-embedded tissue and should therefore not be attempted on tissue that has been embedded or in fixative for longer than 5 years.

3.7.3 Anticipated Results

BAR method immunohistochemistry should result in a clear colocalized stain of streptavidin to the primary antibody of the protein of choice. Streptavidin stain should be absent from the no primary group. The labeling radius should be no more than 400-500 nm in diameter. Typically, 20 coronal slices 35-40 μm thick will generate 1 mg of protein after homogenization via boiling and sonication. Loading of 300 μg to 1 mg of protein onto beads is traditionally enough to provide a good protein coverage in the mass spectrometer.

3.7.4 Time Considerations

This protocol from harvest to data will take 1-2 months depending on the LC-MS/MS run. Once the brain is harvested and sliced, the BAR method will take 3 days from staining to imaging. The beads titration assay will take 2 days from incubation to dot plot. The pull-down and harvest will take 4 days. The LC-MS/MS run will take 2-3 days. The data analysis can take 4-5 days depending on the samples detected. Final interpretation of the data by the researcher can take anywhere from 2 weeks to 4 months depending on how deep and wide the analysis is done.

Chapter: 4 Progranulin is Required for Normal Lysosomal Function

Note: Parts of this chapter are in preprint as: Hasan S*, Fernandopulle MS*, Humble SW*, Frankenfield AM, Li H, Prestil R, Johnson KR, Ryan BJ, Wade-Martins R, Ward ME, Hao L. Multi-modal Proteomic Characterization of Lysosomal Function and Proteostasis in Progranulin-Deficient Neurons. bioRxiv doi: 10.1101/2023.02.24.529955 *equal contribution.

4.1 Introduction

Batten disease, also known as neuronal ceroid lipofuscinosis (NCL), encompasses a group of neurodegenerative disorders with varying underlying lysosomal storage pathologies, yet presenting with similar clinical symptoms (Naseri et al., 2021). These symptoms include progressive cerebellar ataxia, seizures, and visual impairment. Pathologically, patients with NCL exhibit accelerated lysosomal accumulation of autofluorescent lipofuscin, a lipid-containing material (Tyynelä et al., 2004). Recently, complete loss of progranulin has been linked to the development of NCL, while haploinsufficiency leads to familial frontotemporal dementia (FTD) (Smith et al., 2012). This development links progranulin with lysosomal storage disorders. Progranulin resides within the lysosome and has recently been implicated to play a role in lysosomal fusion (Zhao et al, 2021) and perhaps

influences lysosomal pH in cells (Tanaka et al., 2017). Despite extensive research, the precise role of progranulin in cellular function remains elusive and is thought to be highly dependent on the specific type of cell it is present in. In this chapter, I set out to define progranulin's role by probing lysosomal contents, lysosomal proximity proteins and protein turnover rates.

4.1.1 Lysosomal Storage Associated Neurodegeneration

Lysosomal storage disorders are genetic metabolic disorders that usually present as pediatric neurodegenerative cases but may also occur in adulthood (Platt et al., 2018). These disorders are often accompanied by neurodegeneration. Neurons lack the ability to divide and therefore rely heavily on lysosomes to degrade waste products, and so mutations in lysosomal proteins can lead to neuronal dysfunction. In particular, progranulin, a lysosomal protein, has been associated with both familial frontotemporal dementia (FTD) and neuronal ceroid lipofuscinosis (NCL) depending on the degree of loss. Single nucleotide polymorphisms (SNPs) in the gene encoding progranulin, *GRN*, have also been linked to an increased risk for developing Alzheimer's disease and Parkinson's disease, highlighting the crucial role that progranulin plays in lysosomal biology (Nalls et al., 2021).

4.1.2 Progranulin in the Lysosome

GRN gene codes for the holoprotein progranulin which is a heavily glycosylated glycoprotein (Bateman et al., 1990; Ward and Miller, 2011; Kao et al., 2017; Paushter et al., 2018, Sieben et al., 2012). It consists of 7.5 cysteine-rich motifs called granulins, separated by linker sequences

that can be cleaved by several proteases depending on its location (Songsrirote et al., 2010). Progranulin is synthesized in the endoplasmic reticulum (ER) and subsequently transported to the Golgi apparatus before reaching its final destination, the lysosome (Devireddy and Ferguson, 2022). Although progranulin's exact role is still not known, some of its interactors are. Prosaposin, a sphingolipid activator protein (O'Brien and Kishimoto, 1991), helps traffic progranulin into the lysosome via mannose-6-phosphate receptor (M6PR) or lipoprotein receptor related protein 1 (LRP1) (Zhou et al., 2015). Consequently, progranulin chaperones prosaposin into the lysosome via sortilin-mediated endocytosis and trafficking (Zhou et al., 2015). When present intracellularly in lysosomes, lysosomes can be cleaved by cathepsins B and L (Lines et al., 2020; Paushter et al., 2018). Progranulin's glycosylated structure can potentially shield it from the acidic lumen of the lysosome as glycosylation has been shown to be protective against autolysis, proteolytic degradation and free radicals, suggesting a lysosomal function (Russell et al., 2009: Martínek et al., 2010). Other known interactors include pro-cathepsin D, glucocerebrosidase and Rab2 (Zhou et al., 2015; Butler et al., 2019; Jian et al., 2016; Zhao et al., 2021). Progranulin enhances activities of cathepsin D and glucocerebrosidase (Butler et al., 2019; Jian et al., 2016). Prosaposin Rab2-mediated autophagosome-lysosome fusion is critical in Gaucher Disease patients as lack of progranulin exacerbates their pathology (Zhao et al., 2021).

4.1.3 Progranulin's Role in Neurons

Progranulin itself has been implicated in several functions due to its various expression pattern throughout the body. Outside the nervous system, it is expressed by cells such as neutrophils, epithelial cells and sperm (Bateman et al., 1990; Bhandari et al., 1993; Anakwe and Gerton,

1990) resulting in functions such as wound healing, tumorigenesis, inflammation, cell proliferation and vasculogenisis (Lines et al., 2020; Paushter et al., 2018; Kao et al., 2017). In the brain, progranulin is primarily expressed by microglia and neurons of the hippocampus, amygdala, hypothalamus, cerebellar Purkinje neurons, cingulate and piriform cortex (Petkau et al., 2010; Mendsaikhan et al., 2019). It has been shown to promote neuronal survival, neurite outgrowth and neuronal differentiation (Kao et al., 2017; Paushter et al., 2018; Lines et al., 2020). Neurons express sortilin and microglia may release progranulin that is trafficked to neuronal lysosomes (Du et al., 2022). Therefore, this raises the question of whether progranulin deficiency mediated dysfunction is a cell autonomous or non-autonomous issue.

Despite this wealth of knowledge, the primary molecular functions of progranulin and the impact of progranulin deficiency on lysosomal biology and protein homeostasis remain unclear. This is in part due to limited tools available for understanding the role of progranulin in the brain. Lysosomes are highly dynamic organelles, and their interactions are difficult to capture by traditional immunoprecipitation and organelle isolation. Recent advances in intact lysosomal isolation methods via proximity labeling and immunoprecipitation have generated a wealth of information on lysosomal functions, though mostly in non-neuronal contexts (Abu-Remaileh et al., 2017). Other proteomics-based studies in relevant mouse models have only been able to capture global changes regardless of cell type or organelle (Huang et al., 2017; Klein et al., 2017; Miedema et al., 2022). Here, I utilized a combination of *in situ* proximity labeling, organelle isolation, and dynamic stable isotope labeling using amino acids in cell culture (dSILAC) proteomic approaches to map the organellar and cellular architectures of neuronal progranulin deficiency.

4.1.4 Aims

- Define the proteome of lysosomes lacking progranulin.
- Determine the degradative capacity of lysosomes lacking progranulin.
- Define the interactome of progranulin-deficient lysosomes *in situ.*

4.2 Methods

4.2.1 *GRN* KO i^{3}Neurons

The lab generated a *GRN* KO human inducible pluripotent stem cell (hiPSC) line using the WTC11 cell line mentioned in Chapter 3. A mutation was created by creating a 7 base pair insertion in one *GRN* allele and 10 base pair deletion in the other *GRN* allele resulting in complete loss of function. This cell line will be referred to as *GRN* KO from now on. FTD patient cell line labelled i2*GRN* was acquired from Dr. Dimitri Krainc harboring a heterozygous *GRN* mutation (c.26 C > A, p.A9D), along with its isogenic control labelled i2W. The patient was a female former postal worker of Irish descent who presented with progressive dysarthria and stuttering at the age of 63 that worsened over the course of 2 years resulting in death (Wider et al., 2008). These lines will be referred to as ptMut and ptWT from here on. A complete knock out was created in our lab using CRISPR-Cas9 sgRNA gGTGGCCTTAACAGCAGGGC directed against *GRN* in i2W, hereafter referred to as ptKO.

4.2.2 *GRN* KO Mouse Model

Mouse model used were WT:C57BL/6 (Jackson Labs) and *GRN*$^{-/-}$: B6.129S4(FVB)-Grn$^{tm1.1Far}$ (Jackson Labs). The animals were housed in the National Institutes of Health (NIH) animal facility that followed the U.S. Department of Health and Human Services Public Health Service Policy on Humane Care and Use of Laboratory Animals for animal husbandry and euthanasia. Female mice aged 20 months were used for this study.

4.2.3 Lysosomal Proximity Labeling

For each biological replicate, I picked 21 slices evenly from the whole brain. The slices were treated with 0.3% H_2O_2 to quench endogenous peroxidases for 30 mins and blocked for 1 hour with 3% donkey serum and 0.25% Triton X in PBS. Proximity labeling experiments in fixed mouse brain slices were targeted to three bait proteins of interest: a lysosomal marker (Lamp1), progranulin (Pgrn), and a microglial marker (P2y12). Fixed mouse brain slices were incubated in primary antibody of choice in block overnight at 4°C: Lamp1 (Developmental Studies Hybridoma Bank #1D4B), PGRN (R&D Systems #AF2557-SP) or P2y12 (AnaSpec #AS-55043A). Four biological replicates were used for each group. The negative control group was treated the same minus primary antibody. After thoroughly washing off the primary antibody, mouse brain slices were incubated in horseradish peroxidase (HRP)-conjugated secondary antibody in block buffer for 1 hour. The next step was incubation in phenol-biotin [(10μM) in 1% FBS and PBS] for 1 hour and treatment with 0.003% H_2O_2 in the phenol-biotin buffer for 10 minutes. The slices were quenched using cold PBS + 500mM sodium ascorbate + 10mM sodium azide for 5 mins. Mouse brain slices were lysed in 3% SDS and 2% sodium deoxycholate in PBST + protease inhibitor (Sigma-Aldrich

#11873580001) by boiling at 90°C for 1 hour and then sonicating for 40 seconds on and 40 seconds off for 15 mins at 1 ampere. The samples were boiled for an additional 30 mins, spun at 18,000 rcf at 4°C in a centrifuge and the supernatant aliquoted into fresh clean Lo-Bind tubes (Fisher Scientific #13698794).

4.2.4 Lysosomal Immunoprecipitation

LAMP1-3xHA transgenic i^{3}Neuron lines were generated with lentiviral transduction in WT and *GRN* KO genetic backgrounds. A TMEM192-mEmerald-expressing line was used as a control for nonspecific pulldowns. i^{3}Neurons were differentiated as described previously and replated on day 3 at 36 million cells per 15cm dish. Cells were maintained with half media changes every other day until day 14. Immunoprecipitation and routine bottom-up proteomics was performed as described in Chapter 2.

4.3 Lysosomal Assays

4.3.1 Magic Red Assay

Differentiated i^{3}Neurons were plated at a density of 50,000 cells on PLO coated ibidi slides (Ibidi # 80827) and aged till day 10. As controls, one well from each cell line received chloroquine (50μM for 24 hours) prior to Magic Red. For cathepsin B activity visualization, Magic Red (Abcam #AB270772-25TEST) was added to the cells at 1:25 final dilution and incubated in the dark for 30 mins at 37°C. Cells were washed twice with PBS and incubated with Hoechst 33342 (Thermo Scientific #62249) at 1:10,000 for 5-10 mins and then washed with PBS. Wells were imaged

using Nikon spinning disk confocal at 60X oil objective. Images were edited and analyzed using ImageJ software. To ensure true significance, we counted the number of puncta detected per nuclei in the field to account for any changes due to plated cell density.

4.3.2 Dynamic Stable Isotope Labelling in Cell Culture (dSILAC)

Human i^{3}Neurons were maintained on PLO coated 12-well dishes in light amino acid-containing media (DMEM:F12 for SILAC medium (Athena Enzyme Systems #0423), N2 Supplement (Life Technologies Corporation #17502048), B27 Supplement (Life Technologies #NC1001496), NEAA (Life Technologies #11140050), GlutaMAX (Life Technologies #35050061), BDNF (PeproTech #450-02), NT-3 (PeproTech #AF-450-03-100ug), Arg (light) at 0.699M (Sigma #A4599), Lys (light) at 0.499M (Sigma #L7039)). On day 10 of i^{3}Neuron culture, neurons were gently washed with PBS twice and switched into the neuronal media containing heavy stable isotope labeled (13C615N2) lysine (Lys8) at 0.499M (Cambridge Isotope Laboratories #CNLM-291-H-PK). Neurons were harvested after 4 day (96 hours) of media switch (day 14 of i^{3}Neuron culture). Neurons were gently washed with PBS twice and lysed in 100 µL of ice-cold lysis buffer containing 0.1% Rapigest (Neta Scientific Inc #WAT-186001860), 150 mM NaCl, and 50 mM Tris-HCl. Neurons were scraped into 1.5 mL tubes for sonication in the QSonica (Q800R) sonicator for 15 min at 4°C with alternating 40 seconds on, 20 seconds off cycles. Supernatants were collected after centrifugation at 4°C and 16,500 g for 15 min. Total protein concentrations of neuron lysate were determined with DC Protein assay (BioRad). Protein disulfide bonds were reduced by 5 mM of Tris(2-carboxyethyl) phosphine (TCEP) for 30 min, followed by addition of 15 mM of iodoacetamide (IAA) for 30 min and 5

mM of TCEP for 15 min in a ThermoMixer shaking at 800 rpm at 37°C. Proteins were digested with LysC (Promega #VA1170) at 1:30 (enzyme: protein) ratio for 16 hours at 37°C and quenched with 10% trifluoroacetic acid (TFA) until pH<3. Peptides were desalted using a Waters Oasis HLB 96-well extraction plate based on the manufacturer's protocol. Peptide samples were dried under SpeedVac and stored at -80°C until LC-MS/MS analysis.

4.4 Results

4.4.1 Lysosomal Immunoprecipitation Can Be Used on i^{3}Neurons

Lysosomes are highly dynamic organelles that transiently interact with numerous organelles and cellular components (Ballabio and Bonifacino, 2020). Given the unique role of lysosomes in neurons, these interactions likely have a cell type-specific significance (Ferguson, 2019). Neuronal cell anatomy forces their lysosomes to travel incredible distances to get to their destinations (Tsukita and Ishikawa, 1980; Farías et al., 2017). Additionally, mature degradative lysosomes exist primarily in neuronal soma, followed by some in dendrites and very few in axons (Becker et al., 1960; Gorenstein et al., 1985; Parton et al., 1992; Cai et al., 2010; Gowrishankar et al., 2017; Yap et al., 2018). These differentially distributed lysosomes seem to have different compositions depending on their locations. To this effect, it is important to differentiate the identity of neuronal lysosomes from other cell types. Isolating lysosomes from neurons is challenging. This is in part due to the culturing conditions required for generating large volumes of starting material (such as whole organ lysate or 25 million cultured cells using commercially available

isolation kits), as well as the fact that traditional differential centrifugation techniques result in impure admixtures of lysosomes and other organelles with similar densities. Our lab has successfully used the lysosome isolation technique developed by Abu-Remaileh et al. (2017) and is the first to isolate lysosomes from human iPSC derived neurons (i^3Neurons). Abu-Remaileh et al. have demonstrated that the lysosomes isolated using this technique maintain their integrity, as evidenced by the retention of cathepsin D activity and the ability to uptake radiolabeled arginine *in vitro* (Abu-Remaileh et al., 2017). As this feature was not necessary for my experiments, it was not included in the testing. To isolate lysosomes from neurons, we genetically modified hiPSCs to stably express LAMP1-HAx3, using a safe harbor approach developed by Dr. Michael Fernandopulle. These cells are equipped with a doxycycline-inducible neurogenin2 (NGN2) cassette integrated into their genome, enabling them to differentiate into cortical neurons (Fernandopulle et al., 2018). These neurons will be referred to as i^3Neurons. Fernandopulle et al. have demonstrated that i^3Neurons start developing neurites within two days of differentiation. By day 14, these neurons exhibit dendritic spines with pre- and post-synaptic markers, along with other cortical neuronal markers like Tuj1, Map2, and Tau. Moreover, these neurons are capable of generating spontaneous trains of action potentials, indicating functional activity (Fernandopulle et al., 2018). I differentiated and harvested the i^3Neurons at day 14 using a gentle cell homogenizer, followed by a rapid pull-down using magnetic anti-HA beads, as described in Chapter 2. Although Abu-Remaileh et al. recommend using TMEM192 tagged with HA for a cleaner pull-down, I chose to use LAMP1-tagged HA to maintain consistency with other lysosomal experiments targeting Lamp1 in this thesis.

My results showed that lysosomes could be isolated from i^3Neurons using LAMP1-HAx3, as demonstrated by immunoblotting and mass spectrometry analyses. Specifically, lysosome-enriched markers, such as

Lamp2 and Ctsd, were detected in the pull-down, although there was some contamination with peroxidases and Golgi apparatus (**Figure 4-1A**). The negative control used for this set of experiments was a cell line with TMEM192 (a lysosomal transmembrane protein) tagged to monomeric Emerald protein that has no interactions with anti-HA beads. Confocal imaging of day 14 i^3Neurons also revealed colocalization of HA with the lysosomal marker Lamtor4, further supporting lysosome isolation (**Figure 4-1B**). Mass spectrometry analysis revealed that the pull-down group was enriched with 261 proteins compared to the negative control, of which a subset was identified as lysosomal lumen and membrane proteins (**Figure 4-2A**). Protein identification was performed using UniProt.org, and subsequent Gene Ontology (GO) enrichment analysis for cellular compartment revealed terms associated with lytic vacuole, lysosome, lysosomal lumen, and lysosomal membrane (**Figure 4-2B**). Notably, the top Kyoto Encyclopedia of Genes and Genomes (KEGG) pathway GO term was lysosome, identifying 54 of the enriched proteins, including Lamp proteins (Lamp1, Lamp2), cathepsins (Ctsb, Ctsl, Ctsd, Ctsz, Ctsf, Ctsc, Ctsa), hexosaminidases (HexA, HexB), and prosaposin (Psap), among others (see **Supplemental Figure 4-1** for details). Overall, my data suggest that LAMP1-HAx3 can be effectively utilized to isolate lysosomes from neuronal cells, despite minor contaminations.

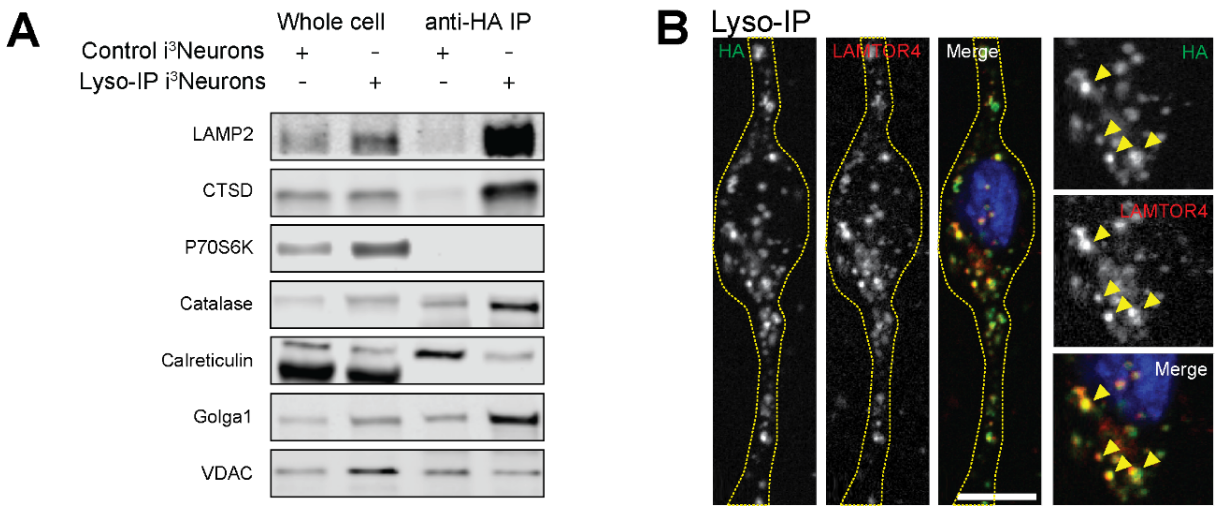

Figure 4-1: HA tagged to LAMP1 pulls down lysosomes and colocalizes with lysosomal marker LAMTOR4.

(A) Day 14 i^{3}Neurons differentiated from human iPSCs were used to pull down intact HA-tagged lysosomes via anti-HA magnetic beads. Lysosomes tagged with the green-fluorescent protein Emerald to TMEM192 were used as controls. Markers for lysosome (LAMP2 at 100-130 kDa, CTSD at 31 kDa), cytoplasm (P70S6K at 70-85 kDa), peroxisome (catalase at 55 kDa), endoplasmic reticulum (calreticulin at 57 kDa), Golgi apparatus (golga1 at 97 kDa), and mitochondria (VDAC at 30 kDa) were used to assess pull-down purity. **(B)** Representative confocal images of Day 14 i^{3}Neurons showing colocalization of lysosomal marker LAMTOR4 and HA tag. Scale bar is 10μm.

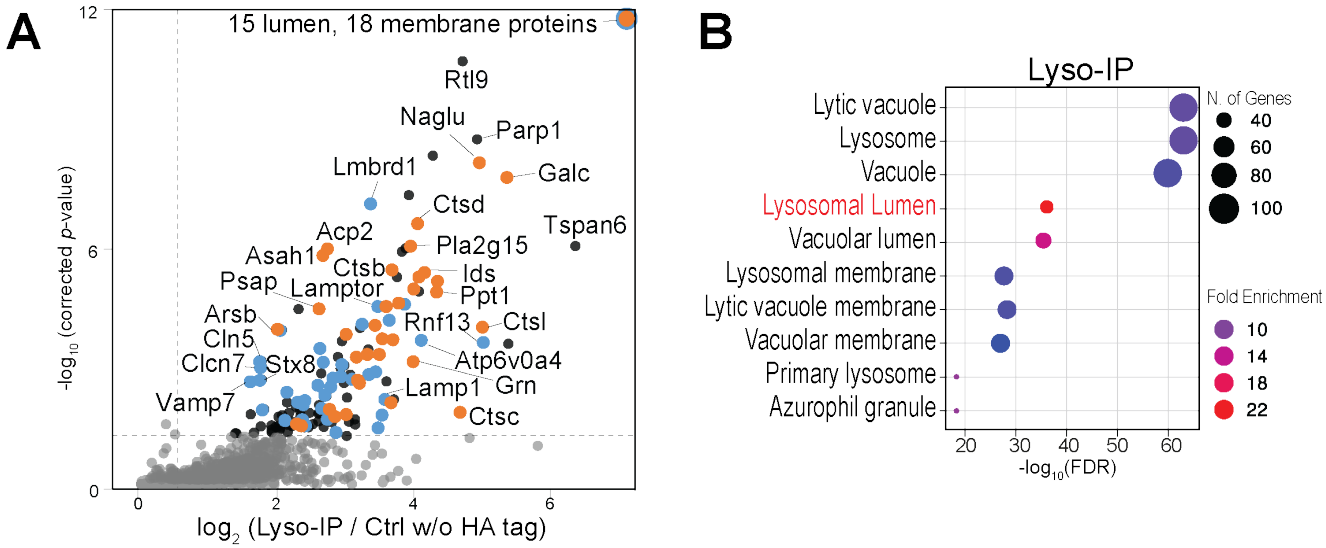

Figure 4-2: Isolated lysosomes are enriched for lysosomal proteins.

(A) Volcano plot shows 261 proteins enriched (n=4) in Lyso-IP from WT i^{3}Neurons. A subset was identified as lysosome lumen proteins (orange dots) and lysosome membrane (blue dots) using uniport.org. **(B)** Top GO enrichment analysis for enriched proteins using ShinyGO shows lysosomal GO terms for Cellular Compartment.

4.4.2 Loss of Progranulin Leads to Increased Lysosomal Enzymes in Neurons

After isolating lysosomes from i^{3}Neurons, I aimed to investigate alterations in lysosomal contents in the absence of progranulin using this technique. First, I confirmed that *GRN* KO i^{3}Neurons did indeed lack progranulin by performing immunofluorescence for progranulin and Lamp1 on day 6 i^{3}Neurons. *GRN* KO cells completely lacked progranulin despite Lamp1 staining being present (**Supplemental Figure 4-2**). I then pulled down lysosomes from i^{3}Neurons with and without progranulin at day 14 using the rapid immunoprecipitation technique described above and detailed in Chapter 2. I processed the samples for mass spectrometry

as described in Chapter 2. Comparing *GRN* KO to wildtype neurons, loss of progranulin led to an increase in 368 and a decrease in 362 proteins in relation to wildtype (**Figure 4-3A**). The 368 increased proteins observed in *GRN* KO neurons had GO term enrichment most significant for lysosomes and steroid biosynthesis KEGG Pathways (**Figure 4-3B**). The most enriched molecular function GO term for increased proteins in *GRN* KO neurons was arylsulfatase and sulfuric ester hydrolase activity. The proteins that contributed to these molecular function GO terms were Arsa, Arsi, Arsf and Sts. To better understand how these proteins interact with one another and others, I performed string analysis and generated the network shown in **Figure 4-3C**. This analysis revealed involvement of these proteins with other networks associated with glycosphingolipid metabolic process, ceramide catabolic process, steroid catabolic process, and steroid biosynthetic process. The grey nodes represent proteins that were not altered in my dataset. The fully labelled string network with legends for fold change and significance is shared in the supplementary (**Supplemental Figure 4-3**). I next looked at how proteins enriched in the lysosomes only (from **Figure 4-2A**) were altered in *GRN* KO neurons. Using the whole dataset, I filtered for the 261 proteins that were enriched in the wildtype LAMP1-HAx3 pull-down compared to the negative control (TMEM192-HAx3) (**Figure 4-4A**). Among the enriched proteins, an increase in 37 proteins was observed in the neuronal lysosomes of the *GRN* KO compared to wildtype, while 26 were decreased, including Grn as anticipated for the *GRN* KO lysosomes. GO analysis performed on the 63 altered proteins identified the lysosome KEGG pathway as the top hit (**Figure 4-4B**), which is in agreement with the criteria used to filter for lysosomal enriched proteins. Other GO terms for molecular function and biological process showed terms associated with bond breakage and lysosomal pH maintenance (**Figure 4-4B**). Proteins responsible for pH maintenance terms that were increased in *GRN* KO were Cln3, Clcn6 and

Ppt1. This is consistent with our data from the lab showing an increase in other pH-maintaining proteins such as v-ATPases on the lysosome's surface using proximity labeling and increase in lysosomal pH using a pH assay (Hasan et al., 2023). The Lyso-IP data supports the observation of disruption in lysosomal pH by capturing an increase in pH-maintaining proteins. The v-ATPases were not altered in the Lyso-IP data, suggesting that the v-ATPases are not incorporated into the lysosomal membrane, although further investigation is needed to verify this.

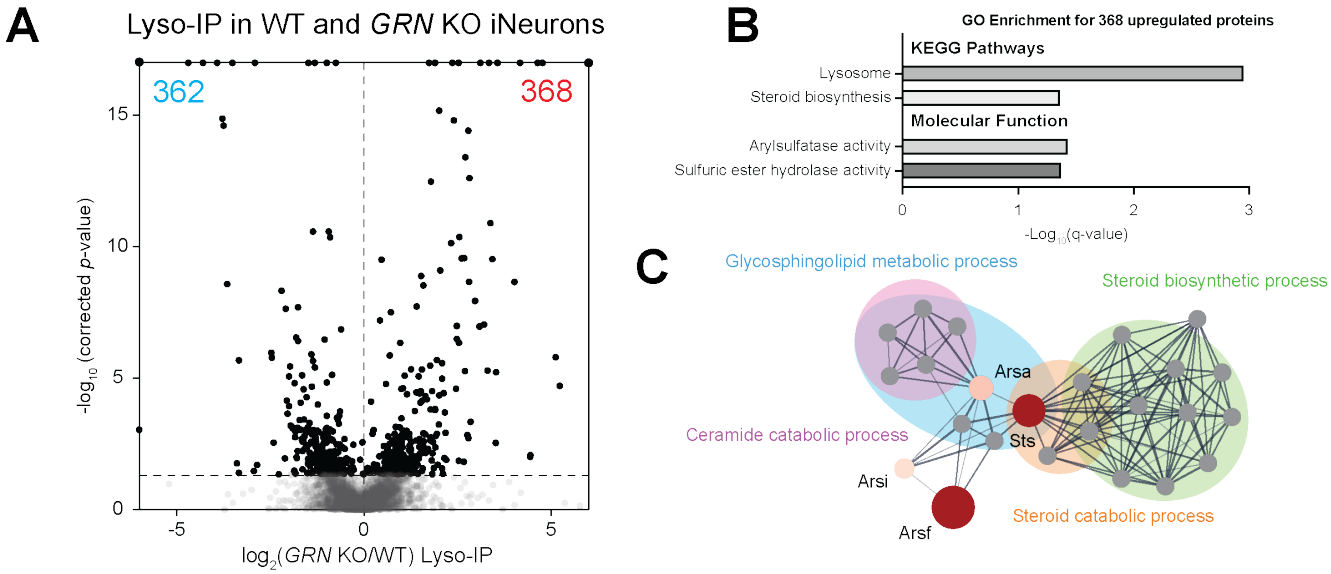

Figure 4-3: Loss of progranulin leads to an increase in lysosomal enzymes in human neurons.

Lysosomes were harvested from day 14 i^{3}Neurons with and without progranulin for LC-MS/MS analysis **(A)** Volcano plot shows 5941 proteins detected (n=4) in both WT and *GRN* KO i^{3}Neurons. A total of 730 proteins were differentially expressed between *GRN* KO and WT with 368 upregulated and 362 downregulated in *GRN* KO (q value < 0.05). **(B)** Top two GO enrichment analysis for 368 upregulated proteins using Enrichr where q is corrected p-value. **(C)** String diagram showing proteins in the molecular function GO term from (B) as labelled nodes. Colored Venn diagrams represent biological process GO terms associated with the next 20 interacting proteins to the labelled nodes. Depth of red shade denotes increased significance (using corrected p-value), node size denotes fold change. Detailed legend in supplementary.

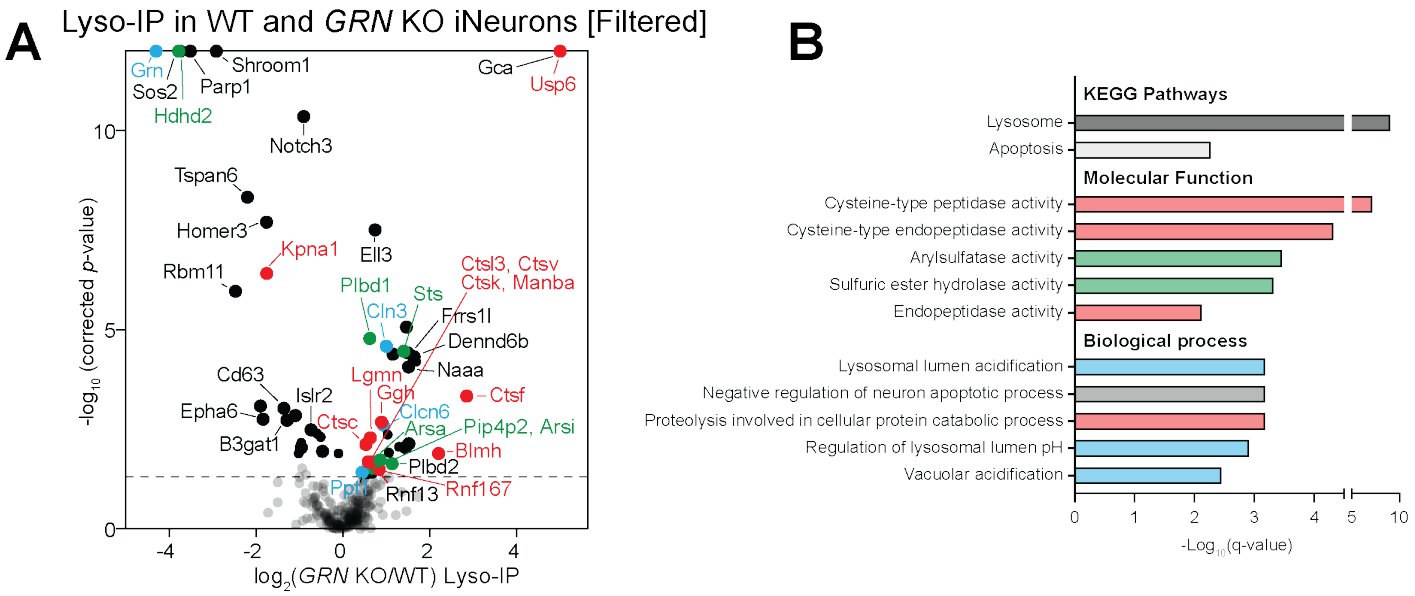

Figure 4-4: Lysosomal proteins related to pH maintenance and bond breakage are upregulated in human neurons with progranulin loss.

This analysis was filtered for lysosome-enriched proteins from Fig 2A. **(A)** Volcano plot shows highlighted lysosomal proteins that were differentially expressed in *GRN* KO i^{3}Neurons compared to WT. q value < 0.05. **(B)** GO term analysis for all the differentially expressed proteins. Colors represent labeled proteins in the volcano plot from (A).

4.4.3 Progranulin-lacking Lysosomes Have Decreased Degradative Capabilities

An increase in catabolic enzymes of the lysosome is often observed in lysosomal storage diseases and may suggest alterations in lysosomal degradative capacity (Moran et al., 2000; Vitner et al., 2010; Moles et al., 2012). In this regard, our lab's data demonstrates a reduction in the degradative function of lysosomes in the absence of progranulin, as revealed by a DQ-BSA assay, where there was a notable decrease in the degradation of DQ-BSA (Hasan et al., 2023). To test a specific lysosomal

enzyme using a commercially available reagent, I tested Cathepsin B (Ctsb) activity in wild type and *GRN* KO neurons. A significant increase in Ctsb expression has been observed in cells with progranulin deficiency (Takana et al., 2017; Klein et al., 2017; Huang et al., 2020). In my dataset, several cathepsins are elevated in lysosomes lacking progranulin, such as Ctsc, Ctsf, Ctsk, Ctsv and Ctsl3 (**Figure 4-4A**). However, Ctsb's increase is not significant here. Changes in enzyme abundance can indicate altered enzyme activity; however, it is important to confirm changes in enzyme activity through appropriate functional assays. Cathepsins require a specific pH for normal function and are processed in the lysosome (Turk et al., 1995; Turk et al., 1993; Almeida et al., 2001; Turk et al., 2012), however, lysosomes lacking progranulin may have altered pH considering the increase in pH-maintaining proteins. I chose to test Ctsb activity given its well documented involvement with progranulin (Mohan et al., 2021; Tanaka et al., 2017; Klein et al., 2017). I used the Magic Red assay which consists of a fluorescently-quenched Ctsb substrate that becomes fluorescent red upon cleavage by Ctsb. Cultured i^3Neurons in Magic Red have a base-line activity of Ctsb as seen in **Figure 4-5A**. This activity can be completely abolished in the presence of chloroquine, a pH neutralizing drug (**Figure 4-5A**). Loss of progranulin leads to significant decrease in Ctsb activity that can be consistently replicated (**Figure 4-5B**). This is congruous to the suggestion of altered pH, which was then confirmed in a pH assay from the lab. The assay showed alkalinization of luminal pH in lysosomes lacking progranulin in neurons (Hasan et al., 2023). Lysosomal enzymes have a narrow range of pH that they operate in. Disruption in this leads to decreased degradative properties of lysosomes, just as this data suggests.

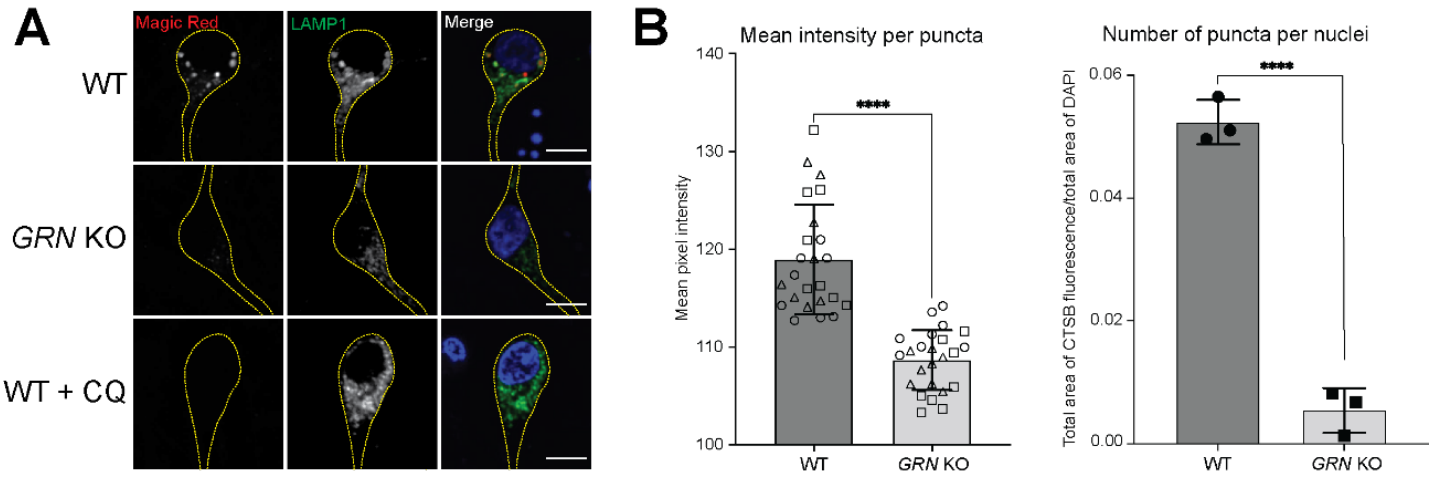

Figure 4-5: Progranulin loss leads to decreased cathepsin B activity.

Day 10 i^{3}Neurons were treated with a Magic Red assay for cathepsin B activity. **(A)** Representative fluorescence imaging of wildtype (WT) and *GRN* KO i^{3}Neurons. Lysosomes are shown via LAMP1, Ctsb activity via Magic Red. Chloroquine (CQ) treatment (50μM for 24 hours) abolishes Magic Red fluorescence. Scale bar is 10μm. **(B)** Quantification of absolute and relative fluorescence intensities indicate decreased cathepsin B activity in *GRN* KO vs. WT i^{3}Neurons. Images were analyzed using 8 fields of view from each replicate using a titled 9x9 image using a 60X oil objective. ****p value<0.0001, mean plotted with standard deviation.

4.4.4 Genes Associated with Neurodegeneration Have Altered Protein Turnover Rates in the Absence of Progranulin

The lysosome is a critical component of the cell's degradation pathway. Protein homeostasis is maintained by the constant rate of synthesis and degradation, whereby any disruption to this pathway may lead to aberrant protein turnover rates. To test for progranulin's role in maintaining canonical protein turnover rates, I utilized a dynamic stable isotope labeling using amino acids in cell culture (dSILAC) method developed by the lab (Hasan et al., 2023). This technique has two key

components: first, the incorporation of heavy isotope amino acids into newly synthesized peptides, and second, subsequent mass spectrometry analysis (**Supplemental Figure 4-4**). By measuring the ratio of heavy to light amino acids in peptides, this method provides a means to track protein turnover. I applied this method to neurons derived from a patient carrying *GRN* heterozygous mutations (ptMut), as well as their isogenic control (ptWT) and a complete *GRN* knockout line from the isogenic control (ptKO) (**Supplemental Figure 4-5A**). To ensure a comprehensive comparison, I also included data from the lab on the *GRN* KO neurons collected by Dr. Ryan Prestil. These differentiated i^3Neurons were aged in SILAC media for 10 days. On the 10^{th} day, media was switched to SILAC media containing heavy isotope of Lysine for 4 days prior to harvesting and processed for mass spectrometry as defined in the methods section and Chapter 2. Protein turnover rates were calculated and can be seen as altered when compared to WT (**Figure 4-6A-C**). The volcano plots depict proteins with different turnover rates. Proteins with longer half-lives, which indicates slower turnover rates, are shown on the right side of the plots. Conversely, proteins with shorter half-lives, indicating faster turnover rates, are shown on the left side of the plots. A more symmetrical plot was observed in the comparison between *GRN* KO and wildtype, compared to the patient-derived groups. Despite differences in the overall plot symmetry, similar patterns in protein turnover rates were observed between the three comparison groups. For example, the protein Ctsb showed a slower turnover rate in all three comparison groups, while Hnrnpa2b1, a member of the heterogeneous nuclear ribonucleoprotein (hnRNP) family of proteins, exhibited a faster turnover rate in all three groups (**Figure 4-6A-C**). The heatmap illustrates this more clearly by grouping proteins with similar turnover rates in two or more groups between the three comparison groups (**Figure 4-6D**). Several of these proteins are annotated in the volcano plots for better visualization.

Despite some proteins not reaching significance in one or two of the plots, they were included in the heatmap to demonstrate gene-dose dependent trends as with Ctsd. The half-life of Ctsd was found to be 1.2 days in the *GRN* KO versus wildtype group, 1.3 days in the patient-derived *GRN* knockout (ptKO) versus isogenic control group (ptWT), and 0.8 days in the patient-derived *GRN* heterozygous mutation (ptMut) versus ptWT. Some of the proteins, such as Pld3, Myh9, Clta, Cltc, Gap43, and Sod1, showed unusual trends in which the *GRN* KO/WT and ptMut/ptWT groups were more similar to each other than the *GRN* KO/WT to ptKO/ptWT group on both sides of the spectrum. This is unexpected since the *GRN* KO/WT and ptKO/ptWT groups should be more similar to each other. One possible explanation for this observation is that the cell lines used for the comparison were derived from different individuals, which could have resulted in genetic differences that could influence the turnover rates of these proteins. Further investigation would be needed to clarify these differences. It is important to note that several proteins, including Snca, Hmgb1, Fus, Vim, Vcp, and Hnrnpa1, exhibited faster turnover rates in the patient-derived cell lines than in the *GRN* KO/WT group. In contrast, these proteins showed slower turnover rates in the *GRN* KO/WT group, further emphasizing the potential underlying genetic differences between these individuals. All of these proteins are classified as FTD/ALS associated proteins. In addition, when considering all the proteins with altered turnover rates and performing a gene ontology term analysis, the top KEGG pathway identified is "pathways of neurodegeneration" (**Supplemental Figure 4-5**). In summary, the findings suggest that loss of progranulin leads to altered protein turnover rates indicative of lysosomal dysfunction, with a significant impact on proteins associated with other neurodegenerative disorders. These results suggest that the lysosome may be a common point of convergence in these diseases.

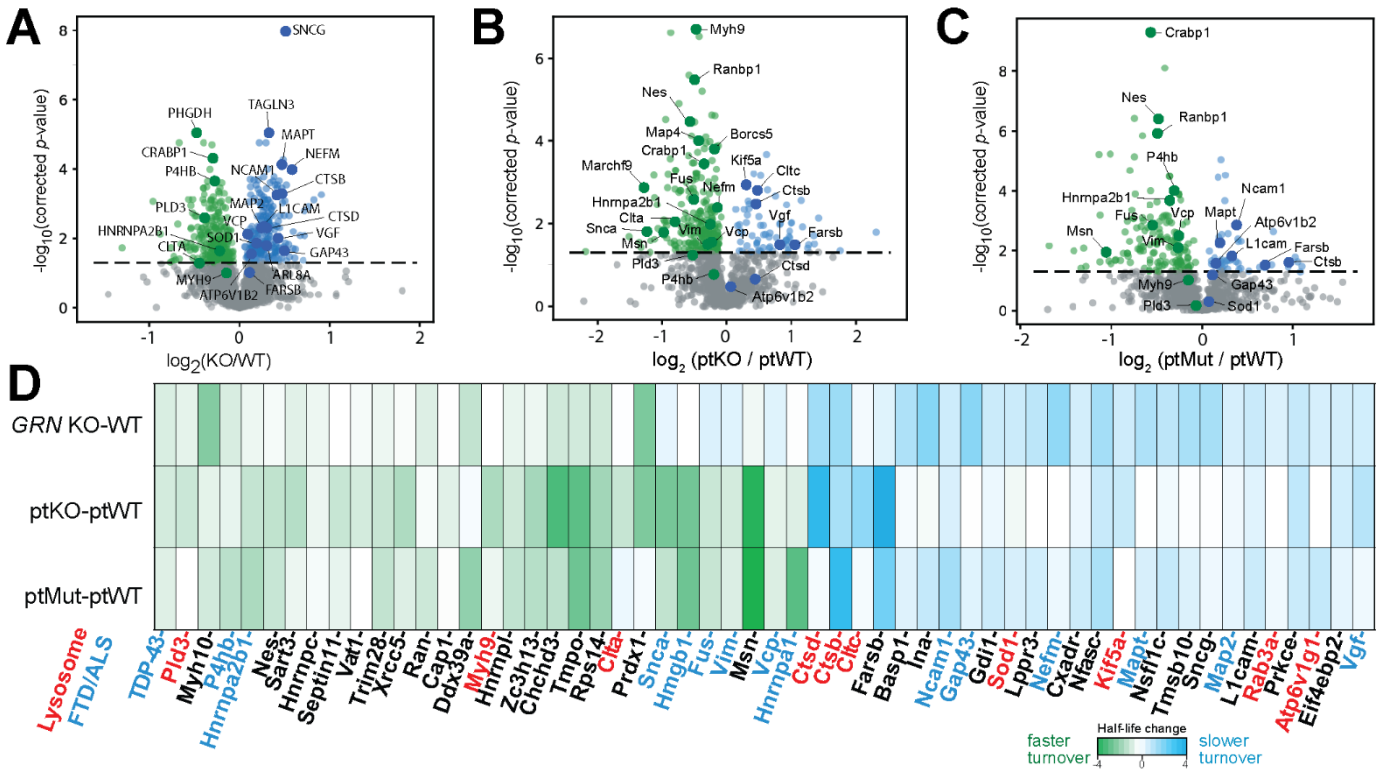

Figure 4-6: Frontotemporal dementia (FTD) patient-derived i^{3}Neurons with mutant *GRN* reveal altered protein turnover of lysosomal enzymes and FTD-associated proteins.

(A) Patient derived i^{3}Neurons (pMut) were used and compared to its isogenic control (pWT) and complete knockout (pKO). **(B)** Volcano plot of protein half-life changes in ptKO vs. ptWT i^{3}Neuron. **(C)** Volcano plot of protein half-life changes in ptMut vs. ptWT i^{3}Neuron. **(D)** Heatmap showing overlapped protein turnover changes in days in all *GRN* KO, Mutant, and WT i^{3}Neurons. Heatmap colors represent the absolute half-life differences between comparison groups. Key proteins from lysosomes and relevant to FTD/ALS are highlighted in red and blue, respectively. *Contribution: cell line ptKO was generated by LH, dSILAC experiment was carried out by RP for GRN KO-WT and SH for ptKO-ptWT and ptMut-ptWT. Analysis was conducted by LH and SH.*

4.4.5 Mouse Brains Lacking Progranulin Upregulate Complement Markers

Considering the unique identities of neuronal lysosomes, it is crucial to assess the potential impact of non-neuronal lysosomes in the disease. As part of this objective, I aimed to collect proteins in proximity to all lysosomes from whole brains *in situ*, utilizing the well-established *GRN*$^{-/-}$ mouse model mentioned in the methods section of this chapter. Whole brains were preferred over 2D tri-culture models (neurons, astrocytes, microglia) *in vitro* due to their better representation of the *in vivo* environment. The enhanced BAR method, as described in Chapter 3, was utilized for this purpose. I targeted lysosomes by using Lamp1 as the bait protein, which I will refer to as Lyso-BAR going forward. Samples were prepared for mass spectrometry as detailed in Chapter 3.

A total of 201 proteins exhibited a significant difference in abundance between *GRN*$^{-/-}$ and WT brains, with 91 increased in *GRN*$^{-/-}$ (**Figure 4-7A**). The lysosomal proteins identified as enriched in Lyso-BAR from WT samples relative to the negative control in **Figure 3-10B** of Chapter 3 were used to highlight their alterations in the *GRN*$^{-/-}$ samples, as depicted in the volcano plot with labelled proteins. Surprisingly, there was a limited overlap between the Lyso-IP and Lyso-BAR datasets, with only 20 shared proteins. This finding was unexpected as more overlap was anticipated. The difference in protein capture could be attributed to the Lyso-BAR method targeting lysosomal changes from other cell types, as well as proteins in the lysosomal vicinity. This further highlights the significance of examining disease-relevant alterations *in situ*. GO term analysis on the 91 increased proteins in *GRN*$^{-/-}$ identified top KEGG pathway terms as lysosome, consisting of proteins such as HexB, Psap, Ap3d1, Tpp1, Ctsb, and Ctsd, all of which except Ap3d1 have been linked to progranulin (Zhou et al., 2017a; Zhou et al., 2017b; Butler et al., 2019; Huang et al., 2020).

Other KEGG terms included endocytosis, autophagy, and antigen processing and presentation (**Figure 4-7B**). The biological process analysis showed that the top term was neutrophil-mediated immunity, which included lysosomal proteins like HexB, Psap, Ctsd, and Ctsb, as well as non-lysosomal proteins such as Surf4, Rhog, Huwe1, Erp44, Ncstn, Psmc2, Rab18, Pgm1, and Hspa1a. It is worth noting that the Lyso-BAR method captures proteins within a 200-300nm radius of the lysosome, which includes both inside and outside the lysosome. Other biological processes included endocytosis, autophagy and response to starvation (**Figure 4-7B**).

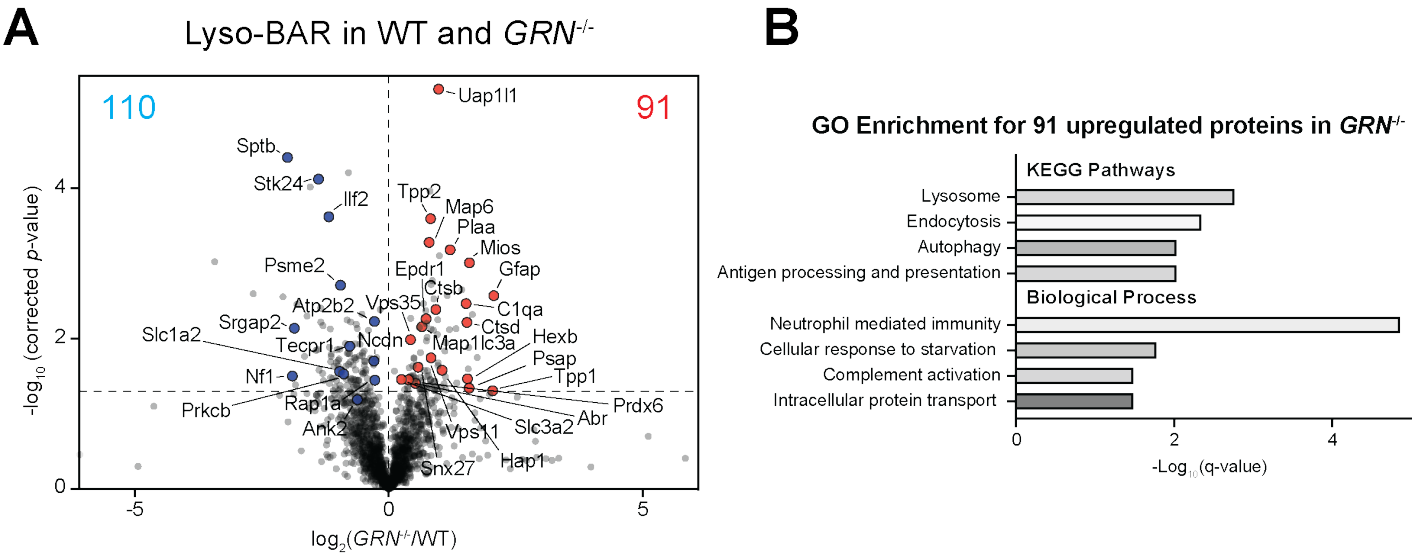

Figure 4-7: Mouse brains lacking progranulin upregulate pathways associated with autophagy, starvation response and complement activation.

Lyso-BAR was performed on wildtype and *GRN*$^{-/-}$ mice at 20 months of age followed by LC-MS/MS. Each group had 4 biological replicates. **(A)** Volcano plot shows a total of 201 proteins as differentially abundant in *GRN*$^{-/-}$ compared to WT. Labelled proteins are lysosomal. **(B)** A GO term analysis on the 91 upregulated proteins shows KEGG pathways associated with relevant terms. Biological process GO terms show an immune response and complement activation.

Previous proteomic studies by Klein et al. and Huang et al. have also reported an increase in proteins such as Ctsb, Ctsd, HexB, Tpp1, Stx7, C1qa, C1qb, Gfap, Uap1|1, and Psap in the brains of *GRN*$^{-/-}$ mice (Klein et al., 2017; Huang et al., 2020). To ensure relevance of the findings to the study at hand, I focused on the Huang et al. dataset as it includes samples from 3- and 19-month-old mice, which are closer in age to the 20 month old mice used in my study, compared to the mice used in the Klein et al. study. There was a 25% overlap between the 91 upregulated proteins detected in Lyso-BAR and the upregulated proteins identified in the Huang et al. proteomics dataset (**Figure 4-8A**). This overlap is reasonable, considering that the Huang et al. dataset was based on whole brain lysates, while the Lyso-BAR specifically targeted lysosomes. The 9 proteins seen upregulated in all 3 datasets were C1qa, C1qb, Uap1|1, HexB, Tpp1, Ctsd, Ctsb, Stx7, and Psap. These are highlighted in the string analysis with node size and shade denoting fold change and significance respectively using Lyso-BAR values (**Figure 4-8B**). Grey nodes were unchanged. Complement proteins have been shown to be increased in these mice before resulting on complement-mediate pruning of synapses (Lui et al., 2016). HexB, Tpp1, Ctsb, Ctsd, and Psap are lysosome enzymes that are known to be upregulated in these mice (Huang et al., 2020).

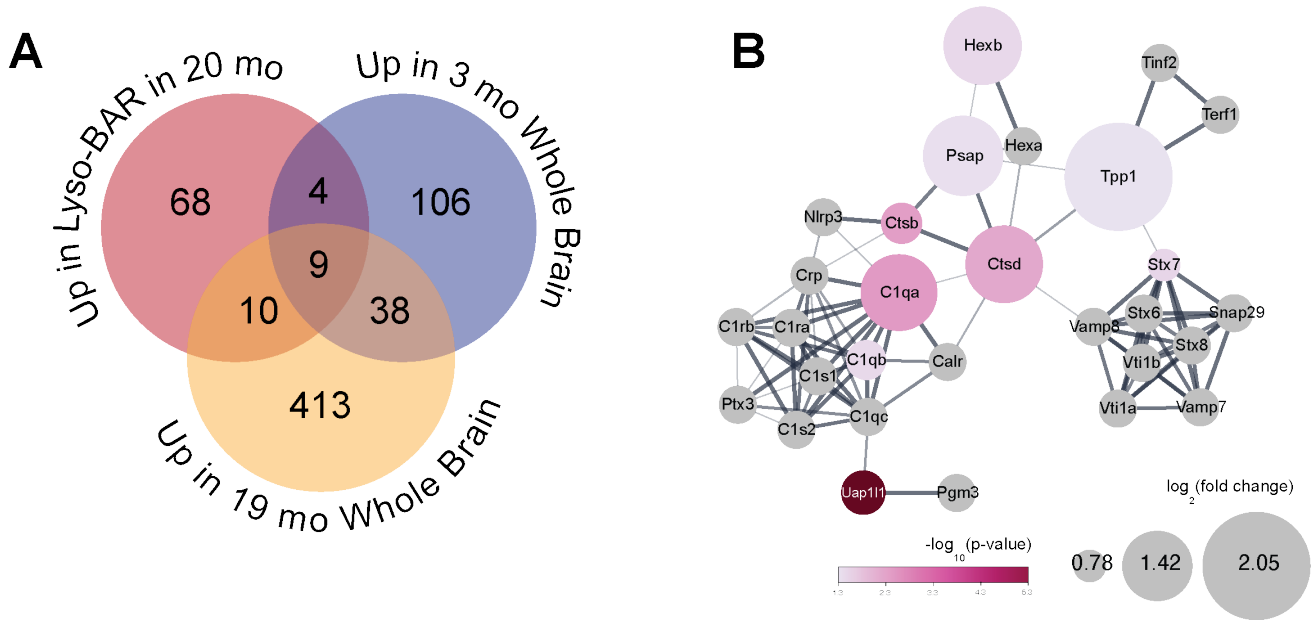

Figure 4-8: Progranulin lacking lysosomes have more synaptic and complement peptides.

(A) Up regulated proteins from Lyso-BAR (91 proteins) were compared to whole brain proteomics on *GRN*$^{-/-}$ mice at 3 and 19 months of age from Huang et al., 2020. Of 91 proteins, 23 were also upregulated in Huang et al. dataset. **(B)** The 9 common proteins between the 3 datasets are represented as colored nodes with their respective fold change and significance. Source: string-db.org.

The Lyso-BAR dataset is distinct because it focuses primarily on lysosomes. Consequently, I conducted a GO term enrichment analysis on the 68 proteins exclusive to my dataset. The results revealed that "synapse" was the most enriched term with a high number of genes and strong statistical significance in the Lyso-BAR dataset (**Supplemental Figure 4-6**). This finding is intriguing given the upregulation of complement and autophagy related proteins. It suggests a possible link between lysosomal dysfunction and synaptic protein degradation. Post-synaptic receptors can either be degraded by lysosomes or reinserted through endosomes, depending on the synaptic stimulus. Previous

studies have emphasized the importance of lysosomal degradation in normal synaptic plasticity (Ehlers, 2000; Fernández-Monreal et al., 2012). It is interesting to note an increased presence of synaptic proteins near lysosomes in cases of progranulin loss. Further investigation is needed to determine whether this increase is due to protein buildup or enhanced trafficking towards the degradation pathway. The upregulation of complement proteins could also indicate neuroinflammation, a common feature of neurodegenerative disorders. It is important to note that HexB has been previously reported to be predominantly expressed in microglia, indicating that significant non-neuronal changes are also occurring in the *GRN*$^{-/-}$ model (Hickman et al., 2013; Masuda et al., 2020). Others have shown that complement proteins, as seen here with C1qa and C1qb, are expressed by microglia that results in engulfment of synapses in disease conditions (Hong et al., 2016; Lui et al., 2017; De Schepper et al., 2023). Further investigation into the microglial changes seen in *GRN*$^{-/-}$ brains is warranted.

4.5 Discussion

In this study, I demonstrated that lysosomes lacking progranulin in i^{3}Neurons have elevated levels of catabolic enzymes and pH-maintaining proteins but have decreased degradative properties as shown with decreased Ctsb activity and dysregulated protein turnover rates. I also showed that lysosomes from whole mouse brains lacking progranulin have higher levels of lysosomal proteins in addition to autophagy and antigen presenting proteins. Most intriguingly, I observed increased synaptic proteins in these lysosomes using Lyso-BAR from progranulin-lacking mouse brains.

4.5.1 Loss of Progranulin Leads to an Increase in Lysosomal Enzymes

Others have consistently shown that progranulin facilitates localization of proteins to the lysosome and it directly interacts with various lysosomal proteins including prosaposin (Psap), Sortilin, CD68, and proCtsd to name a few (Hu et al., 2010; Zhou et al., 2015; Zhou et al., 2017a; Butler et al., 2019; Santos et al., 2022; Du et al., 2022). Sortilin is cell surface receptor on neurons that binds to and trafficks progranulin into the cell and to the lysosome (Hu et al., 2010). Loss of sortilin increases progranulin levels in the brain and serum. Prosaposin is a saposin precursor that activates lysosomal sphingolipid metabolizing enzymes (Matsuda et al., 2007). It binds to progranulin and provides a sortilin-independent pathway to lysosomes for progranulin (Zhou et al., 2015). CD68 is a lysosomal membrane protein expressed in myeloid cells (Chistiakov et al., 2017). Loss of progranulin results in an increase in CD68 levels but a decrease in its molecular weight whereas loss of CD68 leads to decreased levels of granulin E (Santos et al., 2022). And finally, progranulin binding to proCtsd destabilizes the structure, thereby allowing intermolecular cleavage to the mature form (Butler et al., 2019). However, it is interesting to note that Ctsd, unlike other cathepsins, does not cleave progranulin (Mohan et al., 2021). This suggests that progranulin has undiscovered functions within the lysosome that warrant further investigation.

In the Lyso-IP dataset comparing *GRN* KO lysosomes to wildtype from i^{3}Neurons, I have shown that loss of progranulin leads to increased steroid biosynthesis enzymes in the lysosome. One of these enzymes is lathosterol oxidase (Sc5d). Typical sites of steroid biosynthesis are mitochondria and endoplasmic reticulum, and it is interesting to note these proteins in the lysosome (Sewer and Li, 2008; Duarte et al., 2012).

Progranulin loss has been linked to lysosomal lipid metabolism changes and this is consistent with that (Evers et al., 2017). However, Evers et al. have shown that whole brain transcriptomics from progranulin lacking mice have decreased levels of Sc5d transcripts (Evers et al., 2017). This is a clear example of how transcript levels do not necessarily correspond with protein levels. One interpretation of this data could suggest that there is decreased degradation of this enzyme as it accumulates in the lysosome, prompting the cell to counteract this increase by down-regulating transcription. A confirmation experiment for this hypothesis would be to check for Sc5d transcripts in our i^{3}Neurons lacking progranulin.

Other enzymes with increased abundances in the lysosome were arylsulfatases. Loss of arylsulfatases lead to metachromatic leukodystrophy, a lysosome storage disorder (DeLuca et al., 1979; Fluharty et al., 1991). No direct links have been made between progranulin and arysulfatases, yet here I show that with loss of progranulin, arysulfatase A, arysulfatase I and arysulfatase F are all increased in abundance in the lysosome. Since arysulfatases have not been studied in the context of progranulin loss, it would be crucial to follow up on progranulin's role in arysulfatase activities.

4.5.2 Progranulin Deficiency Leads to Lysosomal Degradation Dysregulation

Consistent with what others have shown, I also observed increased levels of lysosomal pH-maintaining proteins congruent with progranulin's involvement in acidifying lysosomes (Tanaka et al., 2017). Subsequently, our lab has shown that progranulin lacking lysosomes in i^{3}Neurons are more alkaline than their wildtype counterparts (Hasan et al., 2023). This is relevant for the cathepsins that reside and operate in the lysosomes.

Cathepsins are initially produced as inactive precursors, or zymogens, which require cleavage to become mature and active enzymes (Turk et al., 2001). Specifically, Ctsb, an enzyme affected by progranulin, has an optimal pH of around 4.5 (Mach et al., 1994; Rozman et al., 1999). At neutral pH, the propeptide is bound to the active site, keeping the enzyme inhibited. As pH lowers, conformation of the proenzyme loosens, allowing autocleavage (Fox et al., 1992; Quraishi et al., 1999). In line with Ctsb activity being pH dependent, I showed decreased Ctsb activity in *GRN* KO i^{3}Neurons, despite no changes in Ctsb abundance seen in the Lyso-IP dataset. Ths is consistent with progranulin-lacking lysosomes being more alkaline than wildtype (Hasan et al., 2023). However, this was different from what I and others have seen regarding upregulated levels of Ctsb in *GRN*$^{-/-}$ mouse brains (Huang et al., 2020). This is most likely due to cell-type differences as Lyso-IP data only takes neurons into account, whereas Lyso-BAR covers lysosomes from the whole brain including glia and other cell types. Note that the Lyso-IP data was obtained from human i^{3}Neurons, while the Lyso-BAR data was obtained from mouse whole brains. However, it is noteworthy that in the absence of progranulin, the turnover rate of Ctsb is reduced in i^{3}Neurons, as demonstrated in the dSILAC dataset. Of note, Ctsd, a known progranulin interactor, also had a slower turnover rate in the absence of progranulin (Zhou et al., 2017b). However, it is unexpected that the Lyso-IP KO data did not show an increased abundance of these proteins, which has been consistently observed by others (Evers et al., 2017; Telpoukhovskaia et al., 2020; Huang et al., 2020). Moreover, considering their slower turnover rate, these proteins are either not being synthesized as fast or not being degraded as efficiently as in wildtype. This should result in a buildup of these proteins, but that is not observed in my data. One possible explanation for the lack of increase could be the relocalization of these proteins outside the lysosome. Ctsb leakage into the cytosol has been

linked to apoptosis and inflammation (de Castro et al., 2016; Amaral et al., 2018). It would be crucial to perform whole cell lysate immunoblots from i^{3}Neurons to determine whether there are any differences in the total amount of these cathepsins. Such studies could shed light on unknown downstream effects, such as cell death or inflammation, resulting from the relocalization of these proteins.

4.5.3 Progranulin-Null Mouse Brains Have Increased Lysosome and Complement Associated Proteins

Du et al. have shown that microglia have a prosaposin and sortilin independent mechanism of trafficking progranulin to their lysosome via an unknown mechanism (Du et al., 2022). This provides insight into how progranulin may play different roles in different cells. Strikingly, complement proteins were upregulated in progranulin lacking Lyso-BAR data. Though Lyso-BAR enriches for lysosomal proteins, it also captures proteins in proximity to those lysosomes. This is both a limitation and advantage. Although I cannot be certain that the proteins I pull down are strictly lysosomal, I can be confident that they are within the lysosome's interactome given the highly enriched lysosomal proteins captured in the bait group vs no bait group (Chapter 3; **Figure 3-10B**). Being cognizant of that, I also note synaptic proteins as more abundant in the Lyso-BAR data from *GRN*$^{-/-}$ brains. It is important to note that Lyso-BAR encompasses all cell types in the brain, and thus, the observed changes may predominantly originate from cells that are most affected by progranulin deficiency. Progranulin is highly expressed by microglia and is known to be upregulated in reactive microglia (Petkau et al., 2010). Progranulin deficient microglia have been shown to prune synapses in a complement-mediated manner before (Lui et al., 2016). Along the same lines, the Lyso-BAR *GRN*$^{-/-}$ data shows an elevation in proteins associated with the

complement system. This data, therefore, supports the argument for examining how microglia change with loss of progranulin next.

In summary, I have shown lysosomes lacking progranulin from human i^3Neurons have increased levels of catabolic enzymes and pH maintaining proteins. These same lysosomes harbor enzymes that are less active and therefore have decreased degradative properties. I have shown that these changes lead to an altered turnover rate of proteins that are associated with other neurodegenerative diseases. In mice, I have reproduced previously seen data where others have shown increased lysosomal enzymes and complement associated proteins in progranulin deficient brains. I have also shown an increase in synaptic proteins in proximity to lysosomes in the absence of progranulin whereas others have shown a general decrease in synapses in these mice. Overall, these findings provide further evidence for the important role that progranulin plays in maintaining proper lysosomal function and protein degradation.

Chapter: 5 Loss of Progranulin Leads to a Reactive Microglial Response

5.1 Introduction

5.1.1 Role of Progranulin in Microglia

Microglia express higher levels of progranulin during development than neurons, and its expression increases in microglial lysosomes when they respond to injury (Moisse et al., 2009; Petkau et al., 2010). Interestingly, microglia lacking progranulin are more prone to becoming inflammatory, as they release higher levels of proinflammatory cytokines (such as TNF-α, IL-6, and IL-1b) when exposed to LPS/IFN-γ and show increased expression of the lysosomal marker CD68 when exposed to traumatic injury (Martens et al., 2012; Tanaka et al., 2013). Loss of progranulin in microglia leads to increased complement-mediated synaptic elimination, independent of neuronal loss of progranulin (Lui et al., 2016). This emphasizes the importance of progranulin as a suppressor of microglial-mediated synaptic pruning through the complement system. During aging, microglia accumulate lipid droplets. However, mice lacking progranulin exhibit a significant increase in the build-up of lipid droplets when compared to wildtype. This highlights the ability of progranulin to delay the development of lipid droplets in aging microglia (Marschallinger et al., 2020). Progranulin loss has been shown to result in the

accumulation of pro-cathepsins within microglial lysosomes hindering cathepsin maturation. This led to the upregulation of lysosomal activity in other cell types (Götzl et al., 2018). Additionally, thalamic microglia from progranulin deficient mice decrease homeostatic markers such as P2ry12 and Tmem119, and upregulate genes implicated in inflammation, lysosomal function and neurodegeneration starting at 7 months and progressing to 19 months when compared to wildtype (Zhang et al., 2020).

Based on the available information, it appears that progranulin plays a role in modulating microglia's proinflammatory function in the brain. However, there is still much to be elucidated in order to fully comprehend the contribution of microglia to disease progression.

5.1.2 Challenges of Studying Microglia in Isolation

Microglia, the resident immune cells of the brain, undergo transcriptional changes throughout their life cycle (Orre et al., 2014; Pan et al., 2020). As they age, microglia become more amoeboid with less complex branching indicative of a primed state (Perry et al., 1993; Divangahi et al., 2021). Aged microglia have a more pronounced proinflammatory response to injury than juvenile microglia suggesting increased sensitivity to insults (Godbout et al., 2005; Keane et al., 2021). Studies have demonstrated that aged microglia express higher levels of proinflammatory cytokines, major histocompatibility complex II (MHC II), and pattern recognition receptors in rodents and humans (Perry et al., 1993; Ogura et al., 1994; Streit and Sparks, 1997; Sheffield and Berman, 1998; Streit et al., 2004; Henry et al., 2009). While changes in gene expression can provide valuable information, proteomic analysis allows for a more comprehensive understanding of the complex protein networks involved in cellular processes. Studies have shown that proteomics can

provide 10-to-20-fold better capture than transcriptomics, and sometimes even capture twice as much information (Sharma et al., 2015; Specht et al., 2021; Johnson et al., 2022). Therefore, proteomics is a better approach to defining microglial states. Furthermore, studying protein-protein interactions can provide insights into the cellular processes that are disrupted in ageing and disease.

Microglia are specialized to sense and react to their environment (Davalos et al., 2005; Nimmerjahn et al., 2005). Butovsky and colleagues have shown that cultured microglia and immortalized microglial cell lines transcriptionally differ from freshly isolated microglia from mouse brains (Butovsky et al., 2014). This creates the challenge of capturing microglial identity *in vivo* without capturing changes influenced by the *in vitro* environment. Therefore, to study unaltered microglia in their natural state, one ideal method is the Biotinylation by Antibody Recognition method, which has been previously tested in Chapters 3 and 4. This method involves using HRP conjugated antibodies against primary antibodies to proteins of interest in fixed tissue. HRP conjugated antibodies are easily available and involve no genetic manipulation to generate cell lines. Despite some limitations of HRP compared to other proximity labeling enzymes such as APEX and BioID, it remains advantageous for proteomic studies. Although HRP has a larger labeling radius and depends on highly specific antibodies, it has the benefit of readily available commercial antibodies for desired targets. Another advantage of BAR is its utilization of fixed tissue, which enables the preservation of microglia in their most physiologic state before harvest. This allows for the capture of microglia in their various states in the brain without any artifacts associated with the isolation of live microglial cells for proteomics or their response to injury at the time of harvest. Therefore, in this chapter, I aimed to characterize the microglial lysosome and potential interactome, using microglial-BAR in mouse brains.

Here, microglial lysosomes were examined using the Lyso-IP technique described in Chapter 4 on human inducible pluripotent stem cell-derived microglia (iMG) to compare lysosomes with and without progranulin. Considering the limitations of *in vitro* systems in studying microglia, the BAR method described in Chapter 3 was also utilized to analyze microglial differences *in situ* in progranulin-deficient mouse brains. Microglial-BAR revealed changes related to lysosomal, immunity, protein transport, and synapse proteins in the vicinity of microglia in progranulin-deficient brains.

5.1.3 Aims

- Characterize human iMicroglial lysosomes.
- Characterize progranulin-lacking microglial lysosomes.
- Determine interactome of microglial lacking progranulin.

5.2 Methods

5.2.1 *GRN* KO iMicroglia

6-TF-iMG lines received from Dr. Martin Kampmann and cultured as described by Dräger et al. in Chapter 2 (Dräger et al., 2022). These cells were matured till day 8, which is when they become ramified and express the canonical microglial markers GPR34 and IBA1. These microglia have also been shown to be phagocytically active at this age (Dräger et al., 2022).

5.2.2 Lysosomal Immunoprecipitation Cell Lines

6-TF-iMG lines received from Dr. Martin Kampmann (Dräger et al., 2022). These lines were transduced with LAMP1-3xHA lentiviral and TMEM192-3xHA plasmids into WT (WTC11; Coriell Institute #GM25256) and *GRN* KO (7/10; WTC11 with a 7 base pair insertion in one GRN allele and 10 base pair deletion in the other *GRN* allele resulting in complete loss of function generated in house) genetic backgrounds. A TMEM192-mEmerald-expressing line was used as a control for nonspecific pulldowns.

5.2.3 *GRN* KO Mouse Model

Mouse models used were WT:C57BL/6 (Jackson Labs) and *GRN*$^{-/-}$: B6.129S4(FVB)-Grn$^{tm1.1Far}$ (Jackson Labs). The *GRN*$^{-/-}$ line was thoroughly backcrossed into C57BL/6 before being used. The animals were housed in the National Institutes of Health (NIH) animal facility that followed the U.S. Department of Health and Human Services Public Health Service Policy on Humane Care and Use of Laboratory Animals for animal husbandry and euthanasia. Three female and one male mice aged 6-8 months were used for this study.

5.2.4 Microglial Proximity Labeling

Four biological replicates were used as described before. For each biological replicate, I picked 21 slices evenly from the whole brain. The slices were treated as described in Chapter 3 for the BAR protocol. Bait protein was P2Y12 (AnaSpec #AS-55043A used at 1:3000). All other secondaries are mentioned in Chapter 2.

5.3 Results

5.3.1 iMicroglia Can Be Used to Isolate Intact Lysosomes

There is a lack of research on whether microglial lysosomes differ from those found in other cell types. Progranulin is a lysosomal protein that is highly expressed in microglia during development and activation, while neurons only upregulate it in mature states (Petkau et al., 2010). CD68 is also a lysosomal protein that is often used as a microglial marker. Despite these findings, there have been no investigations into the inherent differences in lysosome composition between microglia and other cells. Only one study has compared primary microglia to an immortalized macrophage line, J774, and found that microglial lysosomes have increased levels of proteases but a more alkaline pH when unperturbed. Upon activation by LPS, IL-6, or MCSF, microglial lysosomes become more acidic and degradative (Majumdar et al., 2007). Based on this, it is important to investigate microglial lysosomes in disease states. Given the important role lysosomes play in microglial biology, I conducted a preliminary study aimed at characterizing microglial lysosomes by isolating them from cultured microglia. By using the technique developed by our laboratory to extract intact lysosomes, I isolated lysosomes from human iPSC-derived microglia that were generously provided by Dr. Martin Kampmann (Dräger et al., 2022) and genetically modified by Dr. Michael Fernandopulle and Dr. Allison Snyder in our lab. I tested two iMG lines with different lysosomal HA tags to determine the most effective line. The iMG iPSCs were modified to have HA tagged to either LAMP1 or TMEM192, both of which are lysosomal membrane proteins. I isolated lysosomes from both lines at 8 days post-differentiation using the immunoprecipitation technique described in Chapters 2 and 4. To test for

purity of the pull down, I conducted a Western blot using various markers to assess efficiency of the pull down (**Figure 5-1**). As seen in **Figure 5-1**, pulldowns from both lines were enriched for lysosomal markers LAMP2 and CTSD. However, other contaminants were also detected such ER (calreticulin), Golgi (golga1), Catalase and mitochondria (VDAC). After comparing the results from both iMG lines, it was observed that the TMEM192-HAx3 line had lower levels of contamination than the LAMP1-HAx3 line approximately. Hence, for all subsequent experiments, I chose to use the TMEM192-HAx3 line to isolate lysosomes.

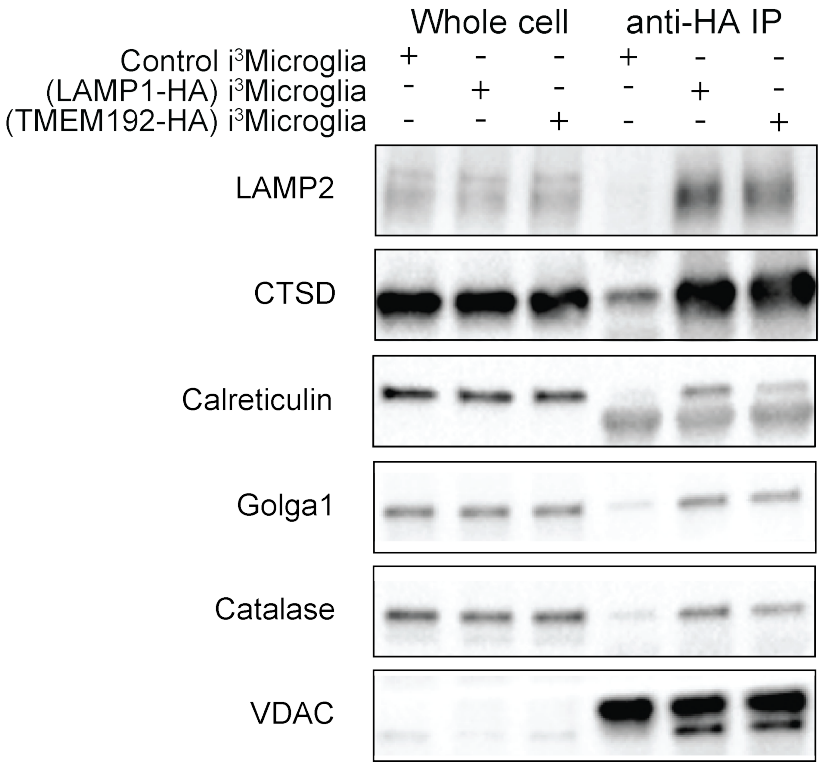

Figure 5-1: HA tagged to TMEM192 pulls down cleaner lysosome lysates than HA tagged to LAMP1.

Day 8 iMicroglia differentiated from human iPSCs were used to pull down intact HA-tagged lysosomes via anti-HA magnetic beads. Lysosomes tagged with the green-fluorescent protein Emerald to TMEM192 were used as controls. Markers for lysosome (LAMP2 at 100-130 kDa, CTSD at 31 kDa),

cytoplasm (P70S6K at 70-85 kDa), peroxisome (catalase at 55 kDa), endoplasmic reticulum (calreticulin at 57 kDa), Golgi apparatus (golga1 at 97 kDa), and mitochondria (VDAC at 30 kDa) were used to assess pull-down purity.

To control for non-specific proteins binding to HA-beads, an iMG line expressing TMEM-192 tagged to monomeric Emerald, which was generated by Dr. Michael Fernandopulle, was used. Since monomeric Emerald theoretically has no interactions, this line serves as a control for non-specific binding proteins. I processed the samples for mass spectrometry as described in the methods and the mass spectrometry was performed by Dr. Andy Qi. In the analysis, a total of 240 proteins were detected that were found to be significant, with 118 of these proteins being enriched (fold change > 0) in the bait group and 122 of them being de-enriched (fold change < 0) as shown in **Figure 5-2A**. Additionally, the bait protein Tmem192 was also detected as enriched in the analysis, as depicted in **Figure 5-2B**. Furthermore, other known lysosomal proteins were also detected such as lysosomal membrane proteins including Lamp2, Pip4p1, Rab12, Glmp, Vps33b, Prcp, Rraga and Cpq (**Figure 5-2C**). Luminal proteins such as Grn, Cln5, Tpp1, Gla, and cathepsins (Ctss, Ctsl, Ctsh) were also enriched (**Figure 5-2C**). A complete list of the 40 lysosomal proteins identified using unirpot.org shown in **Figure 5-2C** is listed in **Supplemental Table 5-1**.

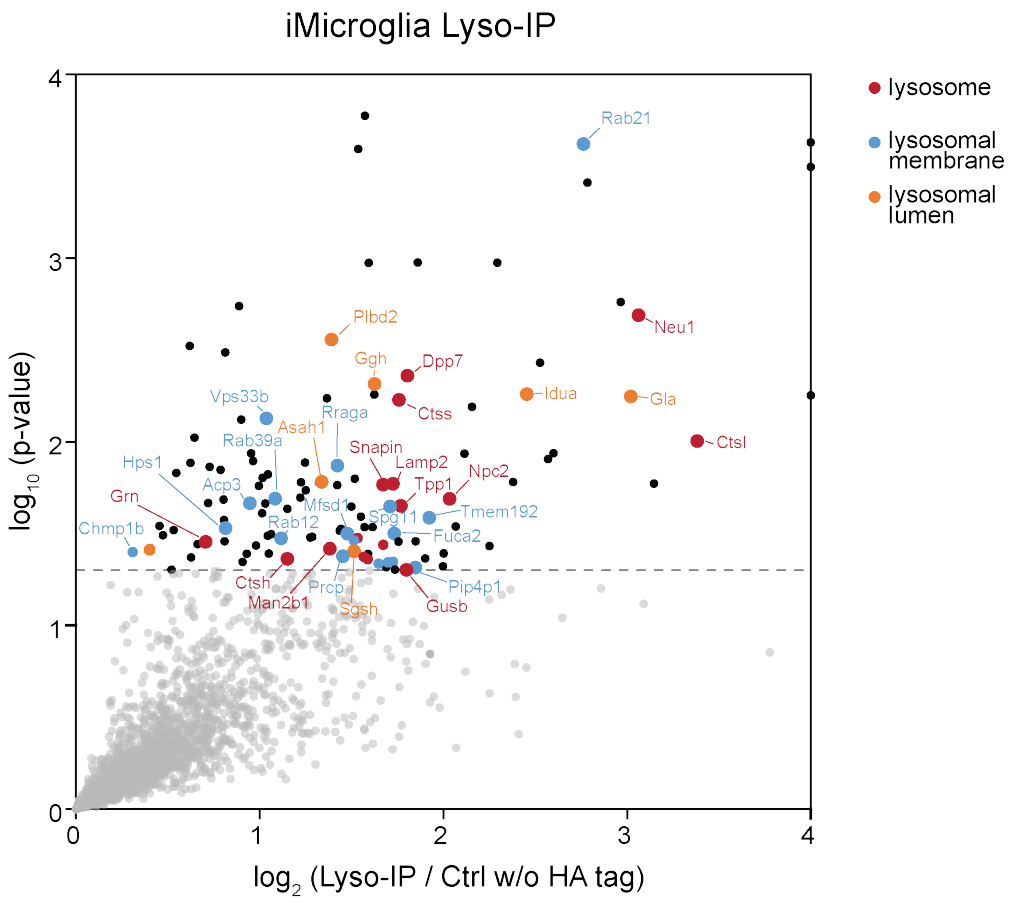

Figure 5-2: Lysosome associated proteins are isolated using HA tagged to TMEM192 from day 8 iMicroglia.

Volcano plot showing enriched proteins in the lysosome lysate from TMEM192-HAx3 line when compared to control (TMEM192-Em). Highlighted proteins are confirmed human lysosomal membrane and lumen proteins from uniport.org. A total of 118 enriched proteins were detected, 40 of which are classified as human lysosome lumen or membrane proteins.

The top GO terms for the 118 enriched proteins were lysosome and lysosome-related functions (**Figure 5-3A**). The GO term 'Lysosome' consisted of 37 proteins, 14 of which were lysosome lumen proteins seen in **Figure 5-2C**, including Gla, Naaa, Npc2, Tpp1, Man2b1, Gusb, Glb1, Ctss, and Ctsl. These are all enzymes with known functions in the

lysosome and linked to lysosomal storage disorders (uniport.org). The remaining 13 were lysosomal membrane proteins (**Figure 5-3B**). Lamp2 was classified as lysosome, lysosome lumen and lysosome membrane. Of note, Prcp is classified as a lysosomal membrane protein by uniport.org, however, Enrichr classifies it as both lysosomal lumen and membrane protein. It also categorizes it as lysosome only.

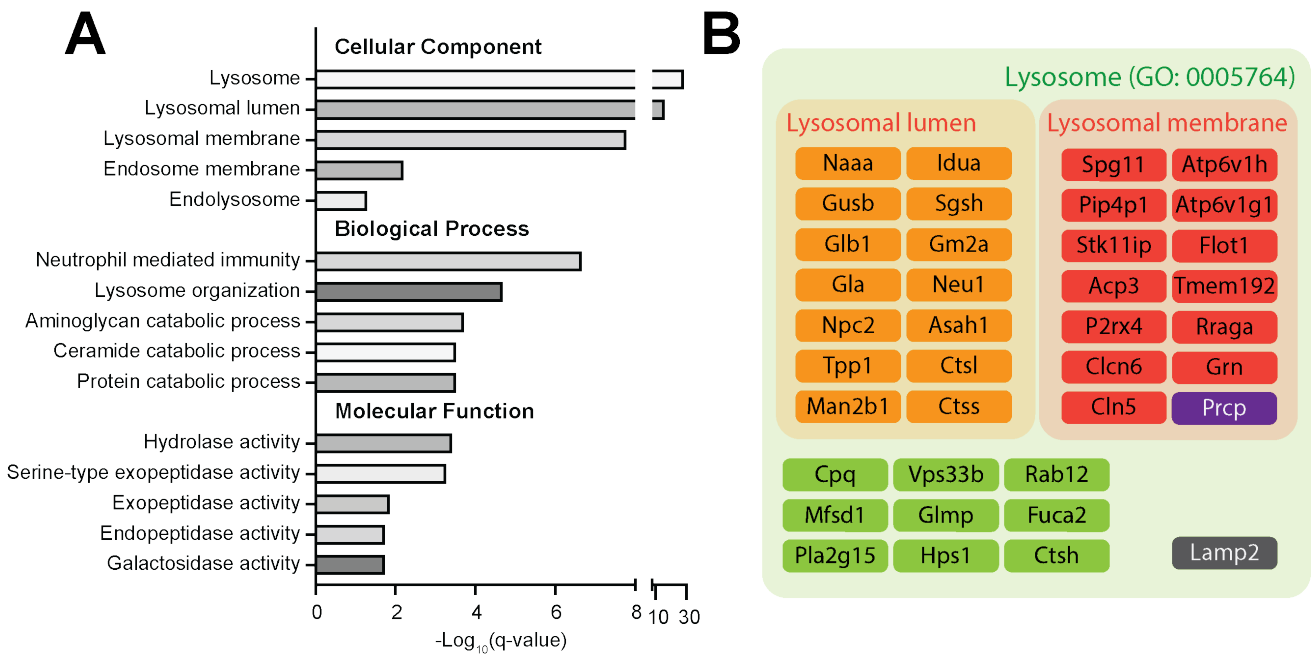

Figure 5-3: Lysosome lysates are enriched for lysosomal proteins.

(A) GO term analysis for the 118 enriched proteins reveals lysosomal terms as top hits using Enrichr. **(B)** Venn diagram shows all the proteins classified under lysosome, lysosomal lumen, and lysosomal membrane GO terms. Lamp2 is highlighted as grey to distinguish it as a shared protein between all three GO terms. Prcp is highlighted in purple to signify that it was classified as lysosomal membrane only.

Based on the GO analysis, the 122 de-enriched proteins that were detected at a higher abundance in the negative control than the bait group are likely to be non-specific proteins that are prone to sticking to surfaces.

There were no clear patterns detected with their KEGG GO terms, which included Yersinia infection, coronavirus disease, and Fc epsilon RI signaling. Additionally, the GO analysis revealed that the proteins were related to cellular components such as focal adhesion, cell-substrate junction, cytoskeleton, and molecular functions such as cadherin binding, RNA binding, and GTPase binding. I speculate that these proteins have a tendency to bind non-specifically.

Based on all the evidence presented, the results indicate that lysosomes can be successfully isolated from iMicroglia at 8 days *in vitro*, although some contamination may occur.

5.3.2 Further Optimizations are Needed to Characterize Lysosomes from iMicroglia Lacking Progranulin

Petkau et al. have shown that microglia express progranulin at higher levels than neurons during development, but at comparable levels during sensing states via immunohistochemistry in mice. However, they showed that in response to NMDA-induced excitotoxic injury via intrastriatal injections, microglia upregulate progranulin expression (Petkau et al., 2010). Microglia lacking progranulin have been shown to exhibit increased pro-inflammatory cytokine production, altered phagocytic activity, and reduced synaptic pruning efficiency (Lui et al., 2016). However, the effect of progranulin loss on microglial lysosome composition is still unknown. Therefore, my aim was to investigate changes seen in microglial lysosomes with loss of progranulin. I isolated lysosomes from day 8 iMG cells with and without progranulin and prepared the samples for mass spectrometry, which was performed by Dr. Andy Qi. The resulting volcano plot shows a total of 138 differentially abundant proteins in knock-out versus wildtype. Majority of these proteins (78.3%) were decreased in the

progranulin knock-out iMG lysosomes (**Figure 5-4A**). A GO term search revealed proteins involved in cell-substrate junctions, actin cytoskeleton, and positive-regulation of substrate adhesion-dependent cell spreading. Proteins classified as cell-substrate junction GO term included Akap12, Lasp1, Cnn3, Triobp, Rac1, Yes1, Rpl31, Ptpra, Pak4, Actc1, Bcar3, and Git2 (**Figure 5-4**). Bcar3 and Git2 were increased in *GRN* KO iMicroglia lysosomes whereas the rest were decreased when compared to WT. Akap12 is also known as Src-suppressed C kinase substrate or SSeCKS. It is not linked to microglia, other than in one study where the authors showed that after chronic constriction injury in the spinal cord, SSeCKS expression was found to be upregulated the most in neurons, followed by astrocytes, and then microglia, but with minimal expression detected in microglia compared to astrocytes and neurons (Xia et al., 2010). Lasp1 is involved in migration of medulloblastoma cells *in vitro*, however, no studies have linked Lasp1 to microglia yet (Traenka et al., 2010). Rac1 has been shown to be increased in microglia post-LPS stimulation resulting in amoeboid formation and is known to have LRRK2 bind to it resulting in a decrease in F-actin formation in microglia (Bettegazzi et al., 2021; Kim et al., 2022). As Petkau et al. have shown that progranulin expression is increased in microglia during development, its loss may affect the maturation of these iPSC-derived microglia *in vitro* (Petkau et al., 2010). Progranulin-null iMicroglia lysosomes have decreased levels of cell-substrate junction proteins in their lysosomes. This observation suggests that either these proteins are not being efficiently degraded within the lysosome or their synthesis is insufficient to maintain normal turnover rates. An alternative interpretation could be that the observed decrease in cell-substrate junction proteins in progranulin-null iMicroglia lysosomes is indicative of reduced cellular motility, as these proteins are crucial for cell adhesion and migration. In contrast, wildtype iMicroglia may be more motile, requiring higher levels of these proteins, which are being

efficiently degraded in their lysosomes. Further experiments, such as assessing the morphology of the cells using immunocytochemistry, evaluating the total protein amount of some of the hits using whole cell lysate immunoblotting, and measuring protein turnover rates using dynamic stable isotope labeling using amino acids in cell culture (dSILAC), would need to be performed to support this claim.

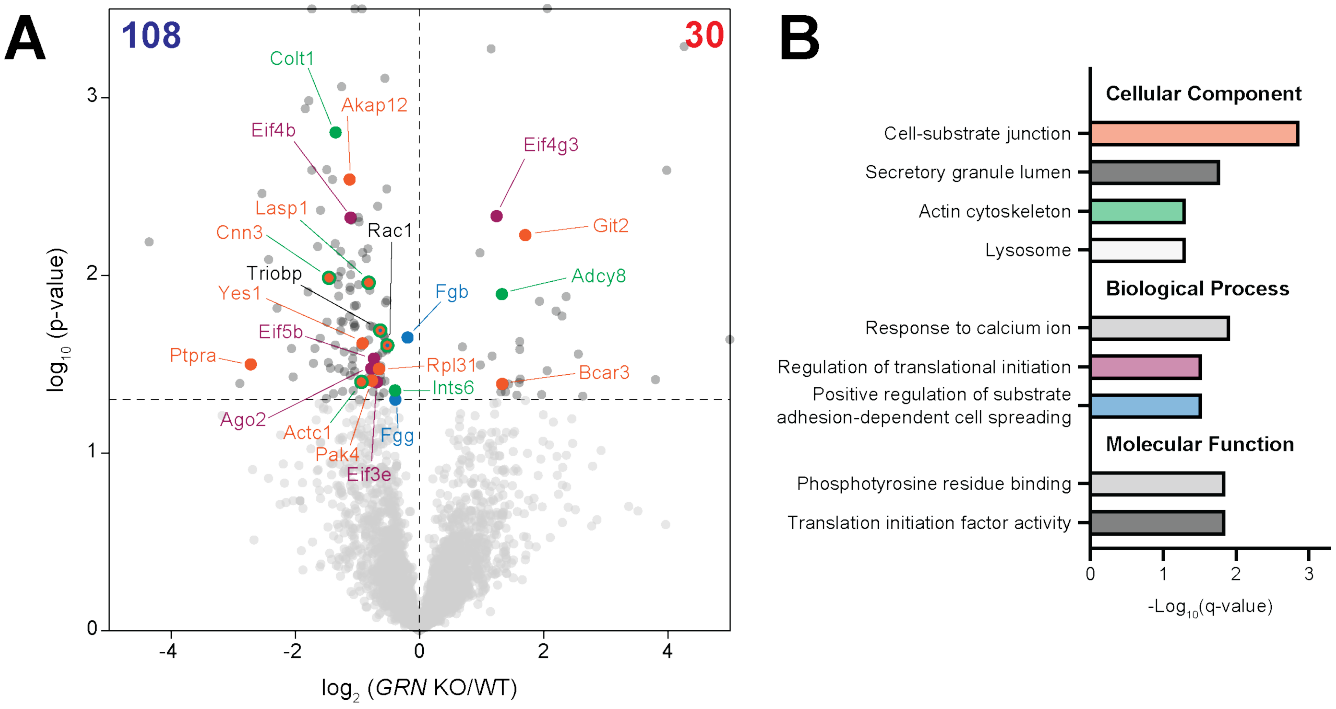

Figure 5-4: Progranulin lacking lysosomes from iMicroglia have altered abundance of proteins associated with translation and cell-cell junctions.

(A) A total of 138 proteins were detected with altered abundance in iMicroglia lysosomes lacking progranulin, majority of which were decreased in abundance. **(B)** Top GO terms for all 138 proteins are shown here. Colors represent proteins under that GO term. Non-colored bars are not represented on the volcano plot.

5.3.3 Progranulin Lacking Mouse Microglia Have Increased Lysosomal, Immunity, and Synapse-pruning Proteins in Their Vicinity.

Given the challenges with the iMG model, I pursued the well-established *GRN*$^{-/-}$ mouse model and set out to determine the interactome of microglia lacking progranulin. Progranulin-deficient mouse models have successfully been used to demonstrate how microglia are affected when progranulin is absent. Many have demonstrated that progranulin-deficient mice have increased staining for Iba1, CD68 and Gfap as these mice age, signifying increased micro- and astrogliosis (Yin et al., 2010; Tanaka et al., 2014; Lui et al., 2016). Therefore, for my purposes, an *in vivo* model is more appropriate as it allows for the development of microglia in their natural environment and is more representative of the physiological conditions. For this, I used *GRN*$^{-/-}$ and WT mouse brains and applied the BAR method targeting P2y12 for microglia at 6-8 months of age, a stage when microgliosis starts to increase (Yin et al., 2010; Nguyen et al., 2018). I first tested to see if there was any gross difference in the morphology of microglia between the control and *GRN*$^{-/-}$ brains. I did not observe any difference in soma size or branching pattern between the *GRN*$^{-/-}$ and WT microglia (**Figure 5-5**). I proceeded with the BAR method and sample preparation for LC-MS/MS analysis and the NIH Core conducted the run. The volcano plot shows a total of 103 proteins with differential abundance and is labelled for GO analysis terms on the 62 significantly increased protein abundances (**Figure 5-6A**). Proteins in the vicinity of microglia lacking progranulin were higher in levels for cell substrate junction (Adam9, Dnm2, Cnn3, Map2k1, Pdia3, Itgb7, Rpl7a, Ezr, Itgb2), membrane raft (Tpp1, Kcna5, Ezr, Itgb2, Ctsd), and lysosome associated proteins (Tpp1, Vps26a, Hexb, Psap, Stx7, Ctsd, Ctsb) (**Figure 5-6B**). This finding is consistent with previous research indicating that these mice have microglia with processes that are more prominent

and aberrant, and lysosomal abnormalities. Although no significant macroscopic changes were observed at this age here, these subtle changes detected by microglial-BAR may have been previously overlooked by others. Other affected biological processes were immunity (Ctsb, Ndufc2, Mif, Hmox2, Itgb2, Hexb, Psap), transport (Dnm2, Sar1a/b, Rab3b, Stx7, Itgb2, Arcn1, Vps26a) and synapse pruning (C1qa, C1qb) related. A consistently seen upregulation of uridylyltransferase was also noted in my dataset (**Figure 5-6B**; Uap1|1, Uap1). Of the 103 significant hits, 41 were decreased in the *GRN*$^{-/-}$ brain and their GO analysis is shown in **Supplemental Table 5-1**. It is interesting to note synaptic KEGG terms representing proteins such as Gnb3, Slc6a11, Gnai1, Adcy5, and Ppp3ca as being decreased in *GRN*$^{-/-}$ microglia interactome. This suggests decreased synaptic proteins in *GRN*$^{-/-}$ neurons which others have shown before (Petkau et al., 2012; Lui et al, 2016). Since the microglial-BAR method targets proteins within 200-300 nm of microglial processes, the decreased levels of synaptic proteins could indicate a reduction in the amount of these proteins in microglia's vicinity. However, it is unexpected that more ubiquitous synaptic proteins such as synaptophysin or PSD-95 did not show a similar reduction. Further investigation through immunoblotting and immunostaining is required to confirm this decrease.

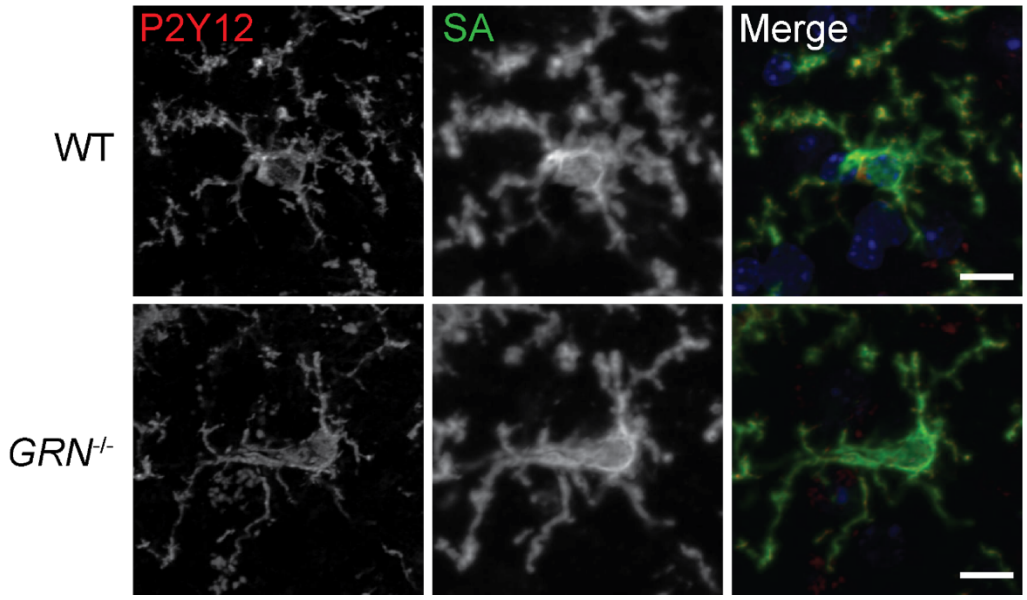

Figure 5-5: Biotinylated proteins colocalize with microglial marker in fixed mouse tissue.

Representative images of biotinylated proteins around microglia in WT and *GRN*$^{-/-}$ mouse cortex using BAR at 6 months of age. P2Y12 was used as a microglial marker, streptavidin (SA) was used to visualize biotinylated proteins. Scale bar is 10 μm.

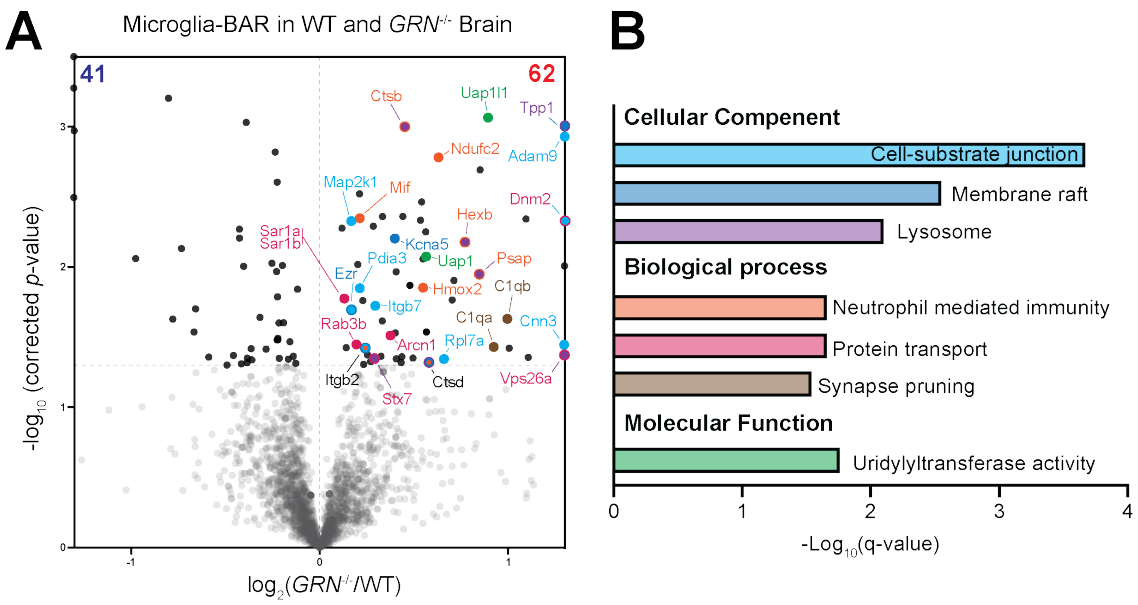

Figure 5-6: Microglia lacking progranulin have increased proteins associated with cell-cell junctions and lysosomes.

(A) 6-month-old mouse brains from WT and *GRN*$^{-/-}$ mice were used to generate volcano plot via LC-MS/MS analysis. A total of 103 proteins were detected with altered abundance, majority of which were increased. **(B)** GO term analysis of the 62 increased proteins is shown here. Color of the bars represents highlighted proteins in volcano plot.

Many studies have reported transcriptomic changes in progranulin deficient mouse brains, including dysfunctions in lysosomal, immunity, and lipid metabolic genes (Lui et al., 2016; Evers et al., 2017; Telpoukhovskaia et al., 2020; Zhang et al., 2020). However, proteomics data is still lacking. Only one such study by Huang et al. has been published thus far using whole brain proteomics (Huang et al., 2020). Huang and colleagues used *GRN*$^{-/-}$ mouse brains to show several proteins differentially regulated resulting in various networks to be identified. They also showed dysregulation of lysosomal and lipid metabolism proteins. They verified two of their hits (Gpnmb and Lgals3) in human FTD patient

brains to confirm the validity of using their mouse model. Here, I have taken it a step further and conducted microglia-centered proteomics using microglial-BAR on *GRN*$^{-/-}$ mouse brains at 6 months of age. Consistent with existing literature, proteins affected were associated with lysosomes and immunity. I compared my dataset with Huang and colleagues' dataset and when compared to their dataset, 29% of my upregulated hits overlap with their datasets (**Supplemental Table 5-2**). Given that their dataset is from whole brain lysates, whereas mine is from microglial-BAR, this overlap is promising. Upon a closer look at these overlapping proteins which consisted of Psap, Hexb, Tpp1, Ctsd, Ctsd, Vps26a, Arcn1, Stx7, Lsp1, Mif, Itgb2, C1qa, C1qb, Uap1|1, Cnn3, Tmem126a, Mtch2, and Fxyd1, we can see that they are involved in protein transport, catabolic process and complement activation (**Figure 5-7**). The string diagram shows my hits in color with no more than 20 interactors included. It is interesting to note that 9 of these 18 proteins shown in **Figure 5-7** were also seen in the Lyso-BAR data from **Figure 4-6** in Chapter 4. These proteins are shown in **Supplemental Table 5-2**. It is important to note that the data obtained from Lyso-BAR pertains to 20-month-old mice, which exhibit more pronounced pathophysiology compared to the 6-month-old mice utilized in microglial-BAR experiments. Consequently, the absence of Gpnmb or Lgals3 in the obtained dataset is likely due to the age-related discrepancy, as Huang et al. had observed this significant variance in 18-month-old mice. Taken together, microglial-BAR captures most significantly increased proteins in progranulin-lacking microglia as having functions involving lysosomal activity, vesicle transport, and complement-mediated response.

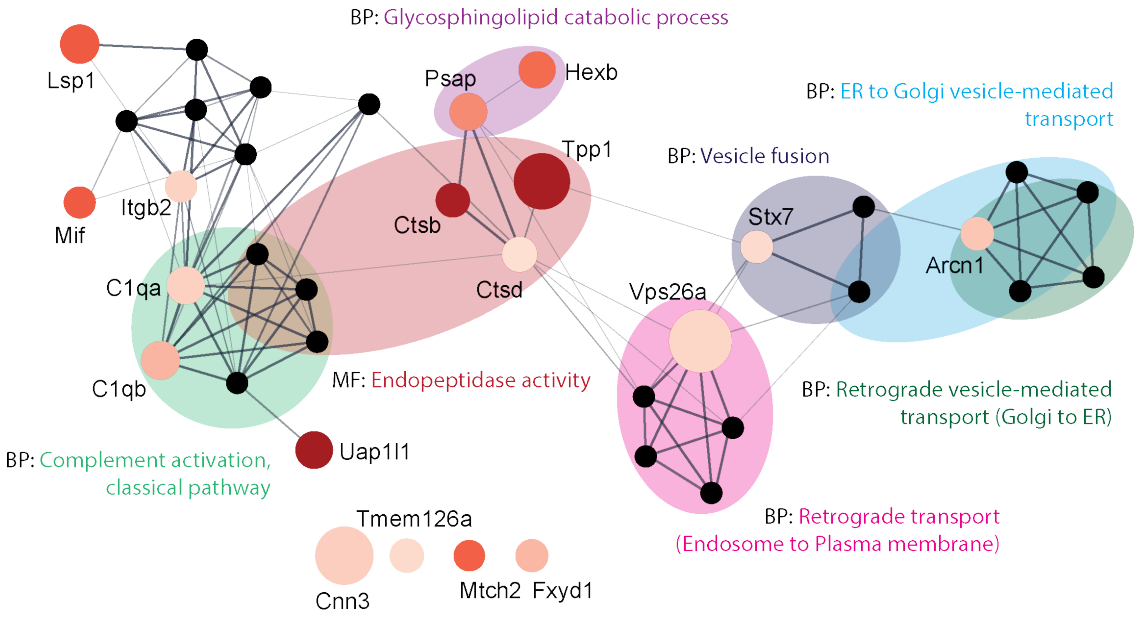

Figure 5-7: Literature confirmed hits from progranulin lacking microglia are associated with protein transport, lysosomal activity, and classical complement pathways.

18 proteins of the 62 increased in progranulin lacking mouse brains are shown in a string diagram here. GO term analysis is highlighted in the network. BP: biological process, MF: molecular function. No more than 20 interactors are included for each hit. Unlabeled nodes were not significantly altered in the dataset. The size of the nodes represents $\log_2$ fold change in increasing order, and the depth of color of the nodes denotes higher significance. All labelled nodes are significant.

5.4 Discussion

Here I've demonstrated that human iPSC-derived microglia (iMicroglia) can be scaled up to successfully pull-down lysosomes for proteomics. However, my results are preliminary, and more experiments are needed to be done to characterize the lysosome's proteome from progranulin lacking iMicroglia. And finally, I captured an *in situ* snapshot of mouse microglia interactome from *GRN*$^{-/-}$ brains showing an increase

in lysosomal, vesicle-mediated transport, and complement-associated proteins.

5.4.1 iMicroglia Can Be Used to Study Microglial Lysosomes

Typically, lysosomal immunoprecipitation experiments require large number of cells, such as whole organ lysate or 35 million cultured cells, as starting material (Bagshaw et al., 2005; Abu-Remaileh et al., 2017). This is a challenge given that only 5-12% of the mouse brain is microglial and isolating and maintaining such large pure primary cultures is challenging and expensive (Lawson et al., 1990; Nikodemova and Watters, 2012; Bohlen et al., 2019; Bordt et al., 2020). In order to circumvent that issue, iPSC derived cells can be cultured at large quantities to generate the sample size needed. We are the first to attempt scaling the iMicroglia line up for lysosomal pull downs. Although the isolation was not free from contamination of other cellular organelles such as ER, Golgi, mitochondria, and peroxisome, it did allow for enrichment of lysosomal proteins. Contamination in the pull-down assay could arise from various factors, including unknown components unique to the lysosome of microglia, either as a cell type or due to *in vitro* artifacts. The study by Abu-Remaileh et al. demonstrated that in human embryonic kidney (HEK) 293T cells, hemagglutinin (HA) tagged to transmembrane protein 192 (TMEM192) resulted in cleaner pull-downs compared to HA tagged to lysosome-associated membrane protein 1 (LAMP1). On the other hand, Xiong et al. demonstrated that fusing LAMP1 with Strep II tag, which mimics the high affinity interaction between biotin and streptavidin, resulted in highly pure lysosome pull-downs from HeLa cells. However, their study only examined this specific lysosomal protein as a tag target

(Xiong et al.,2019). Therefore, cell type-specific lysosomal properties cannot be excluded.

To account for cell type-specific lysosome composition, the Lyso-IP can be reattempted by tagging HA to CD68, a lysosomal marker specific to microglia in the brain. Additionally, a comparison of iMicroglia line to other established microglial cell lines such as BV-2 or HMC3 would be necessary to determine lysosome composition unique to microglia (Blasi et al, 1990; Janabi et al., 1995). However, transcriptional differences between these lines and primary microglia could contribute to false negatives (Butovsky et al., 2014). Another alternative, therefore, would be to use two of the six other iPSC-derived microglial protocols, although these protocols take much longer for differentiation than the 6-TF iMG cells used (Abud et al., 2017; Douvaras et al., 2017; Haenseler, Sansom, et al., 2017; Muffat et al., 2016; Pandya et al., 2017; Takata et al., 2017). Additional experiments could involve performing dynamic stable isotope labeling by amino acids in cell culture (SILAC) to determine if the observed decrease in proteins is due to longer half-life and decreased degradation. However, to ultimately understand the lysosomal content of microglia *in vitro*, it would be necessary to test lysosomal composition in iMicroglia at different stages of maturation.

5.4.2 Microglial-BAR as a Tool to Study *In Situ* Microglial Changes

To avoid the *in vitro* alterations that microglia undergo, I chose to implement the microglial-BAR method to *GRN*$^{-/-}$ brains. This allowed me to capture microglia *in situ* before harvest by fixing the whole brain via perfusion. Immunohistochemistry did not capture any differences between microglia with and without progranulin. Others have observed no changes in microglia through Iba1 and CD68 staining at 3 and 4 months of age but

have noted increased levels of both at 18 and 22.5 months of age (Yin et al., 2010; Tanaka et al., 2014; Lui et al., 2016). Additionally, transcriptomic profiles of progranulin deficient microglia isolated from mouse brains at 4 months revealed similar profiles whereas it greatly differed from wildtype at 16 months (Lui et al. 2016). Therefore, this observation is not surprising as mice in this study were 6-8 months of age. However, when compared to wildtype, microglial-BAR showed an increase in lysosomal proteins in these mice at the same age. This finding is consistent with the Lyso-BAR data presented in Chapter 4, as well as with the work of others, such as Huang et al. (2020). Additionally, Zhang et al. (2020) showed that these mice exhibit increased levels of C1q and C3b at 7 months of age and microglial-BAR captured that increase of C1q subunits. Wu et al. on the other hand have shown progranulin deficient microglia lack the ability to fully degrade myelin at 21 months of age when compared to wildtype, hinting at lysosomal dysfunction as an underlying cause (Wu et al., 2021). Surprisingly, they did not observe an increase in Iba1 and CD68 staining in 12-month-old progranulin-deficient mouse brains, but they did see an increase in these markers at 21 months of age. They also reported no changes in C1q and C3b RNA levels at 12 months of age but observed changes at 21 months of age. However, the interpretation of these results is not entirely clear, and therefore should be interpreted with caution. In contrast, previous work by Lui et al. demonstrated that neonatal primary cultures of progranulin deficient microglia exhibit higher expression of C1qa and C3 transcripts and proteins. Furthermore, in 12-month-old progranulin-deficient brains, they observed increased levels of C1qa in the cytoplasm of microglia. The authors also show a decrease in synaptophysin, a synaptic density marker, in the ventral thalamus of 4-, 7-, 12-, and 19-month-old progranulin deficient brains (Lui et al., 2016). Although microglial-BAR did not capture a decrease in synaptophysin, it did detect other synaptic proteins as decreased. This difference in results

could be due to the fact that microglial-BAR analyzes microglia from whole brains, while Lui et al. focused specifically on the ventral thalamus. Regardless, microglial-BAR produces results consistent with published work in terms of lysosomal dysregulation, immune response, and decreased synaptic proteins in progranulin-deficient mouse brains.

One of the primary limitations associated with microglial-BAR is the labeling radius, which is restricted to a range of 200-300 nm as outlined in Chapter 3. Consequently, this method captures not only microglial processes but also any neighboring structure that it comes into contact with, including microglia-neuronal contact sites. While this feature enables us to examine microglial neighborhoods, it also poses a challenge as it is not limited to the intended target. However, several studies have investigated the importance of microglia-neuronal contact sites in disease and have identified them as significant contributors. Wake et al. first showed that microglial processes contact synapses once every hour for about 5 minutes in steady state, while others demonstrated that microglia have decreased surveillance associated motility in awake mice (Wake et al., 2009; Lui et al, 2019; Stowell et al., 2019). Interestingly, another study conducted recently using super resolution imaging showed that microglial processes have a tendency to contact neuronal somas over neurites (Cserép et al., 2020). Therefore, an interesting experiment to add would be to conduct neuronal-BAR in these mice and overlap them to microglial-BAR. By comparing the hits from neuronal-BAR to those obtained from microglial-BAR, novel information can be gained into the interface of microglial-neuronal contact sites. To accomplish this, it is necessary to select a widely expressed neuronal cell surface marker. The choice of the neuronal marker will determine the outcome of the experiment and can provide valuable insights into potential distinct interactions between neurons and microglia. For instance, using a parvalbumin marker in conjunction with microglial-BAR could potentially reveal

pathophysiological changes occurring at these contact sites. This is especially relevant given that these synapses have been previously shown to be decreased in progranulin-deficient mice (Lui et al., 2016). Genome wide association studies have identified progranulin's gene, *GRN,* polymorphisms as a modifying risk factor for Alzheimer's disease (Brouwers et al., 2008; Cortini et al., 2008; Viswanathan et al., 2009). Studies have shown that microglia with decreased levels of progranulin have decreased phagocytosis of Aβ (Minami et al., 2014). Conversely, a recent study showed that complete loss of progranulin in microglia did not result in any alteration in the phagocytosis of myelin debris, although it prevented the degradation of it (Wu et al., 2021). Given the data from Chapter 4, it is possible that microglia and neurons both experience similar pH dysregulation, and presence of any progranulin may lead to different physiological response resulting in different phagocytic properties. Therefore, I would like to conduct a lysosomal assay to determine the microglial lysosome's ability to degrade substrates. One such assay is the Magic Red assay used in Chapter 4 to assess cathepsin B (Ctsb) activity in primary microglia cultured from *GRN*$^{-/-}$ brains. Magic Red is a fluorescently quenched substrate that is inactive until it is cleaved by the enzyme Ctsb inside living cell. This would determine if lysosomes of progranulin-deficient microglia have higher levels of Ctsb activity, since they have higher levels of Ctsb protein. A complimentary control in addition to wildtype microglia would be performing this assay in primary neurons from the same mice. This experiment would provide insight into any differences in lysosomes from different cell types lacking progranulin. In summary, characterizing microglial lysosomes has been difficult due to the lack of appropriate tools. In this study, iMicroglia was successfully scaled up for lysosomal proteomics, but further optimization is required for iMicroglia maturation. On the other hand, microglial-BAR shows consistency with previous findings of lysosomal dysregulation and

immune-related protein changes in progranulin-deficient microglia, making it a valuable tool for *in situ* proteomics.

Chapter: 6 Pathways Affected in Proximity to Microglia in Early AD Mouse Model

6.1 Introduction

Alzheimer's disease (AD) is characterized by the presence of amyloid-beta (Aβ) plaques and neurofibrillary tangles (NFTs) in the brain (Hardy and Selkoe, 2002). However, the onset of these changes can occur several decades before the onset of cognitive decline in AD patients (Gordon et al., 2018). Synapse loss has been demonstrated to be the most reliable predictor of cognitive decline (Meftah and Gan, 2023).

6.1.1 Synapse Loss Occurs Early in AD

The importance of synaptic density and plasticity in learning and memory has been widely recognized by notable researchers in the field including Donald Hebb, Eric Kandel, and Richard Morris. It has since been widely accepted that the number of synapses is a critical determinant of cognitive ability.

In 1990, DeKosky and Scheff were the first to demonstrate that a decreased number of synapses in AD patients correlates with decreased cognitive scores on the Mini-Mental Status Examination (MMSE) using electron microscopy (DeKosky and Scheff, 1990). Interestingly, they observed that in patients with AD, despite a decrease in the number of

synapses, the overall synaptic contact area per unit volume remained the same which was due to an increase in the size of the remaining synapses early in disease (DeKosky and Scheff, 1990). They noted that patients at advanced stages of AD also exhibited enlarged synapses, but the loss of synapses was greater than the increase in size, suggesting that early changes in AD may be taking place at the synapses during disease progression. Subsequently, Terry and colleagues showed that a decrease in synaptic density, measured by microdensitometry, was observed in AD brains and this decrease correlated with their decreased MMSE score. Notably, this decrease in synaptic density was not associated with plaques and weakly correlated with tangles (Terry et al., 1991). Several studies thereafter have confirmed this observation using sophisticated tools including ELISA-based assays, immunoblotting, immunohistochemistry, and proteomics (Ingelsson et al., 2004; Kashani et al., 2008; Whitfield et al., 2014; Bereczki et al., 2016; Bereczki et al., 2018). The presence of soluble forms of Aβ oligomers, rather than amyloid plaques, has been shown to be the primary contributor to synapse toxicity (Lambert et al., 1998; Gong et al., 2003; Klein, 2006). Koffie et al. demonstrated that toxic oligomers of Aβ surround synapses, and potentially contribute to synaptotoxicity (Koffie et al., 2012). It is worth noting that numerous synaptic studies in AD have utilized transgenic mouse models; however, the results have been inconsistent regarding synapse loss occurring before or after plaque deposition (Subramanian et al., 2020). This may be due to the fact that these models carry exaggerated mutations and may not accurately represent the events that occur in human AD brains. Nevertheless, these models have provided valuable insights into the mechanisms of synapse loss, including the role of microglial engulfment (Hong et al., 2016). Microglial involvement has been implicated in disease. Recent genome-wide association studies have identified multiple microglial genes as potential risk factors for AD,

further supporting the involvement of microglia in the pathogenesis of AD (Lambert et al., 2013). This finding highlights the need for further investigation into the role of microglia in AD.

6.1.2 Microglia's Role in AD

Microglia are the brain's resident immune cells that continuously survey the brain tissue. They are known to interact with synapses and respond to damage, as well as prune synapses in disease (Stephan et al., 2012; Hong et al., 2016; Lui et al., 2020).

Microglia express an array of damage-sensing receptors including pattern recognition receptors, chemokine receptors, Fc receptors, purinergic receptors, cytokine receptors, and scavenger receptors (Hickman et al., 2013). Additionally, microglia use the TREM2 receptor, and studies have shown that microglia lacking this receptor coalesce less around amyloid plaques, which worsens the effects of amyloidosis (Wang et al., 2015). Given their role in early synapse loss in AD, it is crucial to investigate how microglia interact differently in this disease. Therefore, I chose to utilize the *APP*^{NLF} mouse model in this chapter, which is considered a more accurate representation of human AD in mice (Saito et al., 2014) This is given the fact that these mice express a humanized Aβ sequence with two mutations (the Swedish '*NL*' and the Beyreuther/Iberian '*F*' mutations) under the endogenous mouse *APP* promoter. These mice develop plaques beginning at 6 months of age, and progress with cognitive impairments. With this model, I aim to explore the differences in microglial processes at the protein level, as we know they engulf synapses before plaque deposition occurs (De Schepper et al., 2023).

6.1.3 Aims

- Determine microglial interactome in early AD mouse model.
- Validate potential hits.

6.2 Methods

6.2.1 *APP*^{NLF} Mouse Model

Mouse models used were WT:C57BL/6J (Charles River UK) and *APP*^{NLF} mice were obtained from F. A. Edwards (Department of Neuroscience, Physiology & Pharmacology, UCL, UK). The animals were housed under Weizmann Institute Animal Care Committee guidelines at the Cruciform UCL building. Four female mice at 6 months of age were used for this study.

6.2.2 Microglial BAR in *APP*^{NLF} Mouse Brains

Microglial proximity labeling was conducted as described in Chapter 3. Four biological replicates were used. For each biological replicate, 21 slices were picked evenly from the whole brain. The slices were treated as described in Chapter 3 for the BAR protocol. Bait protein was P2Y12 (AnaSpec #AS-55043A used at 1:3000) and IBA1 (Wako Chemicals # 019-19741 used at 1:3000). All other secondaries are mentioned in Chapter 3.

6.3 Results

6.3.1 Comparison of P2y12 and Iba1 for Microglial-BAR on *APP*^{NLF} Cohort

Most AD mouse models involve exaggerated representations of the human disease, which can limit their translational value. Ultimately, no mouse model can truly recapitulate human disease. However, the *APP*^{NLF} model, on the other hand, offers a more physiologically relevant representation of AD in mice, as it expresses *APP* mutations at endogenous levels, thereby excluding overexpression artifacts (Saito et al., 2014). This model provides a more accurate representation of amyloidosis-related pathology, as it does not involve tauopathies. In this chapter, I aimed to investigate microglial biology in the early stages of amyloidosis as initial plaque deposition occurs, with the first signs of synapse loss at 6 months of age (De Schepper et al., 2023). By studying microglial processes at this stage, I aim to identify subtle changes that could potentially be targeted to slow the progression of the disease. To this end, I tested two microglial markers for microglial-BAR on *APP*^{NLF} brains by targeting P2y12 and Iba1. P2y12 is a purinergic cell surface receptor and Iba1 is a calcium-binding protein, both exclusively expressed by microglia in the brain (Imai et al., 1996; Sasaki et al., 2003). Both groups were treated identically, with a common negative control treated with secondary antibodies alone, bypassing incubation with primary antibodies. In these samples, the biotinylated proteins colocalized with both P2y12 and Iba1, respectively, while no staining was detected in the negative control (**Figure 6-1**). Based on this, I processed the samples for mass spectrometry as mentioned in Chapter 3 and proceeded with the LC-MS/MS analysis.

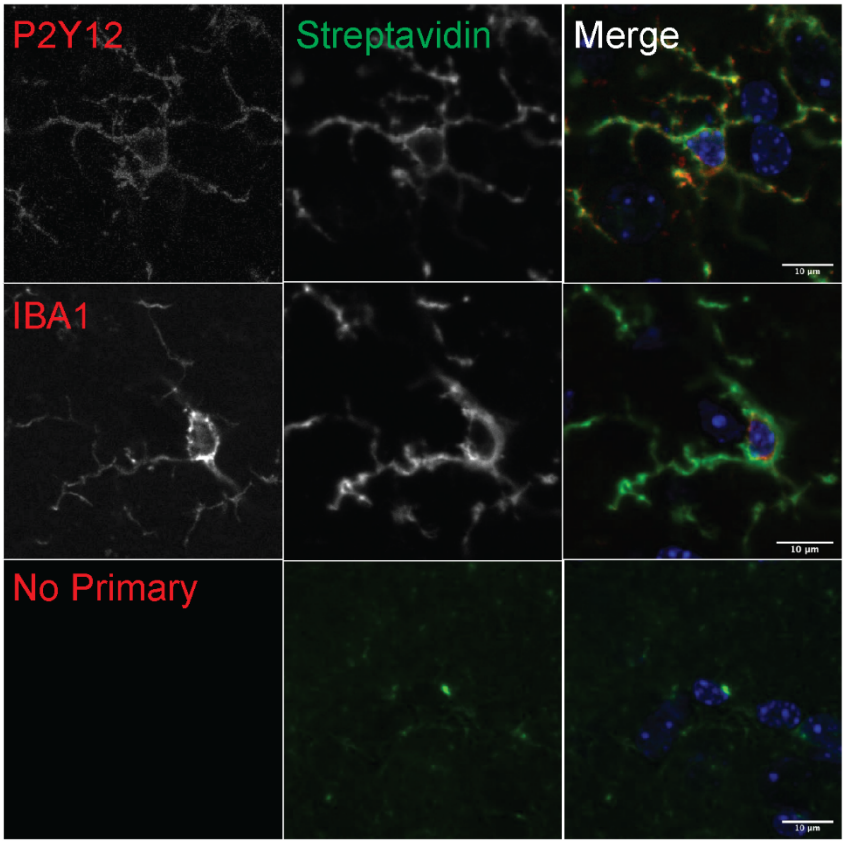

Figure 6-1: P2Y12 and IBA1 as microglial marker for BAR in fixed mouse brain.

Representative images of microglial-BAR in APP-wildtype mice. No primary was used as a negative control for the BAR method. Biotinylated proteins shown in streptavidin stain colocalize with P2Y12 and IBA1. Minimal streptavidin stain was seen in the no primary group. Scale bare is 10 μm.

The mass spectrometry analysis was conducted by Dr. Yan Li at the NIH mass spectrometry core facility, using Proteome Discoverer for the analysis. Initial results yielded intensely skewed volcano plots (**Figure 6-2**). I observed that the Iba1-BAR detected majority of the proteins as increased in wildtype versus *APP*^{NLF}, while P2y12-BAR showed the opposite trend. This was an unexpected result and prompted me to conduct further investigation. To this end, total protein abundances was

examined. The reanalysis revealed that the wildtype samples for Iba1-BAR consisted of a higher protein amount detected when compared to *APP*^{NLF} (**Figure 6-3A**). However, this was not the case for P2y12-BAR, where the total protein abundances detected per animal were comparable to each other (**Figure 6-3B**). Although the samples were loaded and treated identically, it is possible that there was some protein loss somewhere along the processing pipeline. Given this development, Dr. Yan Li recommended normalizing the samples to total peptide abundance detected within each sample and re-ran the analysis. The normalization resulted in an evenly distributed volcano plot for P2y12-BAR, however, the Iba1-BAR plot remained skewed (**Figure 6-4**). The total protein differences in the Iba1-BAR group could not be resolved and would have to be repeated again. For this reason, I proceeded with further analysis on the P2y12-BAR cohort.

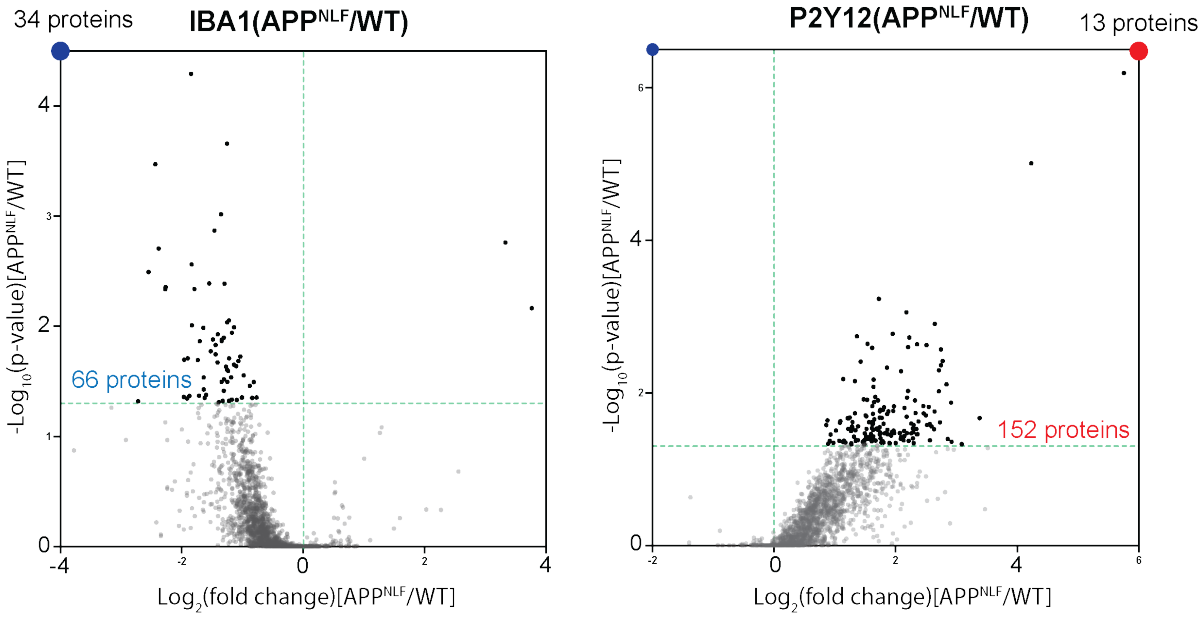

Figure 6-2: Volcano plots for IBA1-BAR and P2Y12-BAR comparing *APP*^{NLF} to wildtype.

Microglial-BAR was performed on wildtype and *APP*^{NLF} mice at 6 months of age followed by LC-MS/MS. Each group had 4 biological replicates. Non-normalized abundance ratios and p-values were plotted here. The graphs were skewed to the left for IBA1 and skewed to right for P2Y12.

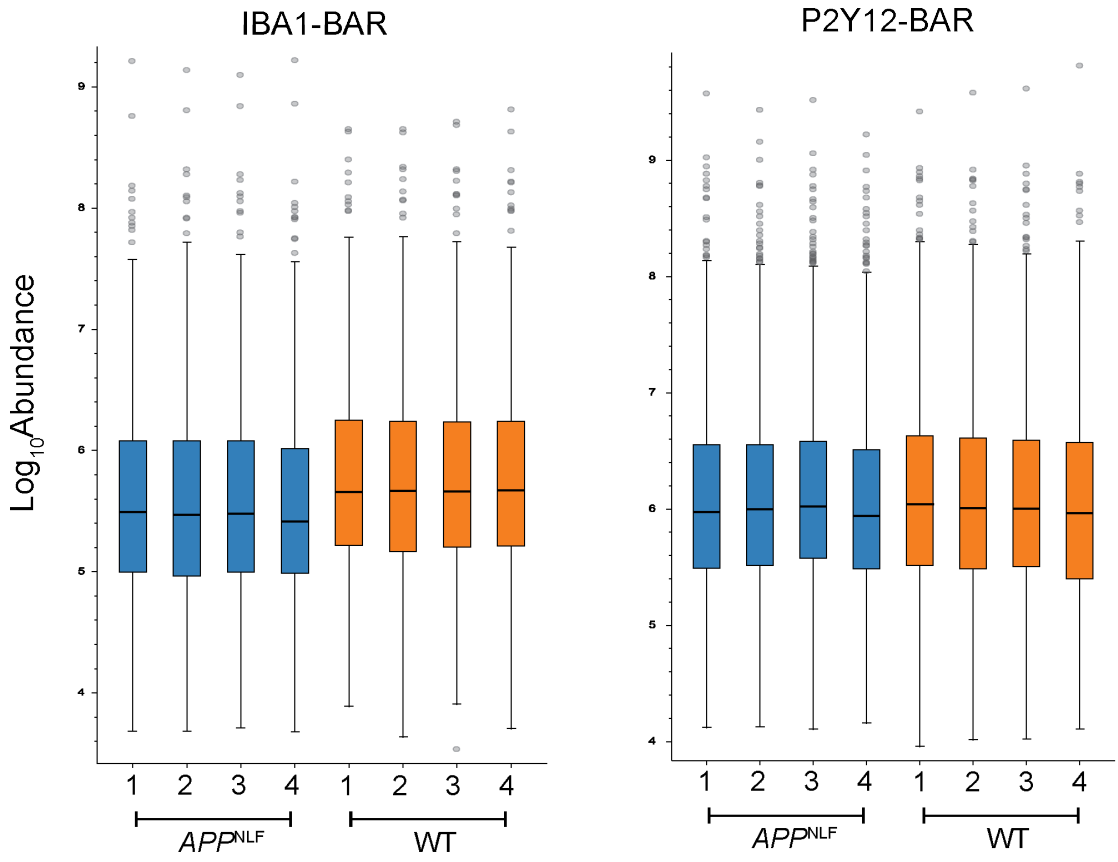

Figure 6-3: Comparison of raw abundances between groups.

Shown here are raw abundances of all proteins detected in each sample. The numbers represent biological replicate, and the labeled bar underneath represents the genotype. IBA1-BAR wildtype samples had more protein quantity detected when compared to IBA1-BAR *APP*^{NLF} samples. Both P2Y12-BAR groups had similar amounts detected and were comparable to each other.

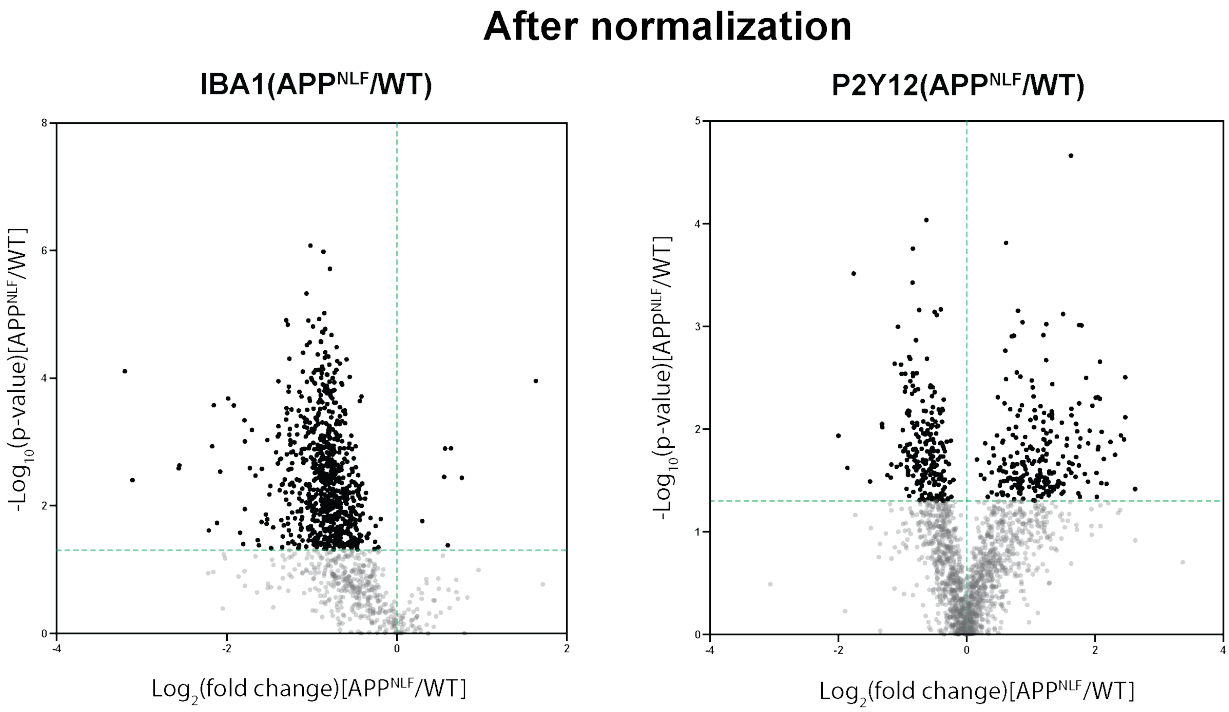

Figure 6-4: IBA1-BAR data could not be used post-normalization.

The samples were normalized to total peptide amount detected within the sample for each group. The plots were generated using all peptides detected. IBA1-BAR plot remained skewed whereas P2Y12-BAR resolved to an evenly distributed volcano plot.

6.3.2 Proteins increased in microglia in early AD are endocytosis-associated.

Given the normalization, I filtered my dataset to include proteins that had more than 2 unique peptides detected. This was to ensure that only true positives were included, and false positives were minimized. The filter resulted in the removal of 34 proteins from the list, leaving a total of 424 proteins detected in *APP*^{NLF} P2y12-BAR above significance. Of those, 215 were increased in *APP*^{NLF} and 209 were decreased (**Figure 6-5A**). To

identify patterns in the proteins with altered abundances, I conducted a Gene Ontology (GO) enrichment analysis, which revealed 45 proteins in the dataset with pathways of neurodegeneration, 25 with oxidative phosphorylation, 25 with endocytosis, 14 with phagosome, and 5 with fatty acid biosynthesis (**Figure 6-5B**). Other biological process GO terms detected terms such as nuclear-transcribed mRNA catabolic process, translation, and phagosome acidification. Most notably, altered cellular components observed were cell-substrate junction with 35 proteins detected 17 of which were increased in *APP*^{NLF}, cytoskeleton with 34 proteins with half as increased in *APP*^{NLF}, and mitochondrial membrane with 37 proteins, 28 of which were increased in wildtype. Based on these findings, I deemed it necessary to further examine the proteins under KEGG pathways of oxidative phosphorylation, endocytosis, and phagosome. Additionally, as neurodegeneration emerged as the top KEGG pathway detected, I also decided to include it in my analysis.

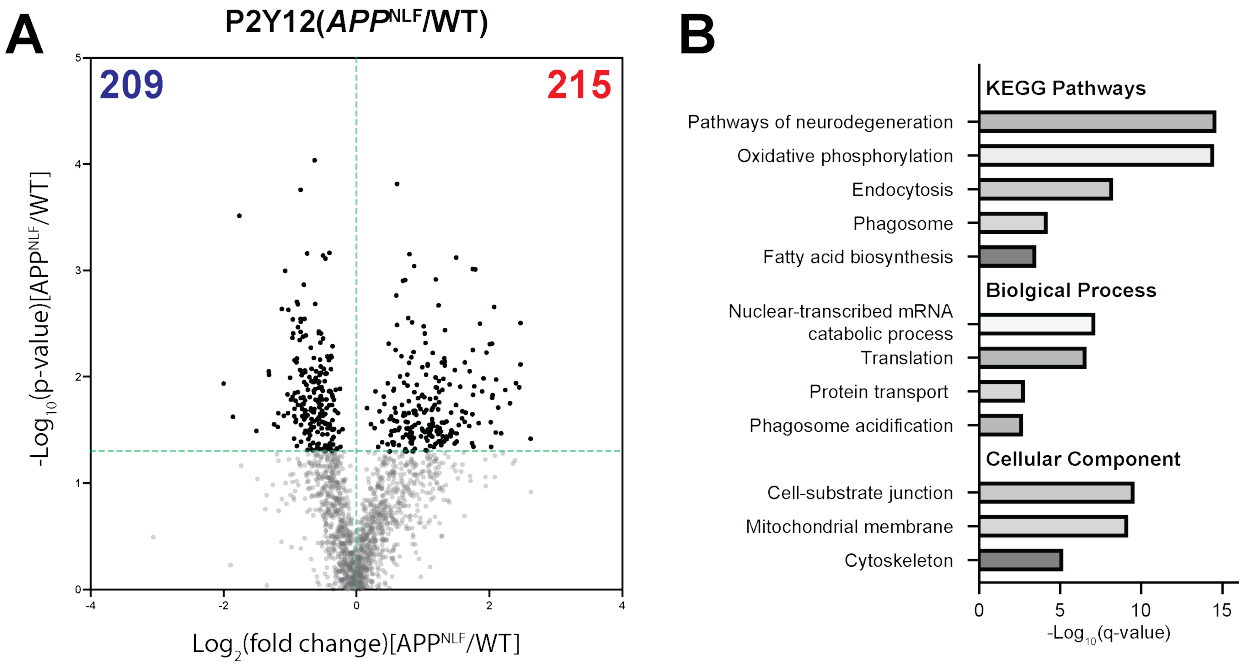

Figure 6-5: *APP*^{NLF} brains have altered protein abundances related to oxidative phosphorylation, phagocytosis, and protein translation.

(A) A total of 424 proteins were differentially abundant in the *APP*^{NLF} microglial-BAR samples when compared to wildtype, 215 of which were increased and 209 were decreased. The volcano plot shows proteins that had more than 2 unique peptides detected. **(B)** Gene Ontology (GO) enrichment analysis of the 424 proteins revealed KEGG pathways associated with pathways of neurodegeneration, oxidative phosphorylation, endocytosis, phagosome, and fatty acid biosynthesis. GO term enrichment for biological processes identified nuclear-transcribed mRNA catabolic process, translation, protein transport, and phagosome acidification proteins. Cellular component GO terms associated with the 424 proteins were cell-substrate junction, mitochondrial membrane, and cytoskeleton.

I examined the distribution of the proteins identified by the aforementioned KEGG pathways on the volcano plot for each GO term (**Figure 6-6**). There was a significant overlap of proteins between pathways of neurodegeneration and oxidative phosphorylation, with a larger portion of the proteins on the left side of the plot than right signifying more decreased proteins in *APP*^{NLF} than wildtype. A larger number of hits for the phagosome and endocytosis terms were located on the right side of the plot compared to the left, indicating a higher abundance in *APP*^{NLF} than wildtype. The identities of these proteins can be seen in **Supplemental Table 6-1**. This was interesting, given that the target protein was P2y12, a microglial cell surface marker involved in chemotaxis to sites of damage (Haynes et al., 2006). Microglia form contact sites at neuronal somas and respond to neuronal activity via P2y12 receptors as shown by Cserép and colleagues (Cserép et al., 2020). Others have shown that this receptor is necessary for stress-induced phagocytosis of dendritic spines in the prefrontal cortex of mice (Bollinger et al., 2022). P2y12 levels did not change in my dataset at this time point, even though it is known to decrease in disease-associated microglia in late stages of disease pathogenesis (Haynes et al., 2006). In order to identify any additional patterns among the increased proteins from these two groups,

I performed a STRING analysis (**Figure 6-7**). The labeled nodes represent proteins that exhibited an increase in abundance in the *APP*^{NLF} microglial-BAR. Three main biological processes were identified, including proton transmembrane transport, regulation of vesicle-mediated transport/protein transport, and actin filament-based processes. Atp6v1g1, Atp6v1d, and Atp6v0d1 were identified as proton transmembrane transport proteins, and interestingly, they were also found to be associated with phagosome and phagosome-acidification GO terms. This finding suggests that further investigation into the phagocytic properties of *APP*^{NLF} microglia at this age point would be worthwhile, especially given that De Schepper et al. have shown an increase in engulfment of synapses labeled with C1q by these microglia in the *APP*^{NLF} mice when synapses are vulnerable (De Schepper et al., 2023). Nedd4l, Sh3kbp1, Arf6, Iqsec2, and Arpc4 were identified as belonging to the actin filament-based process pathway. Among these, Nedd4l, Sh3kbp1, and Arf6 were also found to be involved in protein transport, as indicated by their annotation in the protein transport pathway (**Figure 6-7**). Based on this information, exploring possible structural differences in the processes of microglia from *APP*^{NLF} mice at this age would be an intriguing avenue for further investigation. Other proteins, such as Epn2, Ap2s1, Eps15, Rab5a, Rab5b, Rab8a, Ehd4, Vta1, and Vps37c, are involved in protein transport and may be related to changes occurring in microglial processes, which may require an increase in protein concentration. However, further verification is necessary to support this claim.

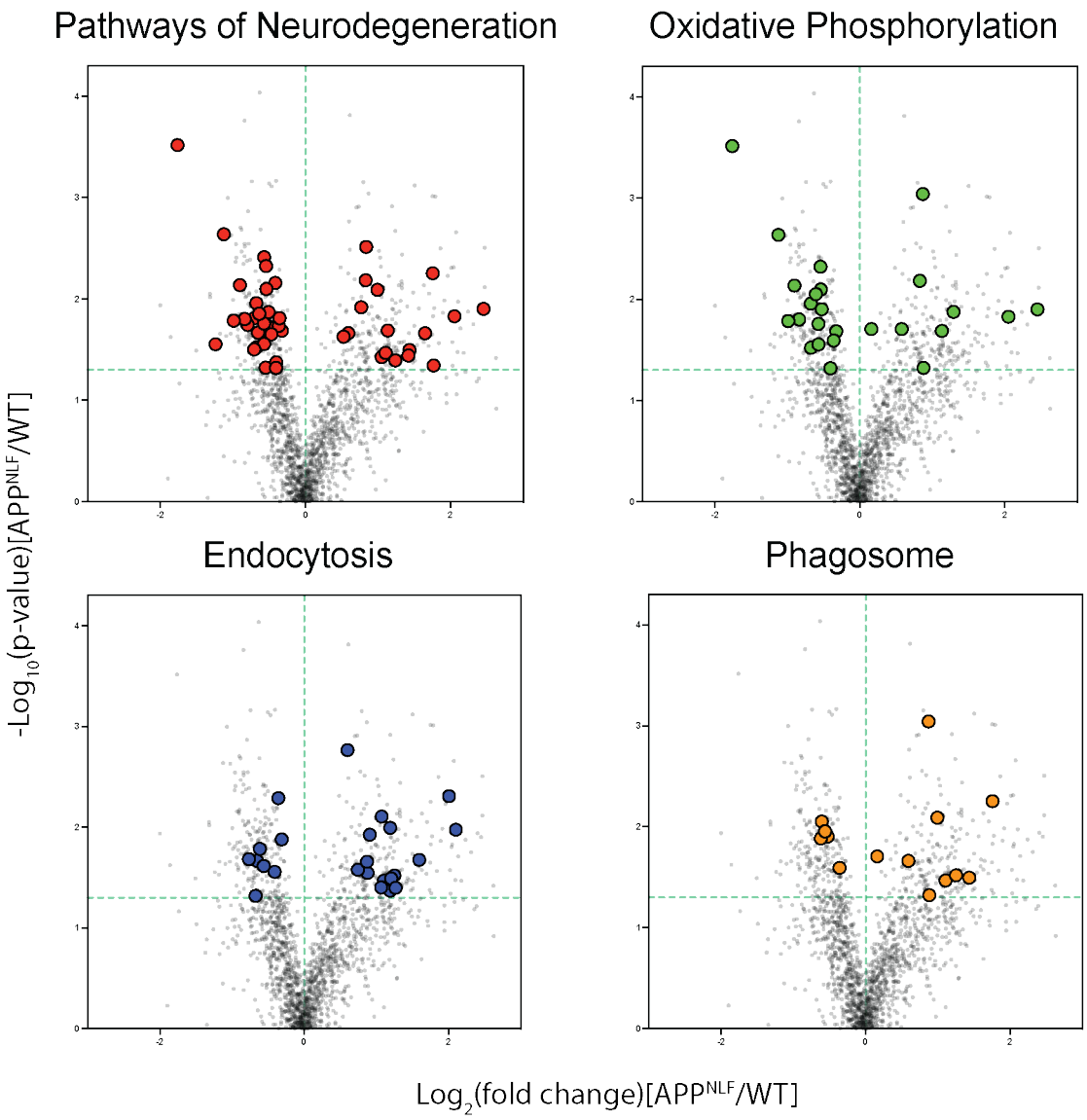

Figure 6-6: *APP*^{NLF} brains have more proteins associated with endocytosis and phagosome increased at 6 months of age.

Each plot represents proteins associated with the respective KEGG pathway term. More proteins associated with pathways of neurodegeneration (28 vs 17) and oxidative phosphorylation (16 vs 9) are decreased in *APP*^{NLF} than wildtype. Contrastingly, more proteins associated with endocytosis (17 vs 8) and phagosome (9 vs 5) are increased in *APP*^{NLF} than wildtype

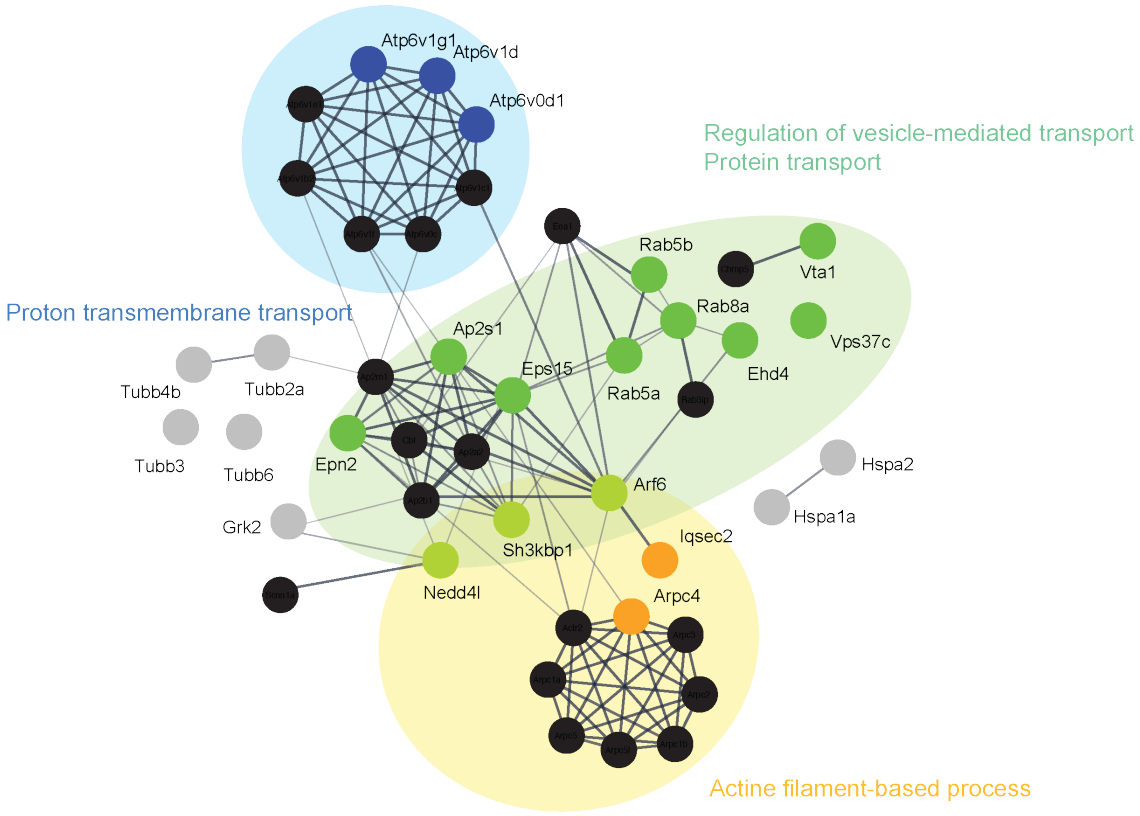

Figure 6-7: String network analysis of increased proteins in *APP*^{NLF} associated with endocytosis and phagosome.

All labeled nodes were increased in *APP*^{NLF} microglial-BAR. No more than 20 interactors are included in this analysis. The highlighted Venn diagram shows Biological Processes GO terms associated with the respective group of proteins.

It's important to note that the BAR labeling radius of 200-300nm covers not only the microglial processes but also neighboring cells. Therefore, changes observed in relation to cytoskeleton-associated proteins may originate from other cell types as well. This is supported by the presence of several shared proteins in the identified KEGG pathways of synaptic vesicle cycle, dopaminergic synapse, GABAergic synapse, and glutamatergic synapse, although a larger number of proteins are

associated to terms such as phagosome and endocytosis rather than synaptic proteins (**Supplemental Figure 6-1**). These shared proteins include Gng3, Gng2, Gng5, Gng7, Gng12, Glul, Gnai1, Gnai2, and Gria1. Majority of these proteins were found to be decreased in *APP*^{NLF} microglial-BAR than wildtype as follows; 64% of synaptic vesicle proteins, 79% of dopaminergic synapse proteins, 73% of GABAergic synapse proteins, and 67% of glutamatergic synapse (**Figure 6-8**). The identities of these proteins can be seen in **Supplemental Table 6-2**. Interestingly, Grk2 was significantly increased and was also identified as an endocytosis KEGG term. Grk2 is a G protein-coupled receptor kinase responsible for G protein-coupled receptor (GPCR) desensitization and internalization (Evron et. al., 2012). Grk2 has been found to be upregulated in a prodromal AD mouse model, with majority of it being localized in the cytosol where it remains inactive. This inactivity has been linked to a lack of desensitization of GPCRs, which has been suggested to cause sub-threshold Aβ-associated GPCR hyperactivity in microglia (Suo et al., 2004). Suo et al. demonstrated that microglia, which were pre-treated with sub-threshold levels of Aβ, responded to GPCR activation by releasing TNF-α. The authors established the GPCR dependence of TNF-α release by stimulating the Aβ-treated microglia with GPCR ligands (thrombin/glutamate) or a non-GPCR ligand (LPS) to test for a tumor necrosis factor (TNF-α) release. There has been limited research on this topic to date, and further investigation into the specific role of microglial dysfunction in AD would be valuable. It would be interesting to conduct a follow-up study to examine the impact of this finding specifically on microglia and its potential contribution to the development of AD.

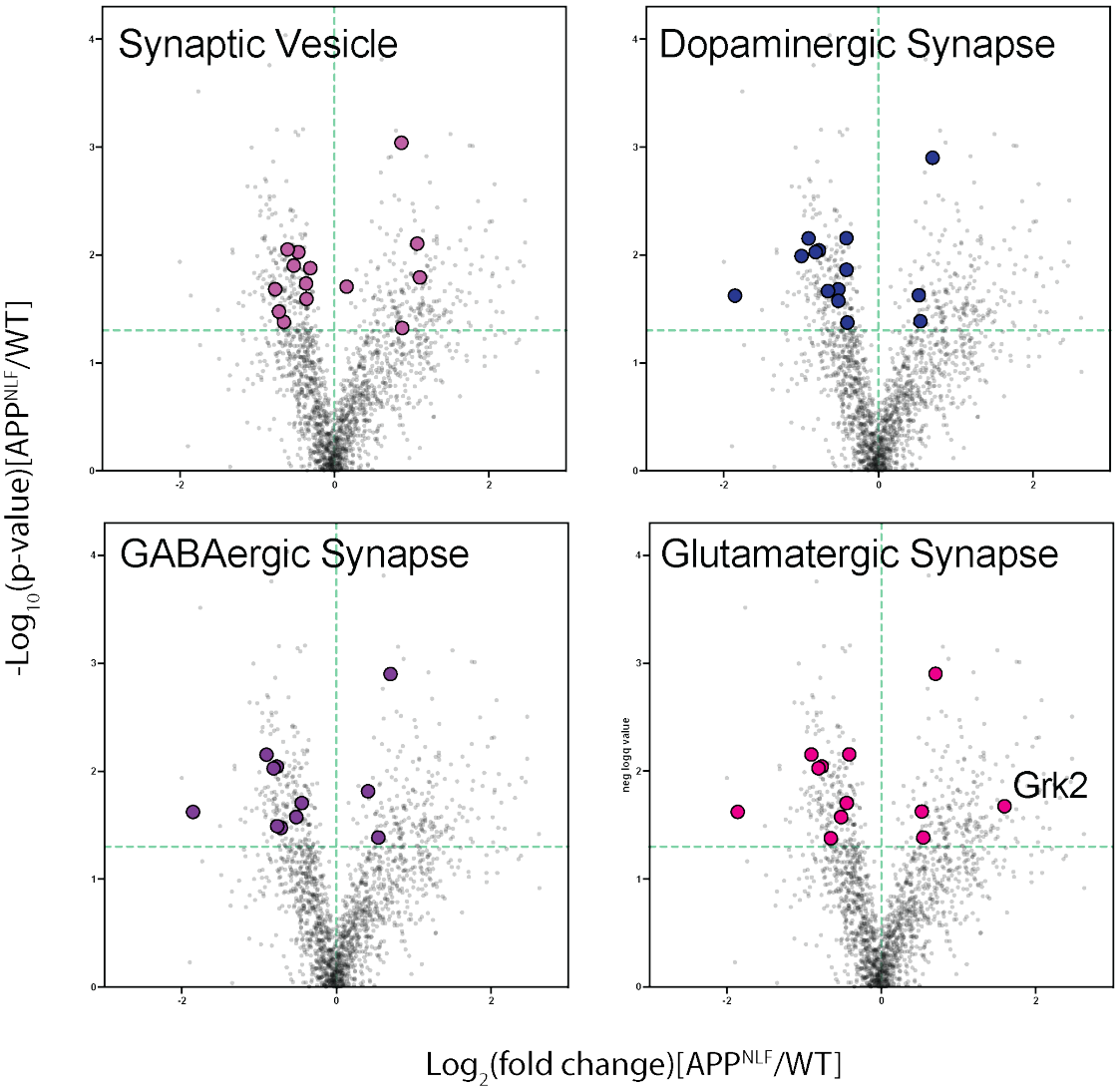

Figure 6-8: KEGG Pathways associated with synaptic terms in *APP*^{NLF} microglial-BAR compared to wildtype.

Each plot shows proteins for respective KEGG terms. More synaptic proteins are decreased in *APP*^{NLF} than wildtype; Synaptic Vesicle (9 out of 14), Dopaminergic Synapse (11 out of 14), GABAergic Synapse (8 out of 11), and Glutamatergic Synapse (8 out of 12).

In summary, the study has revealed early changes in microglial processes, including increased phagocytic and endocytic proteins and decreased oxidative phosphorylation and synaptic proteins in *APP*^{NLF} mice before plaque deposition.

6.4 Discussion

In this chapter, I investigated the early changes in microglial biology in the *APP*^{NLF} mouse model before the onset of Aβ plaque deposition. I used microglial-BAR to identify proteins in proximity to microglial processes in 6-month-old *APP*^{NLF} brains. My results showed that proteins associated with oxidative phosphorylation and synapses were decreased close to microglia, while proteins associated with endocytosis, phagosome, and actin filament-based processes were increased. These findings suggest that microglia may contribute to AD pathology by promoting synaptic loss and altering cellular metabolism in the brain.

Although the BAR method has been performed multiple times through this thesis, it was unexpected to observe non-comparable protein detection between the Iba1-BAR samples despite identical handling and timing with P2y12-BAR. This observation raises the possibility that the protein's inherent properties may make it difficult to detect, and further exploration is necessary. In contrast, the P2y12-BAR data exhibited consistent and robust detection, indicating that P2y12 serves as a reliable BAR method marker across different model organisms. The detection of 424 protein abundance changes between *APP*^{NLF} and wildtype, with many of them associated with pathways of neurodegeneration on KEGG GO term analysis, is a noteworthy finding. Furthermore, majority of these proteins were linked to the KEGG GO term oxidative phosphorylation,

suggesting possible involvement of mitochondria. Most of these proteins were found to be decreased in *APP*^{NLF} microglial-BAR compared to wildtype. Several studies have shown that AD patients exhibit decreased mitochondrial respiratory function, increased oxidative damage, and reduced mitochondrial biogenesis (Lin and Beal, 2006; Wang et al., 2009; Manczak et al., 2011). Animal models of AD have also demonstrated mitochondrial dysfunction, with decreased ATP levels and altered mitochondrial morphology (Reddy, 2009; Du et al., 2010). It is yet to be determined whether the differences noted in the *APP*^{NLF} microglial-BAR are specific to microglial processes or more widespread throughout the brain. Additionally, the detection of decreased synaptic proteins, with the exception of Grk2, is a significant observation. Grk2, which falls under the KEGG GO term of endocytosis, has been reported to increase in a prodromal AD mouse model by Suo et al. (Suo et al., 2004). However, a study by Guimarães and colleagues found no change in Grk2 levels in AD patient brains when compared to age-matched controls (Guimarães et al., 2021). Interestingly, they observed decreased levels of Grk2 specifically in the CA1 region of the hippocampus. To further investigate, it would be intriguing to explore whether Grk2 levels change in aged *APP*^{NLF} brains, particularly after being increased at 6 months of age in microglial-BAR, compared to wildtype. The finding that more endocytic and phagosome proteins were increased in abundance in *APP*^{NLF} microglial-BAR than in wildtype is intriguing as well and warrants further investigation.

One potential approach to investigate the specificity of BAR is to perform microglial-BAR, select a few proteins with validated antibodies, and conduct Western blotting on the biotinylated proteins pulled down, flow-through, and total lysate. This would help determine whether the observed differences are unique to the pull-down sample. Another method would be to conduct immunoassays to investigate whether these proteins are indeed altered and if so, where. Additionally, it would be interesting to

examine microglial-BAR at 12 months of age for *APP*^{NLF} mice, when they develop plaques, to determine if the observed changes are more pronounced or reversed. Furthermore, phagocytosis assays on 6-month-old primary microglia from these mice would be informative, as well as Lyso-BAR analysis to investigate their lysosomal contents and surroundings. Another complementary experiment would be to perform *in vivo* proximity labeling of microglia in *APP*^{NLF} mice using a biotin ligase, TurboID, expressed under the macrophage specific CX3CR1 promoter. However, this would involve crossbreeding the CX3CR1-TurboID mice recently generated by the Hong lab with *APP*^{NLF}, requiring additional time for breeding. This experiment offers the potential to reveal the microglial interactome in plaque-ridden environments compared to the wildtype, providing insights into microglial-specific changes in amyloidosis, such as altered phagocytosis or motility-associated proteins. Another approach would involve generating a mouse colony expressing LAMP1-tagged HA under the CX3CR1 promoter, allowing for the pull-down of intact microglial lysosomes. This would enable the assessment of microglial lysosome contents and the identification of amyloidosis-specific effects between the *APP*^{NLF} model and the wildtype. These proposed experiments have the potential to provide valuable insights into the pathology of AD and should be considered for further investigation.

The data presented here suggests the utility of the BAR method as a potential tool for studying the pathology of Alzheimer's disease. However, this data is still preliminary and needs significant validation using further immunohistochemistry, immunoblotting, and a repeat BAR experiment. The ability to apply this method to other targets will help advance our understanding of the disease further. Importantly, this approach can be applied to human tissue, providing more clinically relevant data on the progression of the disease. However, limitations exist including availability of highly specific antibodies against targets of interest

and suitable fixation methods for human tissue. Despite these limitations, this method has valuable potential for future research.

Chapter: 7 Discussion

7.1 Introduction

In this thesis, I modified and implemented the BAR method to identify potential target-relevant protein interactions in mouse brain tissue. This method added to our understanding of lysosomes in progranulin-deficient mice. The data reiterated the significant contribution of microglia to lysosomal disruption. As microglia are implicated in neurodegeneration, I further explored their role in early Alzheimer's disease model using the BAR method. This analysis revealed dysregulation of mitochondrial and endocytosis/phagocytosis associated proteins, indicating possible microglial dysregulation in early AD. Although the BAR method has limitations, including the risk of false positives resulting from its labeling method, my research has indicated that it may still prove useful for the scientific community due to potential applicability to human tissue. While mouse models and *in vitro* cell culture studies can provide valuable insights into conserved biological mechanisms and relevant biochemical changes in disease, the utilization of human tissue provides a more direct approach to understanding the impact of disease pathology. Hence, there is a need to extend the application of this method to patient brain tissue to gain insights into the underlying pathophysiology of neurodegeneration that occurs in humans, rather than relying on findings from studies conducted in mice or *in vitro* cell culture systems.

7.2 Applicability and Challenges of the BAR Method

In Chapter 3 of my thesis, I discussed the use of Lamp1 and P2y12 antibodies to pull down target-relevant proteins via BAR. Although the efficacy of the BAR method has been demonstrated by the isolation of several cell-substrate proteins using an antibody against the cell surface protein P2y12 and lysosomal lumen and membrane proteins targeting the lysosomal membrane protein Lamp1, it should be noted that the method can also pull-down proteins that are not relevant to the target. One major contributing factor to this is the relatively large labeling radius of HRP, which is around 200-300nm. This means that there may be non-specific proteins that are also pulled down in addition to the target-relevant ones. This can be seen when the Lyso-BAR data was compared to Lyso-IP in Chapter 4. The comparison did not yield a significant overlap. In addition, our preprint (Hasan et al., 2023) demonstrates some but not complete overlap between Lyso-BAR and another proximity labeling technique called Lyso-APEX, which uses genetically modified human iPSC-derived neurons with lysosomes tagged to ascorbate peroxidase. It is worth noting that Lyso-APEX is conducted in live cells without membrane permeabilization, which captures only the outside of the lysosome, while Lyso-BAR captures both inside and outside. This is because the membranes are permeabilized during the labeling process for BAR, allowing for tagging to occur on both sides of the membrane. As a result, proteins on the opposite side of the membrane may be marked as potential target-interactors even if they did not interact with the protein of interest. Therefore, this is another limitation of the BAR method where if a target protein resides in a membrane, such as P2y12 or Lamp1, it can be challenging to differentiate between proteins that interact with the protein on one side of a membrane versus the other. Furthermore, Lyso-BAR

does not distinguish lysosomes from different cell types, whereas Lyso-APEX captures the lysosomal interactome from neurons in culture exclusively. One potential solution is to choose a lysosomal protein that is primarily expressed in one cell type, such as CD68 in microglia (Chistiakov et al., 2017). However, this approach is contingent upon the availability of reliable cell type-specific markers. Identification of cell type-specific markers requires prior knowledge of proteins expressed only in certain cells, which is currently an area of growing understanding.

Future experiments to confirm the BAR results could include targeted immunoblots and immunohistochemistry to validate the changes observed in mouse brains. Additionally, it would be valuable to repeat the Lyso-BAR experiment on i^3Neurons and compare the results to Lyso-APEX data. This would provide a better comparison of the techniques, despite the issue of labeling both sides of the membrane. Other markers can also be tested, such as mitochondrial proteins, by using mito-BAR in human embryonic kidney (HEK) cells and comparing it to existing mito-APEX data from Alice Ting's group (Rhee et al., 2013).

The ultimate goal, however, would be to extend this technique to human brain tissue. While two such attempts have been made in this direction (Killinger et al., 2022; Radford et al., 2023), working with human tissues presents several challenges. Compared to mice, human tissue is a limited resource and the fixation techniques commonly used for human tissues, such as paraffin embedding, have not been tested with the BAR method and may not yield optimal results. Moreover, long-term storage of human tissues can lead to a degradation in quality, making them less than ideal for use with the BAR method. However, successfully adapting the BAR method to human brain tissue would have tremendous potential for expanding our understanding of the human brain and associated diseases. To achieve this, the next steps involve optimizing the technique

for application to human tissue by standardizing the requirements for high-quality tissue. This entails collecting brain tissue from various brain banks and categorizing them based on factors such as post-mortem interval (PMI), fixation method, and duration of fixation storage. The control for this experiment would involve using fresh operating room acquired tissue that is fixed in 4% PFA overnight and subsequently stored in 30% sucrose. By analyzing this data, we can determine the types of brain bank tissue that yield optimal results and establish guidelines for its use. Once this standardization is accomplished, the BAR method can be universally applied to investigate various hypotheses using patient brains. While many therapeutic advancements originate from mouse model studies, their translatability to human disease remains uncertain until clinical trials are conducted. By applying the BAR method on human tissue, it offers the advantage of identifying pathology that is directly relevant to patients and allows comparison to mouse models. This comparison will help determine the similarities and differences between the two, guiding the development of therapies that target patient-specific pathology more efficiently and effectively.

7.3 Progranulin's Role in Lysosomes

Chapter 4 of this thesis demonstrates the use of various tools to characterize the neuronal lysosomes, including lysosomal isolation (Lyso-IP), lysosome functional assays (Ctsb activity and dSILAC), and proximity labeling of lysosomes *in situ* (Lyso-BAR). While our study represents the first use of the Lyso-IP technique developed by Abu-Remaileh et al. in i^{3}Neurons, further troubleshooting may be necessary to optimize the technique's efficacy and accuracy. In the original study, Abu-Remaileh et al. used TMEM192 tagged with HA instead of Lamp1 as they found that

TMEM192 exhibited better lysosomal localization upon overexpression compared to Lamp1 (Abu-Remaileh et al., 2017). This likely resulted in a more efficient and less contaminated pull-down. However, for this thesis, I chose to use Lamp1 tagged with HA to maintain consistency with the other experiments related to Lamp1. This decision may have led to contamination of catalases and Golgi apparatus in the lysosome isolation fraction. This may be due to the dynamic nature of Lamp1, which constantly moves between organelles (Deng and Storrie, 1988). While Lamp1 was previously thought to be a specific marker for lysosomes, it is now recognized that it does not exclusively represent lysosomes containing catalytic enzymes (Cheng et al., 2018). Additionally, neuronal lysosomes exhibit varying contents and internal pH, which can be influenced by their subcellular localization (Cai et al., 2010; Gowrishankar et al., 2017; Farfel-Becker et al., 2019). Therefore, it would be useful to explore other lysosomal markers in i^3Neurons to determine the best target for Lyso-IP. Using more than one lysosomal marker would provide a comprehensive dataset of neuronal lysosomes. However, despite these issues, the Lyso-IP technique on *GRN* KO i^3Neurons provided valuable information, such as increased lysosomal enzymes and proteins associated with pH maintenance.

Although previous studies have suggested that the proteins Ctsd and Ctsb are upregulated in progranulin KO cells, my Lyso-IP data did not show any changes in their levels (Takana et al., 2017; Klein et al., 2017; Huang et al., 2020). However, these studies examined whole cell lysates of Ctsd, which does not consider the protein's location within the cell. Therefore, the Lyso-IP data could suggest a potential change in the protein's localization. Although I assessed Ctsb activity in i^3Neurons, this method is not be reliable for determining its location within the cell since it requires an acidic environment that is absent outside the lysosome.

Further experiments are needed to investigate the location of these enzymes in i^{3}Neurons lacking progranulin.

To determine the neuron's ability to maintain lysosomal activity with loss of progranulin, dynamic stable isotope labeling using amino acids in cell culture (dSILAC) was conducted using progranulin deficient i^{3}Neurons and their isogenic controls. Several proteins associated with neurodegenerations were identified to have altered protein turnover rates with loss of progranulin in a dose-dependent manner based on the data. As a next step, it would be crucial to conduct a synthesis/degradation assay for some of the identified hits to verify the source of the change in turnover. Follow-up immunoblots for the proteins with altered turnover rates would be necessary to identify any buildup or decrease in protein levels, followed by imaging to determine the localization of these proteins in i^{3}Neurons. Moreover, the experiment should be repeated with a pH-neutralizing drug to assess whether the observed changes in turnover rates are due solely to pH changes. Testing a protease inhibitor drug would also be essential to confirm that the observed degradation changes are specific to lysosomal degradation and not other degradation pathways.

Lyso-BAR was applied to *GRN*$^{-/-}$ brains as neurons do not exist in isolation *in vivo*. The data revealed several upregulated lysosomal proteins along with immune-related proteins. However, it's important to realize that neurons are not the most abundant cells in the brain. Therefore, it is likely that glia are driving the observed changes. Microglia, in particular, are the likely culprits as suggested by the upregulation of immune proteins such as C1q subunit (Lui et al., 2016). The dataset shows an increase in Ctsb and Ctsd, as previously noted (Takana et al., 2017; Klein et al., 2017; Huang et al., 2020). Additionally, Uap1|1 consistently appears in two datasets from literature (Lui et al., 2016;

Huang et al., 2020), although there is no known connection between progranulin and UAP1|1 in the literature. Interestingly, UAP1 was recently identified as a crucial step in promoting the activation of type 1 interferon (IFN) signaling for innate antiviral responses, linking UAP to immune response (Yang et al., 2023). Since neuroinflammation plays a role in neurodegeneration, it is important to conduct further experiments to verify the increase of UAP1. These experiments should aim to identify the brain regions where UAP1 is expressed and investigate how its loss affects microglia's immune response by examining cytokine release.

7.4 Microglial Progranulin

In this chapter, I aimed to investigate the microglial lysosome from progranulin deficient cells, as progranulin is a lysosomal protein highly expressed by microglia in the brain. The inducible microglia system generously gifted by Dr. Martin Kampmann was utilized, and the Lyso-IP constructs were added to them by Dr. Allison Snyder. I differentiated these cells to implement the pull-down and determine the optimum cell line for use. Unfortunately, both TMEM192-HA and LAMP1-HA lines failed to pull down lysosomes free of contamination. However, the pull-down was enriched for several lysosomal proteins, leading to a pilot Lyso-IP attempt using the TMEM192-HA line. The preliminary data showed a decrease in proteins associated with cell-substrate junction and substrate-adhesion dependent spreading in progranulin deficient iMicroglia. It is challenging to determine if this is a genuine representation of decreased cell spreading with lack of progranulin or an artifact of the differentiation process. Immunocytochemistry should be performed on these cells to determine and quantify morphological differences, while immunoblots can serve as an alternative validation of the Lyso-IP hits. Another approach to

investigate the lysosomal contents in progranulin-deficient microglia would be to conduct targeted Western blots using primary microglia from *GRN*$^{-/-}$ brains. This would involve testing markers for pH maintenance such as Cln3, Clnc6, and Ppt1, which were identified as up-regulated in neuronal Lyso-IP data from *GRN*$^{-/-}$ i^{3}Neurons in Chapter 4. An alternative option is to perform Magic Red assays to assess the presence of active cathepsins in *GRN*$^{-/-}$ primary microglia. Additionally, Lyso-IP pull-downs can be carried out using CX3CR1-LAMP1-HA mice to examine lysosomal contents of microglia. However, it is important to note that further optimization of this assay is required, as there have been no previous reports of lysosome pull-downs from whole mouse brains.

To investigate the interactome of microglia in the absence of progranulin, Microglial-BAR was performed in progranulin deficient mouse brains. The obtained results demonstrated similar changes to those observed in the Lyso-BAR dataset. This is consistent with the known influence of progranulin on lysosomal function, its high expression by microglia, and the upregulation of progranulin by microglia in response to injury (Moisse et al., 2009; Petkau et al., 2010). However, a direct comparison between Lyso-BAR and microglial-BAR was not conducted due to the different age of the mice used in the two experiments (20 and 6-8 months respectively). To obtain a more comprehensive coverage of the true lysosomal contents, future studies could utilize CD68 as a lysosomal marker specific to microglia to repeat the BAR experiments in these mice. Moreover, performing lysosomal assays on Ctsb and Ctsd activity in primary microglia from these mice could provide further insight into the functional significance of the observed increase in these enzymes.

7.5 Pre-plaque AD-Associated Microglia

Neuroinflammation is a recurring feature in neurodegenerative disorders, and microglia have been extensively linked to disease pathology. Recent studies have demonstrated the involvement of microglia in complement-mediated synapse pruning in Alzheimer's disease (AD), which is also observed in progranulin-deficient mice (Hong et al., 2016; Lui et al., 2016). Thus, the aim of this chapter was to investigate the impact of early AD model changes on microglial function. For this purpose, I conducted microglial-BAR using two markers: a calcium-binding protein, Iba1, and P2y12. However, there was an issue with the Iba1 group where the protein abundances in the wildtype compared to the AD mouse were significantly different, which could not be rectified by normalization. As a result, analysis on that group was stopped. On the other hand, the P2y12 group produced robust data that revealed alterations in the abundance of proteins associated with oxidative phosphorylation and endocytosis/phagocytosis in early AD model. Given that oxidative stress-associated mitochondrial issues are widely reported in AD, the endocytosis/phagosome hits obtained from the microglial-BAR analysis merit further investigation (Caspersen et al., 2005: Olagunju et al., 2023). A repeat experiment should be conducted to account for any unseen issues that resulted in the non-salvageable Iba1 microglial-BAR before proceeding. Interestingly, microglial-BAR from early AD mouse model showed a decrease in oxidative phosphorylation hits, whereas endocytosis/phagosome associated proteins were increased. This could indicate an increase in phagocytic activity of these microglia. Therefore, a follow up experiment would be conducting phagocytic assays in primary microglia from these mice, which should ideally be harvested at 6 months of age. Further immunohistochemistry experiments targeting these endocytosis/phagosome proteins needs to

be conducted to verify the changes seen in microglial-BAR. Moreover, performing Lyso-BAR using CD68 as a target marker in these mice may yield valuable insights into the phagocytic activity of these microglia and any possible lysosomal dysfunction they may be experiencing.

An interesting hypothesis to explore is the interactions between amyloid aggregates and microglia at the interface. This can be achieved through the implementation of a method called split-peroxidase (Martell et al., 2016; Han et al., 2019; Ramirez et al., 2021). I propose the development of a Split-BAR method, where the HRP is divided into two inactive subunits that can rejoin into an enzymatically active form when in close proximity, specifically capturing the interface between two target proteins if they interact. To accomplish this, nanobodies can be used in combination with a split form of the enzyme (APEX or HRP) by linking them together with a flexible linker, enabling subunit movement and joining upon proximity. Split peroxidases and nanobodies have already been engineered and utilized in various studies (Yamagata and Sanes, 2018). By engineering primary antibody heavy-chain specific nanobodies with the split peroxidase attached, we can adapt this technique to different hypotheses of interest. In our case, since the lab commonly uses antibodies raised in mouse or rabbit hosts, the nanobodies would target the Fc portion of these primary antibodies. This approach allows for the utilization of antibodies from mouse and rabbit hosts to study the interaction between amyloid oligomers and microglial cell surfaces, which are the specific targets for this proposal.

7.6 Conclusion

In summary, the purpose of this work was to develop a tool that could aid in the understanding of neurodegenerative diseases in patients and ultimately lead to improved therapeutic options. Although the research here faced various challenges, significant progress was made. The consistent application of BAR to mouse brain tissue enabled the identification of target-relevant hits, which in turn provided insights into the pathophysiology of diseases. Specifically, by applying BAR to the study of progranulin deficiency, this work was able to link microglia to lysosomal dysfunction in progranulin-deficient mouse brains, thereby enhancing our knowledge of the lysosome's role in this disease. Additionally, the application of microglial-BAR to early AD revealed early dysfunctions in phagocytosis, although validation of these implications is crucial. Overall, BAR represents a valuable tool in the scientific arsenal for unraveling the mysteries of neurodegeneration and developing better treatments for patients.

Bibliography

Abiega, O., Beccari, S., Diaz-Aparicio, I., Nadjar, A., Layé, S., Leyrolle, Q., Gómez-Nicola, D., Domercq, M., Pérez-Samartín, A., Sánchez-Zafra, V., Paris, I., Valero, J., Savage, J. C., Hui, C. W., Tremblay, M. È., Deudero, J. J. P., Brewster, A. L., Anderson, A. E., Zaldumbide, L., … Sierra, A. (2016). Neuronal Hyperactivity Disturbs ATP Microgradients, Impairs Microglial Motility, and Reduces Phagocytic Receptor Expression Triggering Apoptosis/Microglial Phagocytosis Uncoupling. *PLoS Biology*, *14*(5). https://doi.org/10.1371/journal.pbio.1002466

Abu-Remaileh, M., Wyant, G. A., Kim, C., Laqtom, N. N., Abbasi, M., Chan, S. H., Freinkman, E., & David, S. M. (2017). Lysosomal metabolomics reveals V-ATPase- and mTOR-dependent regulation of amino acid efflux from lysosomes. *Science*, *358*, 807–813. https://www.science.org

Abud, E. M., Ramirez, R. N., Martinez, E. S., Healy, L. M., Nguyen, C. H. H., Newman, S. A., Yeromin, A. V., Scarfone, V. M., Marsh, S. E., Fimbres, C., Caraway, C. A., Fote, G. M., Madany, A. M., Agrawal, A., Kayed, R., Gylys, K. H., Cahalan, M. D., Cummings, B. J., Antel, J. P., … Blurton-Jones, M. (2017). iPSC-Derived Human Microglia-like Cells to Study Neurological Diseases. *Neuron*, *94*(2), 278-293.e9. https://doi.org/10.1016/j.neuron.2017.03.042

Aebersold, R., & Mann, M. (2003). Mass spectrometry-based proteomics. *Nature*, *422*, 198–207. www.nature.com/nature

Ahmed, R., Irish, M., van Eersel, J., Ittner, A., Ke, Y., Volkerling, A., van der Hoven, J., Tanaka, K., Karl, T., Kassiou, M., Kril, J., Piguet, O., Götz, J., Kiernan, M., Halliday, G., Hodges, J., Ittner, L. (2017) Mouse models of frontotemporal dementia: A comparison of phenotypes with clinical symptomatology. *Neuroscience and*

Biobehavioral Reviews, 126-138, 74. https://doi.org/10.1016/j.neubiorev.2017.01.004

Ahmed, Z., Sheng, H., Xu, Y. F., Lin, W. L., Innes, A. E., Gass, J., Yu, X., Hou, H., Chiba, S., Yamanouchi, K., Leissring, M., Petrucelli, L., Nishihara, M., Hutton, M. L., McGowan, E., Dickson, D. W., & Lewis, J. (2010). Accelerated lipofuscinosis and ubiquitination in granulin knockout mice suggest a role for progranulin in successful aging. *American Journal of Pathology*, *177*(1), 311–324. https://doi.org/10.2353/ajpath.2010.090915

Alliot, F., Godin, I., Pessac, B., & Francé, F. (1999). Microglia derive from progenitors, originating from the yolk sac, and which proliferate in the brain. *Developmental Brain Research*, *117*, 1999–145. www.elsevier.comrlocaterbres

Amaral, E. P., Riteau, N., Moayeri, M., Maier, N., Mayer-Barber, K. D., Pereira, R. M., Lage, S. L., Kubler, A., Bishai, W. R., D'Império-Lima, M. R., Sher, A., & Andrade, B. B. (2018). Lysosomal cathepsin release is required for nlrP3-inflammasome activation by Mycobacterium tuberculosis in infected Macrophages. *Frontiers in Microbiology*, *9*(JUN). https://doi.org/10.3389/fimmu.2018.01427

Anakwe, O. O., & Gerton, G. L. (1990). Acrosome Biogenesis Begins during Meiosis: Evidence from the Synthesis and Distribution of an Acrosomal Glycoprotein, Acrogranin, during Guinea Pig Spermatogenesis. *Biology of Reproduction*, *42*, 317–328. https://academic.oup.com/biolreprod/article/42/2/317/2764327

Arai, T., Hasegawa, M., Akiyama, H., Ikeda, K., Nonaka, T., Mori, H., Mann, D., Tsuchiya, K., Yoshida, M., Hashizume, Y., & Oda, T. (2006). TDP-43 is a component of ubiquitin-positive tau-negative inclusions in frontotemporal lobar degeneration and amyotrophic lateral sclerosis. *Biochemical and Biophysical Research Communications*, *351*(3), 602–611. https://doi.org/10.1016/j.bbrc.2006.10.093

Bagshaw, R. D., Mahuran, D. J., & Callahan, J. W. (2005). A proteomic analysis of lysosomal integral membrane proteins reveals the diverse composition of the organelle. *Molecular and Cellular*

Proteomics, *4*(2), 133–143. https://doi.org/10.1074/mcp.M400128-MCP200

Baker, M., Mackenzie, I. R., Pickering-Brown, S. M., Gass, J., Rademakers, R., Lindholm, C., Snowden, J., Adamson, J., Sadovnick, A. D., Rollinson, S., Cannon, A., Dwosh, E., Neary, D., Melquist, S., Richardson, A., Dickson, D., Berger, Z., Eriksen, J., Robinson, T., … Hutton, M. (2006). Mutations in progranulin cause tau-negative frontotemporal dementia linked to chromosome 17. *Nature*, *442*(7105), 916–919. https://doi.org/10.1038/nature05016

Ballabio, A., & Bonifacino, J. S. (2020). Lysosomes as dynamic regulators of cell and organismal homeostasis. *Nature Reviews Molecular Cell Biology*, *21*(2), 101–118. https://doi.org/10.1038/s41580-019-0185-4

Bar, D. Z., Atkatsh, K., Tavarez, U., Erdos, M. R., Gruenbaum, Y., & Collins, F. S. (2018). Biotinylation by antibody recognition - a method for proximity labeling. *Nature Methods*, *15*(2), 127–133. https://doi.org/10.1038/nmeth.4533

Bateman, A., Belcourt, D., Bennett, H., Lazure, C., & Solomon, S. (1990). Granulin, a novel class of peptide from leukocytes. *Biochemical and Biophysical Research Communications*, *173*(3), 1161–1168.

Becher, B., Spath, S., & Goverman, J. (2017). Cytokine networks in neuroinflammation. *Nature Reviews Immunology*, *17*(1), 49–59. https://doi.org/10.1038/nri.2016.123

Becker, N. H., Goldfischer, S., Shin, W.-Y., & Novikoff, A. B. (1960). The localization of enzyme activities in the brain. *The Journal of Biophysical and Biochemical Cytology*, *8*, 649–663.

Bellenguez, C., Küçükali, F., Jansen, I. E., Kleineidam, L., Moreno-Grau, S., Amin, N., Naj, A. C., Campos-Martin, R., Grenier-Boley, B., Andrade, V., Holmans, P. A., Boland, A., Damotte, V., van der Lee, S. J., Costa, M. R., Kuulasmaa, T., Yang, Q., de Rojas, I., Bis, J. C., … Lambert, J.-C. (2022). New insights into the genetic etiology of Alzheimer's disease and related dementias. *Nature Genetics*, *54*(4), 412–436. https://doi.org/10.1038/s41588-022-01024-z

Bereczki, E., Attems, J., & Jellinger, K. (2018). Proteomics for synaptic markers of cognitive decline in neurodegenerative diseases. *Brain*, *141*(2), 329–331. https://doi.org/10.1093/brain/awx360

Bereczki, E., Francis, P. T., Howlett, D., Pereira, J. B., Höglund, K., Bogstedt, A., Cedazo-Minguez, A., Baek, J. H., Hortobágyi, T., Attems, J., Ballard, C., & Aarsland, D. (2016). Synaptic proteins predict cognitive decline in Alzheimer's disease and Lewy body dementia. *Alzheimer's and Dementia*, *12*(11), 1149–1158. https://doi.org/10.1016/j.jalz.2016.04.005

Bettegazzi, B., Bellani, S., Cattaneo, S., Codazzi, F., Grohovaz, F., & Zacchetti, D. (2021). Gα13 Contributes to LPS-Induced Morphological Alterations and Affects Migration of Microglia. *Molecular Neurobiology*, *58*(12), 6397–6414. https://doi.org/10.1007/s12035-021-02553-0

Bhandari, V., Giaids, A., & Batemans, A. (1993). The Complementary Deoxyribonucleic Acid Sequence, Tissue Distribution, and Cellular Localization of the Rat Granulin Precursor*. *Endocrinology*, *133*(6). https://academic.oup.com/endo/article/133/6/2682/3035991

Blasi, E., Barluzzi, R., Bocchini, V., Mazzolla, R., & Bistoni, F. (1990). Immortalization of murine microglial cells by a v-raf/v-myc carrying retrovirus. *Journal of Neuroimmunology*, *27*, 229–237.

Bohlen, C. J., Bennett, F. C., & Bennett, M. L. (2019). Isolation and Culture of Microglia. *Current Protocols in Immunology*, *125*(1). https://doi.org/10.1002/cpim.70

Bohlen, C. J., Bennett, F. C., Tucker, A. F., Collins, H. Y., Mulinyawe, S. B., & Barres, B. A. (2017). Diverse Requirements for Microglial Survival, Specification, and Function Revealed by Defined-Medium Cultures. *Neuron*, *94*(4), 759-773.e8. https://doi.org/10.1016/j.neuron.2017.04.043

Bollinger, J. L., Dadosky, D. T., Flurer, J. K., Rainer, I. L., Woodburn, S. C., & Wohleb, E. S. (2022). Microglial P2Y12 mediates chronic stress-induced synapse loss in the prefrontal cortex and associated behavioral consequences. *Neuropsychopharmacology*. https://doi.org/10.1038/s41386-022-01519-7

Bordt, E. A., Block, C. L., Petrozziello, T., Sadri-Vakili, G., Smith, C. J., Edlow, A. G., & Bilbo, S. D. (2020). Isolation of Microglia from Mouse or Human Tissue. *STAR Protocols*, *1*(1). https://doi.org/10.1016/j.xpro.2020.100035

Braak, H., & Braak, E. (1991). Neuropathological stageing of Alzheimer-related changes. *Acta Neuropathol*, *82*, 239–259.

Braak, H., Braak, E., Grundke-Iqbal, I., & Iqbal, K. (1986). Occurrence of neuropil threads in the senile human brain and in Alzheimer's disease: a third location of paired helical filaments outside of neurofibrillary tangles and neuritic plaques. *Neuroscience Letters*, *65*, 351–355.

Branon, T. C., Bosch, J. A., Sanchez, A. D., Udeshi, N. D., Svinkina, T., Carr, S. A., Feldman, J. L., Perrimon, N., & Ting, A. Y. (2018). Efficient proximity labeling in living cells and organisms with TurboID. *Nature Biotechnology*, *36*(9), 880–898. https://doi.org/10.1038/nbt.4201

Bright, J., Hussain, S., Dang, V., Wright, S., Cooper, B., Byun, T., Ramos, C., Singh, A., Parry, G., Stagliano, N., & Griswold-Prenner, I. (2015). Human secreted tau increases amyloid-beta production. *Neurobiology of Aging*, *36*(2), 693–709. https://doi.org/10.1016/j.neurobiolaging.2014.09.007

Brouwers, N., Sleegers, M. K., Engelborghs, S., Maurer-Stroh, S., Gijselinck, I., Van Der Zee, J., Pickut, B. A., Van Den Broeck, M., Mattheijssens, M., Peeters, K., Schymkowitz, J., Rousseau, F., Martin, J.-J., Cruts, M., De Deyn, P. P., & Van Broeckhoven, C. (2008). Genetic variability in progranulin contributes to risk for clinically diagnosed Alzheimer disease. *Neurology*, *71*, 656–664. www.neurology.org.

Bruttger, J., Karram, K., Wörtge, S., Regen, T., Marini, F., Hoppmann, N., Klein, M., Blank, T., Yona, S., Wolf, Y., Mack, M., Pinteaux, E., Müller, W., Zipp, F., Binder, H., Bopp, T., Prinz, M., Jung, S., & Waisman, A. (2015). Genetic Cell Ablation Reveals Clusters of Local Self-Renewing Microglia in the Mammalian Central Nervous System. *Immunity*, *43*(1), 92–106. https://doi.org/10.1016/j.immuni.2015.06.012

Bsibsi, M., Ravid, R., & Van Noort, J. M. (2002). Broad Expression of Toll-Like Receptors in the Human Central Nervous System. *Journal of Neuropathology and Experimental Neurology*, *61*(11). https://academic.oup.com/jnen/article/61/11/1013/2916258

Butler, V. J., Cortopassi, W. A., Argouarch, A. R., Ivry, S. L., Craik, C. S., Jacobson, M. P., & Kao, A. W. (2019). Progranulin Stimulates the In Vitro Maturation of Pro-Cathepsin D at Acidic pH. *Journal of Molecular Biology*, *431*(5), 1038–1047. https://doi.org/10.1016/j.jmb.2019.01.027

Butovsky, O., Jedrychowski, M. P., Moore, C. S., Cialic, R., Lanser, A. J., Gabriely, G., Koeglsperger, T., Dake, B., Wu, P. M., Doykan, C. E., Fanek, Z., Liu, L., Chen, Z., Rothstein, J. D., Ransohoff, R. M., Gygi, S. P., Antel, J. P., & Weiner, H. L. (2014). Identification of a unique TGF-β-dependent molecular and functional signature in microglia. *Nature Neuroscience*, *17*(1), 131–143. https://doi.org/10.1038/nn.3599

Butovsky, O., Ziv, Y., Schwartz, A., Landa, G., Talpalar, A. E., Pluchino, S., Martino, G., & Schwartz, M. (2006). Microglia activated by IL-4 or IFN-γ differentially induce neurogenesis and oligodendrogenesis from adult stem/progenitor cells. *Molecular and Cellular Neuroscience*, *31*(1), 149–160. https://doi.org/10.1016/j.mcn.2005.10.006

Cadiz, M. P., Jensen, T. D., Sens, J. P., Zhu, K., Song, W. M., Zhang, B., Ebbert, M., Chang, R., & Fryer, J. D. (2022). Culture shock: microglial heterogeneity, activation, and disrupted single-cell microglial networks in vitro. *Molecular Neurodegeneration*, *17*(1). https://doi.org/10.1186/s13024-022-00531-1

Cai, Q., Lu, L., Tian, J. H., Zhu, Y. B., Qiao, H., & Sheng, Z. H. (2010). Snapin-regulated late endosomal transport is critical for efficient autophagy-lysosomal function in neurons. *Neuron*, *68*(1), 73–86. https://doi.org/10.1016/j.neuron.2010.09.022

Caspersen, C., Wang, N., Yao, J., Sosunov, A., Chen, X., Lustbader, J. W., Xu, H. W., Stern, D., McKhann, G., & Du Yan, S. (2005). Mitochondrial Aβ: a potential focal point for neuronal metabolic

dysfunction in Alzheimer's disease. *The FASEB Journal*, *19*(14), 2040–2041. https://doi.org/10.1096/fj.05-3735fje

Chambers, C. B., Lee, J. M., Troncoso, J. C., Reich, S., & Muma, N. A. (1999). Overexpression of four-repeat tau mRNA isoforms in progressive supranuclear palsy but not in Alzheimer's disease. *Annals of Neurology*, *46*(3), 325–332. https://doi.org/10.1002/1531-8249(199909)46:3<325::AID-ANA8>3.0.CO;2-V

Chen, J. W., Murphy, T. L., Wlllingham, M. C., Pastan, I., & August, J. T. (1985). Identification of Two Lysosomal Membrane Glycoproteins. *The Journal of CEll Biology*, *101*(5), 85–95. http://rupress.org/jcb/article-pdf/101/1/85/1051998/85.pdf

Cheng, X. T., Xie, Y. X., Zhou, B., Huang, N., Farfel-Becker, T., & Sheng, Z. H. (2018). Characterization of LAMP1-labeled nondegradative lysosomal and endocytic compartments in neurons. *Journal of Cell Biology*, *217*(9), 3127–3139. https://doi.org/10.1083/jcb.201711083

Chistiakov, D. A., Killingsworth, M. C., Myasoedova, V. A., Orekhov, A. N., & Bobryshev, Y. V. (2017). CD68/macrosialin: Not just a histochemical marker. *Laboratory Investigation*, *97*(1), 4–13. https://doi.org/10.1038/labinvest.2016.116

Choi-Rhee, E., Schulman, H., & Cronan, J. E. (2004). Promiscuous protein biotinylation by Escherichia coli biotin protein ligase. *Protein Science*, *13*(11), 3043–3050. https://doi.org/10.1110/ps.04911804

Choi, S. Y., Lopez-Gonzalez, R., Krishnan, G., Phillips, H. L., Li, A. N., Seeley, W. W., Yao, W. D., Almeida, S., & Gao, F. B. (2019). C9ORF72-ALS/FTD-associated poly(GR) binds Atp5a1 and compromises mitochondrial function in vivo. *Nature Neuroscience*, *22*(6), 851–862. https://doi.org/10.1038/s41593-019-0397-0

Chopra, G., Shabir, S., Yousuf, S., Kauts, S., Bhat, S. A., Mir, A. H., & Singh, M. P. (2022). Proteinopathies: Deciphering Physiology and Mechanisms to Develop Effective Therapies for Neurodegenerative Diseases. *Molecular Neurobiology*, *59*(12), 7513–7540. https://doi.org/10.1007/s12035-022-03042-8

Cortini, F., Fenoglio, C., Guidi, I., Venturelli, E., Pomati, S., Marcone, A., Scalabrini, D., Villa, C., Clerici, F., Dalla Valle, E., Mariani, C., Cappa, S., Bresolin, N., Scarpini, E., & Galimberti, D. (2008). Novel exon 1 progranulin gene variant in Alzheimer's disease. *European Journal of Neurology*, *15*(10), 1111–1117. https://doi.org/10.1111/j.1468-1331.2008.02266.x

Cox, J., & Mann, M. (2008). MaxQuant enables high peptide identification rates, individualized p.p.b.-range mass accuracies and proteome-wide protein quantification. *Nature Biotechnology*, *26*(12), 1367–1372. https://doi.org/10.1038/nbt.1511

Cras, P., Kawai, M., Siedlak, S., Mulvihill, P., Gambetti, P., Lowery, D., Gonzalez-Dewhitt, P., Greenberg, B., & Perry, G. (1990). Neuronal and Microglial Involvement in f3-Amyloid Protein Deposition in Alzheimer's Disease. *AmericanJournal OfPathology*, *137*(2).

Cruts, M., Gijselinck, I., Van Der Zee, J., Engelborghs, S., Wils, H., Pirici, D., Rademakers, R., Vandenberghe, R., Dermaut, B., Martin, J. J., Van Duijn, C., Peeters, K., Sciot, R., Santens, P., De Pooter, T., Mattheijssens, M., Van Den Broeck, M., Cuijt, I., Vennekens, K., … Van Broeckhoven, C. (2006). Null mutations in progranulin cause ubiquitin-positive frontotemporal dementia linked to chromosome 17q21. *Nature*, *442*(7105), 920–924. https://doi.org/10.1038/nature05017

Cserép, C., Pósfai, B., Lénárt, N., Fekete, R., László, Z. I., Lele, Z., Orsolits, B., Molnár, G., Heindl, S., Schwarcz, A. D., Ujvári, K., Környei, Z., Tóth, K., Szabadits, E., Sperlágh, B., Baranyi, M., Csiba, L., Hortobágyi, T., Maglóczky, Z., … Dénes, Á. (2020). Microglia monitor and protect neuronal function through specialized somatic purinergic junctions. *Science*, *367*, 528–537. https://www.science.org

Dalpke, A. H., K-H Schä fer, M., Frey, M., Zimmermann, S., Tebbe, J., Weihe, E., & Heeg, K. (2002). Immunostimulatory CpG-DNA Activates Murine Microglia 1. *The Journal of Immunology*, *168*, 4854–4863. http://journals.aai.org/jimmunol/article-pdf/168/10/4854/1317385/4854.pdf

Daskoulidou, N., Shaw, B., Torvell, M., Watkins, L., Cope, E. L., Carpanini, S. M., Allen, N. D., & Morgan, B. P. (2023). Complement receptor 1 is expressed on brain cells and in the human brain. *GLIA*. https://doi.org/10.1002/glia.24355

Davalos, D., Grutzendler, J., Yang, G., Kim, J. V., Zuo, Y., Jung, S., Littman, D. R., Dustin, M. L., & Gan, W. B. (2005). ATP mediates rapid microglial response to local brain injury in vivo. *Nature Neuroscience*, *8*(6), 752–758. https://doi.org/10.1038/nn1472

Davis, D., Schmitt, F., Wekstein, D., & Markesbery, W. (1999). Alzheimer neuropathologic alterations in aged cognitively normal subjects. *J Neuropathol Exp Neurol*. 58(4), 376-388.

De Calignon, A., Polydoro, M., Suárez-Calvet, M., William, C., Adamowicz, D. H., Kopeikina, K. J., Pitstick, R., Sahara, N., Ashe, K. H., Carlson, G. A., Spires-Jones, T. L., & Hyman, B. T. (2012). Propagation of Tau Pathology in a Model of Early Alzheimer's Disease. *Neuron*, *73*(4), 685–697. https://doi.org/10.1016/j.neuron.2011.11.033

de Castro, M., Bunt, G., & Wouters, F. (2016). Cathepsin B launches an apoptotic exit effort upon cell death-associated disruption of lysosomes. *Cell Death Discovery*, *2*(1). https://doi.org/10.1038/cddiscovery.2016.12

De Schepper, S., Crowley, G., & Hong, S. (2020). Understanding microglial diversity and implications for neuronal function in health and disease. *Developmental Neurobiology*, *81*(5), 507–523. https://doi.org/10.1002/dneu.22777

De Schepper, S., Ge, J. Z., Crowley, G., Ferreira, L. S. S., Garceau, D., Toomey, C. E., Sokolova, D., Rueda-Carrasco, J., Shin, S. H., Kim, J. S., Childs, T., Lashley, T., Burden, J. J., Sasner, M., Sala Frigerio, C., Jung, S., & Hong, S. (2023). Perivascular cells induce microglial phagocytic states and synaptic engulfment via SPP1 in mouse models of Alzheimer's disease. *Nature Neuroscience*, *26*(3), 406–415. https://doi.org/10.1038/s41593-023-01257-z

Deng, Y., & Storrie, B. (1988). Animal cell lysosomes rapidly exchange membrane proteins. In *Proc. Nati. Acad. Sci. USA* (Vol. 85).

DeJesus-Hernandez, M., Mackenzie, I. R., Boeve, B. F., Boxer, A. L., Baker, M., Rutherford, N. J., Nicholson, A. M., Finch, N. C. A., Flynn, H., Adamson, J., Kouri, N., Wojtas, A., Sengdy, P., Hsiung, G. Y. R., Karydas, A., Seeley, W. W., Josephs, K. A., Coppola, G., Geschwind, D. H., … Rademakers, R. (2011). Expanded GGGGCC Hexanucleotide Repeat in Noncoding Region of C9ORF72 Causes Chromosome 9p-Linked FTD and ALS. *Neuron*, *72*(2), 245–256. https://doi.org/10.1016/j.neuron.2011.09.011

DeKosky, S. T., & Scheff, S. W. (1990). Synapse loss in frontal cortex biopsies in Alzheimer's disease: Correlation with cognitive severity. *Annals of Neurology*, *27*(5), 457–464. https://doi.org/10.1002/ana.410270502

Deluca, C., Brownt, J. A., & Showsf, T. B. (1979). Lysosomal arylsulfatase deficiencies in humans: Chromosome assignments for arylsulfatase A and B (somatic cell hybrids/human chromosomes 5 and 22/metachromatic leukodystrophy/Maroteaux-Lamy syndrome/multiple sulfatase deficiency). *Genetics*, *76*(4), 1957–1961. https://www.pnas.org

Deng, J., Wang, P., Chen, X., Cheng, H., Liu, J., Fushimi, K., Zhu, L., & Wu, J. Y. (2018). FUS interacts with ATP synthase beta subunit and induces mitochondrial unfolded protein response in cellular and animal models. *Proceedings of the National Academy of Sciences of the United States of America*, *115*(41), E9678–E9686. https://doi.org/10.1073/pnas.1806655115

Deng, J., Yang, M., Chen, Y., Chen, X., Liu, J., Sun, S., Cheng, H., Li, Y., Bigio, E. H., Mesulam, M., Xu, Q., Du, S., Fushimi, K., Zhu, L., & Wu, J. Y. (2015). FUS Interacts with HSP60 to Promote Mitochondrial Damage. *PLoS Genetics*, *11*(9). https://doi.org/10.1371/journal.pgen.1005357

Devireddy, S., & Ferguson, S. M. (2022). Efficient progranulin exit from the ER requires its interaction with prosaposin, a Surf4 cargo. *Journal of Cell Biology*, *221*(2). https://doi.org/10.1083/jcb.202104044

DiFiglia, M., Sapp, E., Chase, K., Davies, S., Bates, G., Vonsattel, J., & Aronin, N. (1997). Aggregation of Huntingtin in Neuronal

Intranuclear Inclusions and Dystrophic Neurites in Brain. *Science*. *277*, 1990-1993.

Divangahi, M., Aaby, P., Khader, S. A., Barreiro, L. B., Bekkering, S., Chavakis, T., van Crevel, R., Curtis, N., DiNardo, A. R., Dominguez-Andres, J., Duivenwoorden, R., Fanucchi, S., Fayad, Z., Fuchs, E., Hamon, M., Jeffrey, K. L., Khan, N., Joosten, L. A. B., Kaufmann, E., … Netea, M. G. (2021). Trained immunity, tolerance, priming and differentiation: distinct immunological processes. *Nature Immunology*, *22*(1), 2–6. https://doi.org/10.1038/s41590-020-00845-6

Douvaras, P., Sun, B., Wang, M., Kruglikov, I., Lallos, G., Zimmer, M., Terrenoire, C., Zhang, B., Gandy, S., Schadt, E., Freytes, D. O., Noggle, S., & Fossati, V. (2017). Directed Differentiation of Human Pluripotent Stem Cells to Microglia. *Stem Cell Reports*, *8*(6), 1516–1524. https://doi.org/10.1016/j.stemcr.2017.04.023

Dräger, N. M., Sattler, S. M., Huang, C. T. L., Teter, O. M., Leng, K., Hashemi, S. H., Hong, J., Aviles, G., Clelland, C. D., Zhan, L., Udeochu, J. C., Kodama, L., Singleton, A. B., Nalls, M. A., Ichida, J., Ward, M. E., Faghri, F., Gan, L., & Kampmann, M. (2022). A CRISPRi/a platform in human iPSC-derived microglia uncovers regulators of disease states. *Nature Neuroscience*, *25*(9), 1149–1162. https://doi.org/10.1038/s41593-022-01131-4

Dragicevic, N., Mamcarz, M., Zhu, Y., Buzzeo, R., Tan, J., Arendash, G. W., & Bradshaw, P. C. (2010). Mitochondrial amyloid-β levels are associated with the extent of mitochondrial dysfunction in different brain regions and the degree of cognitive impairment in Alzheimer's transgenic mice. *Journal of Alzheimer's Disease*, *20*(SUPPL.2). https://doi.org/10.3233/JAD-2010-100342

Du, H., Guo, L., Yan, S., Sosunov, A. A., McKhann, G. M., & Yan, S. S. Du. (2010). Early deficits in synaptic mitochondria in an Alzheimer's disease mouse model. *Proceedings of the National Academy of Sciences of the United States of America*, *107*(43), 18670–18675. https://doi.org/10.1073/pnas.1006586107

Du, H., Zhou, X., Feng, T., & Hu, F. (2022). Regulation of lysosomal trafficking of progranulin by sortilin and prosaposin. *Brain*

Communications, *4*(1). https://doi.org/10.1093/braincomms/fcab310

Duarte, A., Poderoso, C., Cooke, M., Soria, G., Cornejo Maciel, F., Gottifredi, V., & Podestá, E. J. (2012). Mitochondrial Fusion Is Essential for Steroid Biosynthesis. *PLoS ONE*, *7*(9). https://doi.org/10.1371/journal.pone.0045829

Edwards-Lee, T., Miller, B. L., Benson, D. F., Cummings, J. L., Russell, G. L., Boone, K., & Mena, I. (1997). The temporal variant of frontotemporal dementia. *Brain*, *120*, 1027–1040.

Ehlers, M. (2000). Reinsertion or Degradation of AMPA Receptors Determined by Activity-Dependent Endocytic Sorting. *Neuron, 28*, 511-525.

Eng, J. K., Mccormack, A. L., & Yates, J. R. (1994). An Approach to Correlate Tandem Mass Spectral Data of Peptides with Amino Acid Sequences in a Protein Database. *American Society for Mass Spectrometry*, *5*, 976–989. https://pubs.acs.org/sharingguidelines

Evers, B. M., Rodriguez-Navas, C., Tesla, R. J., Prange-Kiel, J., Wasser, C. R., Yoo, K. S., McDonald, J., Cenik, B., Ravenscroft, T. A., Plattner, F., Rademakers, R., Yu, G., White, C. L., & Herz, J. (2017). Lipidomic and Transcriptomic Basis of Lysosomal Dysfunction in Progranulin Deficiency. *Cell Reports*, *20*(11), 2565–2574. https://doi.org/10.1016/j.celrep.2017.08.056

Evron, T., Daigle, T. L., & Caron, M. G. (2012). GRK2: Multiple roles beyond G protein-coupled receptor desensitization. In *Trends in Pharmacological Sciences* (Vol. 33, Issue 3, pp. 154–164). https://doi.org/10.1016/j.tips.2011.12.003

Farfel-Becker, T., Roney, J. C., Cheng, X. T., Li, S., Cuddy, S. R., & Sheng, Z. H. (2019). Neuronal Soma-Derived Degradative Lysosomes Are Continuously Delivered to Distal Axons to Maintain Local Degradation Capacity. *Cell Reports*, *28*(1), 51-64.e4. https://doi.org/10.1016/j.celrep.2019.06.013

Farías, G. G., Guardia, C. M., De Pace, R., Britt, D. J., & Bonifacino, J. S. (2017). BORC/kinesin-1 ensemble drives polarized transport of

lysosomes into the axon. *Proceedings of the National Academy of Sciences of the United States of America*, *114*(14), E2955–E2964. https://doi.org/10.1073/pnas.1616363114

Feng, T., Mai, S., Roscoe, J. M., Sheng, R. R., Ullah, M., Zhang, J., Katz, I. I., Yu, H., Xiong, W., & Hu, F. (2020). Loss of TMEM 106B and PGRN leads to severe lysosomal abnormalities and neurodegeneration in mice. *EMBO Reports*, *21*(10). https://doi.org/10.15252/embr.202050219

Ferguson, S. M. (2019). Neuronal lysosomes. *Neuroscience Letters*, *697*(March 2018), 1–9. https://doi.org/10.1016/j.neulet.2018.04.005

Fernández-Monreal, M., Brown, T.C., Royo, M., Esteban, J.A. (2012). The Balance between Receptor Recycling and Trafficking toward Lysosomes Determines Synaptic Strength during Long-Term Depression. *The Journal of Neuroscience, 32(38),* 13200-13205.

Fernandopulle, M. S., Prestil, R., Grunseich, C., Wang, C., Gan, L., & Ward, M. E. (2018). Transcription Factor–Mediated Differentiation of Human iPSCs into Neurons. *Current Protocols in Cell Biology*, *79*(1). https://doi.org/10.1002/cpcb.51

Ferrari, R., Hernandez, D. G., Nalls, M. A., Rohrer, J. D., Ramasamy, A., J Kwok, J. B., Dobson-Stone, C., Brooks, W. S., Schofi eld, P. R., Halliday, G. M., Hodges, J. R., Piguet, O., Bartley, L., Thompson, E., Haan, E., Hernández, I., Ruiz, A., Boada, M., Borroni, B., … Momeni, P. (2014). Frontotemporal dementia and its subtypes: a genome-wide association study. *The Lancet Neurology*, *13*. www.thelancet.com/neurology

Fluharty, A. L., Fluharty, C. B., Bohne, W., Von Figura, K., & Gieselmannt, V. (1991). Two New Arylsulfatase A (ARSA) Mutations in a Juvenile Metachromatic Leukodystrophy (MLD) Patient. *Am. J. Hum. Genet*, *49*, 1340–1350.

Fox, T., De Miguel, E., Mort, J. S., & Storer, A. C. (1992). Potent Slow-Binding Inhibition of Cathepsin B by Its Propeptide* 1 II". *Biochemistry*, *31*, 12571–12576. https://pubs.acs.org/sharingguidelines

Frankenfield, A. M., Fernandopulle, M. S., Hasan, S., Ward, M. E., & Hao, L. (2020). Development and Comparative Evaluation of Endolysosomal Proximity Labeling-Based Proteomic Methods in Human iPSC-Derived Neurons. *Analytical Chemistry*, *92*(23), 15437–15444. https://doi.org/10.1021/acs.analchem.0c03107

Galatro, T. F., Holtman, I. R., Lerario, A. M., Vainchtein, I. D., Brouwer, N., Sola, P. R., Veras, M. M., Pereira, T. F., Leite, R. E. P., Möller, T., Wes, P. D., Sogayar, M. C., Laman, J. D., Den Dunnen, W., Pasqualucci, C. A., Oba-Shinjo, S. M., Boddeke, E. W. G. M., Marie, S. K. N., & Eggen, B. J. L. (2017). Transcriptomic analysis of purified human cortical microglia reveals age-associated changes. *Nature Neuroscience*, *20*(8), 1162–1171. https://doi.org/10.1038/nn.4597

Galloway, D., Phillips, A., Owen, D., Moore, C. (2019). Phagocytosis in the brain: Homeostasis and disease. *Frontiers in Immunology*, 10. https://doi.org/10.3389/fimmu.2019.00790

Gass, J., Prudencio, M., Stetler, C., & Petrucelli, L. (2012). Progranulin: An emerging target for FTLD therapies. *Brain Research*, *1462*, 118–128. https://doi.org/10.1016/j.brainres.2012.01.047

Gavin, A. C., Aloy, P., Grandi, P., Krause, R., Boesche, M., Marzioch, M., Rau, C., Jensen, L. J., Bastuck, S., Dümpelfeld, B., Edelmann, A., Heurtier, M. A., Hoffman, V., Hoefert, C., Klein, K., Hudak, M., Michon, A. M., Schelder, M., Schirle, M., … Superti-Furga, G. (2006). Proteome survey reveals modularity of the yeast cell machinery. *Nature*, *440*(7084), 631–636. https://doi.org/10.1038/nature04532

Ge, S. X., Jung, D., & Yao, R. (2020). ShinyGO: a graphical gene-set enrichment tool for animals and plants. *Bioinformatics*, *36*(8), 2628–2629. https://doi.org/10.5281/zenodo.1451847

Ghoshal, N., Dearborn, J. T., Wozniak, D. F., & Cairns, N. J. (2012). Core features of frontotemporal dementia recapitulated in progranulin knockout mice. *Neurobiology of Disease*, *45*(1), 395–408. https://doi.org/10.1016/j.nbd.2011.08.029

Gijselinck, I., Van Der Zee, J., Engelborghs, S., Goossens, D., Peeters, K., Mattheijssens, M., Corsmit, E., Del-Favero, J., De Deyn, P. P.,

Van Broeckhoven, C., & Cruts, M. (2008). Progranulin locus deletion in frontotemporal dementia. *Human Mutation*, *29*(1), 53–58. https://doi.org/10.1002/humu.20651

Ginhoux, F., Greter, M., Leboeuf, M., Nandi, S., See, P., Gokhan, S., Mehler, M., Conway, S., Guan Ng, L., Stanley, E., Samokhvalov, I., & Merad, M. (2010). Fate Mapping Analysis RevealsThat Adult Microglia Derive fromPrimitive Macrophages. *Science*, *330*(6005), 838–841. https://doi.org/10.1126/science.1194554

Ginhoux, F., Lim, S., Hoeffel, G., Low, D., & Huber, T. (2013). Origin and differentiation of microglia. *Frontiers in Cellular Neuroscience*, *MAR*. https://doi.org/10.3389/fncel.2013.00045

Glenner, G. G., & Wong, C. W. (1984). Alzheimer's Disease: Initial report of the purification and characterization of a novel cerebrovascular amyloid protein. *Biochemical and Biophysical Research Communications*, *120*(3), 885–890.

Godbout, J. P., Chen, J., Abraham, J., Richwine, A. F., Berg, B. M., Kelley, K. W., & Johnson, R. W. (2005). Exaggerated neuroinflammation and sickness behavior in aged mice after activation of the peripheral innate immune system. *The FASEB Journal*, *19*(10), 1329–1331. https://doi.org/10.1096/fj.05-3776fje

Gong, Y., Chang, L., Viola, K. L., Lacor, P. N., Lambert, M. P., Finch, C. E., Krafft, G. A., & Klein, W. L. (2003). Alzheimer's disease-affected brain: Presence of oligomeric A ligands (ADDLs) suggests a molecular basis for reversible memory loss. *PNAS*, *100*(18), 10417–10422. www.pnas.orgcgidoi10.1073pnas.1834302100

Gordon, B. A., Blazey, T. M., Su, Y., Hari-Raj, A., Dincer, A., Flores, S., Christensen, J., McDade, E., Wang, G., Xiong, C., Cairns, N. J., Hassenstab, J., Marcus, D. S., Fagan, A. M., Jack, C. R., Hornbeck, R. C., Paumier, K. L., Ances, B. M., Berman, S. B., … Benzinger, T. L. S. (2018). Spatial patterns of neuroimaging biomarker change in individuals from families with autosomal dominant Alzheimer's disease: a longitudinal study. *The Lancet Neurology*, *17*(3), 241–250. https://doi.org/10.1016/S1474-4422(18)30028-0

Gorenstein, C., Bundman, M. C., Lew, P. J., Olds, J. L., & Ribak, C. E. (1985). Dendritic Transport I. Colchicine Stimulates the Transport of Lysosomal Enzymes from Cell Bodies to Dendrites'. *The Journal of Neutosclence*, *5*(8).

Gorno-Tempini, M. L., Dronkers, N. F., Rankin, K. P., Ogar, J. M., Phengrasamy, L., Rosen, H. J., Johnson, J. K., Weiner, M. W., & Miller, B. L. (2004). Cognition and Amatomy in Three Variants of Primany Progressive Aphasia. *Annals of Neurology*, *55*(3), 335–346. https://doi.org/10.1002/ana.10825

Gosselin, D., Skola, D., Coufal, N. G., Holtman, I. R., Schlachetzki, J. C. M., Sajti, E., Jaeger, B. N., O'Connor, C., Fitzpatrick, C., Pasillas, M. P., Pena, M., Adair, A., Gonda, D. D., Levy, M. L., Ransohoff, R. M., Gage, F. H., & Glass, C. K. (2017). An environment-dependent transcriptional network specifies human microglia identity. *Science*, *356*(6344), 1248–1259. https://doi.org/10.1126/science.aal3222

Götz, J., Halliday, G., & Nisbet, R. M. (2019). Molecular Pathogenesis of the Tauopathies. *Annual Reviews of Pathology: Mechanism of Disease*, *14*, 239–261. https://doi.org/10.1146/annurev-pathmechdis-012418-012936

Götzl, J. K., Colombo, A. V., Fellerer, K., Reifschneider, A., Werner, G., Tahirovic, S., Haass, C., & Capell, A. (2018). Early lysosomal maturation deficits in microglia triggers enhanced lysosomal activity in other brain cells of progranulin knockout mice. *Molecular Neurodegeneration*, *13*(1). https://doi.org/10.1186/s13024-018-0281-5

Gowrishankar, S., Wu, Y., & Ferguson, S. M. (2017). Impaired JIP3-dependent axonal lysosome transport promotes amyloid plaque pathology. *Journal of Cell Biology*, *216*(10), 3291–3305. https://doi.org/10.1083/jcb.201612148

Greaves, C. V., & Rohrer, J. D. (2019). An update on genetic frontotemporal dementia. *Journal of Neurology*, *266*(8), 2075–2086. https://doi.org/10.1007/s00415-019-09363-4

Grundke-Iqbal, I., Iqbal, K., Tung, Y.-C., Quinlan, M., Wisniewski, H. M., & Bindert, L. I. (1986). Abnormal phosphorylation of the microtubule-

associated protein X (tau) in Alzheimer cytoskeletal pathology (Alzheimer disease/neurofibrillary tangles/paired-helical filaments/microtubules). *Medical Sciences*, *83*, 4913–4917. https://www.pnas.org

Guerreiro, R., Wojtas, A., Bras, J., Carrasquillo, M., Rogaeva, E., Majounie, E., Cruchaga, C., Sassi, C., Kauwe, J. S. K., Younkin, S., Hazrati, L., Collinge, J., Pocock, J., Lashley, T., Williams, J., Lambert, J.-C., Amouyel, P., Goate, A., Rademakers, R., … Hardy, J. (2013). TREM2 Variants in Alzheimer's Disease . *New England Journal of Medicine*, *368*(2), 117–127. https://doi.org/10.1056/nejmoa1211851

Guimarães, T. R., Swanson, E., Kofler, J., & Thathiah, A. (2021). G protein-coupled receptor kinases are associated with Alzheimer's disease pathology. *Neuropathology and Applied Neurobiology*, *47*(7), 942–957. https://doi.org/10.1111/nan.12742

Guo, C. Y., Sun, L., Chen, X. P., & Zhang, D. S. (2013). Oxidative stress, mitochondrial damage and neurodegenerative diseases. *Neural Regeneration Research*, *8*(21), 2003–2014. https://doi.org/10.3969/j.issn.1673-5374.2013.21.009

Haenseler, W., Sansom, S. N., Buchrieser, J., Newey, S. E., Moore, C. S., Nicholls, F. J., Chintawar, S., Schnell, C., Antel, J. P., Allen, N. D., Cader, M. Z., Wade-Martins, R., James, W. S., & Cowley, S. A. (2017). A Highly Efficient Human Pluripotent Stem Cell Microglia Model Displays a Neuronal-Co-culture-Specific Expression Profile and Inflammatory Response. *Stem Cell Reports*, *8*(6), 1727–1742. https://doi.org/10.1016/j.stemcr.2017.05.017

Hammond, T. R., Dufort, C., Dissing-Olesen, L., Giera, S., Young, A., Wysoker, A., Walker, A. J., Gergits, F., Segel, M., Nemesh, J., Marsh, S. E., Saunders, A., Macosko, E., Ginhoux, F., Chen, J., Franklin, R. J. M., Piao, X., McCarroll, S. A., & Stevens, B. (2019). Single-Cell RNA Sequencing of Microglia throughout the Mouse Lifespan and in the Injured Brain Reveals Complex Cell-State Changes. *Immunity*, *50*(1), 253-271.e6. https://doi.org/10.1016/j.immuni.2018.11.004

Han, Y., Branon, T., Martell, J., Boassa, D., Shechner, D., Ellisman, M., Ting, A. (2019). Directed Evolution of Split APEX2 Peroxidase. *ACS Chemical Biology,* 619-635, 14(4). https://doi.org/10.1021/acschembio.8b00919

Hanisch, U. K., & Kettenmann, H. (2007). Microglia: Active sensor and versatile effector cells in the normal and pathologic brain. *Nature Neuroscience*, *10*(11), 1387–1394. https://doi.org/10.1038/nn1997

Hardy, J. A., & Higgins, G. A. (1992). Alzheimer's disease: The amyloid cascade hypothesis. *Science*, *256*(5054), 184–185. https://doi.org/10.1126/science.1566067

Hardy, J., & Selkoe, D. J. (2002). The Amyloid Hypothesis of Alzheimer's Disease: Progress and Problems on the Road to Therapeutics. *Science*, *297*, 353–356. https://www.science.org

Haynes, S. E., Hollopeter, G., Yang, G., Kurpius, D., Dailey, M. E., Gan, W. B., & Julius, D. (2006). The P2Y12 receptor regulates microglial activation by extracellular nucleotides. *Nature Neuroscience*, *9*(12), 1512–1519. https://doi.org/10.1038/nn1805

Henry, C. J., Huang, Y., Wynne, A. M., & Godbout, J. P. (2009). Peripheral lipopolysaccharide (LPS) challenge promotes microglial hyperactivity in aged mice that is associated with exaggerated induction of both pro-inflammatory IL-1β and anti-inflammatory IL-10 cytokines. *Brain, Behavior, and Immunity*, *23*(3), 309–317. https://doi.org/10.1016/j.bbi.2008.09.002

Hickman, S. E., Kingery, N. D., Ohsumi, T. K., Borowsky, M. L., Wang, L. C., Means, T. K., & El Khoury, J. (2013). The microglial sensome revealed by direct RNA sequencing. *Nature Neuroscience*, *16*(12), 1896–1905. https://doi.org/10.1038/nn.3554

Hodges, J. R., Davies, ; R, Xuereb, ; J, Kril, ; J, & Halliday, G. (2003). Survival in frontotemporal dementia. *Neurology*, *61*, 349–354.

Hogan, D. B., Jetté, N., Fiest, K. M., Roberts, J. I., Pearson, D., Smith, E. E., Roach, P., Kirk, A., Pringsheim, T., & Maxwell, C. J. (2016). The prevalence and incidence of frontotemporal dementia: A systematic

review. *Canadian Journal of Neurological Sciences*, *43*(S1), S96–S109. https://doi.org/10.1017/cjn.2016.25

Honda, S., Sasaki, Y., Ohsawa, K., Imai, Y., Nakamura, Y., Inoue, K., & Kohsaka, S. (2001). Extracellular ATP or ADP Induce Chemotaxis of Cultured Microglia through G i/o-Coupled P2Y Receptors. *The Journal of Neuroscience*, *21*(6), 1975–1982.

Hong, S., Beja-Glasser, V. F., Nfonoyim, B. M., Frouin, A., Li, S., Ramakrishnan, S., Merry, K. M., Shi, Q., Rosenthal, A., Barres, B. A., Lemere, C., Selkoe, D. J., & Stevens, B. (2016). Complement and microglia mediate early synapse loss in Alzheimer mouse models. *Science*, *352*(6286), 712–716. https://doi.org/10.1001/jama.2016.4226

Houser, M., Uriarte Huaarte, O., Wallings, R., Keating, C., MacPhearson, K., Herrick, M., Kannarkat, G., Kelly, S., Chang, J., Varvel, N., Rexach, J., Tansey, M. (2022). Progranulin loss results in sex-dependent dysregulation of the peripheral and central immune system. *Frontiers in Immunology,* 13. https://doi.org/10.3389/fimmu.2022.1056417

Hu, F., Padukkavidana, T., Vægter, C. B., Brady, O. A., Zheng, Y., Mackenzie, I. R., Feldman, H. H., Nykjaer, A., & Strittmatter, S. M. (2010). Sortilin-mediated endocytosis determines levels of the frontotemporal dementia protein, progranulin. *Neuron*, *68*(4), 654–667. https://doi.org/10.1016/j.neuron.2010.09.034

Huang, D. W., Sherman, B. T., & Lempicki, R. A. (2009). Systematic and integrative analysis of large gene lists using DAVID bioinformatics resources. *Nature Protocols*, *4*(1), 44–57. https://doi.org/10.1038/nprot.2008.211

Huang, M., Modeste, E., Dammer, E., Merino, P., Taylor, G., Duong, D. M., Deng, Q., Holler, C. J., Gearing, M., Dickson, D., Seyfried, N. T., & Kukar, T. (2020). Network analysis of the progranulin-deficient mouse brain proteome reveals pathogenic mechanisms shared in human frontotemporal dementia caused by GRN mutations. *Acta Neuropathologica Communications*, *8*(1), 163. https://doi.org/10.1186/s40478-020-01037-x

Hutton, M., Lendon, C. L., Rizzu, P., Baker, M., Froelich, S., Houlden, H., Pickering-Brown, S., Chakraverty, S., Isaacs, A., Grover, A., Hackett, J., Adamson, J., Lincoln, S., Dickson, D., Davies, P., Petersen, R. C., Stevens, M., De Graaff, E., Wauters, E., … Heutink, P. (1998). Association of missense and 5-splice-site mutations in tau with the inherited dementia FTDP-17. *Nature* , *393*, 702–705.

Ihara, Y., Nukina, N., Miura, R., & Ogawara, M. (1986). Phosphorylated Tau Protein Is Integrated into Paired Helical Filaments in Alzheimer's Disease. *Biochem*, *99*, 1807–1810. https://academic.oup.com/jb/article/99/6/1807/858236

Imai, Y., Ibata, I., Ito, D., Ohsawa, K., & Kohsaka, S. (1996). A Novel Gene iba1 in the Major Histocompatibility Complex Class III Region Encoding an EF Hand Protein Expressed in a Monocytic Lineage. *Biochemical and Biophysical Research Communications*, *224*, 855–862.

Ingelsson M, Fukumoto H, Newell KL, Growdon JH, Hedley-Whyte ET, Frosch MP, Albert MS, Hyman BT, Irizarry MC. Early Abeta accumulation and progressive synaptic loss, gliosis, and tangle formation in AD brain. (2004) Neurology. 62(6):925-31. doi: 10.1212/01.wnl.0000115115.98960.37. PMID: 15037694.

Inoue, K. (2002). Microglial activation by purines and pyrimidines. *GLIA*, *40*(2), 156–163. https://doi.org/10.1002/glia.10150

Ittner, L. M., & Götz, J. (2011). Amyloid-β and tau - A toxic pas de deux in Alzheimer's disease. *Nature Reviews Neuroscience*, *12*(2), 67–72. https://doi.org/10.1038/nrn2967

Janabi, N., Peudenier, S., Héron, B., Ng, K. H., & Tardieu, M. (1995). Establishment of human microglial cell lines after transfection of primary cultures of embryonic microglial cells with the SV40 large T antigen. *Neuroscience Letters*, *195*(2), 105–108. https://doi.org/10.1016/0304-3940(94)11792-H

Jansen, I. E., Savage, J. E., Watanabe, K., Bryois, J., Williams, D. M., Steinberg, S., Sealock, J., Karlsson, I. K., Hägg, S., Athanasiu, L., Voyle, N., Proitsi, P., Witoelar, A., Stringer, S., Aarsland, D., Almdahl, I. S., Andersen, F., Bergh, S., Bettella, F., … Posthuma,

D. (2019). Genome-wide meta-analysis identifies new loci and functional pathways influencing Alzheimer's disease risk. *Nature Genetics*, *51*(3), 404–413. https://doi.org/10.1038/s41588-018-0311-9

Jian, J., Tian, Q. Y., Hettinghouse, A., Zhao, S., Liu, H., Wei, J., Grunig, G., Zhang, W., Setchell, K. D. R., Sun, Y., Overkleeft, H. S., Chan, G. L., & Liu, C. ju. (2016). Progranulin Recruits HSP70 to β-Glucocerebrosidase and Is Therapeutic Against Gaucher Disease. *EBioMedicine*, *13*, 212–224. https://doi.org/10.1016/j.ebiom.2016.10.010

Jiang, Y. X., Cao, Q., Sawaya, M. R., Abskharon, R., Ge, P., DeTure, M., Dickson, D. W., Fu, J. Y., Ogorzalek Loo, R. R., Loo, J. A., & Eisenberg, D. S. (2022). Amyloid fibrils in FTLD-TDP are composed of TMEM106B and not TDP-43. *Nature*, *605*(7909), 304–309. https://doi.org/10.1038/s41586-022-04670-9

Johnson, E. C. B., Carter, E. K., Dammer, E. B., Duong, D. M., Gerasimov, E. S., Liu, Y., Liu, J., Betarbet, R., Ping, L., Yin, L., Serrano, G. E., Beach, T. G., Peng, J., De Jager, P. L., Haroutunian, V., Zhang, B., Gaiteri, C., Bennett, D. A., Gearing, M., … Seyfried, N. T. (2022). Large-scale deep multi-layer analysis of Alzheimer's disease brain reveals strong proteomic disease-related changes not observed at the RNA level. *Nature Neuroscience*, *25*(2), 213–225. https://doi.org/10.1038/s41593-021-00999-y

Johnson, J. K., Diehl, J., Mendez, M. F., Neuhaus, J., Shapira, J. S., Forman, M., Chute, D. J., Roberson, E. D., Pace-Savitsky, C., Neumann, M., Chow, T. W., Rosen, H. J., Forstl, H., Kurz, A., & Miller, B. L. (2005). Frontotemporal Lobar Degeneration Demographic Characteristics of 353 Patients. *Arch Neurol*, *62*, 925–930. https://jamanetwork.com/

Jonsson, T., Stefansson, H., Steinberg, S., Jonsdottir, I., Jonsson, P. V., Snaedal, J., Bjornsson, S., Huttenlocher, J., Levey, A. I., Lah, J. J., Rujescu, D., Hampel, H., Giegling, I., Andreassen, O. A., Engedal, K., Ulstein, I., Djurovic, S., Ibrahim-Verbaas, C., Hofman, A., … Stefansson, K. (2013). Variant of TREM2 Associated with the Risk of Alzheimer's Disease . *New England Journal of Medicine*, *368*(2), 107–116. https://doi.org/10.1056/nejmoa1211103

Josephs, K. A., Hodges, J. R., Snowden, J. S., MacKenzie, I. R., Neumann, M., Mann, D. M., & Dickson, D. W. (2011). Neuropathological background of phenotypical variability in frontotemporal dementia. *Acta Neuropathologica*, *122*(2), 137–153. https://doi.org/10.1007/s00401-011-0839-6

Kalani, K., Chaturvedi, P., Chaturvedi, P., Kumar Verma, V., Lal, N., Awasthi, S. K., & Kalani, A. (2023). Mitochondrial mechanisms in Alzheimer's disease: Quest for therapeutics. *Drug Discovery Today*, *28*(5), 103547. https://doi.org/10.1016/j.drudis.2023.103547

Kao, A. W., McKay, A., Singh, P. P., Brunet, A., & Huang, E. J. (2017). Progranulin, lysosomal regulation and neurodegenerative disease. *Nature Reviews Neuroscience*, *18*(6), 325–333. https://doi.org/10.1038/nrn.2017.36

Kashani, A., Lepicard, È., Poirel, O., Videau, C., David, J. P., Fallet-Bianco, C., Simon, A., Delacourte, A., Giros, B., Epelbaum, J., Betancur, C., & El Mestikawy, S. (2008). Loss of VGLUT1 and VGLUT2 in the prefrontal cortex is correlated with cognitive decline in Alzheimer disease. *Neurobiology of Aging*, *29*(11), 1619–1630. https://doi.org/10.1016/j.neurobiolaging.2007.04.010

Kayasuga, Y., Chiba, S., Suzuki, M., Kikusui, T., Matsuwaki, T., Yamanouchi, K., Kotaki, H., Horai, R., Iwakura, Y., & Nishihara, M. (2007). Alteration of behavioural phenotype in mice by targeted disruption of the progranulin gene. *Behavioural Brain Research*, *185*(2), 110–118. https://doi.org/10.1016/j.bbr.2007.07.020

Keane, L., Antignano, I., Riechers, S. P., Zollinger, R., Dumas, A. A., Offermann, N., Bernis, M. E., Russ, J., Graelmann, F., McCormick, P. N., Esser, J., Tejera, D., Nagano, A., Wang, J., Chelala, C., Biederbick, Y., Halle, A., Salomoni, P., Heneka, M. T., & Capasso, M. (2021). mTOR-dependent translation amplifies microglia priming in aging mice. *Journal of Clinical Investigation*, *131*(1). https://doi.org/10.1172/JCI132727

Kertesz, A., Davidson, W., McCabe, P., Takagi, K., & Munoz, D. (2003). Primary progressive aphasia: Diagnosis, varieties, evolution. *Journal of the International Neuropsychological Society*, *9*(5), 710–719. https://doi.org/10.1017/S1355617703950041

Kierdorf, K., Erny, D., Goldmann, T., Sander, V., Schulz, C., Perdiguero, E. G., Wieghofer, P., Heinrich, A., Riemke, P., Hölscher, C., Müller, D. N., Luckow, B., Brocker, T., Debowski, K., Fritz, G., Opdenakker, G., Diefenbach, A., Biber, K., Heikenwalder, M., … Prinz, M. (2013). Microglia emerge from erythromyeloid precursors via Pu.1-and Irf8-dependent pathways. *Nature Neuroscience*, *16*(3), 273–280. https://doi.org/10.1038/nn.3318

Killinger, B. A., Marshall, L. L., Chatterjee, D., Chu, Y., Bras, J., Guerreiro, R., & Kordower, J. H. (2022). In situ proximity labeling identifies Lewy pathology molecular interactions in the human brain. *PNAS*, *119*(5). https://doi.org/10.1073/pnas.2114405119/-/DCSupplemental

Kim, B., Suh, Y. H., & Joe, E. (2022). LRRK2 decreases microglial actin dynamics by filamentous actin depolymerization and Rac1 inhibition. *Animal Cells and Systems*, *26*(6), 380–387. https://doi.org/10.1080/19768354.2022.2158219

Kim, D. I., Jensen, S. C., Noble, K. A., Kc, B., Roux, K. H., Motamedchaboki, K., & Roux, K. J. (2016). An improved smaller biotin ligase for BioID proximity labeling. *Molecular Biology of the Cell*, *27*(8), 1188–1196. https://doi.org/10.1091/mbc.E15-12-0844

Kim, S. U., & De Vellis, J. (2005). Microglia in health and disease. *Journal of Neuroscience Research*, *81*(3), 302–313. https://doi.org/10.1002/jnr.20562

Klein, W. L. (2006). Synaptic targeting by Aβ oligomers (ADDLS) as a basis for memory loss in early Alzheimer's disease. *Alzheimer's and Dementia*, *2*(1), 43–55. https://doi.org/10.1016/j.jalz.2005.11.003

Klein, Z. A., Takahashi, H., Ma, M., Stagi, M., Zhou, M., Lam, T. K. T., & Strittmatter, S. M. (2017). Loss of TMEM106B Ameliorates Lysosomal and Frontotemporal Dementia-Related Phenotypes in Progranulin-Deficient Mice. *Neuron*, *95*(2), 281-296.e6. https://doi.org/10.1016/j.neuron.2017.06.026

Knopman, D. S., & Roberts, R. O. (2011). Estimating the number of persons with frontotemporal lobar degeneration in the US

population. *Journal of Molecular Neuroscience*, *45*(3), 330–335. https://doi.org/10.1007/s12031-011-9538-y

Koffie, R. M., Hashimoto, T., Tai, H. C., Kay, K. R., Serrano-Pozo, A., Joyner, D., Hou, S., Kopeikina, K. J., Frosch, M. P., Lee, V. M., Holtzman, D. M., Hyman, B. T., & Spires-Jones, T. L. (2012). Apolipoprotein E4 effects in Alzheimer's disease are mediated by synaptotoxic oligomeric amyloid-β. *Brain*, *135*(7), 2155–2168. https://doi.org/10.1093/brain/aws127

Kosik, K. S., Joachim, C. L., & Selkoe, D. J. (1986). Microtubule-associated protein tau (T) is a major antigenic component of paired helical filaments in Alzheimer disease (cytoskeleton/neurofibrillary tangles/neuronal degeneration). *Proc. Nati. Acad. Sci. USA*, *83*, 4044–4048. https://www.pnas.org

Kotani, N., Gu, J., Isaji, T., Udaka, K., Taniguchi, N., & Honke, K. (2008). *Biochemical visualization of cell surface molecular clustering in living cells*. www.pnas.org/cgi/content/full/

Krogan, N. J., Cagney, G., Yu, H., Zhong, G., Guo, X., Ignatchenko, A., Li, J., Pu, S., Datta, N., Tikuisis, A. P., Punna, T., Peregrín-Alvarez, J. M., Shales, M., Zhang, X., Davey, M., Robinson, M. D., Paccanaro, A., Bray, J. E., Sheung, A., … Greenblatt, J. F. (2006). Global landscape of protein complexes in the yeast Saccharomyces cerevisiae. *Nature*, *440*(7084), 637–643. https://doi.org/10.1038/nature04670

Kuleshov, M. V., Jones, M. R., Rouillard, A. D., Fernandez, N. F., Duan, Q., Wang, Z., Koplev, S., Jenkins, S. L., Jagodnik, K. M., Lachmann, A., McDermott, M. G., Monteiro, C. D., Gundersen, G. W., & Maayan, A. (2016). Enrichr: a comprehensive gene set enrichment analysis web server 2016 update. *Nucleic Acids Research*, *44*(1), W90–W97. https://doi.org/10.1093/nar/gkw377

Kwiatkowski Jr, T., Bosco, D., Leclerc, A., Tamrazian, E., & Brown Jr, R. (2009). Mutations in the FUS/TLS gene on chromosome 16 cause familial amyotrophic lateral sclerosis. *Science*, *323*(5918), 1201–1205. https://doi.org/10.1126/science.1164508

Lam, S. S., Martell, J. D., Kamer, K. J., Deerinck, T. J., Ellisman, M. H., Mootha, V. K., & Ting, A. Y. (2014). Directed evolution of APEX2 for electron microscopy and proximity labeling. *Nature Methods*, *12*(1), 51–54. https://doi.org/10.1038/nmeth.3179

Lambert, J. C., Ibrahim-Verbaas, C. A., Harold, D., Naj, A. C., Sims, R., Bellenguez, C., Jun, G., DeStefano, A. L., Bis, J. C., Beecham, G. W., Grenier-Boley, B., Russo, G., Thornton-Wells, T. A., Jones, N., Smith, A. V., Chouraki, V., Thomas, C., Ikram, M. A., Zelenika, D., … Seshadri, S. (2013). Meta-analysis of 74,046 individuals identifies 11 new susceptibility loci for Alzheimer's disease. *Nature Genetics*, *45*(12), 1452–1458. https://doi.org/10.1038/ng.2802

Lambert, M. P., Barlow, A. K., Chromy, B. A., Edwards, C., Freed, R., Liosatos, M., Morgan, T. E., Rozovsky, I., Trommer, B., Viola, K. L., Wals, P., Zhang, C., Finch, C. E., Krafft ¶, G. A., & Klein, W. L. (1998). Diffusible, nonfibrillar ligands derived from A 1-42 are potent central nervous system neurotoxins. *PNAS*, *95*, 6448–6453. www.pnas.org.

Lang, C. M., Fellerer, K., Schwenk, B. M., Kuhn, P. H., Kremmer, E., Edbauer, D., Capell, A., & Haass, C. (2012). Membrane orientation and subcellular localization of transmembrane protein 106B (TMEM106B), a major risk factor for frontotemporal lobar degeneration. *Journal of Biological Chemistry*, *287*(23), 19355–19365. https://doi.org/10.1074/jbc.M112.365098

Lant, S. B., Robinson, A. C., Thompson, J. C., Rollinson, S., Pickering-Brown, S., Snowden, J. S., Davidson, Y. S., Gerhard, A., & Mann, D. M. A. (2014). Patterns of microglial cell activation in frontotemporal lobar degeneration. *Neuropathology and Applied Neurobiology*, *40*(6), 686–696. https://doi.org/10.1111/nan.12092

Lashley, T., Rohrer, J. D., Mead, S., & Revesz, T. (2015). Review: An update on clinical, genetic and pathological aspects of frontotemporal lobar degenerations. *Neuropathology and Applied Neurobiology*, *41*(7), 858–881. https://doi.org/10.1111/nan.12250

Lawson, L. J., Perry, V. H., Dri, P., & Gordon, S. (1990). Heterogeneity in the distribution and morphology of microglia in the normal adult mouse brain. *Neuroscience* , *39*(I), 151–170.

Lee, J. H., Yang, D. S., Goulbourne, C. N., Im, E., Stavrides, P., Pensalfini, A., Chan, H., Bouchet-Marquis, C., Bleiwas, C., Berg, M. J., Huo, C., Peddy, J., Pawlik, M., Levy, E., Rao, M., Staufenbiel, M., & Nixon, R. A. (2022). Faulty autolysosome acidification in Alzheimer's disease mouse models induces autophagic build-up of Aβ in neurons, yielding senile plaques. *Nature Neuroscience*, *25*(6), 688–701. https://doi.org/10.1038/s41593-022-01084-8

Lee, S. E., Rabinovici, G. D., Mayo, M. C., Wilson, S. M., Seeley, W. W., Dearmond, S. J., Huang, E. J., Trojanowski, J. Q., Growdon, M. E., Jang, J. Y., Sidhu, M., See, T. M., Karydas, A. M., Gorno-Tempini, M. L., Boxer, A. L., Weiner, M. W., Geschwind, M. D., Rankin, K. P., & Miller, B. L. (2011). Clinicopathological correlations in corticobasal degeneration. *Annals of Neurology*, *70*(2), 327–340. https://doi.org/10.1002/ana.22424

Li, Y., Du, X. F., Liu, C. S., Wen, Z. L., & Du, J. L. (2012). Reciprocal Regulation between Resting Microglial Dynamics and Neuronal Activity In Vivo. *Developmental Cell*, *23*(6), 1189–1202. https://doi.org/10.1016/j.devcel.2012.10.027

Liao, Y., Wang, J., Jaehnig, E. J., Shi, Z., & Zhang, B. (2019). WebGestalt 2019: gene set analysis toolkit with revamped UIs and APIs. *Nucleic Acids Research*, *47*(W1), W199–W205. https://doi.org/10.1093/nar/gkz401

Lin, M. T., & Beal, M. F. (2006). Mitochondrial dysfunction and oxidative stress in neurodegenerative disease. *Nature*, *443*.

Lines, G., Casey, J. M., Preza, E., & Wray, S. (2020). Modelling frontotemporal dementia using patient-derived induced pluripotent stem cells. *Molecular and Cellular Neuroscience*, *109*. https://doi.org/10.1016/j.mcn.2020.103553

Litvan, I., Agid, ; Y, Calne, ; D, Campbell, ; G, Dubois, ; B, Duvoisin, ; R C, Goetz, ; C G, Golbe, ; L I, Grafman, ; J, Growdon, ; J H, Hallett, ; M, Jankovic, ; J, Quinn, ; N P, Tolosa, ; E, & Zee, D. S. (1996). Clinical research criteria for the diagnosis of progressive supranuclear palsy (Steele-Richardson-Olszewski syndrome): Report of the NINDS-SPSP International Workshop*. *Neurology*, *47*, 1–9.

Liu, L., Drouet, V., Wu, J. W., Witter, M. P., Small, S. A., Clelland, C., & Duff, K. (2012). Trans-synaptic spread of tau pathology in vivo. *PLoS ONE*, *7*(2). https://doi.org/10.1371/journal.pone.0031302

Liu, Y. U., Ying, Y., Li, Y., Eyo, U. B., Chen, T., Zheng, J., Umpierre, A. D., Zhu, J., Bosco, D. B., Dong, H., & Wu, L. J. (2019). Neuronal network activity controls microglial process surveillance in awake mice via norepinephrine signaling. *Nature Neuroscience*, *22*(11), 1771–1781. https://doi.org/10.1038/s41593-019-0511-3

Lopez-Gonzalez, R., Lu, Y., Gendron, T. F., Karydas, A., Tran, H., Yang, D., Petrucelli, L., Miller, B. L., Almeida, S., & Gao, F. B. (2016). Poly(GR) in C9ORF72-Related ALS/FTD Compromises Mitochondrial Function and Increases Oxidative Stress and DNA Damage in iPSC-Derived Motor Neurons. *Neuron*, *92*(2), 383–391. https://doi.org/10.1016/j.neuron.2016.09.015

Luck, K., Kim, D. K., Lambourne, L., Spirohn, K., Begg, B. E., Bian, W., Brignall, R., Cafarelli, T., Campos-Laborie, F. J., Charloteaux, B., Choi, D., Coté, A. G., Daley, M., Deimling, S., Desbuleux, A., Dricot, A., Gebbia, M., Hardy, M. F., Kishore, N., … Calderwood, M. A. (2020). A reference map of the human binary protein interactome. *Nature*, *580*(7803), 402–408. https://doi.org/10.1038/s41586-020-2188-x

Lui, H., Zhang, J., Makinson, S. R., Cahill, M. K., Kelley, K. W., Huang, H. Y., Shang, Y., Oldham, M. C., Martens, L. H., Gao, F., Coppola, G., Sloan, S. A., Hsieh, C. L., Kim, C. C., Bigio, E. H., Weintraub, S., Mesulam, M. M., Rademakers, R., MacKenzie, I. R., … Huang, E. J. (2016). Progranulin Deficiency Promotes Circuit-Specific Synaptic Pruning by Microglia via Complement Activation. *Cell*, *165*(4), 921–935. https://doi.org/10.1016/j.cell.2016.04.001

Mach, L., Mort, J. S., & Glössl, J. (1994). Maturation of human procathepsin B. Proenzyme activation and proteolytic processing of the precursor to the mature proteinase, in vitro, are primarily unimolecular processes. *The Journal of Biological Chemistry*, *269*(17), 13030–13035.

Mackenzie, I. R. A., Baborie, A., Pickering-Brown, S., Plessis, D. Du, Jaros, E., Perry, R. H., Neary, D., Snowden, J. S., & Mann, D. M. A.

(2006). Heterogeneity of ubiquitin pathology in frontotemporal lobar degeneration: Classification and relation to clinical phenotype. *Acta Neuropathologica*, *112*(5), 539–549. https://doi.org/10.1007/s00401-006-0138-9

Mackenzie, I. R. A., Foti, D., Woulfe, J., & Hurwitz, T. A. (2008). Atypical frontotemporal lobar degeneration with ubiquitin-positive, TDP-43-negative neuronal inclusions. *Brain*, *131*(5), 1282–1293. https://doi.org/10.1093/brain/awn061

MacKenzie, I. R. A., Neumann, M., Bigio, E. H., Cairns, N. J., Alafuzoff, I., Kril, J., Kovacs, G. G., Ghetti, B., Halliday, G., Holm, I. E., Ince, P. G., Kamphorst, W., Revesz, T., Rozemuller, A. J. M., Kumar-Singh, S., Akiyama, H., Baborie, A., Spina, S., Dickson, D. W., … Mann, D. M. A. (2010). Nomenclature and nosology for neuropathologic subtypes of frontotemporal lobar degeneration: An update. *Acta Neuropathologica*, *119*(1), 1–4. https://doi.org/10.1007/s00401-009-0612-2

Maezawa, I., Zimin, P. I., Wulff, H., & Jin, L. W. (2011). Amyloid-β protein oligomer at low nanomolar concentrations activates microglia and induces microglial neurotoxicity. *Journal of Biological Chemistry*, *286*(5), 3693–3706. https://doi.org/10.1074/jbc.M110.135244

Magnus, T., Chan, A., Grauer, O., Toyka, K. V., & Gold, R. (2001). Microglial Phagocytosis of Apoptotic Inflammatory T Cells Leads to Down-Regulation of Microglial Immune Activation. *The Journal of Immunology*, *167*(9), 5004–5010. https://doi.org/10.4049/jimmunol.167.9.5004

Manczak, M., Calkins, M. J., & Reddy, P. H. (2011). Impaired mitochondrial dynamics and abnormal interaction of amyloid beta with mitochondrial protein Drp1 in neurons from patients with Alzheimer's disease: Implications for neuronal damage. *Human Molecular Genetics*, *20*(13), 2495–2509. https://doi.org/10.1093/hmg/ddr139

Manczak, M., & Reddy, P. H. (2012). Abnormal interaction between the mitochondrial fission protein Drp1 and hyperphosphorylated tau in Alzheimer's disease neurons: Implications for mitochondrial

dysfunction and neuronal damage. *Human Molecular Genetics*, *21*(11), 2538–2547. https://doi.org/10.1093/hmg/dds072

Maphis, N., Xu, G., Kokiko-Cochran, O. N., Jiang, S., Cardona, A., Ransohoff, R. M., Lamb, B. T., & Bhaskar, K. (2015). Reactive microglia drive tau pathology and contribute to the spreading of pathological tau in the brain. *Brain*, *138*(6), 1738–1755. https://doi.org/10.1093/brain/awv081

Marschallinger, J., Iram, T., Zardeneta, M., Lee, S. E., Lehallier, B., Haney, M. S., Pluvinage, J. V., Mathur, V., Hahn, O., Morgens, D. W., Kim, J., Tevini, J., Felder, T. K., Wolinski, H., Bertozzi, C. R., Bassik, M. C., Aigner, L., & Wyss-Coray, T. (2020). Lipid-droplet-accumulating microglia represent a dysfunctional and proinflammatory state in the aging brain. *Nature Neuroscience*, *23*(2), 194–208. https://doi.org/10.1038/s41593-019-0566-1

Martell, J., Yamagata, M., Deerinck, T., Phan, S., Kwa, C., Ellisman, M., Sanes, J., Ting, A. (2016). A split horseradish peroxidase for the detection of intercellular protein-protein interactions and sensitive visualization of synapses. *Nature Biotechnology*, 774-780, 34(7). https://doi.org/10.1038/nbt.3563

Martens, L. H., Zhang, J., Barmada, S. J., Zhou, P., Kamiya, S., Sun, B., Min, S. W., Gan, L., Finkbeiner, S., Huang, E. J., & Farese, R. V. (2012). Progranulin deficiency promotes neuroinflammation and neuron loss following toxin-induced injury. *Journal of Clinical Investigation*, *122*(11), 3955–3959. https://doi.org/10.1172/JCI63113

Martínek, V., Sklenář, J., Dračínský, M., Šulc, M., Hofbauerová, K., Bezouška, K., Frei, E., & Stiborová, M. (2010). Glycosylation protects proteins against free radicals generated from toxic xenobiotics. *Toxicological Sciences*, *117*(2), 359–374. https://doi.org/10.1093/toxsci/kfq206

Masters, C. L., Simms, G., Weinman, N. A., Multhaupt, G., Mcdonald, B. L., & Beyreuthert, K. (1985). Amyloid plaque core protein in Alzheimer disease and Down syndrome. *PNAS*, *82*, 4245–4249. https://www.pnas.org

Mathew, B., Bathla, S., Williams, K. R., & Nairn, A. C. (2022). Deciphering Spatial Protein-Protein Interactions in Brain Using Proximity Labeling. *Molecular and Cellular Proteomics*, *21*(11). https://doi.org/10.1016/j.mcpro.2022.100422

Matsuda, J., Yoneshige, A., & Suzuki, K. (2007). The function of sphingolipids in the nervous system: lessons learnt from mouse models of specific sphingolipid activator protein deficiencies. *Journal of Neurochemistry*, *103 Suppl 1*, 32–38. https://doi.org/10.1111/j.1471-4159.2007.04709.x

Mcgeer, P. L., Itagaki, S., Tago, H., & Mcgeer, E. G. (1987). Reactive microglia in patients with senile dementia of the Alzheimer type are positive for the histocompatibility glycoprotein HLA-DR. *Neuroscience Letters*, *79*, 195–200.

McNamara, N. B., Munro, D. A. D., Bestard-Cuche, N., Uyeda, A., Bogie, J. F. J., Hoffmann, A., Holloway, R. K., Molina-Gonzalez, I., Askew, K. E., Mitchell, S., Mungall, W., Dodds, M., Dittmayer, C., Moss, J., Rose, J., Szymkowiak, S., Amann, L., McColl, B. W., Prinz, M., … Miron, V. E. (2023). Microglia regulate central nervous system myelin growth and integrity. *Nature*, *613*(7942), 120–129. https://doi.org/10.1038/s41586-022-05534-y

Meftah, S., & Gan, J. (2023). Alzheimer's disease as a synaptopathy: Evidence for dysfunction of synapses during disease progression. *Frontiers in Synaptic Neuroscience*, *15*. https://doi.org/10.3389/fnsyn.2023.1129036

Mendsaikhan, A., Tooyama, I., & Walker, D. G. (2019). Microglial Progranulin: Involvement in Alzheimer's Disease and Neurodegenerative Diseases. *Cells*, *8*(3), 230. https://doi.org/10.3390/cells8030230

Mesulam, M. -M. (1987). Primary progressive aphasia—differentiation from Alzheimer's disease. *Annals of Neurology*, *22*(4), 533–534. https://doi.org/10.1002/ana.410220414

Mesulam, M. -Marsel. (1982). Slowly progressive aphasia without generalized dementia. *Annals of Neurology*, *11*(6), 592–598. https://doi.org/10.1002/ana.410110607

Miedema, S. S. M., Mol, M. O., Koopmans, F. T. W., Hondius, D. C., van Nierop, P., Menden, K., de Veij Mestdagh, C. F., van Rooij, J., Ganz, A. B., Paliukhovich, I., Melhem, S., Li, K. W., Holstege, H., Rizzu, P., van Kesteren, R. E., van Swieten, J. C., Heutink, P., & Smit, A. B. (2022). Distinct cell type-specific protein signatures in GRN and MAPT genetic subtypes of frontotemporal dementia. *Acta Neuropathologica Communications*, *10*(1). https://doi.org/10.1186/s40478-022-01387-8

Miller, B. L., Chang, L., Mena, I., Boone, K., & Lesser, I. M. (1993). Progressive Right Frontotemporal Degeneration: Clinical, Neuropsychological and SPECT Characteristics. *Dementia*, *4*, 204–213.

Minami, S. S., Min, S. W., Krabbe, G., Wang, C., Zhou, Y., Asgarov, R., Li, Y., Martens, L. H., Elia, L. P., Ward, M. E., Mucke, L., Farese, R. V., & Gan, L. (2014). Progranulin protects against amyloid β 2 deposition and toxicity in Alzheimer's disease mouse models. *Nature Medicine*, *20*(10), 1157–1164. https://doi.org/10.1038/nm.3672

Mohan, S., Sampognaro, P. J., Argouarch, A. R., Maynard, J. C., Welch, M., Patwardhan, A., Courtney, E. C., Zhang, J., Mason, A., Li, K. H., Huang, E. J., Seeley, W. W., Miller, B. L., Burlingame, A., Jacobson, M. P., & Kao, A. W. (2021). Processing of progranulin into granulins involves multiple lysosomal proteases and is affected in frontotemporal lobar degeneration. *Molecular Neurodegeneration*, *16*(1). https://doi.org/10.1186/s13024-021-00472-1

Mohandas, E., Rajmohan, V., & Raghunath, B. (2009). Neurobiology of Alzheimer's disease. *Indian Journal of Psychiatry*, *51*(1), 55–61. http://journals.lww.com/indianjpsychiatry

Moisse, K., Volkening, K., Leystra-Lantz, C., Welch, I., Hill, T., & Strong, M. J. (2009). Divergent patterns of cytosolic TDP-43 and neuronal progranulin expression following axotomy: Implications for TDP-43 in the physiological response to neuronal injury. *Brain Research*, *1249*, 202–211. https://doi.org/10.1016/j.brainres.2008.10.021

Morris, G. P., Clark, I. A., & Vissel, B. (2014). Inconsistencies and Controversies Surrounding the Amyloid Hypothesis of Alzheimer's

Disease. *Acta Neuropathologica Communications*, *2*(1). https://doi.org/10.1186/s40478-014-0135-5

Muffat, J., Li, Y., Yuan, B., Mitalipova, M., Omer, A., Corcoran, S., Bakiasi, G., Tsai, L. H., Aubourg, P., Ransohoff, R. M., & Jaenisch, R. (2016). Efficient derivation of microglia-like cells from human pluripotent stem cells. *Nature Medicine*, *22*(11), 1358–1367. https://doi.org/10.1038/nm.4189

Mukherjee, O., Wang, J., Gitcho, M., Chakraverty, S., Taylor-Reinwald, L., Shears, S., Kauwe, J. S. K., Norton, J., Levitch, D., Bigio, E. H., Hatanpaa, K. J., White, C. L., Morris, J. C., Cairns, N. J., & Goate, A. (2008). Molecular characterization of novel progranulin (GRN) mutations in frontotemporal dementia. *Human Mutation*, *29*(4), 512–521. https://doi.org/10.1002/humu.20681

Murrell, J. R., Koller, D., Foroud, T., Goedert, M., Spillantini, M. G., Edenberg, H. J., Farlow, M. R., & Ghetti, B. (1997). Familial Multiple-System Tauopathy with Presenile Dementia Is Localized to Chromosome 17. *Am. J. Hum. Genet*, *61*, 1131–1138. http://gdbwww.gdb.org/

Nalls, M. A., Blauwendraat, C., Sargent, L., Vitale, D., Leonard, H., Iwaki, H., Song, Y., Bandres-Ciga, S., Menden, K., Faghri, F., Heutink, P., Cookson, M. R., & Singleton, A. B. (2021). Evidence for GRN connecting multiple neurodegenerative diseases. *Brain Communications*, *3*(2). https://doi.org/10.1093/braincomms/fcab095

Naseri, N., Sharma, M., & Velinov, M. (2021). Autosomal dominant neuronal ceroid lipofuscinosis: Clinical features and molecular basis. *Clinical Genetics*, *99*(1), 111–118. https://doi.org/10.1111/cge.13829

Neumann, H., Kotter, M. R., & Franklin, R. J. M. (2009). Debris clearance by microglia: An essential link between degeneration and regeneration. *Brain*, *132*(2), 288–295. https://doi.org/10.1093/brain/awn109

Neumann, M., Rademakers, R., Roeber, S., Baker, M., Kretzschmar, H. A., & MacKenzie, I. R. A. (2009). A new subtype of frontotemporal

lobar degeneration with FUS pathology. *Brain*, *132*(11), 2922–2931. https://doi.org/10.1093/brain/awp214

Neumann, M., Sampathu, D. M., Kwong, L. K., Truax, A. C., Micsenyi, M. C., Chou, T. T., Bruce, J., Schuck, T., Grossman, M., Clark, C. M., McCluskey, L. F., Miller, B. L., Masliah, E., Mackenzie, I. R., Feldman, H., Feiden, W., Kretzschmar, H. A., Trojanowski, J. Q., & M-Y Lee, V. (2006). Ubiquitinated TDP-43 in Frontotemporal Lobar Degeneration and Amyotrophic Lateral Sclerosis. *Science*, *314*, 130–133. https://www.science.org

Nguyen, A. D., Nguyen, T. A., Zhang, J., Devireddy, S., Zhou, P., Karydas, A. M., Xu, X., Miller, B. L., Rigo, F., Ferguson, S. M., Huang, E. J., Walther, T. C., & Farese, R. V. (2018). Murine knockin model for progranulin-deficient frontotemporal dementia with nonsensemediated mRNA decay. *Proceedings of the National Academy of Sciences of the United States of America*, *115*(12), E2849–E2858. https://doi.org/10.1073/pnas.1722344115

Nikodemova, M., & Watters, J. J. (2012). Efficient isolation of live microglia with preserved phenotypes from adult mouse brain. *Journal of Neuroinflammation*, *9*(147). http://www.jneuroinflammation.com/content/9/1/147

Nimmerjahn, A., Kirchhoff, F., & Helmchen, F. (2005). Resting Microglial Cells AreHighly Dynamic Surveillants of Brain Parenchyma in Vivo. *Science*, *308*(5726), 1314–1318. https://doi.org/10.1126/science.1107891

Niraula, A., Sheridan, J. F., & Godbout, J. P. (2017). Microglia Priming with Aging and Stress. *Neuropsychopharmacology*, *42*(1), 318–333. https://doi.org/10.1038/npp.2016.185

Norden, D. M., & Godbout, J. P. (2013). Review: Microglia of the aged brain: Primed to be activated and resistant to regulation. *Neuropathology and Applied Neurobiology*, *39*(1), 19–34. https://doi.org/10.1111/j.1365-2990.2012.01306.x

O'Brien, J. S. and Kishimoto. (1991) Saposin proteins: structure, function, and role in human lysosomal storage disorders. The FASEB Journal. (5)301-308 https://doi.org/10.1096/fasebj.5.3.2001789

Ogura, K., Ogawa, M., & Yoshida, M. (1994). Effects of ageing on microglia in the normal rat. *NeuroReport*, *5*(10), 1224–1226.

Olagunju, A. S., Ahammad, F., Alagbe, A. A., Otenaike, T. A., Teibo, J. O., Mohammad, F., Alsaiari, A. A., Omotoso, O., & Talukder, M. E. K. (2023). Mitochondrial dysfunction: A notable contributor to the progression of Alzheimer's and Parkinson's disease. *Heliyon*, *9*(3), e14387. https://doi.org/10.1016/j.heliyon.2023.e14387

Olney, N. T., Spina, S., & Miller, B. L. (2017). Frontotemporal Dementia. *Neurologic Clinics*, *35*(2), 339–374. https://doi.org/10.1016/j.ncl.2017.01.008

Olson, J. K., & Miller, S. D. (2004). Microglia Initiate Central Nervous System Innate and Adaptive Immune Responses through Multiple TLRs 1. *The Journal of Immunology*, *173*, 3916–3924. http://journals.aai.org/jimmunol/article-pdf/173/6/3916/1189450/3916.pdf

Onesto, E., Colombrita, C., Gumina, V., Borghi, M. O., Dusi, S., Doretti, A., Fagiolari, G., Invernizzi, F., Moggio, M., Tiranti, V., Silani, V., & Ratti, A. (2016). Gene-specific mitochondria dysfunctions in human TARDBP and C9ORF72 fibroblasts. *Acta Neuropathologica Communications*, *4*(1), 47. https://doi.org/10.1186/s40478-016-0316-5

Orre, M., Kamphuis, W., Osborn, L. M., Melief, J., Kooijman, L., Huitinga, I., Klooster, J., Bossers, K., & Hol, E. M. (2014). Acute isolation and transcriptome characterization of cortical astrocytes and microglia from young and aged mice. *Neurobiology of Aging*, *35*(1), 1–14. https://doi.org/10.1016/j.neurobiolaging.2013.07.008

Oughtred, R., Rust, J., Chang, C., Breitkreutz, B. J., Stark, C., Willems, A., Boucher, L., Leung, G., Kolas, N., Zhang, F., Dolma, S., Coulombe-Huntington, J., Chatr-aryamontri, A., Dolinski, K., & Tyers, M. (2021). The BioGRID database: A comprehensive biomedical resource of curated protein, genetic, and chemical interactions. *Protein Science*, *30*(1), 187–200. https://doi.org/10.1002/pro.3978

Palomba, A., Abbondio, M., Fiorito, G., Uzzau, S., Pagnozzi, D., & Tanca, A. (2021). Comparative Evaluation of MaxQuant and Proteome Discoverer MS1-Based Protein Quantification Tools. *Journal of Proteome Research*, *20*(7), 3497–3507. https://doi.org/10.1021/acs.jproteome.1c00143

Pan, J., Ma, N., Yu, B., Zhang, W., & Wan, J. (2020). Transcriptomic profiling of microglia and astrocytes throughout aging. *Journal of Neuroinflammation*, *17*(1). https://doi.org/10.1186/s12974-020-01774-9

Pandya, H., Shen, M. J., Ichikawa, D. M., Sedlock, A. B., Choi, Y., Johnson, K. R., Kim, G., Brown, M. A., Elkahloun, A. G., Maric, D., Sweeney, C. L., Gossa, S., Malech, H. L., McGavern, D. B., & Park, J. K. (2017). Differentiation of human and murine induced pluripotent stem cells to microglia-like cells. *Nature Neuroscience*, *20*(5), 753–759. https://doi.org/10.1038/nn.4534

Parton, R. G., Simons, K., & Dotti, C. G. (1992). Axonal and Dendritic Endocytic Pathways in Cultured Neurons. *The Journal of Cell Biology*, *119*(1), 123–137. http://rupress.org/jcb/article-pdf/119/1/123/1063455/123.pdf

Paushter, D. H., Du, H., Feng, T., & Hu, F. (2018). The lysosomal function of progranulin, a guardian against neurodegeneration. *Acta Neuropathologica*, *136*(1). https://doi.org/10.1007/s00401-018-1861-8

Perneel, J., Manoochehri, M., Huey, E. D., Rademakers, R., & Goldman, J. (2023). Case report: TMEM106B haplotype alters penetrance of GRN mutation in frontotemporal dementia family. *Frontiers in Neurology*, *14*. https://doi.org/10.3389/fneur.2023.1160248

Perry, V. H., & Gordon, S. (1988). Macrophages and microglia in the nervous system. *Channels of Excitable Membranes*, *312*, 589–593.

Perry, V. H., Matyszak, M. K., & Fearn, S. (1993). Altered antigen expression of microglia in the aged rodent CNS. *Glia*, *7*(1), 60–67. https://doi.org/10.1002/glia.440070111

Petkau, T. L., Neal, S. J., Orban, P. C., MacDonald, J. L., Hill, A. M., Lu, G., Feldman, H. H., MacKenzie, I. R. A., & Leavitt, B. R. (2010). Progranulin expression in the developing and adult murine brain. *Journal of Comparative Neurology*, *518*(19), 3931–3947. https://doi.org/10.1002/cne.22430

Pickford, F., Marcus, J., Camargo, L. M., Xiao, Q., Graham, D., Mo, J. R., Burkhardt, M., Kulkarni, V., Crispino, J., Hering, H., & Hutton, M. (2011). Progranulin is a chemoattractant for microglia and stimulates their endocytic activity. *American Journal of Pathology*, *178*(1), 284–295. https://doi.org/10.1016/j.ajpath.2010.11.002

Platt, F. M., d'Azzo, A., Davidson, B. L., Neufeld, E. F., & Tifft, C. J. (2018). Lysosomal storage diseases. *Nature Reviews Disease Primers*, *4*(1). https://doi.org/10.1038/s41572-018-0025-4

Prada, C. E., & Grabowski, G. A. (2013). Neuronopathic lysosomal storage diseases: Clinical and pathologic findings. *Developmental Disabilities Research Reviews*, *17*(3), 226–246. https://doi.org/10.1002/ddrr.1116

Price, J. L., McKeel, D. W., Buckles, V. D., Roe, C. M., Xiong, C., Grundman, M., Hansen, L. A., Petersen, R. C., Parisi, J. E., Dickson, D. W., Smith, C. D., Davis, D. G., Schmitt, F. A., Markesbery, W. R., Kaye, J., Kurlan, R., Hulette, C., Kurland, B. F., Higdon, R., … Morris, J. C. (2009). Neuropathology of nondemented aging: Presumptive evidence for preclinical Alzheimer disease. *Neurobiology of Aging*, *30*(7), 1026–1036. https://doi.org/10.1016/j.neurobiolaging.2009.04.002

Primiani, C. T., Ryan, V. H., Rao, J. S., Cam, M. C., Ahn, K., Modi, H. R., & Rapoport, S. I. (2014). Coordinated gene expression of neuroinflammatory and cell signaling markers in dorsolateral prefrontal cortex during human brain development and aging. *PLoS ONE*, *9*(10). https://doi.org/10.1371/journal.pone.0110972

Prince, M., Bryce, R., Albanese, E., Wimo, A., Ribeiro, W., & Ferri, C. P. (2013). The global prevalence of dementia: A systematic review and metaanalysis. *Alzheimer's and Dementia*, *9*(1), 63-75.e2. https://doi.org/10.1016/j.jalz.2012.11.007

Prince, M., Wimo, A., Guerchet, M., Gemma-Claire Ali, M., Wu, Y.-T., Prina, M., Yee Chan, K., & Xia, Z. (2015). *World Alzheimer Report 2015 The global impact of dementia an analysis of prevalence, incidence, cost and trends*. www.alz.co.uk/worldreport2015corrections

Quraishi, O., Nägler, D. K., Fox, T., Sivaraman, J., Cygler, M., Mort, J. S., & Storer, A. C. (1999). The occluding loop in cathepsin B defines the pH dependence of inhibition by its propeptide. *Biochemistry*, *38*(16), 5017–5023. https://doi.org/10.1021/bi981950o

Radford, R.A.W., Rayner, S. L., Szwaja, P., Morsch, M., Cheng, F., Zhu., T., Widagdo, J., Anggono, V., Pountney, D.L., Chung, R., Lee, A. (2023). Identification of phosphorylated tau protein interactors in progressive supranuclear palsy (PSP) reveals networks involved in protein degradation, stress response, cytoskeletal dynamics, metabolic processes, and neurotransmission. *J Neurochem* . 2023 May;165(4):563-586. https://doi.org/10.1111/jnc.15796

Ramanathan, M., Majzoub, K., Rao, D. S., Neela, P. H., Zarnegar, B. J., Mondal, S., Roth, J. G., Gai, H., Kovalski, J. R., Siprashvili, Z., Palmer, T. D., Carette, J. E., & Khavari, P. A. (2018). RNA-protein interaction detection in living cells. *Nature Methods*, *15*(3), 207–212. https://doi.org/10.1038/nmeth.4601

Ramirez, C., Egetemaier, S., Béthune, J. (2021). Context-Specific and Proximity-Dependent Labeling for the Proteomic Analysis of Spatiotemporally Defined Protein Complexes with Split-BioID. *Methods in Molecular Biology,* 303-318, 2247.

Rankin, K. P., Gorno-Tempini, M. L., Allison, S. C., Stanley, C. M., Glenn, S., Weiner, M. W., & Miller, B. L. (2006). Structural anatomy of empathy in neurodegenerative disease. *Brain*, *129*(11), 2945–2956. https://doi.org/10.1093/brain/awl254

Raudvere, U., Kolberg, L., Kuzmin, I., Arak, T., Adler, P., Peterson, H., & Vilo, J. (2019). G:Profiler: A web server for functional enrichment analysis and conversions of gene lists (2019 update). *Nucleic Acids Research*, *47*(W1), W191–W198. https://doi.org/10.1093/nar/gkz369

Reimand, J., Kull, M., Peterson, H., Hansen, J., & Vilo, J. (2007). G:Profiler-a web-based toolset for functional profiling of gene lists from large-scale experiments. *Nucleic Acids Research*, *35*(SUPPL.2). https://doi.org/10.1093/nar/gkm226

Rgen Cox, J., Hein, M. Y., Luber, C. A., Paron, I., Nagaraj, N., & Mann, M. (2014). Accurate Proteome-wide Label-free Quantification by Delayed Normalization and Maximal Peptide Ratio Extraction, Termed MaxLFQ* □ S Technological Innovation and Resources. *Molecular & Cellular Proteomics*, *13*, 2513–2526. https://doi.org/10.1074/mcp

Rhee, H.-W., Zou, P., Udeshi, N. D., Martell, J. D., Mootha, V. K., Carr, S. A., & Ting, A. Y. (2013). Proteomic Mapping of Mitochondria in Living Cells via Spatially Restricted Enzymatic Tagging. *Science*, *339*(6125), 1323–1328. https://doi.org/10.1126/science.1228792

Ritzel, R. M., Patel, A. R., Pan, S., Crapser, J., Hammond, M., Jellison, E., & McCullough, L. D. (2015). Age- and location-related changes in microglial function. *Neurobiology of Aging*, *36*(6), 2153–2163. https://doi.org/10.1016/j.neurobiolaging.2015.02.016

Roberson, E., Scearce-Levie, K., Palop, J., Yan, F., Cheng, I., Wu, T., Gerstein, H., Yu, G., & Mucke, L. (2007). Reducing Endogenous Tau Ameliorates Amyloid ß-Induced Deficits in an Alzheimer's Disease Mouse Model. *Science*, *316*(5825), 747–750. https://doi.org/10.1126/science.1140030

Roberson, E. D. (2012). Mouse models of frontotemporal dementia. *Annals of Neurology*, *72*(6), 837–849. https://doi.org/10.1002/ana.23722

Rock, R. B., Hu, S., Deshpande, A., Munir, S., May, B. J., Baker, C. A., Peterson, P. K., & Kapur, V. (2005). Transcriptional response of human microglial cells to interferon-γ. *Genes and Immunity*, *6*(8), 712–719. https://doi.org/10.1038/sj.gene.6364246

Roeber, S., Mackenzie, I. R. A., Kretzschmar, H. A., & Neumann, M. (2008). TDP-43-negative FTLD-U is a significant new clinico-pathological subtype of FTLD. *Acta Neuropathologica*, *116*(2), 147–157. https://doi.org/10.1007/s00401-008-0395-x

Root, J., Merino, P., Nuckols, A., Johnson, M., & Kukar, T. (2021). Lysosome dysfunction as a cause of neurodegenerative diseases: Lessons from frontotemporal dementia and amyotrophic lateral sclerosis. *Neurobiology of Disease*, *154*. https://doi.org/10.1016/j.nbd.2021.105360

Rosen, H. J., Allison, S. C., Schauer, G. F., Gorno-Tempini, M. L., Weiner, M. W., & Miller, B. L. (2005). Neuroanatomical correlates of behavioural disorders in dementia. *Brain*, *128*(11), 2612–2625. https://doi.org/10.1093/brain/awh628

Ross, C. A., & Poirier, M. A. (2004). Protein aggregation and neurodegenerative disease. *Nature Medicine*, *10*(7), S10. https://doi.org/10.1038/nm1066

Rosso, S. M., Roks, G., Stevens, M., De Koning, I., Tanghe, H. L. J., Kamphorst, W., Ravid, R., Niermeijer, M. F., & Van Swieten, J. C. (2001). Complex compulsive behaviour in the temporal variant of frontotemporal dementia. *J Neurol*, *248*, 965–970.

Roux, K. J., Kim, D. I., Raida, M., & Burke, B. (2012). A promiscuous biotin ligase fusion protein identifies proximal and interacting proteins in mammalian cells. *Journal of Cell Biology*, *196*(6), 801–810. https://doi.org/10.1083/jcb.201112098

Rozman, J., Stojan, J., Kuhelj, R., Turk, V., & Turk, B. (1999). Autocatalytic processing of recombinant human procathepsin B is a bimolecular process. *FEBS Letters*, *459*(3), 358–362. https://doi.org/10.1016/S0014-5793(99)01302-2

Russell, D., Oldham, N. J., & Davis, B. G. (2009). Site-selective chemical protein glycosylation protects from autolysis and proteolytic degradation. *Carbohydrate Research*, *344*(12), 1508–1514. https://doi.org/10.1016/j.carres.2009.06.033

Saito, T., Matsuba, Y., Mihira, N., Takano, J., Nilsson, P., Itohara, S., Iwata, N., & Saido, T. C. (2014). Single App knock-in mouse models of Alzheimer's disease. *Nature Neuroscience*, *17*(5), 661–663. https://doi.org/10.1038/nn.3697

Salter, M. W., & Stevens, B. (2017). Microglia emerge as central players in brain disease. *Nature Medicine*, *23*(9), 1018–1027. https://doi.org/10.1038/nm.4397

Santos, M. N., Paushter, D. H., Zhang, T., Wu, X., Feng, T., Lou, J., Du, H., Becker, S. M., Fragoza, R., Yu, H., & Hu, F. (2022). Progranulin-derived granulin E and lysosome membrane protein CD68 interact to reciprocally regulate their protein homeostasis. *Journal of Biological Chemistry*, *298*(9). https://doi.org/10.1016/j.jbc.2022.102348

Sasaki, A., Yamaguchi, H., Ogawa, A., Sugihara, S., & Nakazato, Y. (1997). Microglial activation in early stages of amyloid-beta protein deposition. *Acta Neuropathologica*, *94*(4), 316–322.

Sasaki, Y., Hoshi, M., Akazawa, C., Nakamura, Y., Tsuzuki, H., Inoue, K., & Kohsaka, S. (2003). Selective Expression of Gi/o-Coupled ATP Receptor P2Y12 in Microglia in Rat Brain. *GLIA*, *44*(3), 242–250. https://doi.org/10.1002/glia.10293

Satoh, J. I., Kino, Y., Yanaizu, M., Tosaki, Y., Sakai, K., Ishida, T., & Saito, Y. (2017). Microglia express ABI3 in the brains of Alzheimer's disease and Nasu-Hakola disease. *Intractable and Rare Diseases Research*, *6*(4), 262–268. https://doi.org/10.5582/irdr.2017.01073

Schafer, D. P., Lehrman, E. K., Kautzman, A. G., Koyama, R., Mardinly, A. R., Yamasaki, R., Ransohoff, R. M., Greenberg, M. E., Barres, B. A., & Stevens, B. (2012). Microglia Sculpt Postnatal Neural Circuits in an Activity and Complement-Dependent Manner. *Neuron*, *74*(4), 691–705. https://doi.org/10.1016/j.neuron.2012.03.026

Scheltens, P., Blennow, K., Breteler, M. M. B., de Strooper, B., Frisoni, G. B., Salloway, S., & Van der Flier, W. M. (2016). Alzheimer's disease. *The Lancet*, *388*(10043), 505–517. https://doi.org/10.1016/S0140-6736(15)01124-1

Seeley, W. W., Bauer, ; A M, Miller, ; B L, Gorno-Tempini, ; M L, Kramer, ; J H, Weiner, ; M, & Rosen, H. J. (2005). The natural history of temporal variant frontotemporal dementia. *Neurology*, *64*, 1384–1390.

Seeley, W. W., Crawford, ; Richard, Rascovsky, K., Kramer, J. H., Weiner, M., Miller, B. L., & Gorno-Tempini, M. L. (2008). Frontal Paralimbic Network Atrophy in Very Mild Behavioral Variant Frontotemporal Dementia. *Arch Neurol*, *65*(2), 249–255. https://jamanetwork.com/

Selkoe, D. J., & Hardy, J. (2016). The amyloid hypothesis of Alzheimer's disease at 25 years. *EMBO Molecular Medicine*, *8*(6), 595–608. https://doi.org/10.15252/emmm.201606210

Selkoe, D. J., Abraham, C. R., Podlisny, M. B., & Duffy, L. K. (1986). Isolation of Low-Molecular-Weight Proteins from Amyloid Plaque Fibers in Alzheimer's Disease. *Journal of Neurochemistry*, *46*(6), 1820–1834. https://doi.org/10.1111/j.1471-4159.1986.tb08501.x

Serrano-Pozo, A., Qian, J., Monsell, S. E., Blacker, D., G Omez-Isla, T., Betensky, R. A., Growdon, J. H., Johnson, K. A., Frosch, M. P., Sperling, R. A., & Hyman, B. T. (2014). Mild to Moderate Alzheimer Dementia with Insufficient Neuropathological Changes. *Annals of Neurology*, *75*, 597–601. https://doi.org/10.1002/ana

Sewer, M. B., & Li, D. (2008). Regulation of steroid hormone biosynthesis by the cytoskeleton. *Lipids*, *43*(12), 1109–1115. https://doi.org/10.1007/s11745-008-3221-2

Shankaran, S. S., Capell, A., Hruscha, A. T., Fellerer, K., Neumann, M., Schmid, B., & Haass, C. (2008). Missense mutations in the progranulin gene linked to frontotemporal lobar degeneration with ubiquitin-immunoreactive inclusions reduce progranulin production and secretion. *Journal of Biological Chemistry*, *283*(3), 1744–1753. https://doi.org/10.1074/jbc.M705115200

Shannon, P., Markiel, A., Ozier, O., Baliga, N. S., Wang, J. T., Ramage, D., Amin, N., Schwikowski, B., & Ideker, T. (2003). Cytoscape: A software Environment for integrated models of biomolecular interaction networks. *Genome Research*, *13*(11), 2498–2504. https://doi.org/10.1101/gr.1239303

Sharma, K., Schmitt, S., Bergner, C. G., Tyanova, S., Kannaiyan, N., Manrique-Hoyos, N., Kongi, K., Cantuti, L., Hanisch, U. K., Philips, M. A., Rossner, M. J., Mann, M., & Simons, M. (2015). Cell type-

and brain region-resolved mouse brain proteome. *Nature Neuroscience*, *18*(12), 1819–1831. https://doi.org/10.1038/nn.4160

Sheffield, L. G., & J Berman, N. E. (1998). Microglial Expression of MHC Class II Increases in Normal Aging of Nonhuman Primates. *Neurobiology of Aging*, *19*(1), 47–44.

Sieben, A., Van Langenhove, T., Engelborghs, S., Martin, J. J., Boon, P., Cras, P., De Deyn, P. P., Santens, P., Van Broeckhoven, C., & Cruts, M. (2012). The genetics and neuropathology of frontotemporal lobar degeneration. *Acta Neuropathologica*, *124*(3), 353–372. https://doi.org/10.1007/s00401-012-1029-x

Sierra, A., Encinas, J. M., Deudero, J. J. P., Chancey, J. H., Enikolopov, G., Overstreet-Wadiche, L. S., Tsirka, S. E., & Maletic-Savatic, M. (2010). Microglia shape adult hippocampal neurogenesis through apoptosis-coupled phagocytosis. *Cell Stem Cell*, *7*(4), 483–495. https://doi.org/10.1016/j.stem.2010.08.014

Smith, J. A., Das, A., Ray, S. K., & Banik, N. L. (2012). Role of pro-inflammatory cytokines released from microglia in neurodegenerative diseases. *Brain Research Bulletin*, *87*(1), 10–20. https://doi.org/10.1016/j.brainresbull.2011.10.004

Smith, K. R., Damiano, J., Franceschetti, S., Carpenter, S., Canafoglia, L., Morbin, M., Rossi, G., Pareyson, D., Mole, S. E., Staropoli, J. F., Sims, K. B., Lewis, J., Lin, W. L., Dickson, D. W., Dahl, H. H., Bahlo, M., & Berkovic, S. F. (2012). Strikingly different clinicopathological phenotypes determined by progranulin-mutation dosage. *American Journal of Human Genetics*, *90*(6), 1102–1107. https://doi.org/10.1016/j.ajhg.2012.04.021

Songsrirote, K., Li, Z., Ashford, D., Bateman, A., & Thomas-Oates, J. (2010). Development and application of mass spectrometric methods for the analysis of progranulin N-glycosylation. *Journal of Proteomics*, *73*(8), 1479–1490. https://doi.org/10.1016/j.jprot.2010.02.013

Specht, H., Emmott, E., Petelski, A. A., Huffman, R. G., Perlman, D. H., Serra, M., Kharchenko, P., Koller, A., & Slavov, N. (2021). Single-cell proteomic and transcriptomic analysis of macrophage

heterogeneity using SCoPE2. *Genome Biology*, *22*(1). https://doi.org/10.1186/s13059-021-02267-5

Spillantini, M. G., Murrell, J. R., Goedert, M., Farlow, M. R., Klug, A., & Ghetti, B. (1998). Mutation in the tau gene in familial multiple system tauopathy with presenile dementia alternative mRNA splicingFour-repeat tau isoformsFrontotemporal dementiamicrotubule bindingTau filaments. *Neurobiology*, *95*, 7737–7741. www.pnas.org.

Spillantini, M. G., Goedert, M., Crowther, R. A., Murrell, J. R., Farlow, M. R., & Ghetti, B. (1997). Familial multiple system tauopathy with presenile dementia: A disease with abundant neuronal and glial tau filaments (microtubule-associated protein taufamilial disease). *Neurobiology*, *94*, 4113–4118. www.pnas.org.

Spillantini, M., Schmidt, M., Lee, V. M.-Y., Trojanowski, J., Jakes, R., & Goedert, M. (1997). a-Synuclein in Lewy bodies. *Nature*, *388*, 839–840.

Stalder, M., Phinney, A., Probst, A., Sommer, B., Staufenbiel, M., & Jucker, M. (1999). Association of Microglia with Amyloid Plaques in Brains of APP23 Transgenic Mice. *Am J Pathol*, *154*, 1673–1684.

Stence, N., Waite, M., & Dailey, M. E. (2001). Dynamics of microglial activation: A confocal time-lapse analysis in hippocampal slices. *GLIA*, *33*(3), 256–266. https://doi.org/10.1002/1098-1136(200103)33:3<256::AID-GLIA1024>3.0.CO;2-J

Stephan, A. H., Barres, B. A., & Stevens, B. (2012). The complement system: An unexpected role in synaptic pruning during development and disease. *Annual Review of Neuroscience*, *35*, 369–389. https://doi.org/10.1146/annurev-neuro-061010-113810

Stewart, C. R., Stuart, L. M., Wilkinson, K., Van Gils, J. M., Deng, J., Halle, A., Rayner, K. J., Boyer, L., Zhong, R., Frazier, W. A., Lacy-Hulbert, A., Khoury, J. El, Golenbock, D. T., & Moore, K. J. (2010). CD36 ligands promote sterile inflammation through assembly of a Toll-like receptor 4 and 6 heterodimer. *Nature Immunology*, *11*(2), 155–161. https://doi.org/10.1038/ni.1836

Stowell, R. D., Sipe, G. O., Dawes, R. P., Batchelor, H. N., Lordy, K. A., Whitelaw, B. S., Stoessel, M. B., Bidlack, J. M., Brown, E., Sur, M., & Majewska, A. K. (2019). Noradrenergic signaling in the wakeful state inhibits microglial surveillance and synaptic plasticity in the mouse visual cortex. *Nature Neuroscience*, *22*(11), 1782–1792. https://doi.org/10.1038/s41593-019-0514-0

Streit, W. J., & Sparks, D. L. (1997). Activation of microglia in the brains of humans with heart disease and hypercholesterolemic rabbits. *Journal of Molecular Medicine*, *75*, 130–138.

Streit, W. J., Sammons, N. W., Kuhns, A. J., & Sparks, D. L. (2004). Dystrophic Microglia in the Aging Human Brain. *GLIA*, *45*(2), 208–212. https://doi.org/10.1002/glia.10319

Subramanian, J., Savage, J. C., & Tremblay, M. È. (2020). Synaptic Loss in Alzheimer's Disease: Mechanistic Insights Provided by Two-Photon in vivo Imaging of Transgenic Mouse Models. *Frontiers in Cellular Neuroscience*, *14*. https://doi.org/10.3389/fncel.2020.592607

Suo, Z., Wu, M., Citron, B. A., Wong, G. T., & Festoff, B. W. (2004). Abnormality of G-Protein-Coupled Receptor Kinases at Prodromal and Early Stages of Alzheimer's Disease: An Association with Early β-Amyloid Accumulation. *Journal of Neuroscience*, *24*(13), 3444–3452. https://doi.org/10.1523/JNEUROSCI.4856-03.2004

Szklarczyk, D., Gable, A. L., Lyon, D., Junge, A., Wyder, S., Huerta-Cepas, J., Simonovic, M., Doncheva, N. T., Morris, J. H., Bork, P., Jensen, L. J., & Von Mering, C. (2019). STRING v11: Protein-protein association networks with increased coverage, supporting functional discovery in genome-wide experimental datasets. *Nucleic Acids Research*, *47*(D1), D607–D613. https://doi.org/10.1093/nar/gky1131

Takahashi, K., Tanabe, K., Ohnuki, M., Narita, M., Ichisaka, T., Tomoda, K., & Yamanaka, S. (2007). Induction of Pluripotent Stem Cells from Adult Human Fibroblasts by Defined Factors. *Cell*, *131*(5), 861–872. https://doi.org/10.1016/j.cell.2007.11.019

Takata, K., Kozaki, T., Lee, C. Z. W., Thion, M. S., Otsuka, M., Lim, S., Utami, K. H., Fidan, K., Park, D. S., Malleret, B., Chakarov, S., See, P., Low, D., Low, G., Garcia-Miralles, M., Zeng, R., Zhang, J., Goh, C. C., Gul, A., … Ginhoux, F. (2017). Induced-Pluripotent-Stem-Cell-Derived Primitive Macrophages Provide a Platform for Modeling Tissue-Resident Macrophage Differentiation and Function. *Immunity*, *47*(1), 183-198.e6. https://doi.org/10.1016/j.immuni.2017.06.017

Tanaka, Y., Matsuwaki, T., Yamanouchi, K., & Nishihara, M. (2013). Increased lysosomal biogenesis in activated microglia and exacerbated neuronal damage after traumatic brain injury in progranulin-deficient mice. *Neuroscience*, *250*, 8–19. https://doi.org/10.1016/j.neuroscience.2013.06.049

Tanaka, Y., Suzuki, G., Matsuwaki, T., Hosokawa, M., Serrano, G., Beach, T. G., Yamanouchi, K., Hasegawa, M., & Nishihara, M. (2017). Progranulin regulates lysosomal function and biogenesis through acidification of lysosomes. *Human Molecular Genetics*, *26*(5), 969–988. https://doi.org/10.1093/hmg/ddx011

Telpoukhovskaia, M. A., Liu, K., Sayed, F. A., Etchegaray, J. I., Xie, M., Zhan, L., Li, Y., Zhou, Y., Le, D., Bahr, B. A., Bogyo, M., Ding, S., & Gan, L. (2020). Discovery of small molecules that normalize the transcriptome and enhance cysteine cathepsin activity in progranulin-deficient microglia. *Scientific Reports*, *10*(1). https://doi.org/10.1038/s41598-020-70534-9

Terry, R. D., Masliah, E., Salmon, D. P., Butters, N., DeTeresa, R., Hill, R., Hansen, L. A., & Katzman, R. (1991). Physical basis of cognitive alterations in alzheimer's disease: Synapse loss is the major correlate of cognitive impairment. *Annals of Neurology*, *30*(4), 572–580. https://doi.org/10.1002/ana.410300410

Town, T., Nikolic, V., & Tan, J. (2005). The microglial "activation" continuum: From innate to adaptive responses. *Journal of Neuroinflammation*, *2*. https://doi.org/10.1186/1742-2094-2-24

Tradewell, M. L., Yu, Z., Tibshirani, M., Boulanger, M. C., Durham, H. D., & Richard, S. (2012). Arginine methylation by prmt1 regulates nuclear-cytoplasmic localization and toxicity of FUS/TLS harbouring

ALS-linked mutations. *Human Molecular Genetics*, *21*(1), 136–149. https://doi.org/10.1093/hmg/ddr448

Traenka, C., Remke, M., Korshunov, A., Bender, S., Hielscher, T., Northcott, P. A., Witt, H., Ryzhova, M., Felsberg, J., Benner, A., Riester, S., Scheurlen, W., Grunewald, T. G. P., Von Deimling, A., Kulozik, A. E., Reifenberger, G., Taylor, M. D., Lichter, P., Butt, E., & Pfister, S. M. (2010). Role of LIM and SH3 protein 1 (LASP1) in the metastatic dissemination of medulloblastoma. *Cancer Research*, *70*(20), 8003–8014. https://doi.org/10.1158/0008-5472.CAN-10-0592

Tranel, D., Bechara, A., & Denburg, N. L. (2002). Asymmetric functional roles of right and left ventromedial prefrontal cortices in social conduct, decision-making, and emotional processing. *Cortex*, *38*, 589–612.

Tsoi, P. S., Quan, M. D., Ferreon, J. C., & Ferreon, A. C. M. (2023). Aggregation of Disordered Proteins Associated with Neurodegeneration. *International Journal of Molecular Sciences*, *24*(4). https://doi.org/10.3390/ijms24043380

Tsukita, S., & Ishikawa, H. (1980). The movement of membranous organelles in axons. Electron Microscopic Identification of Anterogradely and Retrogradely Transported Organelles. *Journal of Cell Biology*, *84*, 513–530. http://rupress.org/jcb/article-pdf/84/3/513/1400993/513.pdf

Turk, V., Turk, B., & Turk, D. (2001). Lysosomal cysteine proteases: Facts and opportunities. *EMBO Journal*, *20*(17), 4629–4633. https://doi.org/10.1093/emboj/20.17.4629

Tyynelä, J., Cooper, J. D., Khan, M. N., Shemilt, S. J. A., & Haltia, M. (2004). Hippocampal pathology in the human neuronal ceroid-lipofuscinoses: Distinct patterns of storage deposition, neurodegeneration and glial activation. *Brain Pathology*, *14*(4), 349–357. https://doi.org/10.1111/j.1750-3639.2004.tb00077.x

Uffelmann, E., Huang, Q. Q., Munung, N. S., de Vries, J., Okada, Y., Martin, A. R., Martin, H. C., Lappalainen, T., & Posthuma, D. (2021).

Genome-wide association studies. *Nature Reviews Methods Primers*, *1*(1). https://doi.org/10.1038/s43586-021-00056-9

Valdez, C., Wong, Y. C., Schwake, M., Bu, G., Wszolek, Z. K., & Krainc, D. (2017). Progranulin-mediated deficiency of cathepsin D results in FTD and NCL-like phenotypes in neurons derived from FTD patients. *Human Molecular Genetics*, *26*(24), 4861–4872. https://doi.org/10.1093/hmg/ddx364

Van Deerlin, V. M., Sleiman, P. M. A., Martinez-Lage, M., Chen-Plotkin, A., Wang, L. S., Graff-Radford, N. R., Dickson, D. W., Rademakers, R., Boeve, B. F., Grossman, M., Arnold, S. E., Mann, D. M. A., Pickering-Brown, S. M., Seelaar, H., Heutink, P., Van Swieten, J. C., Murrell, J. R., Ghetti, B., Spina, S., … Lee, V. M. Y. (2010). Common variants at 7p21 are associated with frontotemporal lobar degeneration with TDP-43 inclusions. *Nature Genetics*, *42*(3), 234–239. https://doi.org/10.1038/ng.536

Viswanathan, J., Mäkinen, P., Helisalmi, S., Haapasalo, A., Soininen, H., & Hiltunen, M. (2009). An association study between granulin gene polymorphisms and Alzheimer's disease in finnish population. *American Journal of Medical Genetics, Part B: Neuropsychiatric Genetics*, *150*(5), 747–750. https://doi.org/10.1002/ajmg.b.30889

Vogel, J. W., Iturria-Medina, Y., Strandberg, O. T., Smith, R., Levitis, E., Evans, A. C., & Hansson, O. (2020). Spread of pathological tau proteins through communicating neurons in human Alzheimer's disease. *Nature Communications*, *11*(1), 2612. https://doi.org/10.1038/s41467-020-15701-2

Wake, H., Moorhouse, A. J., Jinno, S., Kohsaka, S., & Nabekura, J. (2009). Resting microglia directly monitor the functional state of synapses in vivo and determine the fate of ischemic terminals. *Journal of Neuroscience*, *29*(13), 3974–3980. https://doi.org/10.1523/JNEUROSCI.4363-08.2009

Wang, D., Kowalewski, E., Koch, G. (2022). Application of Meta-analysis to Evaluate Relationships Among ARIA-E Rate, Amyloid Reduction Rate, and Clinical Cognitive Response in Amyloid Therapeutic Clinical Trials for Early Alzheimer's Disease. *Therapeutic Innovation*

& Regulatory Science, 56:501–516 https://doi.org/10.1007/s43441-022-00390-4

Wang, J., Van Damme, P., Cruchaga, C., Gitcho, M. A., Vidal, J. M., Seijo-Martínez, M., Wang, L., Wu, J. Y., Robberecht, W., & Goate, A. (2010). Pathogenic cysteine mutations affect progranulin function and production of mature granulins. *Journal of Neurochemistry*, *112*(5), 1305–1315. https://doi.org/10.1111/j.1471-4159.2009.06546.x

Wang, P., Deng, J., Dong, J., Liu, J., Bigio, E. H., Mesulam, M., Wang, T., Sun, L., Wang, L., Lee, A. Y. L., McGee, W. A., Chen, X., Fushimi, K., Zhu, L., & Wu, J. Y. (2019). TDP-43 induces mitochondrial damage and activates the mitochondrial unfolded protein response. *PLoS Genetics*, *15*(5). https://doi.org/10.1371/journal.pgen.1007947

Wang, W., Li, L., Lin, W. L., Dickson, D. W., Petrucelli, L., Zhang, T., & Wang, X. (2013). The ALS disease-associated mutant TDP-43 impairs mitochondrial dynamics and function in motor neurons. *Human Molecular Genetics*, *22*(23), 4706–4719. https://doi.org/10.1093/hmg/ddt319

Wang, X., Su, B., Lee, H. G., Li, X., Perry, G., Smith, M. A., & Zhu, X. (2009). Impaired balance of mitochondrial fission and fusion in Alzheimer's disease. *Journal of Neuroscience*, *29*(28), 9090–9103. https://doi.org/10.1523/JNEUROSCI.1357-09.2009

Ward, M. E., Chen, R., Huang, H.-Y., Ludwig, C., Telpoukhovskaia, M., Taubes, A., Boudin, H., Minami, S. S., Reichert, M., Albrecht, P., Gelfand, J. M., Cruz-Herranz, A., Cordano, C., Alavi, M. V, Leslie, S., Seeley, W. W., Miller, B. L., Bigio, E., Mesulam, M.-M., … Green, A. J. (2017). Individuals with progranulin haploinsufficiency exhibit features of neuronal ceroid lipofuscinosis. *Science Translational Medicine*, *9*. https://www.science.org

Ward, M. E., & Miller, B. L. (2011). Potential mechanisms of progranulin-deficient FTLD. *Journal of Molecular Neuroscience*, *45*(3), 574–582. https://doi.org/10.1007/s12031-011-9622-3

Wegiel, J., Wang, K.-C., Imaki, H., Rubenstein, R., Wronska, A., Osuchowski, M., Lipinski, W. J., Walker, L. C., & Levine, H. (2001). The role of microglial cells and astrocytes in fibrillar plaque evolution in transgenic APP SW mice. *Neurobiology of Aging*, *22*, 49–61. www.elsevier.com/locate/neuaging

Weingarten, M. D., Lockwood, A. H., Hwo, S.-Y., & Kirschner, M. W. (1975). A Protein Factor Essential for Microtubule Assembly (tau factor/tubulin/electron microscopy/phosphocellulose). *PNAS*, *72*(5), 1858–1862. https://www.pnas.org

Whitfield, D. R., Vallortigara, J., Alghamdi, A., Howlett, D., Hortobágyi, T., Johnson, M., Attems, J., Newhouse, S., Ballard, C., Thomas, A. J., O'Brien, J. T., Aarsland, D., & Francis, P. T. (2014). Assessment of ZnT3 and PSD95 protein levels in Lewy body dementias and Alzheimer's disease: Association with cognitive impairment. *Neurobiology of Aging*, *35*(12), 2836–2844. https://doi.org/10.1016/j.neurobiolaging.2014.06.015

Whitwell, J. L., Sampson, E. L., Loy, C. T., Warren, J. E., Rossor, M. N., Fox, N. C., & Warren, J. D. (2007). VBM signatures of abnormal eating behaviours in frontotemporal lobar degeneration. *NeuroImage*, *35*(1), 207–213. https://doi.org/10.1016/j.neuroimage.2006.12.006

Wider, C., Uitti, R. J., Wszolek, Z. K., Fang, J. Y., Joesephs, K. A., Baker, M. C., Rademakers R., Hutton, M. J., Dickson, D. W. (2008) Progranulin Gene Mutation with an Unusual Clinical and Neuropathologic Presentation. *Movement Disorders, 23(8),* 1168-1173. https://doi.org/10.1002/mds.22065

Wightman, D. P., Jansen, I. E., Savage, J. E., Shadrin, A. A., Bahrami, S., Holland, D., Rongve, A., Børte, S., Winsvold, B. S., Drange, O. K., Martinsen, A. E., Skogholt, A. H., Willer, C., Bråthen, G., Bosnes, I., Nielsen, J. B., Fritsche, L. G., Thomas, L. F., Pedersen, L. M., … Posthuma, D. (2021). A genome-wide association study with 1,126,563 individuals identifies new risk loci for Alzheimer's disease. *Nature Genetics*, *53*(9), 1276–1282. https://doi.org/10.1038/s41588-021-00921-z

Woolley, J. D., Gorno-Tempini, M.-L., Seeley, W. W., Rankin, K., Lee, S. S., Matthews, B. B. R., & Miller, B. L. (2007). Binge eating is associated with right orbitofrontal-insular-striatal atrophy in frontotemporal dementia. *Neurology*, *69*, 1424–1433. www.neurology.org

Wu, Y., Shao, W., Todd, T. W., Tong, J., Yue, M., Koga, S., Castanedes-Casey, M., Librero, A. L., Lee, C. W., Mackenzie, I. R., Dickson, D. W., Zhang, Y. J., Petrucelli, L., & Prudencio, M. (2021). Microglial lysosome dysfunction contributes to white matter pathology and TDP-43 proteinopathy in GRN-associated FTD. *Cell Reports*, *36*(8). https://doi.org/10.1016/j.celrep.2021.109581

Xia, Y., Liu, H., Shen, A., Liu, Y., Sun, L., Tao, T., Ke, Q., & Cheng, C. (2010). A critical role of Src-suppressed C kinase substrate in rat astrocytes after chronic constriction injury. *NeuroMolecular Medicine*, *12*(3), 205–216. https://doi.org/10.1007/s12017-009-8093-y

Xiong, J., He, J., Xie, W. P., Hinojosa, E., Ambati, C. S. R., Putluri, N., Kim, H. E., Zhu, M. X., & Du, G. (2019). Rapid affinity purification of intracellular organelles using a twin strep tag. *Journal of Cell Science*, *132*(24). https://doi.org/10.1242/jcs.235390

Yamagata, M. and Sanes, J. (2018). Reporter–nanobody fusions (RANbodies) as versatile, small, sensitive immunohistochemical reagents. *Proceedings of the National Academy of Sciences of the United States of America*, 2126-2131, 115(9). https://doi.org/10.1073/pnas.1722491115

Yang, S., Jin, S., Xian, H., Zhao, Z., Wang, L., Wu, Y., Zhou, L., Li, M., & Cui, J. (2023). Metabolic enzyme UAP1 mediates IRF3 pyrophosphorylation to facilitate innate immune response. *Molecular Cell*, *83*(2), 298-313.e8. https://doi.org/10.1016/j.molcel.2022.12.007

Yap, C. C., Digilio, L., McMahon, L. P., Garcia, A. D. R., & Winckler, B. (2018). Degradation of dendritic cargos requires Rab7-dependent transport to somatic lysosomes. *Journal of Cell Biology*, *217*(9), 3141–3159. https://doi.org/10.1083/jcb.201711039

Yeh, F. L., Hansen, D. V., & Sheng, M. (2017). TREM2, Microglia, and Neurodegenerative Diseases. *Trends in Molecular Medicine*, *23*(6), 512–533. https://doi.org/10.1016/j.molmed.2017.03.008

Yin (a), F. (A), Banerjee, R., Thomas, B., Zhou, P., Qian, L., Jia, T., Ma, X., Ma, Y., Iadecola, C., Beal, M. F., Nathan, C., & Ding, A. (2010). Exaggerated inflammation, impaired host defense, and neuropathology in progranulin-deficient mice. *Journal of Experimental Medicine*, *207*(1), 117–128. https://doi.org/10.1084/jem.20091568

Yin, F., Dumont, M., Banerjee, R., Ma, Y., Li, H., Lin, M. T., Beal, M. F., Nathan, C., Thomas, B., & Ding, A. (2010). Behavioral deficits and progressive neuropathology in progranulin-deficient mice: a mouse model of frontotemporal dementia. *The FASEB Journal*, *24*(12), 4639–4647. https://doi.org/10.1096/fj.10-161471

Yokoyama, M., Kobayashi, H., Tatsumi, L., & Tomita, T. (2022). Mouse Models of Alzheimer's Disease. *Frontiers in Molecular Neuroscience*, *15*. https://doi.org/10.3389/fnmol.2022.912995

Young, J. J., Lavakumar, M., Tampi, D., Balachandran, S., & Tampi, R. R. (2018). Frontotemporal dementia: latest evidence and clinical implications. *Therapeutic Advances in Psychopharmacology*, *8*(1), 33–48. https://doi.org/10.1177/2045125317739818

Zhang, H., Cao, Y., Ma, L., Wei, Y., & Li, H. (2021). Possible Mechanisms of Tau Spread and Toxicity in Alzheimer's Disease. *Frontiers in Cell and Developmental Biology*, *9*. https://doi.org/10.3389/fcell.2021.707268

Zhang, J., Velmeshev, D., Hashimoto, K., Huang, Y. H., Hofmann, J. W., Shi, X., Chen, J., Leidal, A. M., Dishart, J. G., Cahill, M. K., Kelley, K. W., Liddelow, S. A., Seeley, W. W., Miller, B. L., Walther, T. C., Farese, R. V., Taylor, J. P., Ullian, E. M., Huang, B., … Huang, E. J. (2020). Neurotoxic microglia promote TDP-43 proteinopathy in progranulin deficiency. *Nature*, *588*(7838), 459–465. https://doi.org/10.1038/s41586-020-2709-7

Zhang, T., Feng, T., Wu, K., Guo, J., Nana, A., Yang, G., Seeley, W., Hu, F. (2023). Progranulin deficiency results in sex-dependent

alterations in microglia in response to demyelination. *Acta Neuropathologica volume* 146, 97–119. https://doi.org/10.1007/s00401-023-02578-w

Zhang, Y. W., Thompson, R., Zhang, H., & Xu, H. (2011). APP processing in Alzheimer's disease. *Molecular Brain*, *4*(1). https://doi.org/10.1186/1756-6606-4-3

Zhao, L., Cong, X., Zhai, L., Hu, H., Xu, J. Y., Zhao, W., Zhu, M., Tan, M., & Ye, B. C. (2020). Comparative evaluation of label-free quantification strategies. *Journal of Proteomics*, *215*. https://doi.org/10.1016/j.jprot.2020.103669

Zhao, X., Liberti, R., Jian, J., Fu, W., Hettinghouse, A., Sun, Y., & Liu, C. ju. (2021). Progranulin associates with Rab2 and is involved in autophagosome-lysosome fusion in Gaucher disease. *Journal of Molecular Medicine*, *99*(11), 1639–1654. https://doi.org/10.1007/s00109-021-02127-6

Zhou, X. (A), Sun, L., Bracko, O., Choi, J. W., Jia, Y., Nana, A. L., Brady, O. A., Hernandez, J. C. C., Nishimura, N., Seeley, W. W., & Hu, F. (2017). Impaired prosaposin lysosomal trafficking in frontotemporal lobar degeneration due to progranulin mutations. *Nature Communications*, *8*. https://doi.org/10.1038/ncomms15277

Zhou, X., Paushter, D. H., Feng, T., Pardon, C. M., Mendoza, C. S., & Hu, F. (2017). Regulation of cathepsin D activity by the FTLD protein progranulin. *Acta Neuropathologica*, *134*(1), 151–153. https://doi.org/10.1007/s00401-017-1719-5

Zhou, X., Sun, L., de Oliveira, F. B., Qi, X., Brown, W. J., Smolka, M. B., Sun, Y., & Hu, F. (2015). Prosaposin facilitates sortilin-independent lysosomal trafficking of progranulin. *Journal of Cell Biology*, *210*(6), 991–1002. https://doi.org/10.1083/jcb.201502029

Appendix

Supplemental Figures

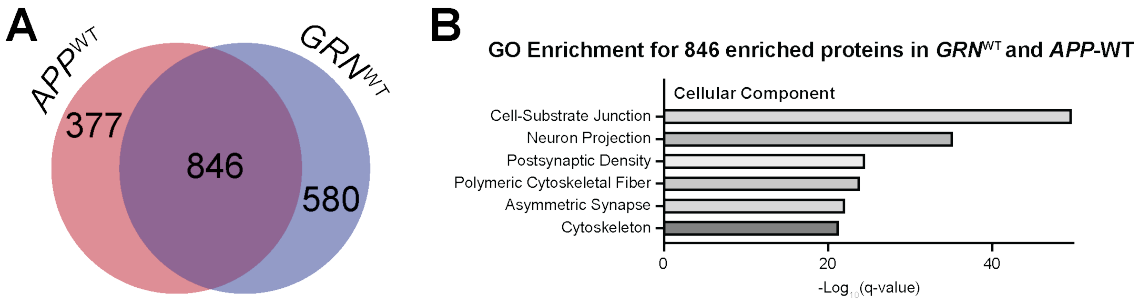

Supplemental Figure 3-1: Overlap of P2Y12-BAR enriched proteins from *GRN*^{WT} and *APP*-WT mouse brains.

(A) Venn diagram showing 846 proteins overlapping between the 1426 P2Y12-BAR enriched proteins from GRNWT and 1224 from APP-WT. **(B)** Gene Ontology analysis using Enrichr reveals cell-substrate junction as the most enriched term, followed by neuron projection, postsynaptic density, polymeric cytoskeletal fiber, asymmetric synapse, and cytoskeleton.

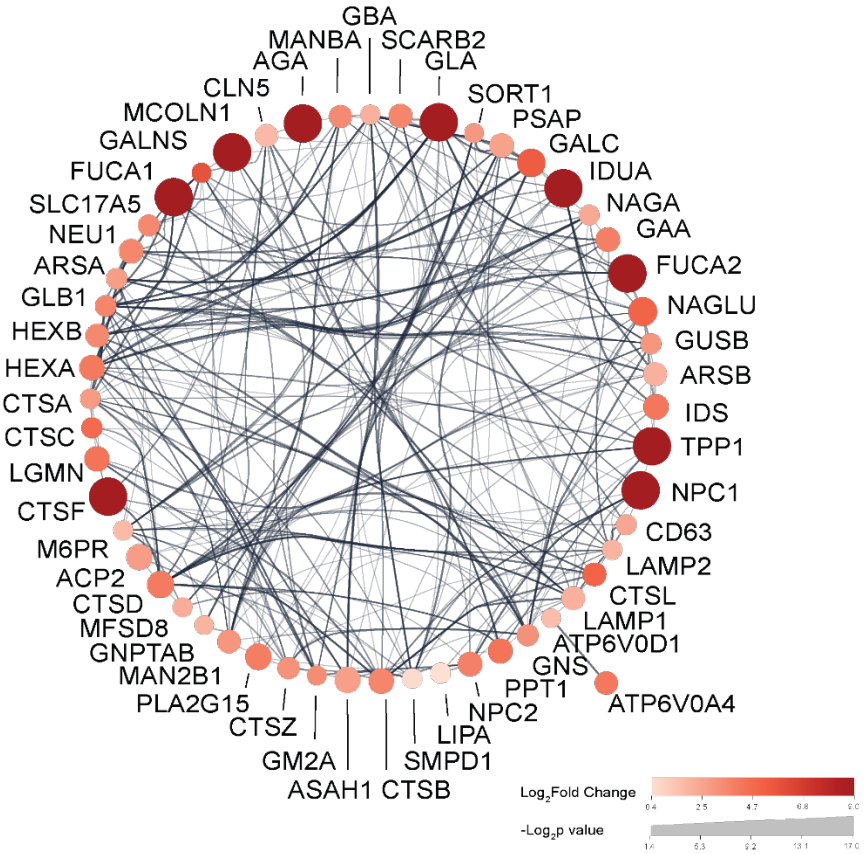

Supplemental Figure 4-1: Lysosomal proteins from i^{3}Neurons Lyso-IP pull down.

Of the 261 proteins enriched in the Lyso-IP dataset, 54 were classified under the lysosome KEGG Pathway GO term. They are shown here in a string network created using string-db.org and Cytoscape.

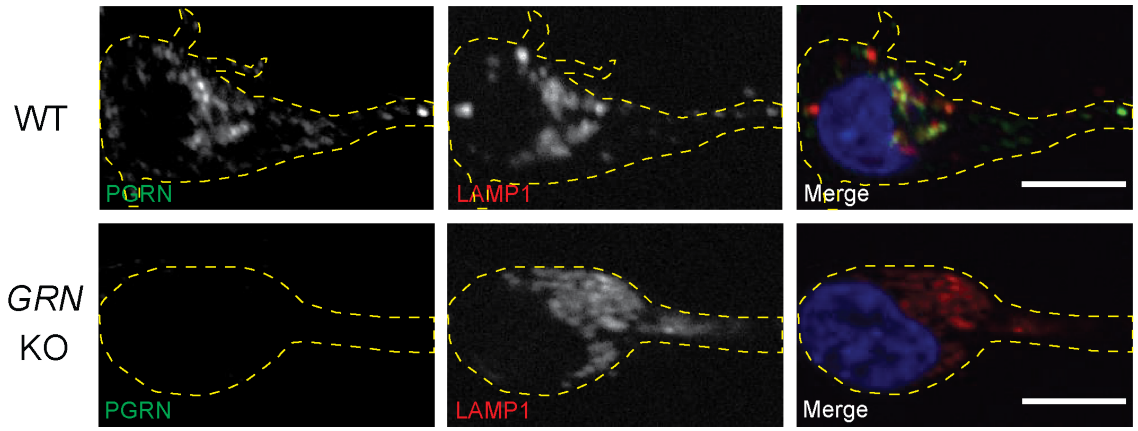

Supplemental Figure 4-2: Complete loss of progranulin in i^{3}Neurons.

Fluorescence imaging shows complete loss of progranulin (PRGN) in *GRN* KO i^{3}Neurons and colocalization of PGRN with lysosomes (LAMP1) in WT i^{3}Neurons. Scale bar is 10μM.

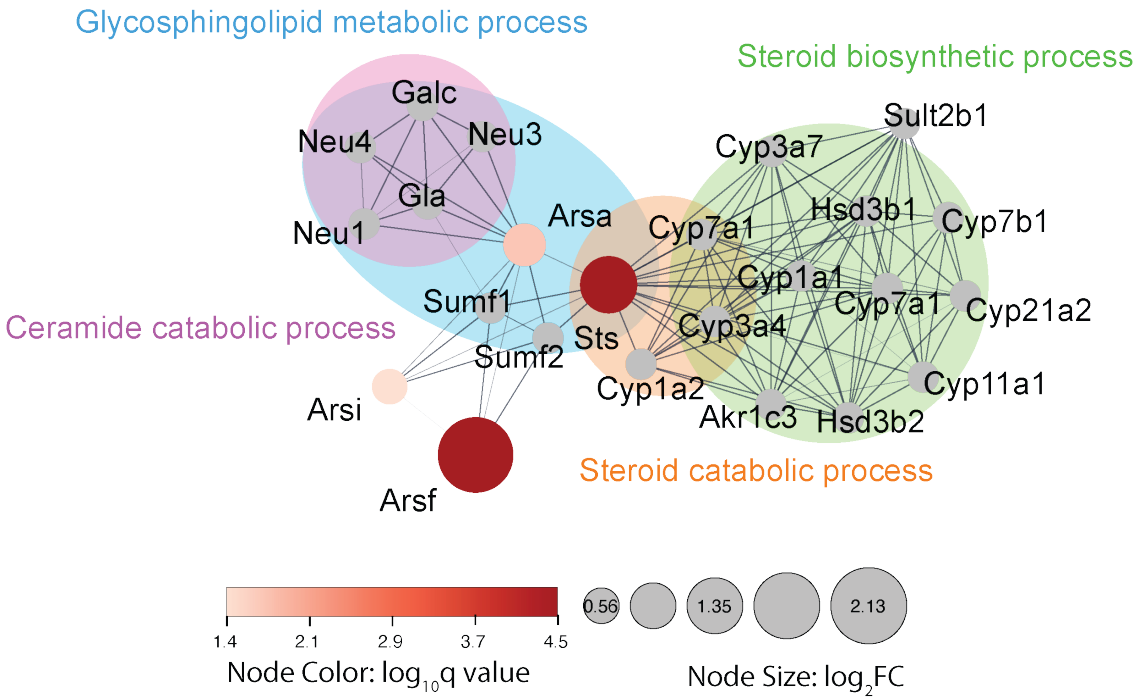

Supplemental Figure 4-3: Complete STRING diagram for Arsa, Sts, Arsf and Arsi.

Diagram was generated using string-db.org and edited in Cytoscape. Grey nodes represent interactors that were not altered in the dataset. No more than 20 interactors were visualized for these 4 proteins. Biological process GO analysis was done using string-db.org's analysis tab. Detailed legend included.

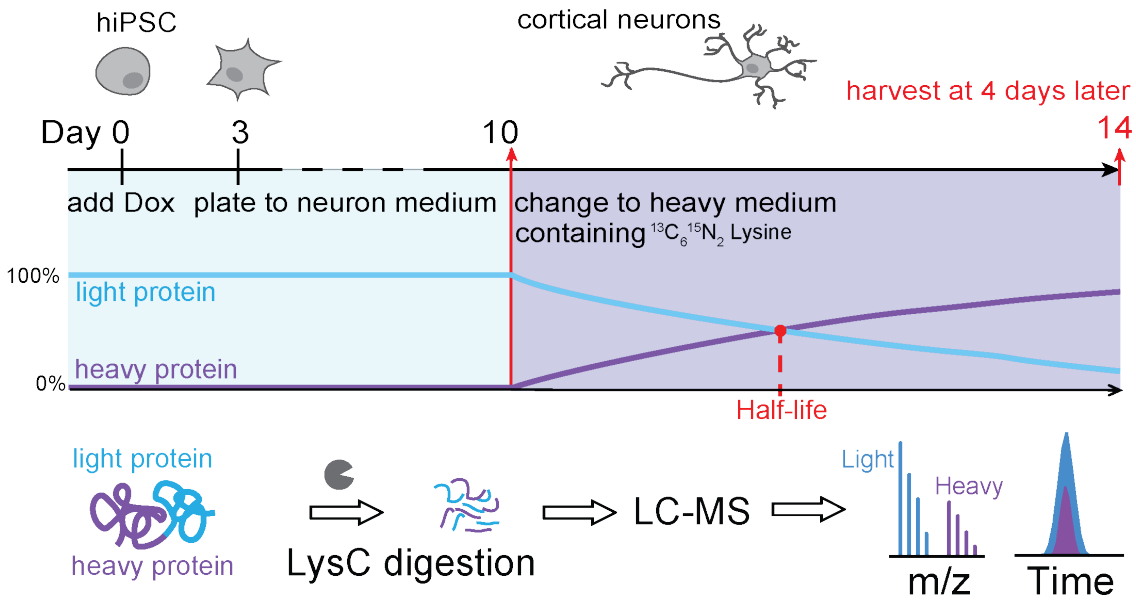

Supplemental Figure 4-4: Dynamic Stable Isotope Labelling using Amino acids in Cell culture (dSILAC) workflow.

Human inducible pluripotent stem cells (hiPSCs) are grown in culture media until use. Doxycycline is added to media to induce differentiation at day 0. The cells differentiate for 3 days before they are replated as neurons (i^{3}Neurons) in SILAC media and matured to day 10. Media is replaced with SILAC media containing heavy isotope of Lysine at day 10 and cells are harvested 4 days later.

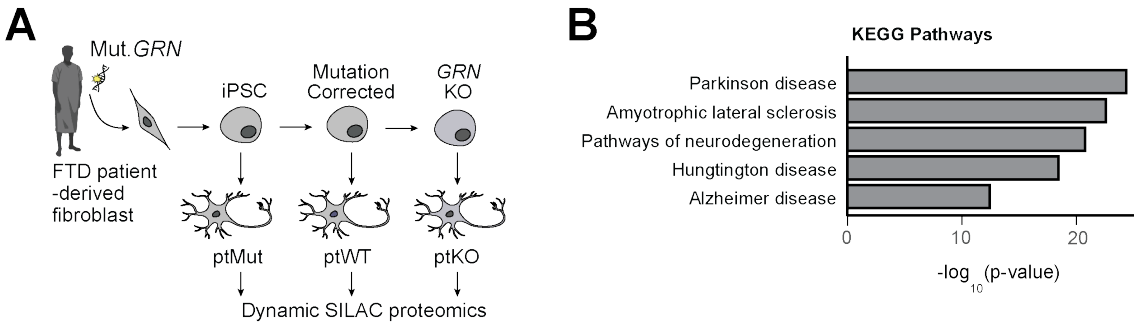

Supplemental Figure 4-5: KEGG Pathways GO enrichment all proteins with changed turnover rates in *GRN* KO neurons.

(A) Patient derived i^{3}Neurons (pMut) were used and compared to its isogenic control (pWT) and complete knockout (pKO). **(B)** Gene Ontology (GO) analysis on all proteins with altered turnover rates in *GRN* KO neurons. Pathways relevant to several neurogenerative disorders are highlighted here. Source: Enrichr.

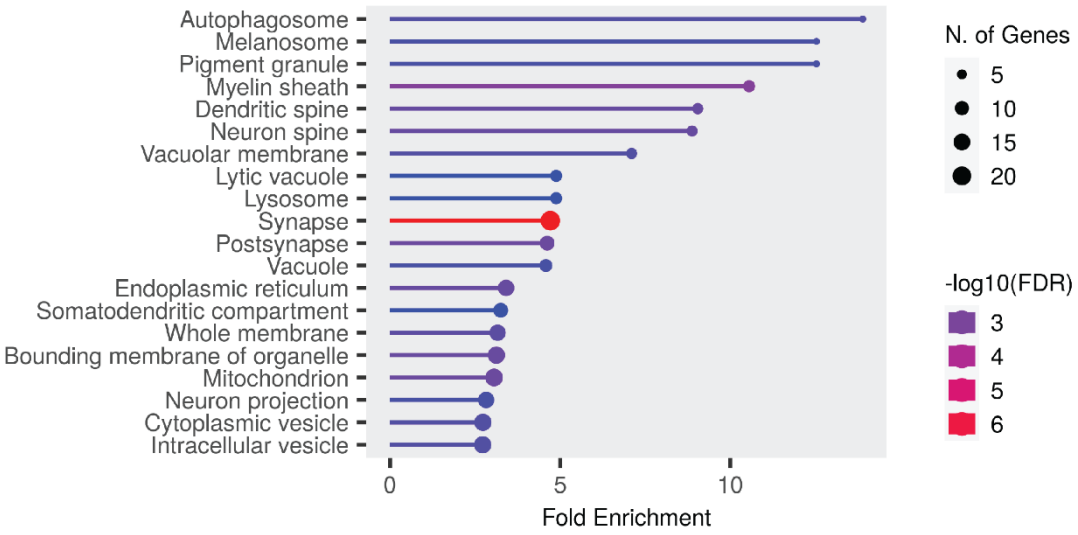

Supplemental Figure 4-6: Cellular component GO enrichment for 68 proteins upregulated only in Lyso-BAR from *GRN*$^{-/-}$ brains.

These proteins were not detected in the Kukar dataset and are unique to Lyso-BAR in *GRN*$^{-/-}$ brains. Synapse is the highly enriched term with the most proteins. Source: ShinyGo 0.77.

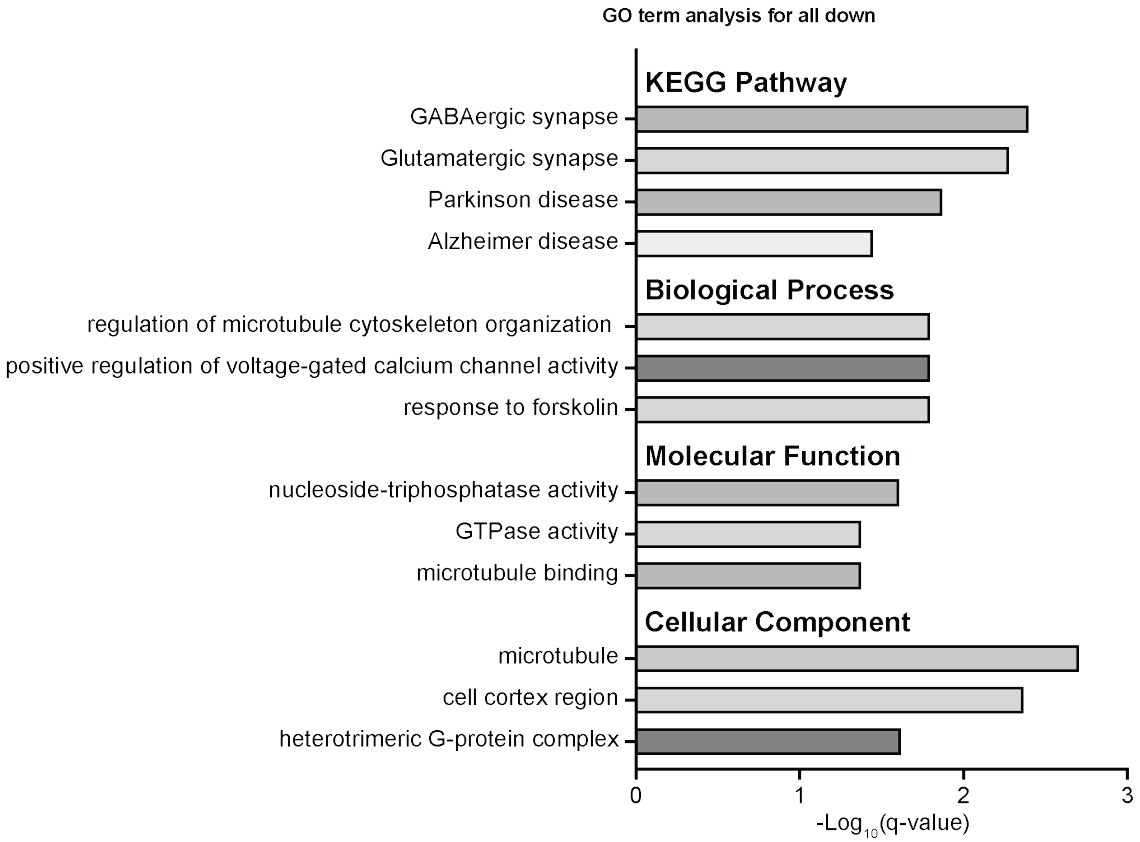

Supplemental Figure 5-1: GO term analysis for 41 decreased proteins in *GRN*$^{-/-}$ microglial-BAR.

Proteins in each term are as follows. GABAergic synapse; Gnb3, Slc6a11, Gnai1, Adcy5. Glutamatergic synapse; Ppp3ca, Gnb3, Gnai1, Adcy5. Parkinson Disease; Tubb2a, Mapt, Gnai1, Adcy5. Alzheimer disease; Ppp3ca, Tubb2a, Csnk2a1, Mapt. Regulation of microtubule cytoskeleton organization; Map6d1, Mapt, Mapre1. Positive response of voltage-gated calcium channel activity; Cacnb3, Nipsnap2. Response to forskolin; Gnai1, Adcy5. Nucleoside-triphosphatase activity; Diras1, Rab24, Gnb3, Gnai1, Kif15. GTPase activity; Diras1, Rab24, Gnb3, Gnai1. Microtubule binding; Map6d1, Mapt, Mapre1, Kif15. Microtubule; Tubb2a, Map6d1, Mapt, Mapre1, Kif15. Cell cortex region; Eno1, Gnai1. Heterotrimeric G-protein complex; Gnb3, Gnai1.

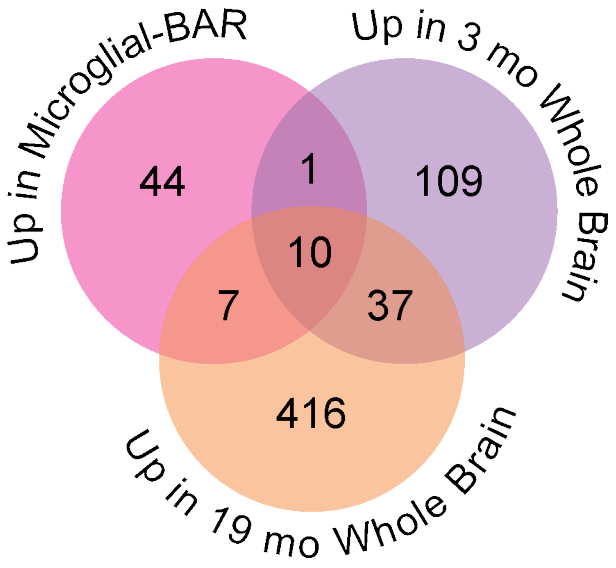

Supplemental Figure 5-2: 29% of microglia-BAR hits from *GRN*$^{-/-}$ brains overlap with existing literature.

62 increased proteins in *GRN*$^{-/-}$ microglia's vicinity were compared to whole brain proteomics from 3-month-old and 19-month-old *GRN*$^{-/-}$ mice from Huang et al, 2020.

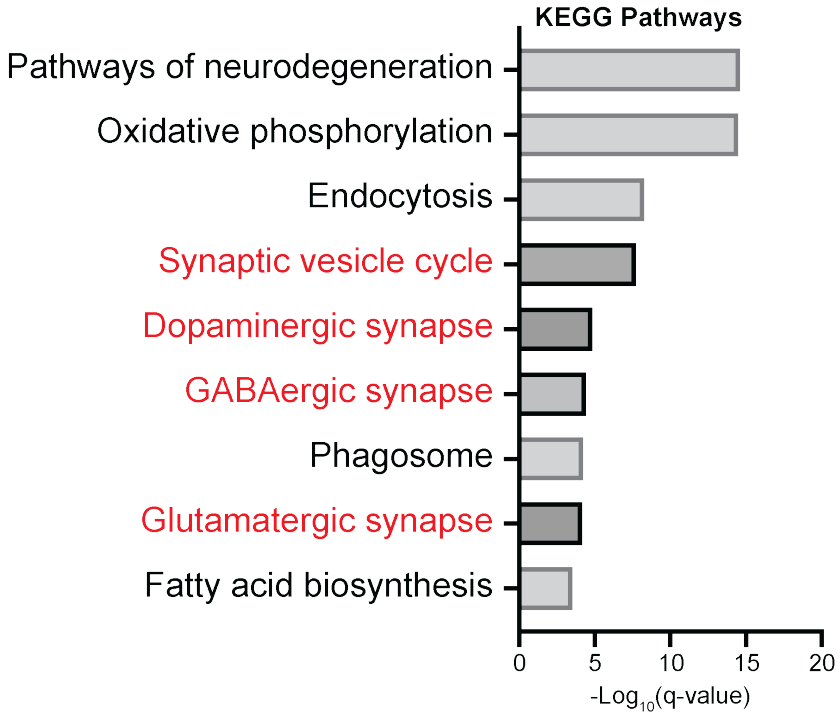

Supplemental Figure 6-1: KEGG Pathway Gene Ontology analysis showing synaptic terms in *APP*^{NLF} microglial-BAR compared to wildtype.

Analysis of 424 altered proteins in *APP*^{NLF} microglial-BAR shows KEGG pathways associated with synaptic vesicle (14 proteins), dopaminergic synapse (14 proteins), GABAergic synapse (11 proteins), and glutamatergic synapse (12 proteins).

Supplemental Tables

Supplemental Table 5-1: Known human lysosome, lysosomal membrane, and lysosomal lumen proteins from Uniprot.org.

Lysosome	Lysosomal lumen	Lysosomal membrane
Cln5	Gla	Prcp
Npc2	Asah1	Chmp1b
Fuca2	Ggh	Spg11
Man2b1	Plbd2	Rab21
Neu1	Sgsh	Hps1
Ctss	Idua	Rraga
Dpp7		Vps33b
Gm2a		Mfsd1
Snapin		Cpq
Tpp1		Glmp
Naaa		Pla2g15
Ctsl		Rbsn
Gusb		Acp3
Grn		Rab12
Lamp2		Rab39a
Ctsh		Tmem192
Glb1		Pip4p1

Supplemental Table 5-2: Increased Lyso- and Microglial-BAR proteins overlap with whole brain proteomics in *GRN*$^{-/-}$ brains.

Proteins with increased abundance in *GRN*$^{-/-}$ brains from Lyso-BAR and Microglial-BAR dataset compared to Huang and colleagues' whole brain proteomics dataset show microglial and lysosomal specific changes (Huang et al., 2020). Proteins highlighted in red are shared between all 4 datasets.

Lyso-BAR (20 mo)			Microglial-BAR (6 mo)		
19 mo and 3 mo	**19 mo**	**3 mo**	**19 mo and 3 mo**	**19 mo**	**3 mo**
C1qb	Wdr81	Tom1l2	**C1qb**	Arcn1	Vps26a
C1qa	Aspa	Ap3d1	**C1qa**	Lsp1	
Uap1l1	Vps35	Stard3nl	**Uap1l1**	Fxyd1	
Hexb	Gja1	Epdr1	**Hexb**	Tmem126a	
Tpp1	Rpn1		**Tpp1**	Itgb2	
Ctsd	Gfap		**Ctsd**	Cnn3	
Stx7	Prdx6		**Stx7**	Mtch2	
Psap	Eea1		**Psap**		
Ctsb	Lxn		**Ctsb**		
	Pkp4		Mif		

Supplemental Table 6-1: Proteins with altered abundances from *APP*^{NLF} brains compared to wildtype with their respective top KEGG pathways.

Of the 424 altered proteins in *APP*^{NLF}, 45 account for pathways of neurodegeneration, 25 account for oxidative phosphorylation, 25 account for endocytosis, and 14 for phagosome.

Pathways of Neurodegeneration		Oxidative Phosphorylation		Endocytosis		Phagosome	
Up	Down	Up	Down	Up	Down	Up	Down
Ndufs8	Uqcrc1	Ndufs8	Uqcrc1	Epn2	Dnm1	Tubb2a	Atp6v1a
Ndufs2	Ppid	Ndufs2	Atp6v1a	Sh3kbp1	Amph	Tubb6	Atp6v1c1
Htt	Stx1a	Ppa1	Sdhb	Grk2	Usp8	Rab5b	Stx12
Tubb2a	Camk2a	Ndufs6	Atp6v1c1	Vps37c	Cdc42	Rab5a	Atp6v1e1
Psma5	Sdhb	Atp6v1d	Uqcrc2	Rab5b	Agap1	Tubb4b	Sec22b
Tubb6	Ppp3ca	Atp6v1g1	Atp5pf	Rab8a	Kif5c	Atp6v1d	
Actr1b	Klc2	Ndufb8	Atp5f1e	Nedd4l	Iqsec1	Atp6v1g1	
Rab8a	Slc25a4	Ppa2	Ndufa12	Arpc4	Clta	Tubb3	
Ndufs6	Nefl	Atp6v0d1	Atp6v1e1	Arf6		Atp6v0d1	
Rab5a	Uqcrc2		Uqcrfs1	Rab5a			
Vdac3	Atp5pf		Ndufb3	Ap2s1			
Tubb4b	Rab1A		Ndufb10	Eps15			
Pik3r4	Nefm		Atp5pb	Hspa2			
Ndufb8	Atp5f1e		Atp5f1d	Iqsec2			
Vdac1	Ndufa12		Cox6c	Ehd4			
Tubb3	Atxn2l		Uqcrb	Vta1			
Gria1	Kif5c			Hspa1a			
	Uqcrfs1						
	Ndufb3						
	Nefh						
	Eif2s1						
	Sod1						
	Ndufb10						
	Atp5pb						
	Atp5f1d						
	Cox6c						
	App						
	Uqcrb						

Supplemental Table 6-2: Proteins with altered abundances from *APP*^{NLF} brains compared to wildtype with their respective synaptic KEGG pathways.

Of the 424 altered proteins in *APP*^{NLF}, 14 account for synaptic vesicle, 14 account for dopaminergic synapse, 11 account for GABAergic synapse, and 12 account for glutamatergic synapse.

Synaptic Vesicle		Dopaminergic Synapse		GABAergic Synapse		Glutamatergic Synapse	
Up	Down	Up	Down	Up	Down	Up	Down
Syt1	Dnm1	Gnai1	Camk2a	Gnai1	Glul	Grk2	Ppp3ca
Ap2s1	Atp6v1a	Gnai2	Ppp2r1a	Gnai2	Gng2	Gnai1	Glul
Atp6v1d	Stx1a	Gria1	Ppp3ca	Plcl1	Slc6a11	Gnai2	Gng2
Atp6v1g1	Rims1		Maob		Gabra1	Gria1	Slc17a7
Atp6v0d1	Atp6v1c1		Gng2		Gng3		Gng3
	Atp6v1e1		Kif5c		Gng12		Gng12
	Slc17a7		Gng3		Gng7		Gng7
	Slc6a11		Gng12		Gng5		Gng5
	Clta		Gng7				
			Ppp2r2a				
			Gng5				

List of Publications

Saadia Hasan, Michael S. Fernandopulle, Stewart W. Humble, Ashley M. Frankenfield, Haorong Li, Ryan Prestil, Kory R. Johnson, Brent J. Ryan, Richard Wade-Martins, Michael E. Ward, Ling Hao. *Multi-modal Proteomic Characterization of Lysosomal Function and Proteostasis in Progranulin-Deficient Neurons.* bioRxiv 2023.02.24.529955; doi: https://doi.org/10.1101/2023.02.24.529955

Archana Yadav, Kaya J.E. Matson, Li Li, Isabelle Hua, Joana Petrescu, Kristy Kang, Mor R. Alkaslasi, Dylan I. Lee, **Saadia Hasan**, Ahmad Galuta, Annemarie Dedek, Sara Ameri, Jessica Parnell, Mohammad M. Alshardan, Feras Abbas Qumqumji, Saud M. Alhamad, Alick Pingbei Wang, Gaetan Poulen, Nicolas Lonjon, Florence Vachiery-Lahaye, Pallavi Gaur, Mike A. Nalls, Yue A. Qi, Michael E. Ward, Michael E. Hildebrand, Pierre-Francois Mery, Emmanuel Bourinet, Luc Bauchet, Eve C. Tsai, Hemali Phatnani, Claire E. Le Pichon, Vilas Menon, Ariel J. Levine. *A Cellular Taxonomy of the Adult Human Spinal Cord.* Neuron. 2023;111(3):328-344.

Ashley Frankenfield, Michael S. Fernandopulle, **Saadia Hasan**, Michael E. Ward, Ling Hao. *Development and Comparative Evaluation of Endolysosomal Proximity Labeling-based Proteomic Methods in Human iPSC-derived Neurons*. Anal. Chem. 2020, 92, 23, 15437–15444.

bioRxiv preprint doi: https://doi.org/10.1101/2023.02.24.529955; this version posted February 24, 2023. The copyright holder for this preprint (which was not certified by peer review) is the author/funder, who has granted bioRxiv a license to display the preprint in perpetuity. It is made available under aCC-BY-ND 4.0 International license.

Multi-modal Proteomic Characterization of Lysosomal Function and Proteostasis in Progranulin-Deficient Neurons

Saadia Hasan[1,2,3#], Michael S. Fernandopulle[1,4,5#], Stewart W. Humble[1,6#], Ashley M. Frankenfield[7], Haorong Li[7], Ryan Prestil[4], Kory R. Johnson[1], Brent J. Ryan[6], Richard Wade-Martins[6], Michael E. Ward[1,*], Ling Hao[7,*]

[1]National Institute of Neurological Disorders and Stroke (NINDS), National Institutes of Health (NIH), Bethesda, MD, USA.

[2]UK Dementia Research Institute, Department of Neurodegenerative Disease, Institute of Neurology, University College London, London, UK.

[3]MD-PhD program, Augusta University/University of Georgia Medical Partnership, Athens, GA, USA.

[4]Cambridge Institute for Medical Research, University of Cambridge, Cambridge, UK.

[5]Medical Scientist Training Program, Feinberg School of Medicine, Northwestern University, Chicago, IL, USA.

[6]Oxford Parkinson's Disease Centre, Kavli Institute for Nanoscience Discovery, Department of Physiology, Anatomy and Genetics, Dorothy Crowfoot Hodgkin Building, University of Oxford, South Parks Road, Oxford, OX1 3QU UK.

[7]Department of Chemistry, George Washington University, Washington, DC, USA.

[#]Contributed equally to this paper

*Co-corresponding authors:

Michael E. Ward

Investigator, NIH/NINDS

wardme@nih.gov

Ling Hao

Assistant Professor, George Washington University

linghao@gwu.edu

bioRxiv preprint doi: https://doi.org/10.1101/2023.02.24.529955; this version posted February 24, 2023. The copyright holder for this preprint (which was not certified by peer review) is the author/funder, who has granted bioRxiv a license to display the preprint in perpetuity. It is made available under aCC-BY-ND 4.0 International license.

Abstract

Progranulin (PGRN) is a lysosomal protein implicated in various neurodegenerative diseases. Over 70 mutations discovered in the *GRN* gene all result in reduced expression of PGRN protein. However, the detailed molecular function of PGRN within lysosomes and the impact of PGRN deficiency on lysosomal biology remain unclear. Here we leveraged multifaceted proteomic techniques to comprehensively characterize how PGRN deficiency changes the molecular and functional landscape of neuronal lysosomes. Using lysosome proximity labeling and immuno-purification of intact lysosomes, we characterized lysosome compositions and interactomes in both human induced pluripotent stem cell (iPSC)-derived glutamatergic neurons (i^3Neurons) and mouse brains. Using dynamic stable isotope labeling by amino acids in cell culture (dSILAC) proteomics, we measured global protein half-lives in i^3Neurons for the first time and characterized the impact of progranulin deficiency on neuronal proteostasis. Together, this study indicated that PGRN loss impairs the lysosome's degradative capacity with increased levels of v-ATPase subunits on the lysosome membrane, increased catabolic enzymes within the lysosome, elevated lysosomal pH, and pronounced alterations in neuron protein turnover. Collectively, these results suggested PGRN as a critical regulator of lysosomal pH and degradative capacity, which in turn influences global proteostasis in neurons. The multi-modal techniques developed here also provided useful data resources and tools to study the highly dynamic lysosome biology in neurons.

bioRxiv preprint doi: https://doi.org/10.1101/2023.02.24.529955; this version posted February 24, 2023. The copyright holder for this preprint (which was not certified by peer review) is the author/funder, who has granted bioRxiv a license to display the preprint in perpetuity. It is made available under aCC-BY-ND 4.0 International license.

Introduction

As the primary degradative organelle of the cell, the lysosome orchestrates proteostasis via the autophagy-lysosome pathway and degrades macromolecules such as proteins, lipids, carbohydrates, and RNA[1–3]. Neurons are particularly sensitive to lysosomal perturbations, as evidenced by numerous neurodegeneration-related mutations in genes that regulate lysosomal biology[4–6]. In particular, pathogenic mutations in genes that encode lysosomal or lysosome-associated proteins (e.g., *GRN, LRRK2, GBA, TMEM106B, C9orf72*) are major causes of inherited neurodegenerative diseases[5–7]. Genetic mutations associated with defective lysosomal enzymes lead to the accumulation of degradative substrates within the lysosomal lumen, consistent with chronic lysosomal dysfunction[8]. However, the molecular mechanisms by which many of these mutated genes cause lysosomal dysfunction and disease remain unclear.

Mutations in the *GRN* gene cause inherited frontotemporal dementia (FTD) and have also been linked to other neurodegenerative diseases, including neuronal ceroid lipofuscinosis (NCL), Alzheimer's disease (AD) and Parkinson's disease (PD)[9–12]. Over 70 pathogenic mutations in the *GRN* gene have been discovered, and all of these mutations result in reduced expression of progranulin (PGRN) protein[13–15]. Progranulin is trafficked to the lysosome and cleaved by cathepsins into smaller intra-lysosomal proteins called granulins[16]. Functionally, progranulin loss leads to a host of lysosome-related phenotypes, including defective autophagy and autophagosome-lysosome fusion[17,18]. Recently, lysosomal lipid dysregulation was found to be a major element of *GRN*-related disease pathogenesis[19,20]. However, the molecular cascade by which loss of intra-lysosomal progranulin impacts lysosomal biology and eventually leads to FTD remains elusive.

bioRxiv preprint doi: https://doi.org/10.1101/2023.02.24.529955; this version posted February 24, 2023. The copyright holder for this preprint (which was not certified by peer review) is the author/funder, who has granted bioRxiv a license to display the preprint in perpetuity. It is made available under aCC-BY-ND 4.0 International license.

Capturing the dynamic lysosomal activities in highly polarized neurons is a challenging task, particularly in a high-throughput fashion. Our human induced pluripotent stem cells (iPSCs)-derived glutamatergic neuron (i^{3}Neuron[21–23]) platform provides pure and scalable human neurons and can be genetically edited to create *GRN* null neurons as a neuronal model to study progranulin deficiency. Recent advances in capturing organelle dynamics have provided useful tools, such as proximity labeling in living cells via engineered ascorbate peroxidase (APEX[24]) or biotin ligases[25], immunopurification of intact organelles[26], and biotinylation by antibody recognition (BAR[27]) in primary tissues, though mostly in non-neuronal contexts. Other proteomics-based studies in progranulin mouse models mostly captured global changes regardless of cell type or organelle[28–30]. Developing proteomic techniques to probe lysosomes in neurons can provide valuable insights in the converging pathway of lysosomal dysfunctions in neurodegenerative diseases. We recently developed a lysosome proximity labeling method (Lyso-APEX) to characterize the dynamic lysosome interactome in wild-type (WT) i^{3}Neurons[31–33]. In this study, we further expanded the lysosome toolbox by implementing the immunopurification of intact lysosomes (Lyso-IP) technique in our i^{3}Neuron platform and Lyso-BAR technique in mouse brains. We comprehensively characterized lysosomal content and interactions using Lyso-APEX and Lyso-IP in i^{3}Neurons and Lyso-BAR in fixed mouse brain tissues. To characterize global proteostasis in human neurons, we also designed a dynamic stable isotope labeling by amino acids in cell culture (dSILAC[34]) proteomic method that was suitable for iPSC-derived neuron cell type to measure global protein half-lives in i^{3}Neurons for the first time.

Leveraging these multifaceted proteomic techniques, we systematically characterized the impact of progranulin loss using multi-modal readouts of lysosomal biology in i^{3}Neurons and mouse brain. We found that loss of PGRN in human neurons presented increased levels of v-

bioRxiv preprint doi: https://doi.org/10.1101/2023.02.24.529955; this version posted February 24, 2023. The copyright holder for this preprint (which was not certified by peer review) is the author/funder, who has granted bioRxiv a license to display the preprint in perpetuity. It is made available under aCC-BY-ND 4.0 International license.

ATPase subunits on the lysosome membrane, increased catabolic enzymes within the lysosome, and elevated lysosomal pH. Mouse brains lacking PGRN also present elevated levels of lysosomal catabolic enzymes and bi-directional protein changes related to lysosomal transport. Using fluorescence microscopy, we confirmed that PGRN-deficient lysosomes are less acidic and have decreased cathepsin B activity compared to WT lysosomes. Consistent with impairments in protein homeostasis, *GRN* deficient i^{3}Neurons have pronounced alterations in protein turnover, which was validated by FTD patient-derived i^{3}Neurons carrying *GRN* mutation. Collectively, these results show that progranulin loss leads to a downstream molecular cascade involving lysosomal alkalinization and decreased degradative capacity, thereby impacting neuronal proteostasis. Multiple downstream proteins affected by these changes are involved in neurodegenerative pathways, suggesting molecular convergence of multiple neurodegeneration-related genes at the lysosome.

Results

Multi-modal proteomics captures holistic lysosomal biology

Lysosomes play critical roles in neurons such as degradation, endocytosis, signal transduction, nutrient sensing, and long-distance trafficking through axons[35–37]. Different methods of characterizing lysosomal composition and interactions now exist, each with its own strengths[33,38,39]. However, a comprehensive characterization of lysosomal biology in neurons with these modern tools has not been performed. We optimized and implemented three complementary proteomic strategies to characterize dynamic lysosomal interactions and lysosomal contents in both human neurons and mouse brain (**Figure 1A**). Lysosome proximity labeling using ascorbate peroxidase (Lyso-APEX) captured neuronal lysosome interactions with other cellular components

bioRxiv preprint doi: https://doi.org/10.1101/2023.02.24.529955; this version posted February 24, 2023. The copyright holder for this preprint (which was not certified by peer review) is the author/funder, who has granted bioRxiv a license to display the preprint in perpetuity. It is made available under aCC-BY-ND 4.0 International license.

as well as lysosome membrane proteins in living human neurons. Rapid lysosomal immunopurification (Lyso-IP) provided both lysosome lumen and membrane proteins in human neurons. Lysosomal biotinylation by antibody recognition (Lyso-BAR) revealed lysosome interactions *in situ* from fixed mouse brains. Proper location of these probes was validated by immunofluorescence and western blotting (**Figure 1B and Supplemental Figure S1**). Control groups were carefully selected for each probe to reduce nonspecific labeling and ensure intracellular spatial specificity (**Figure 1C**).

Lyso-APEX, Lyso-IP, and Lyso-BAR proteomics provided complementary coverage of the lysosomal microenvironment in human neurons and mouse brain tissues (**Figure 1D, Supplemental Figure S1**). Lysosomal membrane proteins such as v-ATPase subunits, LAMP proteins, and Ragulator subunits are identified and enriched by all three probes compared to corresponding controls. Lysosomal lumen proteins, especially hydrolases, are highly enriched in Lyso-IP proteomics, consistent with the degradative nature of the isolated organelles. Besides lysosome-resident proteins, both Lyso-APEX and Lyso-BAR proteomics captured dynamic lysosomal interaction partners related to organelle trafficking and axon transport (*e.g.*, Kinesins, MAPs). Lyso-APEX favored surface-bound and surface-interacting proteins over luminal proteins due to the limited membrane permeability of reactive phenol-biotin generated on the cytosolic face of lysosomes during APEX-mediated labeling (**Figure 1C**). By contrast, Lyso-BAR revealed more intraluminal lysosomal proteins since BAR activation in fixed brain tissues requires membrane permeabilization. Lyso-BAR proteomics in mouse brain also captured numerous synaptic proteins, likely due to enhanced synaptic maturation *in vivo* compared to cultured iPSC-derived i^3Neurons (**Figure 1D, Supplemental Figure S1**). Collectively, combining Lyso-APEX, Lyso-IP, and Lyso-BAR proteomic strategies allows us to obtain comprehensive lysosomal lumen and membrane

bioRxiv preprint doi: https://doi.org/10.1101/2023.02.24.529955; this version posted February 24, 2023. The copyright holder for this preprint (which was not certified by peer review) is the author/funder, who has granted bioRxiv a license to display the preprint in perpetuity. It is made available under aCC-BY-ND 4.0 International license.

proteomes as well as lysosomal interactomes in both cultured human i^{3}Neurons and fixed mouse brains.

Neuronal progranulin loss results in upregulation of vacuolar ATPases and alkalinization of lysosomal pH

Equipped with these new tools, we characterized how progranulin loss altered lysosomal biology. Using CRISPR-Cas9, we knocked out the *GRN* gene in wild type (WT) iPSCs harboring the Lyso-APEX probe and differentiated them into cortical neurons (**Figure 2A**). Immunofluorescence microscopy showed that progranulin protein colocalizes with lysosomes in WT i^{3}Neurons as expected, and that no progranulin signal was observed in *GRN* KO i^{3}Neurons (**Figure 2B**). Using Lyso-APEX proteomics, we found that PGRN depletion altered the abundance of many lysosome membrane proteins and lysosome interaction partners in human neurons (**Figure 2C**). Gene Ontology (GO) enrichment analysis revealed upregulation of proteins related to lysosomal acidification and autophagy (**Figure 2D**). Numerous vacuolar ATPase (v-ATPase) and chloride channel proteins (CLCNs) were substantially up-regulated in *GRN* KO vs. WT i^{3}Neurons (**Figure 2E, Supplementary Figure S2A**). GO enrichment analysis of significantly down-regulated proteins indicated impairment of lysosomal transport and RNA processing (**Supplementary Figure S2B**). Given the centrality of v-ATPases in establishing the acidic lysosomal lumen pH and the strong upregulation of acidification-related proteins in PGRN deficiency, we hypothesized that lysosomal pH could be perturbed by the loss of PGRN inside the neuronal lysosome[40].

To measure neuronal lysosomal acidification, we used a ratiometric fluorescent dextran assay. We co-generated an *in-situ* calibration curve using buffers of known pH, allowing accurate calculations of absolute pH within the lysosome with both nonlinear and linear curve fitting models

bioRxiv preprint doi: https://doi.org/10.1101/2023.02.24.529955; this version posted February 24, 2023. The copyright holder for this preprint (which was not certified by peer review) is the author/funder, who has granted bioRxiv a license to display the preprint in perpetuity. It is made available under aCC-BY-ND 4.0 International license.

(**Figure 2F, Supplementary Figure S2E**). Lysosomal pH is significantly increased in *GRN* KO i^{3}Neurons (4.81 ± 0.24) compared to WT i^{3}Neurons (4.31 ± 0.16). While this difference in pH may seem like a subtle change, it equates to a nearly three-fold decrease in the concentration of protons in the lysosomal compartment of *GRN* KO i^{3}Neurons compared to WT counterparts due to the logarithmic nature of the pH scale ([H^+] in WT ≈ 52±19 μM, *GRN* KO ≈ 18±9 μM). These observations show that *GRN* KO i^{3}Neurons have alkalinized lysosomes, which could trigger the upregulation of acidification machinery to compensate for this effect.

Progranulin-null lysosomes contain increased abundance of catabolic enzymes but have decreased enzymatic activity

Lysosomes require acidic luminal pH to degrade proteins using hydrolases[41]. Since lysosomes from progranulin-null neurons are less acidic, we hypothesized that these lysosomes may have altered abundances or activity of pH-dependent proteases. Using Lyso-IP proteomics, we characterized lysosome composition in *GRN* KO vs. WT i^{3}Neurons (**Figure 3A**). PGRN protein was indeed enriched in WT Lyso-IP data and absent in *GRN* KO i^{3}Neurons (**Supplementary Figure S3A**). Proteins involved in catabolism and lysosomal acidification were significantly increased in PGRN-deficient lysosomes in human neurons (**Figure 3B, 3C, Supplementary Figure S3B**). To investigate the impact of progranulin deficiency on lysosomes in mouse brain, we conducted Lyso-BAR proteomics in *GRN*$^{-/-}$ vs. WT fixed mouse brains (**Figure 3D**). Similar protein catabolic processes were upregulated in *GRN*$^{-/-}$ mice as indicated in Lyso-IP proteomics, particularly lysosomal proteases such as cathepsins (**Figure 3E, 3F, Supplementary Figure S3C**).

Prior studies of *GRN*$^{-/-}$ mouse models have suggested that cathepsins may be less active in progranulin-null cells, despite increased abundance[30,42,43]. To directly evaluate the impact of

bioRxiv preprint doi: https://doi.org/10.1101/2023.02.24.529955; this version posted February 24, 2023. The copyright holder for this preprint (which was not certified by peer review) is the author/funder, who has granted bioRxiv a license to display the preprint in perpetuity. It is made available under aCC-BY-ND 4.0 International license.

progranulin depletion on lysosomal activity in human neurons, we quantified cathepsin B activity using a Magic Red assay in living WT and *GRN* KO i^{3}Neurons. We observed a significant decrease in cathepsin B activity in PGRN-null i^{3}Neurons compared to WT, indicating impaired proteolytic function (**Figure 3G, 3H**, **Supplementary Figure S3D**). To mimic alkalinization-related phenotypes observed in *GRN* KO i^{3}Neurons, we treated neurons with chloroquine, an agent that neutralizes lysosomal pH. As predicted, direct alkalinization of lysosomes with chloroquine treatment reduced Magic Red fluorescence (**Figure 3G**). These findings confirm that although lysosomal hydrolases were upregulated in the absence of progranulin, their activity was decreased, likely due to alkalinized lysosomal lumens.

Characterizing global protein turnover in human iPSC-derived neurons

Since lysosomes are major proteostatic organelles and their degradative function is impaired in progranulin-depleted neurons, we hypothesized that progranulin deficiency could influence global proteostasis. To measure the global protein turnover in neurons, we designed a dynamic SILAC proteomic method in cultured i^{3}Neurons to obtain protein half-lives with multiple-time-point and single-time-point approaches (**Figure 4A**). By modeling the peptide degradation curves in WT i^{3}Neurons, we found that most peptides' degradation curves follow first-order exponential decay (**Figure 4B, Supplementary Figure S4A**). Peptide level and protein level half-lives correlate well with each other, with a median half-life of 4 days (**Figure 4C, 4D and Supplementary Figure S4B, S4C)**. Therefore, peptide and protein half-lives can be obtained using a single-time-point at 4 days (96 hrs) after heavy medium switch (**Supplementary Figure S4D)**. As we examined the distribution of protein half-lives, we found that numerous histones, nucleoporin proteins (Nups), proteins inside lysosomes as autophagy machinery (WDR45, GAA), and inner mitochondrial

bioRxiv preprint doi: https://doi.org/10.1101/2023.02.24.529955; this version posted February 24, 2023. The copyright holder for this preprint (which was not certified by peer review) is the author/funder, who has granted bioRxiv a license to display the preprint in perpetuity. It is made available under aCC-BY-ND 4.0 International license.

membrane proteins have extremely long half-lives (> 20 days) in i^{3}Neurons, in agreement with recent studies in primary rodent neurons and brain tissues[44–46]. In contrast, proteins related to neurosecretion (GPM6B, VGF), axonal transport (kinesins), and ubiquitination (UBL4, USP11) have very short half-lives (0.3-2 days) (**Figure 4E, Supplemental Figure S4B**). Notably, one of the shortest half-life proteins in the entire neuronal proteome was STMN2, a microtubule-binding, golgi-localized protein implicated in ALS pathogenesis[47,48]. Lysosomal proteins have a median half-life of 3.6 days, slightly shorter than the median half-life of global neuronal proteins. Further investigation into the lysosomal compartment revealed a median half-life of 7.5 days for degradative enzymes, 3.5 days for V-ATPases, 6.2 days for lysosome-associated membrane glycoproteins (Lamps), 3.5 days for LAMTOR and HOPS complex subunits, and 3.1 days for BLOC1 complex subunits (**Figure 4F**). Together, this method enabled us to calculate global protein half-lives in live human i^{3}Neurons for the first time.

Progranulin deficiency alters neuronal protein turnover and decreases lysosomal degradative function

Using our dynamic SILAC proteomics approach, we evaluated protein turnover in WT vs. *GRN* KO i^{3}Neurons (**Figure 5A**). The median of protein half-lives remained unchanged, but a remarkable 25% of all measured proteins presented significantly altered half-lives in *GRN* KO vs. WT i^{3}Neurons (**Figure 5B and 5C**). Proteins related to polymerization and fiber organization showed significantly slower turnover, which may indicate a propensity for protein misfolding and aggregation in *GRN* KO neurons related to FTD pathogenesis (**Figure 5D**)[49]. Despite the significantly slower turnover of both cathepsin B and cathepsin D, proteins related to RNA catabolic processes showed faster turnover, which further implicates the disturbance of molecular

bioRxiv preprint doi: https://doi.org/10.1101/2023.02.24.529955; this version posted February 24, 2023. The copyright holder for this preprint (which was not certified by peer review) is the author/funder, who has granted bioRxiv a license to display the preprint in perpetuity. It is made available under aCC-BY-ND 4.0 International license.

degradation pathways (**Figure 5E**). Several proteins with altered half-lives (either faster or slower turnover) are involved in ALS/FTD and other neurodegenerative diseases, suggesting potential converging pathways among different neurodegenerative diseases and dysfunction of key regulators of proteostasis (**Figure 5F**).

Given our observations that lysosomes within *GRN* KO i^{3}Neurons are alkalinized, have reduced cathepsin activity, and exhibit major changes in global protein homeostasis, we predicted that *GRN* KO lysosomes would exhibit impaired lysosome-mediated protein degradation. We directly assayed lysosomal degradative capacity using a fluorescent DQ-BSA Red assay (**Figure 5G, 5H**)[50,51]. The DQ-BSA substrate is initially self-quenching due to the close spatial proximity of the fluorophores. Once cleaved in acidic lysosomes, the DQ-BSA substrate exhibit bright fluorescence signals. The mean DQ-BSA intensity in *GRN* KO i^{3}Neurons was significantly decreased compared to WT neurons (**Figure 5I**), similar to pharmacological inhibition of lysosomal degradation using chloroquine (**Supplemental Figure S5A**). The change in active proteolysis was independent of lysosomal biogenesis, as there was no change in the number of puncta per cell in *GRN* KO vs. WT (**Supplemental Figure S5B**). Taken together, these results show that *GRN* KO lysosomes have significantly hindered proteolytic capacity, consistent with our observations of pathological impairment in lysosomal acidification and impaired lysosomal hydrolase activity.

An isogenic series of *GRN* mutation patient-derived iPSC neurons exhibit altered protein homeostasis

To further explore the relationship between *GRN* insufficiency and protein homeostasis abnormalities, we created i^{3}Neurons from an FTD patient-derived iPSC line with a heterozygous

bioRxiv preprint doi: https://doi.org/10.1101/2023.02.24.529955; this version posted February 24, 2023. The copyright holder for this preprint (which was not certified by peer review) is the author/funder, who has granted bioRxiv a license to display the preprint in perpetuity. It is made available under aCC-BY-ND 4.0 International license.

GRN mutation[52] (c.26 C>A, p.A9D; referred subsequently as ptMut), as well as the isogenic iPSC control line with corrected *GRN* mutation (ptWT). We further knocked out *GRN* in this control line to create an additional isogenic *GRN* KO iPSC line (ptKO) (**Figure 6A**). After differentiating each of these lines to i^{3}Neurons, performing dSILAC, and measuring their protein half-lives, we found that over 25% of proteins showed significantly altered half-lives in ptKO compared to ptWT i^{3}Neurons (**Figure 6B**), consistent with *GRN*-KO vs. WT comparison in **Figure 5C**. About 15% of protein half-lives were significantly altered in ptMut compared to ptWT group (**Figure 6B and 6C**). Principal component analysis and hierarchical clustering showed complete separations of both genetic background and *GRN* genotypes from five i^{3}Neurons lines (*GRN*-KO, WT, ptKO, ptMut, ptWT) based on protein half-lives (**Figure 6D, 6E**). The overall protein half-life changes also suggested a potential gene dosage effect, in which many proteins have greater fold changes in *GRN*-KO neurons compared to *GRN*-mutant neurons (**Figure 6F, Supplementary Figure S6A**). Half-life changes of key overlapping proteins in the three comparisons (*GRN*-KO vs. WT, ptKO vs. ptWT, ptMut vs. ptWT) are highlighted in **Figure 6G and Supplementary Figure S6B**.

The findings in patient-derived *GRN* mutant and KO neurons validate our observations of dysregulated protein homeostasis in settings of *GRN* depletion and insufficiency, including alterations in the half-lives of numerous neurodegeneration-associated proteins. Many lysosomal enzymes showed prolonged protein half-lives, such as cathepsins (CTSD, CTSB), which was especially notable given our direct measurements of increased cathepsin levels and reduced CTSB activity in *GRN* KO neurons. Our findings additionally show that substantial upregulation of numerous lysosomal-associated proteins and enzymes occurs in *GRN*-deficient neurons – many via prolongation in protein half-lives – but that these homeostatic changes are insufficient to normalize lysosomal degradative capacity. As summarized in **Figure 6H**, we propose that GRN

bioRxiv preprint doi: https://doi.org/10.1101/2023.02.24.529955; this version posted February 24, 2023. The copyright holder for this preprint (which was not certified by peer review) is the author/funder, who has granted bioRxiv a license to display the preprint in perpetuity. It is made available under aCC-BY-ND 4.0 International license.

mutations that cause PGRN deficiency inside neuronal lysosomes result in alkalinized lysosomal pH, decreased proteolytic activities, and impaired global protein homeostasis that eventually lead to frontotemporal dementia.

Discussion

Lysosomal dysfunction is a convergent pathological mechanism across multiple neurodegenerative diseases[5,6]. Progranulin, a glycoprotein linked to FTD, ALS, PD, and AD, is trafficked to, processed by, and resides within the lysosome[15]. Despite this knowledge, the primary molecular functions of progranulin and the impact of progranulin deficiency on lysosomal biology and protein homeostasis remain unclear. This is in part due to limited tools available for understanding the role of progranulin in the highly dynamic lysosomes in the brain. Here, we designed a combination of *in vitro* and *in situ* proximity labeling, lysosome immunopurification, and dynamic SILAC proteomic approaches to map the organellar and cellular architectures of neuronal progranulin deficiency.

For the first time, we implemented the antibody-guided biotinylation strategy to measure lysosomal composition in the brain and the lysosomal immunopurification method to characterize neuronal lysosomes. We additionally developed and optimized a neuron dynamic SILAC proteomic method to calculate protein half-lives in i^{3}Neurons for the first time. Despite the application of dynamic SILAC in various cell culture and mouse models, it remains challenging to measure protein turnover rates in non-dividing cells, particularly in human neurons[44,45,53]. Many neuronal proteins exhibit extremely long half-lives, particularly nuclear proteins due to a lack of cell division. For the first time, we measured the global protein turnover in i^{3}Neurons and found that the dynamics of most proteins can be modeled using first-order exponential decay. This

bioRxiv preprint doi: https://doi.org/10.1101/2023.02.24.529955; this version posted February 24, 2023. The copyright holder for this preprint (which was not certified by peer review) is the author/funder, who has granted bioRxiv a license to display the preprint in perpetuity. It is made available under aCC-BY-ND 4.0 International license.

enabled the measurement of global neuron protein half-lives using a 4-day single time point method, significantly reducing the starting materials and reagents compared to multiple-time-point method and allowing the streamlined comparison of multiple i^{3}Neuron lines with different genome backgrounds and *GRN* genotypes.

Using these new multi-modal proteomic strategies, we discovered that progranulin deficiency leads to increased expression of v-ATPases on the lysosomal membrane in i^{3}Neurons. Upon further investigation, we discovered that progranulin deficiency had a severe impact on the lysosomes' ability to properly acidify, which results in impaired hydrolytic activity despite an upregulation of acidification machinery. These results suggest that progranulin plays an important role in maintaining lysosomal pH, with v-ATPases either contributing to that effect or providing a compensatory response for that effect. Since alkalinized lysosomes cannot properly hydrolyze substrates, we next looked at how the contents of progranulin-null lysosomes were affected. We found that several lysosomal enzymes were upregulated both in the mouse and human dataset, notably cathepsins. We showed decreased cathepsin B activity in live neurons, a phenomenon only shown in *in vitro* assays before[52,54–56]. Similar perturbations of lysosomal acidification have been reported in non-neuron cells and other neurodegenerative diseases[57,58].

Mutations in the *GRN* gene cause progranulin deficiency inside the lysosome and have been shown to impair lysosomal function and the autophagy pathway[13,18]. However, whether progranulin deficiency alters protein turnover in human neurons has not been systematically investigated previously. We found that progranulin deficiency broadly influenced proteostasis, altering the half-lives of over 15% and 25% neuron proteins in *GRN* mutant and KO i^{3}Neurons, respectively. Lysosomes degradative capacity was compromised by PGRN deficiency, as evidenced in our DQ-BSA assay. Critically, the recapitulation of global proteostasis defects in

bioRxiv preprint doi: https://doi.org/10.1101/2023.02.24.529955; this version posted February 24, 2023. The copyright holder for this preprint (which was not certified by peer review) is the author/funder, who has granted bioRxiv a license to display the preprint in perpetuity. It is made available under aCC-BY-ND 4.0 International license.

FTD-patient-derived neurons suggests that altered protein turnover rates are relevant to disease pathophysiology.

Although we have established exciting new tools and characterized the neuronal lysosome quite extensively, there are several limitations in this study. Although LAMP1 is a classic lysosome marker, it is also expressed on late endosomes and other endocytic species[59]. Despite this limitation, our data is consistent with degradative lysosome proteomics, and we obtained new insights into neuronal lysosomes specifically. We also recognize that human iPSC-derived neurons are not fully mature and representative of late-stage disease, and therefore have supplemented i^{3}Neuron data with lysosomal proteomics in aged mice. As neuron is the major cell type of the brain, LysoBAR proteomics provide consistent and complementary lysosomal changes compared to cultured i^{3}Neuron. However, LysoBAR method is not cell-type specific and will also include lysosome profiles from other cell types such as microglia, which has higher expression level of progranulin compared to neurons[9,15]. It will be important to investigate whether aged human neurons exhibit different proteomic changes and if human microglial lysosomes behave differently compared to neurons in future studies. Furthermore, future research can focus on individual proteins with altered lysosomal enrichment and half-lives as novel handles for elucidating disease mechanisms, discovering disease biomarkers, and further assessing whether these neuronal proteostatic changes manifest in established mechanisms of neurodegenerative pathology, such as stress granule persistence, impaired macroautophagy, and failed fusion of lysosomes to autophagosomes.

Overall, this study developed and implemented a set of novel proteomics techniques to decipher neuronal lysosomal biology and proteostasis in the context of *GRN* insufficiency that causes frontotemporal dementia. We provided new insights of progranulin function in regulating

bioRxiv preprint doi: https://doi.org/10.1101/2023.02.24.529955; this version posted February 24, 2023. The copyright holder for this preprint (which was not certified by peer review) is the author/funder, who has granted bioRxiv a license to display the preprint in perpetuity. It is made available under aCC-BY-ND 4.0 International license.

lysosomal pH, lysosomal catabolic activity, and global proteostasis in neurons, opens numerous avenues for future follow-up studies to determine specific molecular mechanisms underpinning the protein changes discovered here. This work also illustrated a roadmap for how multi-modal proteomics can be used to illuminate lysosomal biology, providing useful data and technical resources that can be applied to characterize other organelle dynamics in neurons.

Methods

Human i^{3}Neuron Culture

Human iPSC-derived cortical neurons (i^{3}Neurons) were cultured based on our previously established protocol[23]. Briefly, human iPSCs were maintained on Matrigel (Corning Incorporated #354277) coated tissue culture dishes in Essential 8 medium (Gibco #A1517001). Several iPSC lines were used in this study as listed in **Table 1**. A doxycycline-inducible neurogenin2 (NGN2) cassette (Addgene #105840) was stably integrated into each iPSC line, enabling rapid differentiation to glutamatergic cortical neurons (i^{3}Neurons) in a week. Between day 0 and day 3, iPSCs were maintained in neuronal induction medium[23]. Day-3 neurons were replated on poly-L-ornithine coated plates in Brainphys neuron medium and maintained by half-medium change every two days until neuronal maturation in two weeks.

Table 1: List of human iPSC lines used in this study.

Cell line	Description	Source
WT	WTC 11 line, Healthy 30-year-old Japanese male donor	Coriell Institute #GM25256

bioRxiv preprint doi: https://doi.org/10.1101/2023.02.24.529955; this version posted February 24, 2023. The copyright holder for this preprint (which was not certified by peer review) is the author/funder, who has granted bioRxiv a license to display the preprint in perpetuity. It is made available under aCC-BY-ND 4.0 International license.

GRN KO	WTC11 line with a 7 base pair insertion in one GRN allele and 10 base pair deletion in the other *GRN* allele resulting in complete loss of function	Generated in house
ptMut	FTD patient cell line harboring a heterozygous *GRN* mutation (c.26 C > A, p.A9D)	Dr. Dimitri Krainc[52]
ptWT	Isogenic control line by correcting the *GRN* mutation in ptMut line.	Dr. Dimitri Krainc[52]
ptKO	Complete knock out of *GRN* in ptWT line using CRISPR-Cas9	Generated in house

Animals

All mice used in this study were obtained from the Jackson Laboratory and housed in the NIH animal facility that followed NINDS/NIDCD/NCCAM Animal Care and Use Committee (ACUC) Policy for animal husbandry and euthanasia. WT (C57BL/6J) and *GRN*$^{-/-}$ (B6.129S4(FVB)-Grntm1.1Far/Mmjax, MMRRC stock#036771-JAX) mice were used here[60]. Whole brains were dissected from 20-month-old male WT and *GRN*$^{-/-}$ mice after cardiac perfusion with 4% paraformaldehyde (PFA). Cortex was fixed in 4% PFA overnight, incubated in 30% sucrose for 24 hours, and snap frozen on dry ice. A microtome was used to generate 40 μm thick coronal slices that were stored in cryoprotectant at -30°C.

Lysosomal proximity labeling in i^{3}Neurons

Lysosomal proximity labeling was achieved by stable integration of ascorbate peroxidase (APEX2) enzyme onto the C terminus of LAMP1 protein in human iPSCs and differentiating

bioRxiv preprint doi: https://doi.org/10.1101/2023.02.24.529955; this version posted February 24, 2023. The copyright holder for this preprint (which was not certified by peer review) is the author/funder, who has granted bioRxiv a license to display the preprint in perpetuity. It is made available under aCC-BY-ND 4.0 International license.

iPSCs into i^{3}Neurons, as the previously established KuD-LAMP1-APEX (Lyso-APEX) line[32]. A cytosolic localized nuclear exporting signal (NES) APEX i^{3}Neuron line was used as the spatial control[31,32]. Prior to proximity labeling, i^{3}Neurons were incubated in 500 μM biotin-tyramide (Adipogen, #41994-02-9) for 30 min in a CO_2 incubator. Proximity labeling was induced by incubating the cells in 1 mM of hydrogen peroxide for exactly 1 min followed by rapid quenching using ice-cold quench buffer (10 mM sodium azide, 10 mM sodium ascorbate, 5 mM TROLOX in PBS). Neurons were lysed with cold lysis buffer (50 mM Tris-Cl pH 7.4, 500 mM NaCl, 0.2% SDS, 1 mM DTT, 10 mM sodium azide, 10 mM sodium ascorbate, 5 mM TROLOX, cOmplete mini protease inhibitor tablets). Detailed sample preparation procedures have been described previously[33]. Briefly, neuron lysates were sonicated with QSonica (Q800R) sonicator for 15 min at 2°C and clarified by centrifugation. Total protein concentrations were measured using a detergent-compatible (DC) Colorimetric Protein Assay (Bio-Rad #5000111). Biotinylated proteins were enriched with streptavidin (SA) magnetic beads (Cytiva, # 28-9857-99) for 18 h rotating at 4°C and washed extensively to reduce non-specific bindings. Biotinylated proteins were reduced, alkalized, and digested into peptides on the SA beads. The optimal SA beads-to-protein ratio and trypsin-to-SA beads ratio were previously determined[32]. After overnight digestion using Trypsin/Lys-C (Promega, #V5073), supernatant was collected from the magnetic beads, and the digestion reaction was quenched with 10% trifluoroacetic acid until pH < 3. Peptides were desalted with a Waters Oasis HLB 96-well extraction plate, dried under SpeedVac, and stored at -30 °C until LC-MS analysis.

Rapid Lysosome Immunopurification from i^{3}Neurons

bioRxiv preprint doi: https://doi.org/10.1101/2023.02.24.529955; this version posted February 24, 2023. The copyright holder for this preprint (which was not certified by peer review) is the author/funder, who has granted bioRxiv a license to display the preprint in perpetuity. It is made available under aCC-BY-ND 4.0 International license.

Lysosome Immunopurification (Lyso-IP) iPSC line was generated by the stable expression of LAMP1-3xHA in WT and *GRN* KO iPSC lines. i^{3}Neurons were differentiated as described above and maintained in 15cm dishes until day 14. A control i^{3}Neurons line without HA expression (mEmerald) was used to control nonspecific labeling background. Neurons were washed 2 times with PBS and dissociated from the plate using forceful pipetting of 10 ml of PBS. Next, neurons were resuspended in 1ml cold KPBS (136 mM KCl, 10 mM KH2PO4, pH 7.25 adjusted with KOH) and gently homogenized with 21 strokes through an isobiotec balch-style cell homogenizer with a 10µm ball bearing. Each neuron lysate sample was incubated with 150 µL of pre-washed anti-HA magnetic beads (Thermo #88836/88837) for 3 min on a rotator and gently washed three times with KPBS. Beads bound with intact lysosomes were resuspended in 100 µl of Lyso-IP lysis buffer (50 mM HEPES, 50 mM NaCl, 5 mM EDTA, 1% SDS, 1% TritonX, 1% NP-40, 1% Tween 20, 1% deoxycholate, 1% glycerol, 5 mM TCEP) and heated at 60 °C for 30 mins at 1000 g agitation. The supernatant was collected, and the beads were washed with an additional 50 µl of lysis buffer. Supernatant was combined into a new tube for routine bottom-up proteomics steps as described below.

Lysosomal proximity labeling in mouse brains

Mouse brain slices were picked evenly throughout the whole brain and washed with PBS three times. Endogenous peroxidase activity in brain slices was quenched with 0.3% H_2O_2 in PBS for 30 minutes. The slices were blocked using 3% donkey serum and 0.25% Triton X in PBS followed by primary antibodies in blocking buffer at 4°C on a rocker overnight. After the slices were washed thoroughly with PBST, they were incubated with secondary antibody conjugated to HRP in blocking buffer for 1 hour at room temperature and extensively washed in PBST. The slices were

bioRxiv preprint doi: https://doi.org/10.1101/2023.02.24.529955; this version posted February 24, 2023. The copyright holder for this preprint (which was not certified by peer review) is the author/funder, who has granted bioRxiv a license to display the preprint in perpetuity. It is made available under aCC-BY-ND 4.0 International license.

then incubated in biotin-tyramide with 1% fetal bovine serum (FBS) in PBS for 30 min, and then 0.003% H_2O_2 for 10 min, immediately followed by washing with quench buffer (10 mM sodium azide and 500 mM sodium ascorbate). Brain slices without primary antibody treatment were used as the negative control group to compare with Lyso-BAR. One slice from each group was further treated with appropriate Alexa Fluor for microscopy imaging. Twenty brain slices from each group were transferred to 100 μL of Lyso-BAR lysis buffer (3% SDS + 2% sodium deoxycholate in PBS), boiled at 99°C for 1 hour at 1200 g agitation, and sonicated with QSonica Sonicator for 15 min. The lysate was boiled again at 99°C for an additional 30 min until all tissues were homogenized and dissolved into solution. The lysate was diluted using PBS to reduce SDS concentration and clarified by centrifugation. Biotinylated proteins were enriched following the same steps described above for Lyso-APEX sample preparation with optimized SA beads-to-protein ratio and trypsin-to-beads ratio for Lyso-BAR samples.

Dynamic SILAC proteomics in i^{3}Neurons

Human i^{3}Neurons were maintained on PLO coated 12-well dishes in light amino acid-containing media (DMEM:F12 for SILAC medium (Athena Enzyme Systems #0423), N2 Supplement (Life Technologies Corporation #17502048), B27 Supplement (Life Technologies #NC1001496), NEAA (Life Technologies #11140050), GlutaMAX (Life Technologies #35050061), BDNF (PeproTech #450-02), NT-3 (PeproTech #AF-450-03-100ug), 0.3 mM of Arginine (Sigma #A4599), and 0.5 mM of Lysine (Sigma #L7039)). On day 10 of i^{3}Neuron culture, neurons were gently washed with PBS twice and switched into media containing the same components except for replacing light lysine with heavy stable isotope labeled ($^{13}C_6{}^{15}N_2$) lysine (Cambridge Isotope Laboratories #CNLM-291-H-PK). For multiple time point experiments, neurons were harvested

bioRxiv preprint doi: https://doi.org/10.1101/2023.02.24.529955; this version posted February 24, 2023. The copyright holder for this preprint (which was not certified by peer review) is the author/funder, who has granted bioRxiv a license to display the preprint in perpetuity. It is made available under aCC-BY-ND 4.0 International license.

418 at 1, 2, 4, and 6 days (accurate to within 10 min) after media switch. For single time point
419 experiments, neurons were harvested after 4 days (96 hours) of media switch. Neurons were gently
420 washed with PBS twice, lysed in 100 µL of ice-cold lysis buffer containing 0.1% Rapigest (Waters
421 #186008740), 150 mM NaCl, and 50 mM Tris-HCl, sonicated for 15 min, and clarified by
422 centrifugation. Total protein concentrations were determined by DC Protein assay (BioRad).
423 Protein disulfide bonds were reduced by 5 mM of Tris(2-carboxyethyl) phosphine (TCEP) for 30
424 min, followed by addition of 15 mM of iodoacetamide (IAA) for 30 min in a ThermoMixer shaking
425 at 800 g at 37°C. Proteins were digested with LysC (Promega #VA1170) at 1:30 (enzyme:protein)
426 ratio for 16 hours at 37°C and quenched with 10% trifluoroacetic acid (TFA) until pH<3. Peptides
427 were desalted using a Waters Oasis HLB 96-well extraction plate based on the manufacturer's
428 protocol. Peptide samples were dried under SpeedVac and stored at -80°C until LC-MS analysis.
429
430 **LC-MS/MS analysis**
431 LC-MS/MS analyses were conducted on a Dionex UltiMate3000 nanoLC system coupled with a
432 Thermo Scientific Q-Exactive HFX or a Fusion Lumos mass spectrometer. Before injection,
433 peptide samples were reconstituted in 2% acetonitrile (ACN), 0.1% formic acid (FA) in LC-MS
434 grade water and centrifuged to collect supernatant. Easy-spray PepMap C18 columns (2 µm, 100
435 Å, 75 µm ×75 cm) were used for peptide separation with a flow rate of 0.2 µL/min and column
436 temperature of 60°C. The mobile phase buffer A was 0.1% FA in water, and buffer B was 0.1%
437 FA in acetonitrile. A two-hour gradient was used for proximity labeling proteomics, and a three-
438 hour gradient was used for SILAC proteomics. LC-MS/MS analyses were conducted with a top
439 40 data dependent acquisition with MS range of m/z 400-1500, MS resolution of 120K, isolation
440 window of m/z 1.4, dynamic exclusion of 22.5 s, and collision energy of 30% for higher-energy

bioRxiv preprint doi: https://doi.org/10.1101/2023.02.24.529955; this version posted February 24, 2023. The copyright holder for this preprint (which was not certified by peer review) is the author/funder, who has granted bioRxiv a license to display the preprint in perpetuity. It is made available under aCC-BY-ND 4.0 International license.

collisional dissociation (HCD) fragmentation. Automatic gain control (AGC) targets were 1×10^6 for MS and 2×10^5 for MS/MS. Maximum injection times were 30 ms for MS and 35 ms for MS/MS.

Proteomics Data analysis

LC-MS/MS raw files from Lyso-APEX, Lyso-IP, and Lyso-BAR proteomic experiments were analyzed with Thermo Fisher Proteome Discoverer (2.4.1.15) software. For dynamic SILAC proteomic data, MaxQuant (1.6.17.0) software was used for data analysis. Swiss-Prot *Homo sapiens* database was used for i^{3}Neuron data and *Mus musculus* database was used for mouse data with 1% false discovery rate (FDR) for protein identification. Custom-made contaminant protein libraries (https://github.com/HaoGroup-ProtContLib) were included in the data analysis pipeline to identify and remove contaminant proteins[61]. Trypsin was selected as the enzyme with a maximum of two missed cleavages. Cysteine carbamidomethylation was included as fixed modification, and oxidation of methionine and acetylation of the protein N-terminus were selected as variable modifications.

Protein/peptide identification and peak intensities were output as excel files for further analysis using Python or R. Statistical analyses (t-test) and volcano plots for Lyso-APEX, Lyso-IP, and Lyso-BAR proteomics were conducted in Python. Lyso-APEX and Lyso-BAR data were normalized to the most abundant endogenously biotinylated protein (PCCA) before statistical analysis as described previously[32]. For dynamic SILAC data, Maxquant output files were further processed with R to calculate heavy/light peptide ratios and construct the degradation and synthesis curves as well as curve-fitting to the first-order kinetic in multiple time point experiment. For single time point experiments, peptide level Maxquant output files were processed with Python to calculate the peptide half-lives using the equation: $t_{1/2} = t_s \times [\ln 2 / \ln (1+\Psi)]$, where t_s represents

bioRxiv preprint doi: https://doi.org/10.1101/2023.02.24.529955; this version posted February 24, 2023. The copyright holder for this preprint (which was not certified by peer review) is the author/funder, who has granted bioRxiv a license to display the preprint in perpetuity. It is made available under aCC-BY-ND 4.0 International license.

464 the sampling time after media switch, and Ψ represents the heavy-to-light abundance ratio of the
465 peptide. Protein level half-lives were calculated by averaging the half-lives of unique peptides
466 belonging to the specific protein. Statistical analysis was conducted with t-test, and multiple half-
467 life datasets were merged by uniprot protein accession in Python. Protein GO enrichment analysis
468 was conducted using ShinyGO[62]. Protein network analysis was conducted with STRING[63].
469
470 **Live Cell Ratiometric pH Assay**
471 Live cell ratiometric lysosomal pH measurements were conducted using a modified method from
472 Saric et al[64], further optimized for high content imaging and analysis. WT and *GRN*-KO i^{3}Neurons
473 were maintained on 96-well dishes. On day 10, neurons were loaded with 50 μg/mL pH-sensitive
474 Oregon Green-488 dextran (Invitrogen, #D7171), and 50 μg/mL pH-insensitive/loading control
475 Alexa Fluor-555 red dextran (Invitrogen, #D34679) for 4 hours, before washing three times with
476 PBS then chased overnight with neuronal media after PBS washes the day before imaging. These
477 dextrans accumulate in lysosomes, and high-content microscopy quantification of their
478 fluorescence enables ratiometric calculations of pH within individual lysosomes. Physiological
479 buffers of known pH (4-8) containing 10 μg/mL nigericin were placed on WT neurons to generate
480 a calibration curve. Live cell spinning disk confocal microscopy was performed using a Opera
481 Phenix HCS System (PerkinElmer); calibration and sample wells were imaged at 63×;
482 counterstaining was done with NucBlue Live ReadyProbes Reagent (Invitrogen, #R37605) to
483 count and segment nuclei. Lysosome pH was calculated as ratiometric measurement of lysosomes
484 (488/555nm), with subsequent calculation of the pH of those compartments based on the
485 corresponding calibration curve. All analysis was performed using PerkinElmer's Harmony HCA

bioRxiv preprint doi: https://doi.org/10.1101/2023.02.24.529955; this version posted February 24, 2023. The copyright holder for this preprint (which was not certified by peer review) is the author/funder, who has granted bioRxiv a license to display the preprint in perpetuity. It is made available under aCC-BY-ND 4.0 International license.

Software (PerkinElmer). Statistical analyses for all imaging data were conducted using independent student's t-test.

Magic Red cathepsin B activity assay

Human i^{3}Neurons were plated at a density of 50,000 cells on PLO-coated ibidi slides (Ibidi # 80827) and maintained to day 10. Magic Red (Abcam #AB270772-25TEST) was added to the cells at 1:25 final dilution and incubated in the dark for 30 mins at 37°C. Cells were washed twice with PBS and incubated with Hoechst 33342 (Thermo Scientific #62249) at 1:10,000 for 5-10 mins and then washed with PBS. Neurons were imaged using Nikon spinning disk confocal at 60× oil objective. Images were edited and analyzed using ImageJ software[65]. Statistical analysis was conducted using independent student's t-test.

Live cell DQ-BSA Assay in i^{3}Neurons

WT and *GRN*-KO i^{3}Neurons were plated on 384-well dishes. On day 10, neurons were incubated with 45 μg/mL DQ-BSA Red (Invitrogen, #D12051) for 5 hours to allow for substrate endocytosis. Live-cell spinning disk confocal microscopy was performed via Opera Phenix HCS System (PerkinElmer); control and sample wells were imaged at 40× and counterstaining was done with NucBlue Live ReadyProbes Reagent (Invitrogen, #R37605) to count and segment nuclei. All analysis was performed via PerkinElmer's Harmony HCA Software (PerkinElmer).

Western blotting

Intact lysosomes were isolated via immunopurification as described above. The intact lysosomes on beads were boiled with sample buffer at 95°C for 5 mins. The beads were magnetized, and the

bioRxiv preprint doi: https://doi.org/10.1101/2023.02.24.529955; this version posted February 24, 2023. The copyright holder for this preprint (which was not certified by peer review) is the author/funder, who has granted bioRxiv a license to display the preprint in perpetuity. It is made available under aCC-BY-ND 4.0 International license.

supernatant was used for immunoblotting. Lysates were separated using 4-15% precast polyacrylamide gels (Bio-Rad, # 4561083) at **100 V** and then transferred using the Trans-Blot Turbo transfer kit onto nitrocellulose membranes (Bio-Rad, #1704270). Membranes were blocked with 5% nonfat dry milk prepared in TBST (Tris-buffered saline with Tween 20) for 1 hour at room temperature and probed with primary antibodies in 5% bovine serum albumin (BSA) in TBST at 4°C overnight (See **Table 2** for antibodies and dilutions). Following incubation, membranes were washed 3× with TBST and incubated in secondary antibodies diluted 1:5000 in 5% BSA for 1 hour at room temperature. Membranes were then washed 3× with TBST and visualized using ECL western blotting substrate.

Fluorescence imaging

i^{3}Neurons were cultured on PLO-coated ibidi slides (Ibidi #81506) for fluorescence imaging. Neurons were fixed in 4% PFA for 10 mins, washed very gently with PBS, and incubated in blocking buffer (1% bovine serum albumin + 0.1% TritonX) for 1 hour at room temperature (RT). Next, neurons were incubated with primary antibody in blocking buffer overnight at 4°C, gently washed with PBS, and incubated in secondary antibody for 1 hour at RT. Following thorough washes, neurons were ready to be imaged. Mouse brain slices were prepared in the same steps as neuron culture for fluorescence imaging. All antibodies and their respective applications and dilutions are listed in **Table 2**. Confocal images were obtained using a Nikon Eclipse Ti spinning disk confocal microscope at 60× using an oil immersion objective with constant setting between experimental groups. Data analysis was conducted in ImageJ.

bioRxiv preprint doi: https://doi.org/10.1101/2023.02.24.529955; this version posted February 24, 2023. The copyright holder for this preprint (which was not certified by peer review) is the author/funder, who has granted bioRxiv a license to display the preprint in perpetuity. It is made available under aCC-BY-ND 4.0 International license.

532 **Table 2**. Antibodies used for immunostaining.

Antibody	Company	Catalog	Application	Dilution
LAMP1	Developmental Studies Hybridoma Bank	#H4A3	Immunofluorescence	1:3000
LAMTOR4	Cell Signaling Technology	#13140S	Immunofluorescence	1:500
HA	Millipore Sigma	# 11867423001	Immunofluorescence	1:500
HOECHST	Millipore Sigma	#63493	Immunofluorescence	1:10000
Streptavidin-680	Jackson ImmunoResearch	#016-620-084	Immunofluorescence	1:1000
Streptavidin-488	Jackson ImmunoResearch	#016-540-084	Immunofluorescence	1:1000
PGRN	R&D systems	#AF2420	Immunofluorescence	1:1000
Rhodamine Red Donkey anti-Mouse IgG (H+L)	Jackson ImmunoResearch	#715-295-151	Immunofluorescence	1:1000
Rhodamine Red Donkey anti-Rabbit IgG (H+L)	Jackson ImmunoResearch	(#711-295-152	Immunofluorescence	1:1000
Rhodamine Red Donkey anti-Rat IgG (H+L)	Jackson ImmunoResearch	#711-295-153	Immunofluorescence	1:1000
Alexa Fluor 488 Donkey anti-Mouse IgG	Jackson ImmunoResearch	#715-545-151	Immunofluorescence	1:1000
Rodamine Red Donkey anti-Goat IgG	Jackson ImmunoResearch	#705-295-147	Immunofluorescence	1:1000
LAMP2	Cell Signaling Technology	#D5C2P	Western blot	1:5000
Calreticulin	Cell Signaling Technology	#D3E6	Western blot	1:5000
CTSD	Proteintech	#21327-I-AP	Western blot	1:5000
Catalase	Proteintech	#2126-1-AP	Western blot	1:5000
P70 S6 Kinase	Cell Signaling Technology	#49D7	Western blot	1:5000
PGRN	R&D systems	#AF2420		

533

bioRxiv preprint doi: https://doi.org/10.1101/2023.02.24.529955; this version posted February 24, 2023. The copyright holder for this preprint (which was not certified by peer review) is the author/funder, who has granted bioRxiv a license to display the preprint in perpetuity. It is made available under aCC-BY-ND 4.0 International license.

Author Contributions

Author contributions: L.H. and M.E.W. initiated the project with help from S.H. and M.S.F. to design the experimental plan. S.H., M.S.F., S.W.H., R.P., and L.H. conducted iPSC-neuron culture and sample preparation. S.H. conducted mouse brain sample preparation. S.H., M.S.F., A.M.F., H.L., and L.H. conducted proteomics experiments. A.M.F., K.J., and L.H. performed proteomics data analysis. S.H. and M.S.F. performed western blotting and microscopy experiments. S.W.H., S.H., and B.J.R. conducted live cell assays. S.H. and L.H. wrote the manuscript with input from M.S.F. and M.E.W. and edits from all coauthors.

The authors declare no competing financial interests.

Acknowledgements

This study is supported by the NIH grant (R01NS121608, Hao), GW intramural grant (UFF, Hao), the Intramural Research Program at NIH/NINDS (Ward), and MRC Dementias Platform UK Stem Cell Network Capital Equipment Awards MR/M024962/1 (Wade-Martins). We would like to thank Maia Parsadanian for her assistance with mouse brain immunostaining and cell culture, Dr. Dimitri Krainc for providing the FTD patient iPSC lines, and Dr. Lingnan Lin for his help in Python data analysis.

Data Availability

All proteomics RAW files have been deposited in the PRIDE database (ProteomeXchange Consortium) with the data identifier PXD040251 and will be released upon publication. All other supporting data are available within the article and the supplementary files.

bioRxiv preprint doi: https://doi.org/10.1101/2023.02.24.529955; this version posted February 24, 2023. The copyright holder for this preprint (which was not certified by peer review) is the author/funder, who has granted bioRxiv a license to display the preprint in perpetuity. It is made available under aCC-BY-ND 4.0 International license.

References

1. De Duve, C. & Wattiaux, R. Functions of lysosomes. *Annual review of physiology* 28 (1), 435–492 (1966) doi:10.1146/annurev.ph.28.030166.002251.

2. Mizushima, N., Levine, B., Cuervo, A. M. & Klionsky, D. J. Autophagy fights disease through cellular self-digestion. *Nature* (2008) doi:10.1038/nature06639.

3. Lawrence, R. E. & Zoncu, R. The lysosome as a cellular centre for signalling, metabolism and quality control. *Nat. Cell Biol.* **21**, 133–142 (2019).

4. Ferguson, S. M. Neuronal lysosomes. *Neurosci. Lett.* **697**, 1–9 (2019).

5. Wang, C., Telpoukhovskaia, M. A., Bahr, B. A., Chen, X. & Gan, L. Endo-lysosomal dysfunction: a converging mechanism in neurodegenerative diseases. *Current Opinion in Neurobiology* (2018) doi:10.1016/j.conb.2017.09.005.

6. Wallings, R. L., Humble, S. W., Ward, M. E. & Wade-Martins, R. Lysosomal Dysfunction at the Centre of Parkinson's Disease and Frontotemporal Dementia/Amyotrophic Lateral Sclerosis. *Trends Neurosci.* **42**, 899–912 (2019).

7. Root, J., Merino, P., Nuckols, A., Johnson, M. & Kukar, T. Lysosome dysfunction as a cause of neurodegenerative diseases: Lessons from frontotemporal dementia and amyotrophic lateral sclerosis. *Neurobiology of Disease* vol. 154 (2021).

8. Platt, F. M., Boland, B. & van der Spoel, A. C. Lysosomal storage disorders: The cellular impact of lysosomal dysfunction. *J. Cell Biol.* **199**, 723–734 (2012).

9. Paushter, D. H., Du, H., Feng, T. & Hu, F. The lysosomal function of progranulin, a guardian against neurodegeneration. *Acta Neuropathol.* **136**, 1–17 (2018).

10. Nalls, M. A. *et al.* Evidence for GRN connecting multiple neurodegenerative diseases. *Brain Commun.* **3**, (2021).

bioRxiv preprint doi: https://doi.org/10.1101/2023.02.24.529955; this version posted February 24, 2023. The copyright holder for this preprint (which was not certified by peer review) is the author/funder, who has granted bioRxiv a license to display the preprint in perpetuity. It is made available under aCC-BY-ND 4.0 International license.

579 11. Ward, M. E. *et al.* Early retinal neurodegeneration and impaired Ran-mediated nuclear
580 import of TDP-43 in progranulin-deficient FTLD. *J. Exp. Med.* **211**, 1937–1945 (2014).
581 12. Brouwers, N. *et al.* Genetic variability in progranulin contributes to risk for clinically
582 diagnosed Alzheimer disease. *Neurology* **71**, 656–64 (2008).
583 13. Baker, M. *et al.* Mutations in progranulin cause tau-negative frontotemporal dementia
584 linked to chromosome 17. *Nature* (2006) doi:10.1038/nature05016.
585 14. Cruts, M. *et al.* Null mutations in progranulin cause ubiquitin-positive frontotemporal
586 dementia linked to chromosome 17q21. *Nature* (2006) doi:10.1038/nature05017.
587 15. Kao, A. W., McKay, A., Singh, P. P., Brunet, A. & Huang, E. J. Progranulin, lysosomal
588 regulation and neurodegenerative disease. *Nature Reviews Neuroscience* (2017)
589 doi:10.1038/nrn.2017.36.
590 16. Zhou, X. *et al.* Lysosomal processing of progranulin. *Mol. Neurodegener.* **12**, (2017).
591 17. Zhao, X. *et al.* Progranulin associates with Rab2 and is involved in autophagosome-
592 lysosome fusion in Gaucher disease. *J. Mol. Med.* **99**, 1639–1654 (2021).
593 18. Chang, M. C. *et al.* Progranulin deficiency causes impairment of autophagy and TDP-43
594 accumulation. *J. Exp. Med.* **214**, 2611–2628 (2017).
595 19. Boland, S. *et al.* Deficiency of the frontotemporal dementia gene GRN results in
596 gangliosidosis. *Nat. Commun.* **13**, (2022).
597 20. Logan, T. *et al.* Rescue of a lysosomal storage disorder caused by Grn loss of function with
598 a brain penetrant progranulin biologic. *Cell* **184**, 4651-4668.e25 (2021).
599 21. Wang, C. *et al.* Scalable Production of iPSC-Derived Human Neurons to Identify Tau-
600 Lowering Compounds by High-Content Screening. *Stem Cell Reports* **9**, 1221–1233 (2017).
601 22. Zhang, Y. *et al.* Rapid single-step induction of functional neurons from human pluripotent

bioRxiv preprint doi: https://doi.org/10.1101/2023.02.24.529955; this version posted February 24, 2023. The copyright holder for this preprint (which was not certified by peer review) is the author/funder, who has granted bioRxiv a license to display the preprint in perpetuity. It is made available under aCC-BY-ND 4.0 International license.

stem cells. *Neuron* **78**, 785–798 (2013).

23. Fernandopulle, M. S. *et al.* Transcription Factor–Mediated Differentiation of Human iPSCs into Neurons. *Curr. Protoc. Cell Biol.* **79**, 1–48 (2018).

24. Rhee, H. W. *et al.* Proteomic mapping of mitochondria in living cells via spatially restricted enzymatic tagging. *Science (80-.).* **339**, 1328–1331 (2013).

25. Go, C. D. *et al.* A proximity-dependent biotinylation map of a human cell. *Nature* **595**, 120–124 (2021).

26. Wolfson, R. L. *et al.* KICSTOR recruits GATOR1 to the lysosome and is necessary for nutrients to regulate mTORC1. *Nature* **543**, 438–442 (2017).

27. Bar, D. Z. *et al.* Biotinylation by antibody recognition - a method for proximity labeling. *Nat. Methods* **15**, 127–133 (2018).

28. Klein, Z. A. *et al.* Loss of TMEM106B Ameliorates Lysosomal and Frontotemporal Dementia-Related Phenotypes in Progranulin-Deficient Mice. *Neuron* **95**, 281-296.e6 (2017).

29. Miedema, S. S. M. *et al.* Distinct cell type-specific protein signatures in GRN and MAPT genetic subtypes of frontotemporal dementia. *Acta Neuropathol. Commun.* **10**, (2022).

30. Huang, M. *et al.* Network analysis of the progranulin-deficient mouse brain proteome reveals pathogenic mechanisms shared in human frontotemporal dementia caused by GRN mutations. *Acta Neuropathol. Commun.* **8**, 163 (2020).

31. Liao, Y. C. *et al.* RNA Granules Hitchhike on Lysosomes for Long-Distance Transport, Using Annexin A11 as a Molecular Tether. *Cell* **179**, 147-164.e20 (2019).

32. Frankenfield, A. M., Fernandopulle, M. S., Hasan, S., Ward, M. E. & Hao, L. Development and Comparative Evaluation of Endolysosomal Proximity Labeling-Based Proteomic

bioRxiv preprint doi: https://doi.org/10.1101/2023.02.24.529955; this version posted February 24, 2023. The copyright holder for this preprint (which was not certified by peer review) is the author/funder, who has granted bioRxiv a license to display the preprint in perpetuity. It is made available under aCC-BY-ND 4.0 International license.

Methods in Human iPSC-Derived Neurons. *Anal. Chem.* **92**, 15437–15444 (2020).

33. Frankenfield, A., Ni, J. & Hao, L. Characterization of Neuronal Lysosome Interactome with Proximity Labeling Proteomics. *J. Vis. Exp.* 1–19 (2022) doi:10.3791/64132.

34. Ross, A. B., Langer, J. D. & Jovanovic, M. Proteome turnover in the spotlight: Approaches, applications, and perspectives. *Mol. Cell. Proteomics* **20**, 100016 (2021).

35. De Pace, R. *et al.* Synaptic Vesicle Precursors and Lysosomes Are Transported by Different Mechanisms in the Axon of Mammalian Neurons. *Cell Rep.* **31**, (2020).

36. Ballabio, A. & Bonifacino, J. S. Lysosomes as dynamic regulators of cell and organismal homeostasis. *Nat. Rev. Mol. Cell Biol.* **21**, 101–118 (2020).

37. Fernandopulle, M. S., Lippincott-Schwartz, J. & Ward, M. E. RNA transport and local translation in neurodevelopmental and neurodegenerative disease. *Nat. Neurosci.* **24**, (2021).

38. Abu-Remaileh, M. *et al.* Lysosomal metabolomics reveals V-ATPase- and mTOR-dependent regulation of amino acid efflux from lysosomes. *Science (80-.).* **358**, 807–813 (2017).

39. Muthukottiappan, P. & Winter, D. A Proteomic View on Lysosomes. *Mol. Omi.* (2021) doi:10.1039/d1mo00205h.

40. Vasanthakumar, T. & Rubinstein, J. L. Structure and Roles of V-type ATPases. *Trends in Biochemical Sciences* vol. 45 295–307 (2020).

41. Nowosad, A. & Besson, A. Lysosomes at the Crossroads of Cell Metabolism, Cell Cycle and Stemness. *Int. J. Mol. Sci.* **23**, (2022).

42. Lui, H. *et al.* Progranulin Deficiency Promotes Circuit-Specific Synaptic Pruning by Microglia via Complement Activation. *Cell* **165**, 921–935 (2016).

bioRxiv preprint doi: https://doi.org/10.1101/2023.02.24.529955; this version posted February 24, 2023. The copyright holder for this preprint (which was not certified by peer review) is the author/funder, who has granted bioRxiv a license to display the preprint in perpetuity. It is made available under aCC-BY-ND 4.0 International license.

43. Götzl, J. K. *et al.* Common pathobiochemical hallmarks of progranulin-associated frontotemporal lobar degeneration and neuronal ceroid lipofuscinosis. *Acta Neuropathol.* **127**, 845–60 (2014).

44. Mathieson, T. *et al.* Systematic analysis of protein turnover in primary cells. *Nat. Commun.* **9**, 1–10 (2018).

45. Dörrbaum, A. R., Alvarez-Castelao, B., Nassim-Assir, B., Langer, J. D. & Schuman, E. M. Proteome dynamics during homeostatic scaling in cultured neurons. *Elife* **9**, 1–28 (2020).

46. Bomba-Warczak, E., Edassery, S. L., Hark, T. J. & Savas, J. N. Long-lived mitochondrial cristae proteins in mouse heart and brain. *J. Cell Biol.* **220**, (2021).

47. Klim, J. R. *et al.* ALS-implicated protein TDP-43 sustains levels of STMN2, a mediator of motor neuron growth and repair. *Nat. Neurosci.* **22**, 167–179 (2019).

48. Krus, K. L. *et al.* Loss of Stathmin-2, a hallmark of TDP-43-associated ALS, causes motor neuropathy. *Cell Rep.* **39**, (2022).

49. Neary, D., Snowden, J. & Mann, D. Frontotemporal dementia. *Lancet Neurol.* **4**, 771–780 (2005).

50. Reis, R. C. M., Sorgine, M. H. F. & Coelho-Sampaio, T. A novel methodology for the investigation of intracellular proteolytic processing in intact cells. *Eur. J. Cell Biol.* **75**, 192–197 (1998).

51. Carling, P. J. *et al.* Multiparameter phenotypic screening for endogenous TFEB and TFE3 translocation identifies novel chemical series modulating lysosome function. *Autophagy* 1–14 (2022) doi:10.1080/15548627.2022.2095834.

52. Valdez, C. *et al.* Progranulin-mediated deficiency of cathepsin D results in FTD and NCL-like phenotypes in neurons derived from FTD patients. *Hum. Mol. Genet.* **26**, 4861–4872

bioRxiv preprint doi: https://doi.org/10.1101/2023.02.24.529955; this version posted February 24, 2023. The copyright holder for this preprint (which was not certified by peer review) is the author/funder, who has granted bioRxiv a license to display the preprint in perpetuity. It is made available under aCC-BY-ND 4.0 International license.

(2017).

53. Dörrbaum, A. R., Kochen, L., Langer, J. D. & Schuman, E. M. Local and global influences on protein turnover in neurons and glia. *Elife* **7**, 1–24 (2018).

54. Mohan, S. *et al.* Processing of progranulin into granulins involves multiple lysosomal proteases and is affected in frontotemporal lobar degeneration. *Mol. Neurodegener.* **16**, (2021).

55. Zhang, T. *et al.* Differential regulation of progranulin derived granulin peptides. *Mol. Neurodegener.* **17**, (2022).

56. Götzl, J. K. *et al.* Early lysosomal maturation deficits in microglia triggers enhanced lysosomal activity in other brain cells of progranulin knockout mice. *Mol. Neurodegener.* **13**, (2018).

57. Lee, J. H. *et al.* Presenilin 1 Maintains Lysosomal Ca2+ Homeostasis via TRPML1 by Regulating vATPase-Mediated Lysosome Acidification. *Cell Rep.* **12**, 1430–1444 (2015).

58. Tanaka, Y. *et al.* Progranulin regulates lysosomal function and biogenesis through acidification of lysosomes. *Hum. Mol. Genet.* **26**, 969–988 (2017).

59. Cheng, X. T. *et al.* Characterization of LAMP1-labeled nondegradative lysosomal and endocytic compartments in neurons. *J. Cell Biol.* **217**, 3127–3139 (2018).

60. Kao, A. W. *et al.* A neurodegenerative disease mutation that accelerates the clearance of apoptotic cells. *Proc. Natl. Acad. Sci. U. S. A.* **108**, 4441–6 (2011).

61. Frankenfield, A. M., Ni, J., Ahmed, M. & Hao, L. Protein Contaminants Matter: Building Universal Protein Contaminant Libraries for DDA and DIA Proteomics. *J. Proteome Res.* **21**, 2104–2113 (2022).

62. Ge, S. X., Jung, D., Jung, D. & Yao, R. ShinyGO: A graphical gene-set enrichment tool for

bioRxiv preprint doi: https://doi.org/10.1101/2023.02.24.529955; this version posted February 24, 2023. The copyright holder for this preprint (which was not certified by peer review) is the author/funder, who has granted bioRxiv a license to display the preprint in perpetuity. It is made available under aCC-BY-ND 4.0 International license.

694 animals and plants. *Bioinformatics* (2020) doi:10.1093/bioinformatics/btz931.

695 63. Szklarczyk, D. *et al.* STRING v11: Protein-protein association networks with increased
696 coverage, supporting functional discovery in genome-wide experimental datasets. *Nucleic*
697 *Acids Res.* (2019) doi:10.1093/nar/gky1131.

698 64. Saric, A., Grinstein, S. & Freeman, S. A. Measurement of Autolysosomal pH by Dual-
699 Wavelength Ratio Imaging. in *Methods in Enzymology* vol. 588 15–29 (Academic Press
700 Inc., 2017).

701 65. Schneider, C. A., Rasband, W. S. & Eliceiri, K. W. NIH Image to ImageJ: 25 years of image
702 analysis. *Nature Methods* (2012) doi:10.1038/nmeth.2089.

703

bioRxiv preprint doi: https://doi.org/10.1101/2023.02.24.529955; this version posted February 24, 2023. The copyright holder for this preprint (which was not certified by peer review) is the author/funder, who has granted bioRxiv a license to display the preprint in perpetuity. It is made available under aCC-BY-ND 4.0 International license.

Figures and Figure legends

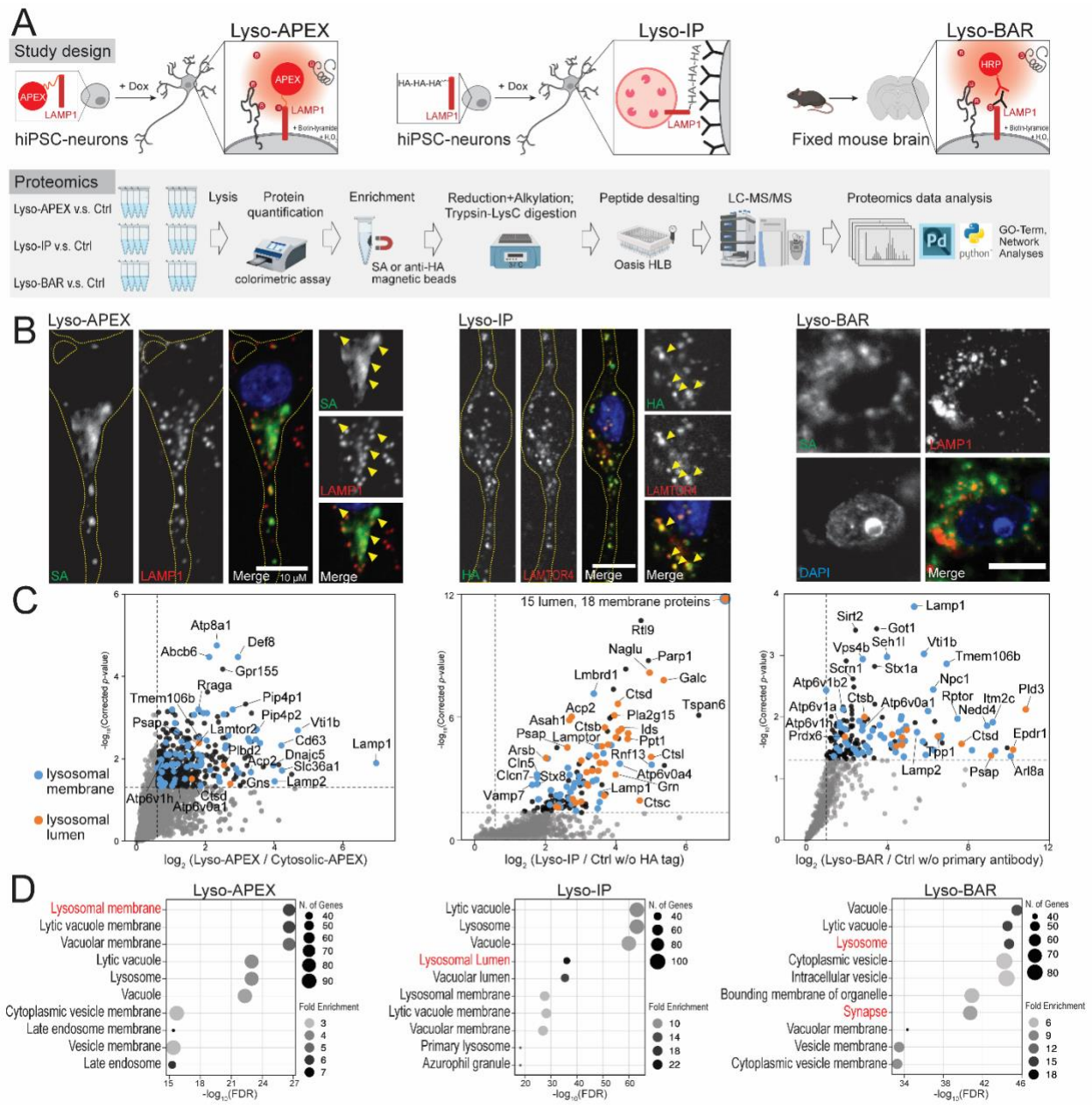

Figure 1. A map of the lysosomal proteome and interactome in human neurons and mouse brain. (**A**) Schematics of lysosomal proximity labeling (Lyso-APEX) in i^{3}Neurons, lysosomal immunopurification (Lyso-IP) in i^{3}Neurons, and lysosomal biotinylation by antibody recognition

bioRxiv preprint doi: https://doi.org/10.1101/2023.02.24.529955; this version posted February 24, 2023. The copyright holder for this preprint (which was not certified by peer review) is the author/funder, who has granted bioRxiv a license to display the preprint in perpetuity. It is made available under aCC-BY-ND 4.0 International license.

(Lyso-BAR) in fixed mouse brain tissues. (**B**) Fluorescence imaging of Lyso-APEX, Lyso-IP, and Lyso-BAR activities in i^3Neurons and fixed mouse brain. Biotinylated proteins, stained with streptavidin (SA), colocalize with lysosomal markers in i^3Neurons and fixed mouse brain tissues. HA-tagged lysosomes colocalize with lysosomal markers in i^3Neurons. Scale bars are 10μm. (**C**) Volcano plots showing significantly enriched proteins from WT Lyso-APEX compared to cytosolic-APEX, Lyso-IP compared to control group without HA expression, and Lyso-BAR compared to control group without primary antibody staining (N=4). Dotted lines denote corrected *p*-value of 0.05 (y-axis) and ratio of 1.5 (x-axis). Known lysosomal membrane and lumen proteins are highlighted in blue and orange colors, respectively. (**D**) GO-term analyses of significantly enriched proteins in Lyso-APEX, Lyso-IP, and Lyso-BAR proteomics.

bioRxiv preprint doi: https://doi.org/10.1101/2023.02.24.529955; this version posted February 24, 2023. The copyright holder for this preprint (which was not certified by peer review) is the author/funder, who has granted bioRxiv a license to display the preprint in perpetuity. It is made available under aCC-BY-ND 4.0 International license.

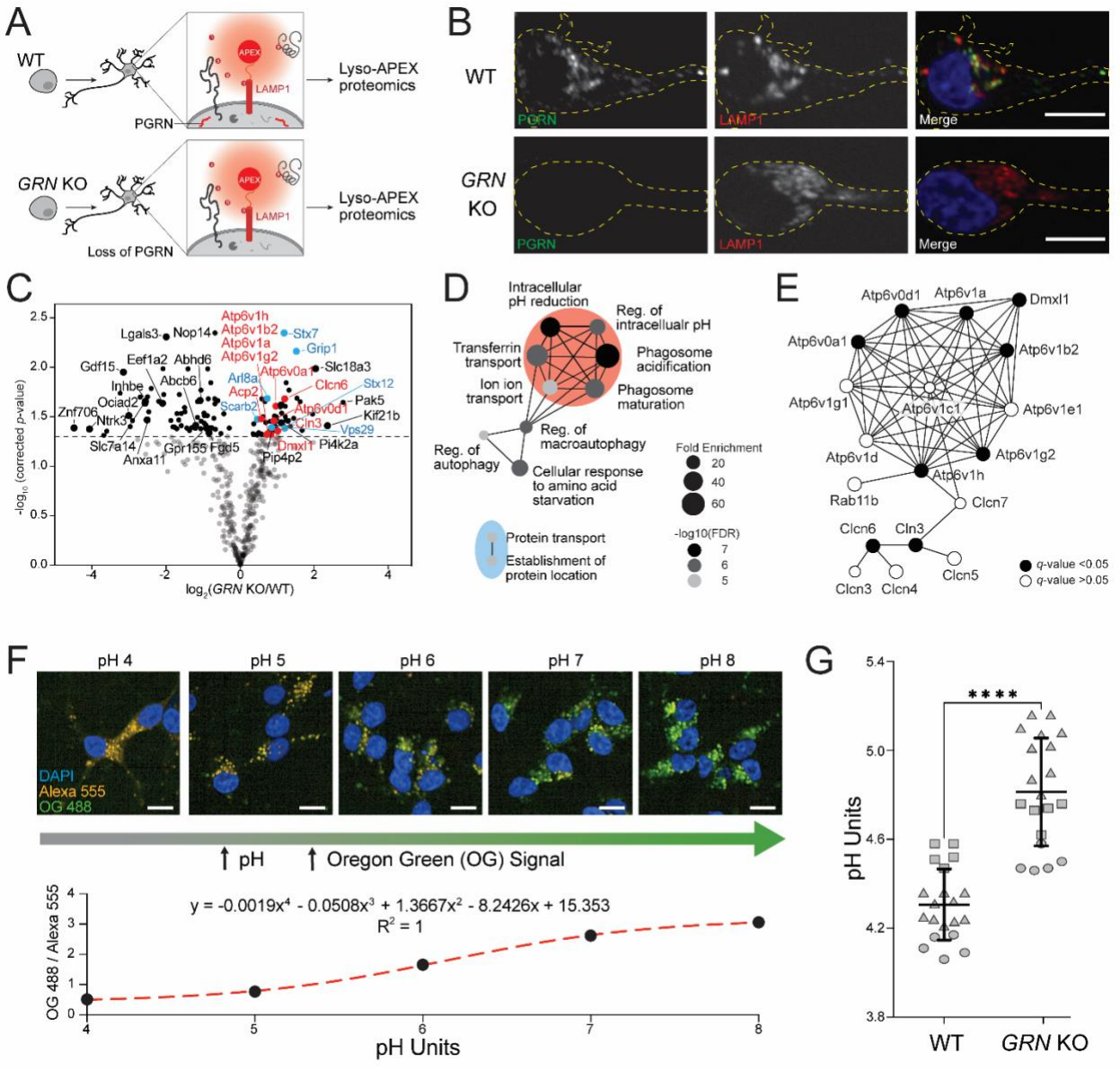

Figure 2. Lysosomal membrane proteins and pH are altered in i^{3}Neurons with loss of progranulin. (**A**) Schematic of Lyso-APEX in WT and isogenic *GRN* KO i^{3}Neurons. (**B**) Fluorescence imaging showing the colocalization of PGRN with lysosomes in WT i^{3}Neurons and loss of progranulin (PGRN) signal in *GRN* KO i^{3}Neurons. Scale bar is 10μm. (**C**) Volcano plot of Lyso-APEX proteomics in *GRN* KO vs. WT i^{3}Neurons. Cytosolic enriched proteins and nonspecific labelings were removed from the volcano plot based on WT LysoAPEX vs. Cytosolic-

bioRxiv preprint doi: https://doi.org/10.1101/2023.02.24.529955; this version posted February 24, 2023. The copyright holder for this preprint (which was not certified by peer review) is the author/funder, who has granted bioRxiv a license to display the preprint in perpetuity. It is made available under aCC-BY-ND 4.0 International license.

737 APEX comparison. Red and blue colored proteins belong to lysosomal pH and protein transport
738 GO-terms, respectively. (**D**) GO-term network analysis of significantly up-regulated biological
739 processes in *GRN* KO vs. WT Lyso-APEX proteomics. (**E**) Protein network analysis of identified
740 vacuolar-ATPase subunits and their interactors. (**F**) Live cell ratiometric lysosome pH assay. pH
741 calibration curve is generated based on the ratio of pH-sensitive Oregon Green-488 dextran signal
742 and pH-insensitive/loading control Alexa Fluor-555 red dextran in WT i^{3}Neurons. Scale bar is
743 10μm. Other linear and nonlinear curve fitting models are provided in Supplementary Figure S2E.
744 (**G**) Lysosome pH measurements in WT vs. *GRN* KO i^{3}Neurons; multiple biological replicates
745 from three independent experiments are represented with different shapes (**** denotes *p*-value
746 < 0.0001).

bioRxiv preprint doi: https://doi.org/10.1101/2023.02.24.529955; this version posted February 24, 2023. The copyright holder for this preprint (which was not certified by peer review) is the author/funder, who has granted bioRxiv a license to display the preprint in perpetuity. It is made available under aCC-BY-ND 4.0 International license.

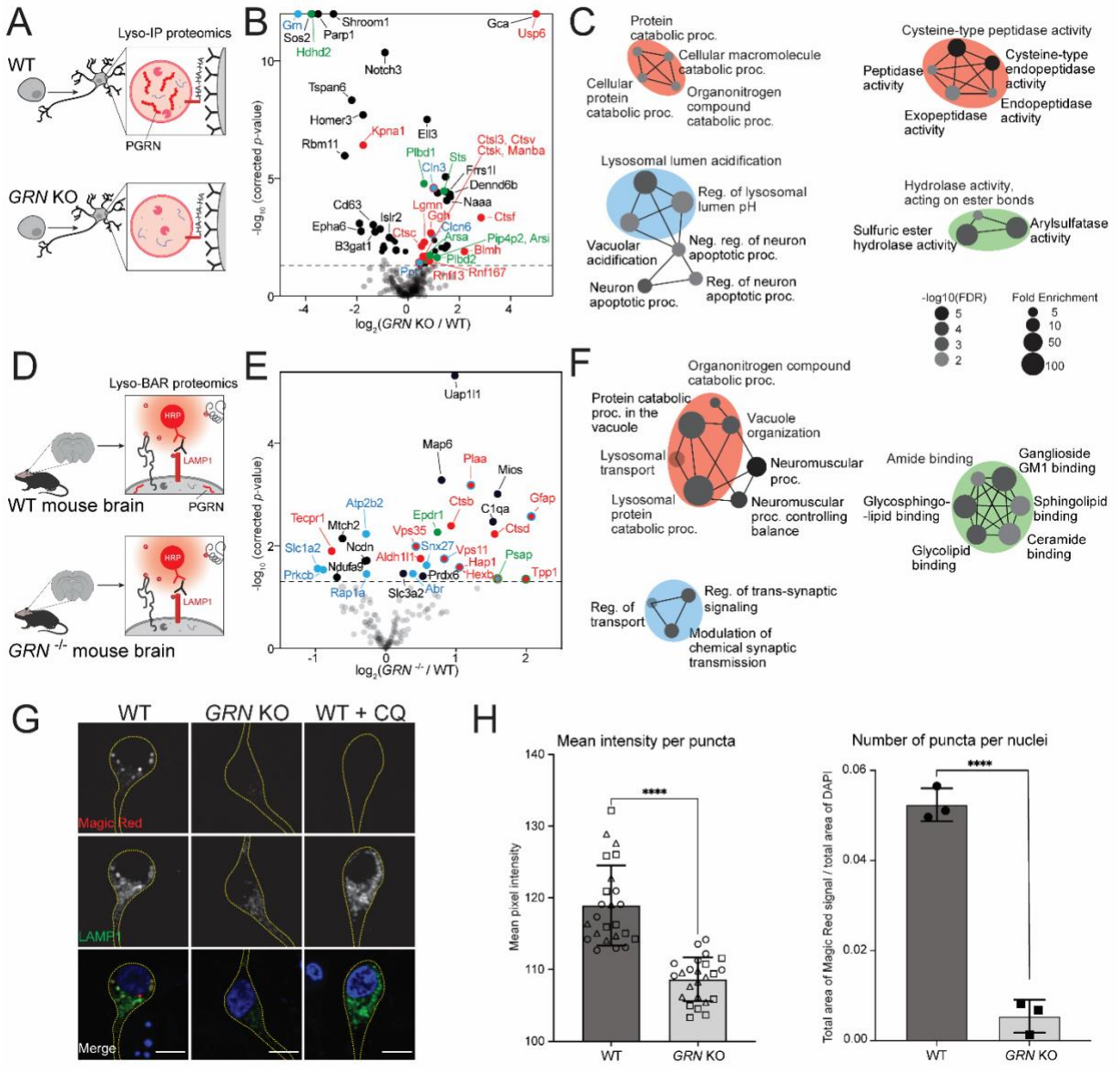

Figure 3. Progranulin-null lysosomes from human neurons and mouse brains have increased levels of lysosomal catabolic enzymes and decreased cathepsin B activity. (**A**) Schematic of intact lysosomal isolation (Lyso-IP) proteomics in *GRN* KO vs. WT i^{3}Neurons. (**B**) Volcano plot of Lyso-IP proteomics showing protein changes related to protein catabolic processes (red), lysosomal pH (blue), and hydrolase activities (green). Nonspecific labeling proteins were removed based on WT LysoIP vs. control i^{3}Neurons without HA expression. (**C**) GO-term network analysis

bioRxiv preprint doi: https://doi.org/10.1101/2023.02.24.529955; this version posted February 24, 2023. The copyright holder for this preprint (which was not certified by peer review) is the author/funder, who has granted bioRxiv a license to display the preprint in perpetuity. It is made available under aCC-BY-ND 4.0 International license.

of significantly changed proteins in *GRN* KO vs. WT Lyso-IP proteomics. Enriched biological processes are shown on the left. Molecular functions are shown on the right. Color code corresponds to the volcano plot. (**D**) Schematic of mouse brain Lyso-BAR labeling in *GRN*$^{-/-}$ vs. WT mice. (**E**) Volcano plot showing Lyso-BAR protein changes in *GRN*$^{-/-}$ vs. WT mouse brain. Nonspecific labeling proteins were removed based on WT LysoBAR vs. control without primary antibody staining. (**F**) GO-term network analysis of significantly changed proteins in *GRN* $^{-/-}$ vs. WT Lyso-BAR proteomics. (**G**) Fluorescence imaging of Magic Red assay to measure cathepsin B activity in i^{3}Neurons. CQ stands for chloroquine treatment (50 μM for 24 hours). Scale bar is 10 μm. (**H**) Quantification of absolute and relative fluorescence intensities indicate decreased cathepsin B activity in *GRN* KO vs. WT i^{3}Neurons (**** denotes p-value < 0.0001).

bioRxiv preprint doi: https://doi.org/10.1101/2023.02.24.529955; this version posted February 24, 2023. The copyright holder for this preprint (which was not certified by peer review) is the author/funder, who has granted bioRxiv a license to display the preprint in perpetuity. It is made available under aCC-BY-ND 4.0 International license.

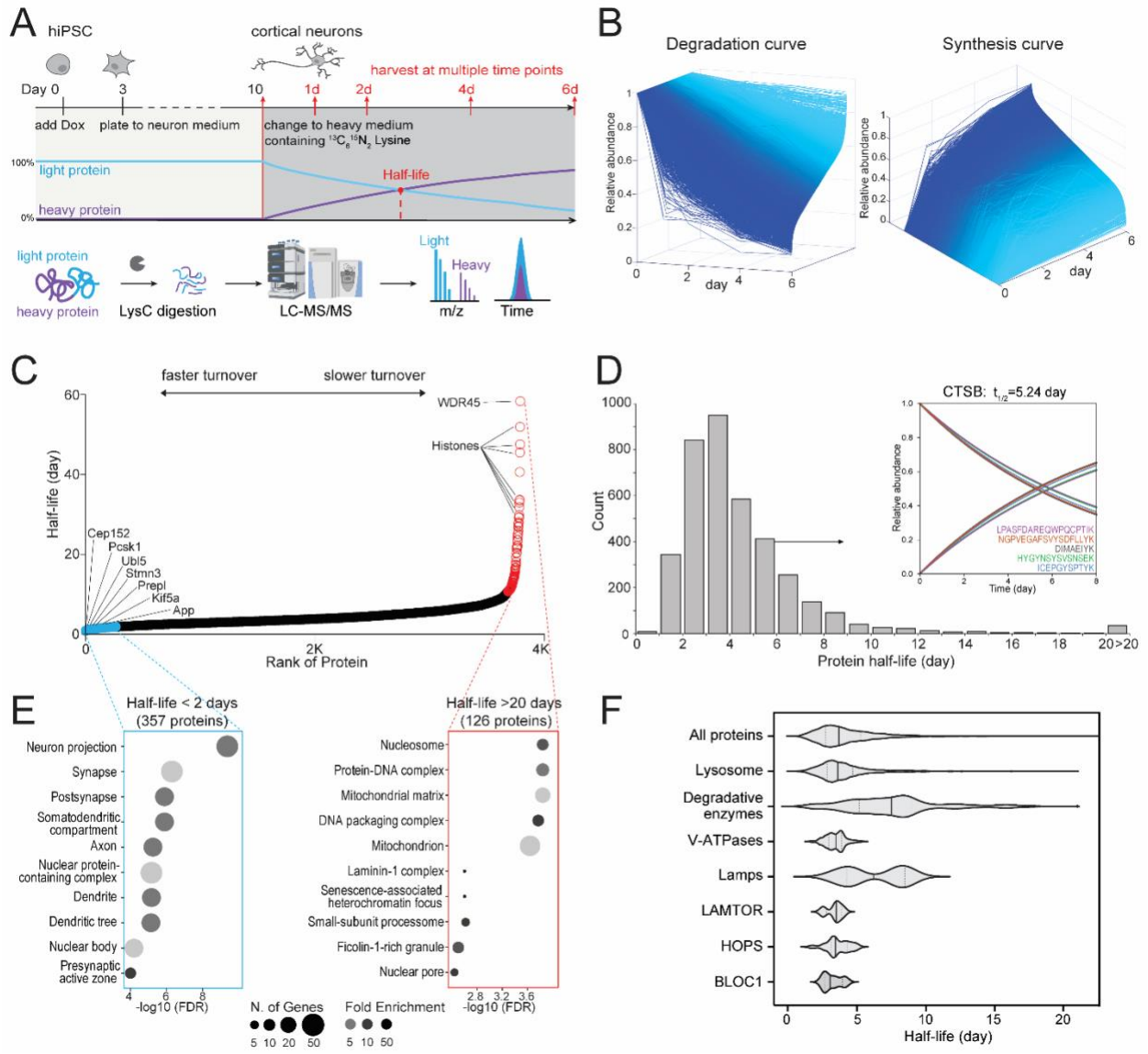

Figure 4. Measuring global protein half-lives in cultured human i^{3}Neurons. (**A**) Schematic of dynamic stable isotope labeling by amino acids in cell culture (dSILAC) proteomics to measure global protein half-lives in cultured human i^{3}Neurons. Cortical neurons were grown in normal medium until day 10 and then switched to heavy lysine-containing medium. Neurons are harvested at 1, 2, 4, and 6 days after medium switch followed by bottom-up proteomics. (**B**) Degradation and synthesis curves of all quantified proteins in WT i^{3}Neurons. (**C**) Scatter plot of protein half-lives measured in WT i^{3}Neurons ranked from fastest turnover to slowest turnover. (**D**) Histogram

bioRxiv preprint doi: https://doi.org/10.1101/2023.02.24.529955; this version posted February 24, 2023. The copyright holder for this preprint (which was not certified by peer review) is the author/funder, who has granted bioRxiv a license to display the preprint in perpetuity. It is made available under aCC-BY-ND 4.0 International license.

773 distribution of protein half-lives in WT i^{3}Neurons. An example cathepsin B (CTSB) protein with
774 five identified unique peptide sequences is illustrated in the inset. (**E**) GO-term analysis of the fast
775 (left) and slow (right) turnover proteins in WT i^{3}Neurons. (**F**) Violin plots of half-life distributions
776 from all proteins and lysosomal proteins in WT i^{3}Neurons.
777

bioRxiv preprint doi: https://doi.org/10.1101/2023.02.24.529955; this version posted February 24, 2023. The copyright holder for this preprint (which was not certified by peer review) is the author/funder, who has granted bioRxiv a license to display the preprint in perpetuity. It is made available under aCC-BY-ND 4.0 International license.

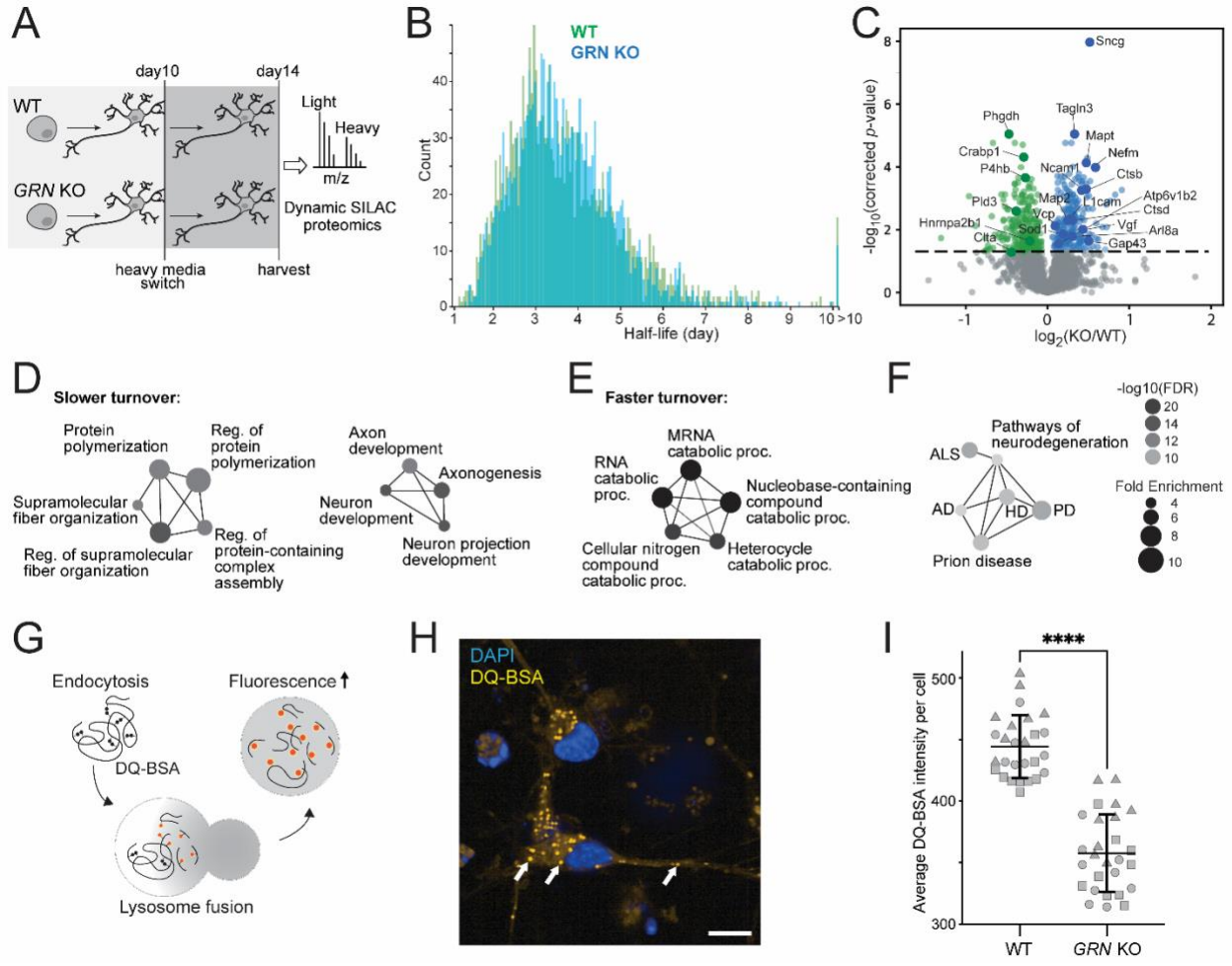

Figure 5. Global protein turnover and lysosomal degradative function are impaired in i^{3}Neurons with loss of progranulin. (**A**) Schematic of protein half-life measurements in *GRN* KO vs. WT i^{3}Neurons using dynamic SILAC proteomics. (**B**) Histogram distribution of global protein half-lives in *GRN* KO (blue) vs. WT (green) i^{3}Neurons. (**C**) Volcano plot of protein half-life changes in *GRN* KO vs. WT i^{3}Neurons. (**D**) GO-term network analysis of enriched biological processes from proteins with significantly slower turnover. (**E**) GO-term network analysis of enriched biological processes from proteins with significantly faster turnover. (**F**) KEGG pathways enriched from significantly altered protein half-lives in *GRN* KO vs. WT i^{3}Neurons. (**G**) Schematic of the DQ-BSA Red assay to measure lysosomal degradative function. Extracellular DQ-BSA with

bioRxiv preprint doi: https://doi.org/10.1101/2023.02.24.529955; this version posted February 24, 2023. The copyright holder for this preprint (which was not certified by peer review) is the author/funder, who has granted bioRxiv a license to display the preprint in perpetuity. It is made available under aCC-BY-ND 4.0 International license.

788 self-quenched dye is endocytosed into i^{3}Neurons and trafficed to the lysosome, where it isdegraded
789 into smaller protein fragments with isolated fluorophores with fluorescence signals. (**H**)
790 Representative fluorescence imaging of DQ-BSA Red assay showing DQ-positive lysosomes in
791 i^{3}Neurons. Scale bar is 10μm. (**I**) Quantification of the fluorescence intensities of the DQ-BSA
792 Red assay in WT vs. *GRN* KO i^{3}Neurons, normalized to the total number of puncta in two groups
793 (**** denotes p-value < 0.0001).
794

bioRxiv preprint doi: https://doi.org/10.1101/2023.02.24.529955; this version posted February 24, 2023. The copyright holder for this preprint (which was not certified by peer review) is the author/funder, who has granted bioRxiv a license to display the preprint in perpetuity. It is made available under aCC-BY-ND 4.0 International license.

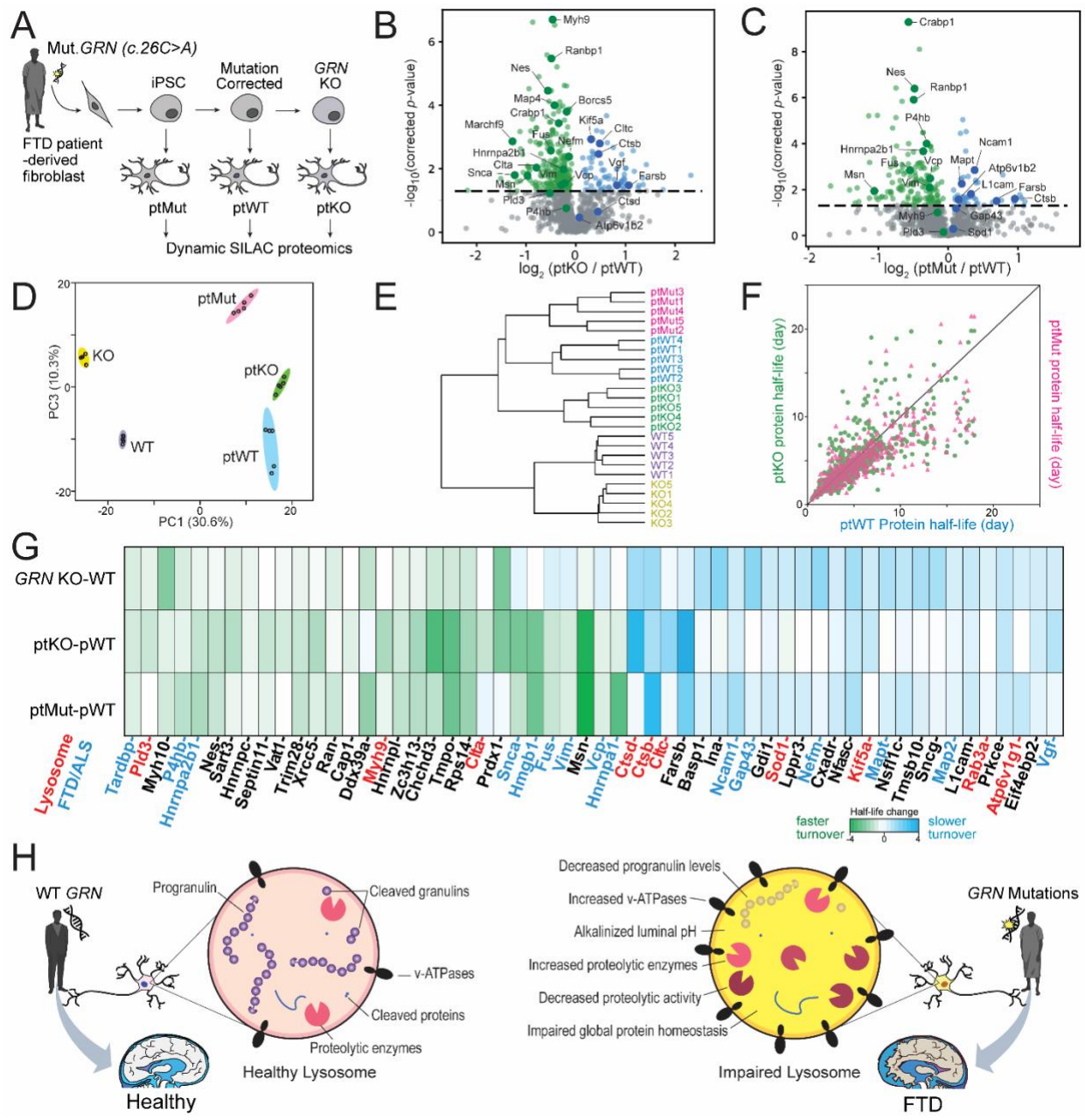

Figure 6. Frontotemporal dementia (FTD) patient-derived i^{3}Neurons with muatant *GRN* reveal altered protein turnover of lysosomal enzymes and FTD-associated proteins. (**A**) Generation of a set of FTD patient fibroblast-derived i^{3}Neurons. First, CRISPR-Cas9 was used to insert an inducible *NGN2* cassette into the *AAVS1* locus of a patient fibroblast-derived iPSC line (ptMut). Next, CRISPR-Cas9 was used to correct the *GRN* mutation in ptMut to create an isogenic

bioRxiv preprint doi: https://doi.org/10.1101/2023.02.24.529955; this version posted February 24, 2023. The copyright holder for this preprint (which was not certified by peer review) is the author/funder, who has granted bioRxiv a license to display the preprint in perpetuity. It is made available under aCC-BY-ND 4.0 International license.

control iPSC line (ptWT) and then to knockout *GRN* in pWT to create the ptKO iPSC line. These iPSC lines were then differentiated into i^{3}Neurons and dSILAC proteomics was performed. (**B**) Volcano plot of protein half-life changes in ptKO vs. ptWT i^{3}Neuron. (**C**) Volcano plot of protein half-life changes in ptMut vs. ptWT i^{3}Neuron. (**D**) Principal component analysis using protein half-lives in GRN-KO, WT, ptKO, ptMut, and ptWT i^{3}Neurons groups. (**E**) Hierarchical clutering of five i^{3}Neurons groups. (**F**) Scatter plot of protein half-life changes in ptKO vs.ptWT and ptMut vs. ptWT comparisons showing the consistency and potential gene dosage effect of ptKO and ptMut i^{3}Neurons. (**G**) Heatmap showing key overlapping protein turnover changes in *GRN* KO vs. WT, ptKO vs. ptWT, and ptMut vs. ptWT i^{3}Neurons. Heatmap colors represent the absolute half-life differences between comparison groups. Key proteins from lysosomes and relevant to FTD/ALS are highlighted in red and blue, respectively. (**H**) Schematic of proposed lysosomal impairment in progranulin-deficient neurons caused by GRN mutations in FTD patients.